Pre-eruptive volatile contents and degassing systematics of rhyolitic magmas from the Taupo Volcanic Zone, New Zealand

Nelia W. Dunbar

Submitted in Partial Fulfullment
of the Requirements for the Degree of
Doctor of Philosophy in Geology

November, 1988

Table of Contents

List of Figures

List of Tables

Appendix D

Appendix E

Appendix F

Appendix G

ACKNOWLEDGEMENTS

First, I would like to acknowledge my advisor and friend, Phil Kyle, who initiated this project, and also provided continual academic and financial support throughout the duration of this work.

Thanks also go to a number of people whose input, and expertise in various fields was extremely helpful to me during this project. Colin Wilson devoted a week of his time to giving us a tour of the Taupo Volcanic Center, and field sampling in this area was greatly facilitated by his detailed mapping. Ian Nairn was equally helpful in the sampling of the Okataina Volcanic Center. Discussions with, and input from Hank Westrich, Rick Hervig, Bruce Taylor, John Eichelberger, Colin Wilson, Bill McIntosh, Paul Sylvester, Andy Campbell, Dave Norman and Dave Caldwell have been very valuable.

There a number of people whose help has been essential to the analytical work which has gone into this project. Rick Hervig and the chemistry department of Arizona State University provided the instrument and the analytical expertise for the ion microprobe analyses done in this study. The geochemistry division of Sandia National Laboratory provided the Karl-Fischer titrimeter and Dupont Moisture analyser used in this project. Hank

Westrich and John Eichelberger showed me how to operate these instruments, and were helpful throughout the time that I was doing these analyses. Electron microprobes from Victoria University, and the University of New Mexico were used in this study, and thanks go to Ken Palmer, John Gamble, and George Conrad for analytical assistance. Ongoing isotopic analyses were done with Bruce Taylor at the U.S.G.S. lab in Menlo Park, and also at the Canadian Geological Survey. Neutron activation and x-ray fluorescence analyses were done at New Mexico Institute of Mining and Technology, and Phil Kyle was very helpful in this part of the analytical work.

I would particularly like to thank my thesis committee; Andy Campbell, John Eichelberger, Phil Kyle, Dave Norman, and Jim Smith, for their discussions and input to my thesis.

I am greatly indepted to the Department of the Interior's Mineral Institute program, and Arpad Torma, who have provided me with four years of financial support under allotment grant number G1164135.

I would like to thank my family, whose continued enthusiasm and encouragment throughout my academic career have allowed me to complete this research.

Finally, I would like to thank Bill McIntosh for all of his help.

ABSTRACT

Melt inclusions in magmatic phenocrysts from rhyolitic Taupo Volcanic Zone tephras represent pre-eruptive magma composition. The pre-eruptive H_2O and F contents of Taupo Volcanic Center (TVC) magmas which produced the Taupo plinian (2 ka), Hatepe plinian (2 ka) and Okaia (23 ka) tephras are 4.3 wt.% and 450 ppm; 4.3 wt.% and 430 ppm; 5.9 wt.% and 470 ppm respectively, as determined by ion microprobe analyses of melt inclusions. The Cl contents of these magmas, as determined by electron microprobe analysis of melt inclusions, are 0.17, 0.17 and 0.21 wt.% respectively, and the range of Cl contents for all 25 tephra units analysed from the TVC and Okataina Volcanic Center (OVC) is 0.13 to 0.23 wt.%. The consistency of the volatile content determinations of the magmas which produced the Taupo and Hatepe plinian tephras indicate that there was no significant volatile gradient in the ~8.2 km^3 of magma which produced these, and the two intermediate eruptions. Therefore, the highly explosive nature of the Taupo "ultraplinian" event, which produced the Taupo plinian tephra was not due solely to an anomalously high water content, as the water content of the less-explosive Hatepe plinian and

Okaia tephra eruptions are similar or greater. Based on the pre-eruptive H_2O and Cl contents of these magmas and estimates of atmospheric equilibrium of these volatiles in rhyolites, petrological estimates of H_2O emitted to the atmosphere during these eruptions are 4.9×10^{14}, 1.3×10^{14}, and 4.6×10^{14} g for the Taupo, Hatepe and Okaia plinian eruptions, and 5.5×10^{12}, 1.5×10^{12} and 6.5×10^{12} g of Cl respectively. The Cl outputs for all other TVC and OVC tephras range from 1.2×10^{11} to 1.9×10^{14} g. If the eruptive columns from these eruptions penetrated into the stratosphere, and if even a small percentage of this magmatic H_2O and HCl remained at high altitude, destruction of stratospheric ozone may have occurred. The amount of H_2O, Cl, Cu, Sn, and Mo which would have been emitted if the post-20 ka Taupo magma chamber formed a crystalline pluton rather than erupting are each on the order of 10^{11} g, enough to form a porphyry ore deposit under the right conditions.

Obsidian in tephra deposits from the TVC and OVC eruptions is co-genetic with the bulk of the tephra, based on its trace element composition. Water contents of obsidian are generally above the atmospheric equilibrium, and range from 0.1 to 2.8 wt.%. The water contents of obsidian from individual tephra units vary widely about the unit mean value. The water contained in obsidian is thought to be primary magmatic water, based on degassing spectra, physical characteristics, and isotopic composition of obsidian. The obsidian represents partially degassed magma which quenched at variable depths during the eruption. The water contents of the obsidian may indicate quenching depths of 0-1.5 km. Limited hydrogen isotopic data of water in obsidian suggests that the melt may have undergone open-system degassing. The Cl contents of obsidian range from 0.119 to 0.168 wt.%, and are invariably lower than Cl in melt inclusions from the same eruption. There is a rough correlation between the mean H_2O and Cl contents of TVC obsidian, which suggests that during degassing, Cl was partitioned into a H_2O vapor phase, or that H_2O and Cl degassed at roughly similar rates. Extension of this correlation to include the H_2O and Cl contents of melt inclusions from the Taupo, Hatepe and Okaia plinian tephras suggests that these volatiles were near saturation in the respective magma chambers, and that the older Okaia magma chamber was deeper in the crust than the Taupo/Hatepe magma chamber. However, lack of vapor phase inclusions in magmatic phenocrysts suggest that these magmas were not saturated.

Based on the pre-eruptive water contents of the magmas, the depths of saturation for the Taupo and Hatepe magmas and the Okaia magma were 3.8 and 7.5 km respectively. The depth of fragmentation (3:1 vapor:melt) at which the explosive phase of the eruptions begin was ~500 m for the Taupo and Hatepe magmas, and ~600 m for the Okaia magma. Based on water contents, most obsidian quenched after the magma had fragmented, possibly due to efficient cooling of fragmented magma.

Trace element compositions of post-20 ka tephras from the TVC are extremely consistent, and show no evidence of systematic compositional zonation in the magma chamber. The pre-20 ka TVC tephras are also compositionally similar, but are distinct from those erupted post-20 ka. The temperature/oxygen fugacity buffer trends of these two groups are also distinct. Tephras from the OVC all fall on a single temperature/oxygen fugacity buffer trend, but are compositionally diverse. They do not, however, show any systematic compositional zonation.

1. INTRODUCTION

Volatile compounds are fundamental components of magmatic systems and influence many aspects of magmatic behavior. Volatiles, particularly H_2O, play a central role in the petrogenetic evolution and eruptive behavior of igneous systems. Stability of both hydrous and anhydrous mineral phases are strongly influenced by the H_2O content of the melt (Naney, 1983; Carmichael et al., 1974). The content and composition of volatiles in melts will dictate the formation of ore deposits during crystallization, providing both the transport medium and complexing agents for ore-forming metals (Burnham, 1979b). Finally, magmatic volatiles partly govern the nature of volcanic eruptions (Fisher and Schmincke, 1984). Volatiles exsolve as magmas rise towards the earth's surface, forming a free vapor phase that expands, and drives explosive eruptions.

The dominant volatile components of magmas are in the C-O-H-S system, particularly H_2O (35-90 mole %), CO_2 (5 to 50 mole %), and SO_2 (2 to 30 mole %) or H_2S depending on oxygen fugacity (Fisher and Schmincke, 1984). Minor components include H_2, CO, COS, S_2, O_2, HCl, N_2, HF, HBr, HI, metal halogens, and noble gases (Fisher and Schmincke, 1984). Some magmas may contain up to 20 wt% of dissolved volatiles, although values of 3-5 wt% are probably more typical (Holloway, 1981). Due to the low atomic weight of most volatile components, the molecular percentage in melts is much higher than the weight percent (Burnham, 1979a). For example, an albite melt containing 6 wt.% H_2O is composed of 50 mole % H_2O.

The exact concentrations and composition of volatile components in magmas are difficult to determine, because before and during eruption a large proportion of pre-eruptive magmatic volatiles are lost and the relative abundances of volatile components are altered. A number of different approaches have been used to estimate the pre-eruptive volatile content of melts, including thermodynamic calculations, experimental determinations based on mineral stabilities, measurements of gases emitted from active volcanoes, and direct determinations from primary volcanic materials (Clemens, 1984). The first three approaches are problematic for the following reasons: thermodynamic constants are not very well known, natural conditions of mineral growth are difficult to simulate in laboratory conditions, gas emissions from volcanoes are subject to atmospheric contamination, and are not directly representative of pre-eruptive magmatic volatiles. The fourth approach, direct determinations from volcanic material, is the most viable of these approaches, and is the one that has been used in this study.

Two types of primary samples of magma are useful for determinations of pre-eruptive volatiles: quenched volcanic glass and melt inclusions trapped in magmatic phenocrysts (Eichelberger and Westrich, 1981, Harris, 1981b; Sommer and Schramm, 1983; Druitt et al., 1982). Volcanic glass, or obsidian, can retain some portion of pre-eruptive volatiles trapped during quenching. Analyses can be used as minimum estimates of magmatic volatiles. Furthermore, because hydrogen isotopes fractionate between H_2O dissolved in the melt, and H_2O in a free vapor phase, the hydrogen isotope composition of a suite of quenched volcanic glasses can be used to trace the degassing process of the melt, and to differentiate between open and closed system degassing (Taylor et al., 1983). The isotopic composition of quenched glass can also be used to project back to the pre-eruptive volatile content of the melt, using determined fractionation factors for the isotope in question.

Melt inclusions trapped in magmatic phenocrysts provide the only samples of pristine, pre-eruptive magma available. If the inclusion glass is unaltered, the volatile content of the glass should represent the original volatile content of the pre-eruptive melt. However, specialized analytical techniques are necessary for the analysis of melt inclusions due to their small size.

The primary objectives of this study are to determine the pre-eruptive volatile contents of magmas that produced a number of rhyolitic eruptions from the

Taupo Volcanic Zone, New Zealand, and to study the degassing conditions of these magmas during eruption. Two approaches were taken to address these objectives. First, melt inclusions were analysed for their volatile contents. Second, trace element abundances, volatile contents and isotopic composition of hydrous obsidian in tephra deposits were determined. The volatile content of the obsidian was used to assess the degassing systematics and infer the volatile contents of the entire magmatic system.

The volatile components analysed in this study were H_2O, Cl and F, because these are the dominant species in rhyolitic systems. These measurements of H_2O, Cl and F are among the first direct determinations of volatile components of a major rhyolitic magmatic system. Two other volatile species, S and CO_2, are generally less important in silicic systems, and were not analysed in detail. Preliminary analyses were made of S, and abundances found to be below the detection limits (<100 ppm) of the analytical technique used. CO_2 was not measured because it is relatively insoluble in rhyolitic melts (Mysen and Virgo, 1980), and is difficult to analyse in low abundances.

The secondary objectives of this study were to determine the thermal and chemical evolution of the magmatic systems that produced the two sequences of rhyolitic eruptions. This was done by determining detailed bulk trace element chemistry and magnetite-ilmenite geothermometry for sequences of tephra from the Taupo and Okataina eruptive centers.

The Taupo Volcanic Zone, in the central North Island of New Zealand, was chosen for this study for several reasons. First, a large number of explosive rhyolitic eruptions of similar major element chemistry have occurred in the Taupo and Okataina volcanic centers over the last 50 ka, and the stratigraphy, chemistry and petrology of these tephras have been well documented (eg. Ewart, 1963,1966; Ewart et al., 1971; Froggatt, 1982b; Howorth, 1976; Nairn, 1972, 1980, 1981; Vucetich and Howorth, 1976; Vucetich and Pullar, 1969, 1973; Walker, 1981a and c; Wilson et al., 1980, 1984). Second, the tephra deposits from these centers represent a range of eruptive styles, from ultraplinian to plinian to phreatoplinian. These differences in eruptive style may relate to initial volatile contents of the melt, or to degassing systematics during the eruptions. Third, there is no evidence of magma mixing in most of these eruptions, which would introduce contaminants into the rhyolitic melts (Froggatt, 1982b). Finally, the tephra units are young and usually unaltered, most contain obsidian fragments that are glassy and appear non-hydrated by meteoric water. Melt inclusions are abundant in phenocrysts.

2. TAUPO VOLCANIC ZONE

General Background

The Taupo Volcanic Zone (TVZ), in the central North Island of New Zealand, covers an area of 200x40 km, and is a main center of Quaternary volcanism. The TVZ is a major volcano-tectonic depression which is the expression of a volcanic arc and/or marginal basin at the southern end of the Tonga-Kermadec subduction zone (Cole, 1982). Volcanism in the TVZ over the last 2 million years (ma) has produced over 10^4 km^3 of magma (Wilson et al., 1984). Volcanism has been dominantly rhyolitic, with subordinant andesites, basalts and dacites (Cole, 1984). The crust in the TVZ is approximately 15 km thick, compared to 30-35 km outside the basin. Consequently, heat flow in the TVZ is high (Cole, 1984; Stern, 1985, 1987).

A large part of the volcanism in the TVZ has been concentrated in the 6 calderas shown in Fig 2-1: Rotorua, Okataina, Maroa, Kapenga, Mangakino, and Taupo. The calderas are not obvious structures, but are defined by depressed areas in the underlying basement rocks and clustering of eruptive vents (Wilson et al., 1984). Positions of 4 calderas, Okataina, Mangakino, Maroa, and

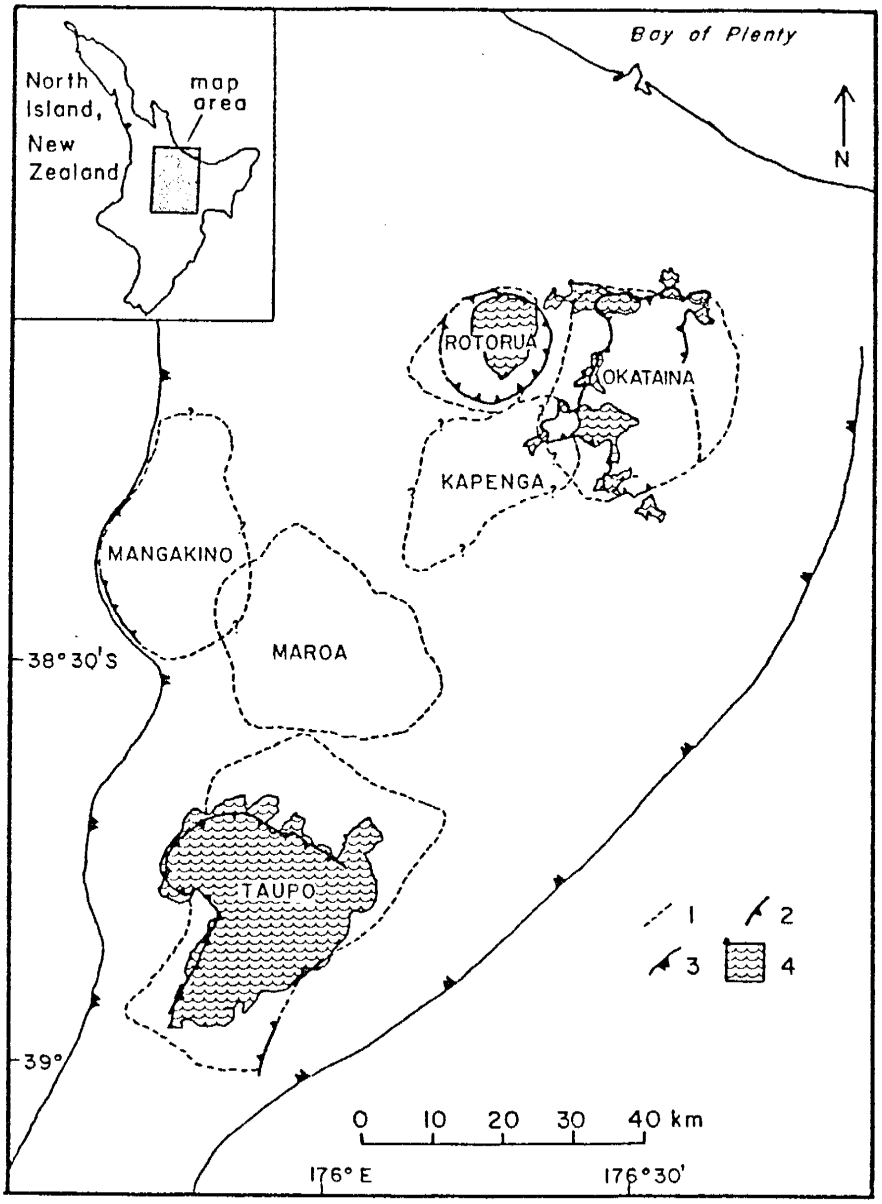

Figure 2-1. Location map of caldera volcanoes of the Taupo Volcanic Zone, New Zealand. Symbols represent (1) outer limits of named centers, (2) caldera margins as mapped by surface geology, (3) limit of basement subsidence associated with the Taupo Volcanic Zone, and (4) lakes. After Wilson et al., 1984.

Taupo, may result from intersections of NW trending structures and the trend of the TVZ, which is NNE (Wilson et al., 1984). However, in some cases, caldera boundaries cut across major regional faults. Rhyolitic plinian tephras, ignimbrites and domes have been erupted from these calderas. Presently, the Taupo and Okataina calderas are most active, and have produced the largest number of recent tephra deposits, Rotorua and Maroa are slightly active, and Kapenga and Mangakino are extinct (Wilson et al., 1984). No evidence of resurgent doming is seen in the TVZ (Wilson et al., 1984).

The eruptive behavior of the Taupo and Okataina calderas, or volcanic centers, contrasts with similar sized calderas in the western United States. Eruptions from the TVZ calderas are generally smaller, but more frequent, than their western U.S. counterparts. For example, over the last 50 thousand years (ka), the Taupo Volcanic Center (TVC) has produced at least 15 separate eruptions, ranging from <1 to about 300 km^3 of tephra, whereas some comparable calderas in the western U.S. have produced only 1 or 2 large eruptions in their lifetime each several 100's to 1000's of km^3 in volume (Wilson et al., 1984). Wilson et al. (1984) suggest that the reason for this difference is that the thin and fractured TVZ crust will not allow formation of large, high level magma chambers that could evolve and produce very large eruptions.

Two major theories have been proposed for the genesis of the large volumes of rhyolite present in the TVZ (Cole, 1979). The first, fractional crystallization of TVZ andesites or high-Al basalts, is geochemically feasible, but seems unlikely when the large volume of rhyolite is considered. About 88% fractional crystallization of a basaltic lava is necessary to generate the observed rhyolitic chemistry, and this would leave a huge volume of mafic residue, for which there is no evidence (Cole, 1979). Isotopic evidence is also at variance with this origin (Blattner and Reid, 1982). The second possibility, partial melting of basement rocks, seems more probable. TVZ rhyolites can be generated by 35% partial melting of a metamorphic greywacke, based on their major, trace element, and isotopic compositions (Cole, 1979, Reid, 1983).

Taupo and Okataina volcanic centers

Background

The tephras studied in this project are from the Taupo Volcanic Center (TVC) and the Okataina Volcanic Center (OVC) (Figs. 2-2 and 2-3). These two centers have erupted a number of rhyolitic plinian and phreatoplinian

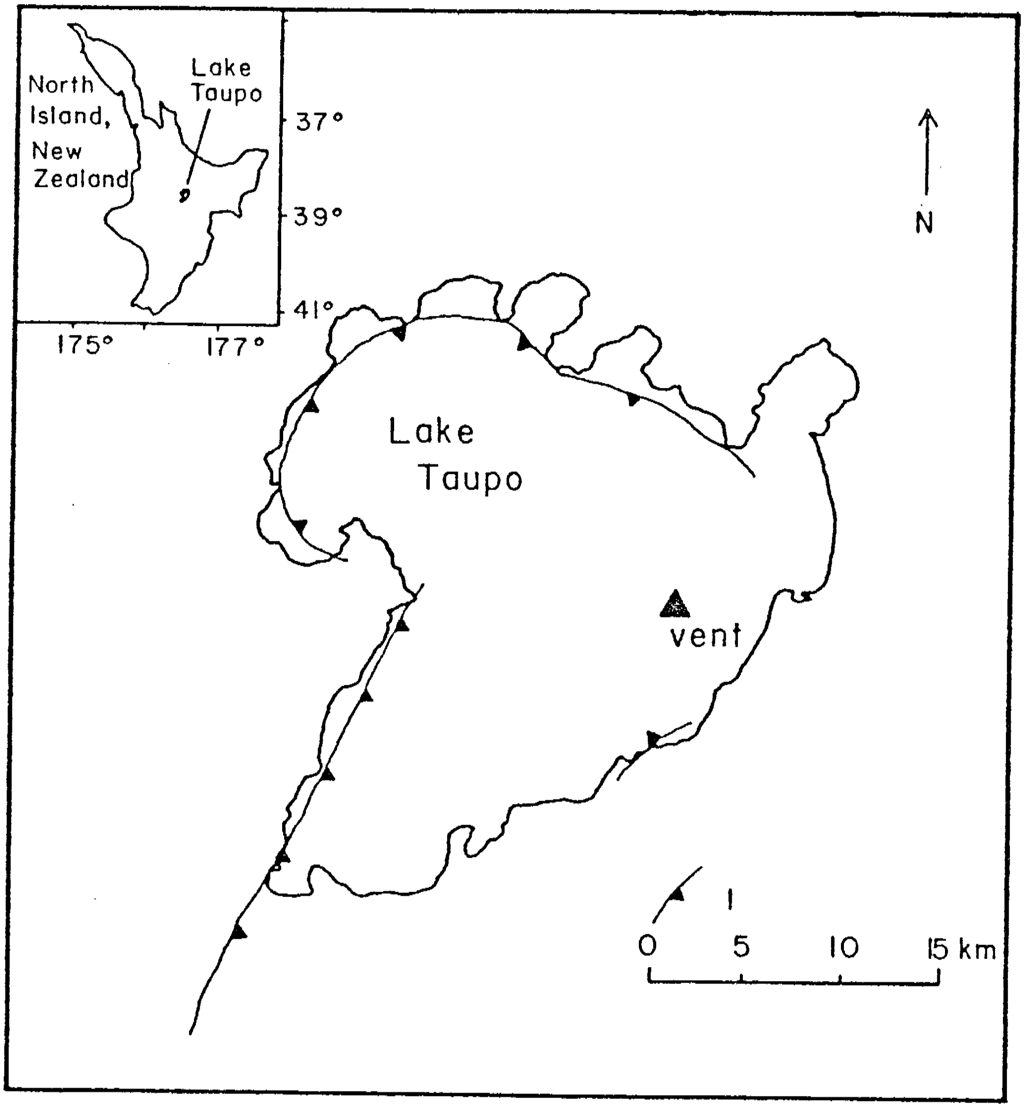

Figure 2-2. Map of the Taupo Volcanic Center. Symbol 1 represents the caldera margins as mapped by surface geology. The vent indicated on the figure is the vent for 4 <10 ka eruptions, including the 2 ka Taupo eruption. Other vents are thought to be within the lake area (Wilson et al, 1984). After Wilson et al., 1984.

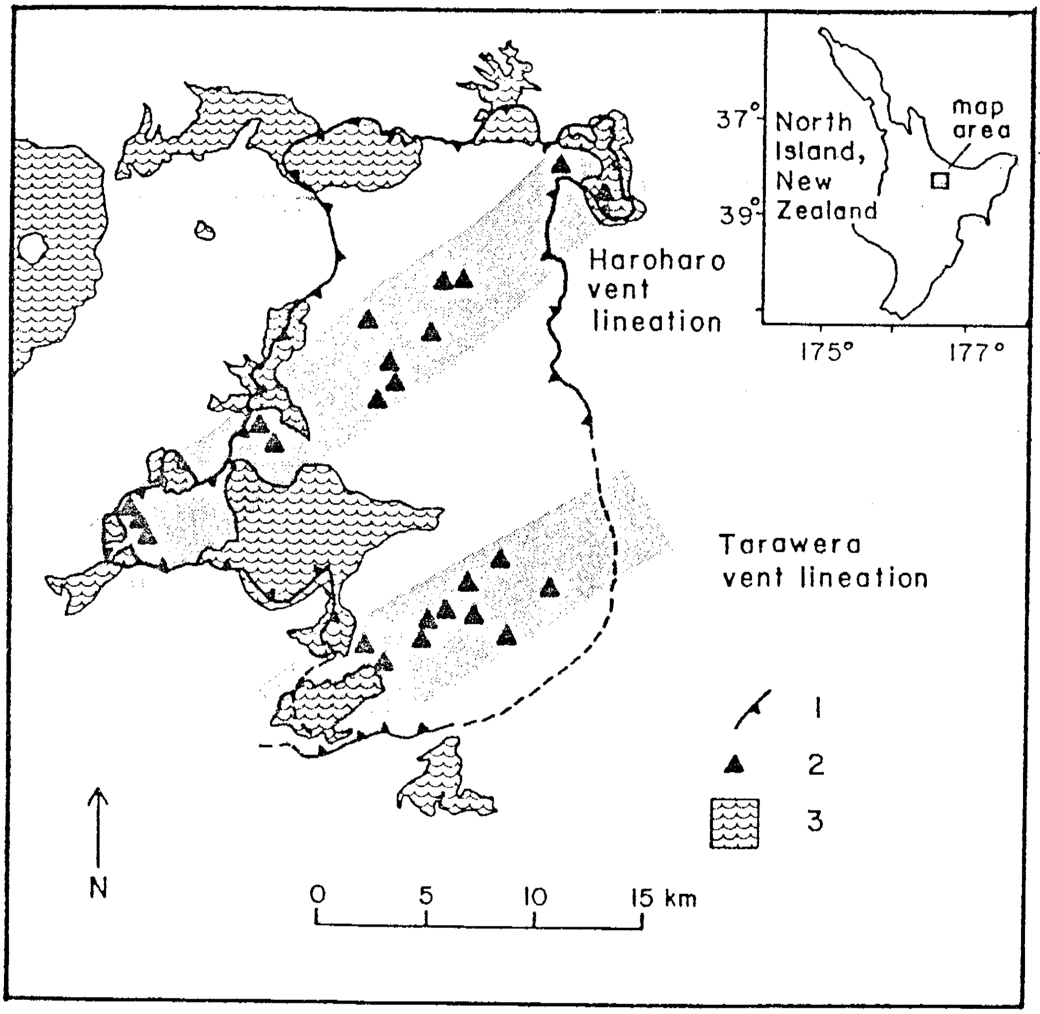

Figure 2-3. Map of the Okataina Volcanic Center. Symbol 1 represents the caldera margins as mapped by surface geology, symbol 2 represents vents for post 20 ka rhyolitic eruptions, and symbol 3 represents lakes. The shaded areas are the Haroharo and Tawarewa vent lineations. After Nairn, 1981, and Wilson et al., 1984.

tephras, ignimbrites and lavas over the last 50 ka. Only the plinian and phreatoplinian tephras are considered in this study, and those sampled are listed in Tables 2-1 and 2-2 (more detailed sample information is given in Appendix A). Most plinian and phreatoplinian tephras chosen for sampling were less than 20 ka old, because the young age reduces the probability that the obsidians have been hydrated. A few older units were sampled as well.

The OVC contains two distinct sub-centers, Haroharo and Tawarewa, both of which have produced holocene eruptions. The Haroharo and Tawarewa trends are shown in Fig 2-3, and the eruptive center for specific OVC eruptions is noted in Table 2-2. It is not known if the Tawarewa and Haroharo centers represent two vents for a single plumbing system, or two separate plumbing systems. A number of eruptive vents have been located, and are shown in Fig. 2-3 (Nairn, 1981). Four of the <10 ka eruptions from the TVC are thought to be derived from essentially a single vent, shown in Fig. 2-2 (Wilson et al., 1984). The vent areas for the other TVC eruptions discussed in this study are thought to be within Lake Taupo, but exact vent positions are not known (Wilson et al., 1984).

The stratigraphy and petrology of these deposits have been well studied (Ewart, 1963, 1966; Ewart et al., 1971, 1975; Froggatt, 1981; Howorth, 1976; Nairn, 1972,

Table 2–1. Major silicic plinian tephra units from the Taupo Volcanic Center. Volume is in situ unless marked with an asterix, in which case volumes are of magma. References: 1) Froggatt, 1981a; 2) Froggatt, 1982a; 3) Lowe, 1986 4) Vucetich and Pullar, 1973; 5) Walker, 1981c; 6) Wilson et al., 1984; 7) Wilson and Walker, 1985 8) Wilson et al., 1986; 9) Froggatt, 1982b; 10) Self, 1983; 11) Wilson et al., 1988.

TAUPO CENTER

Eruptive Unit	Age (ka BP)	Volume (km3)	Mineralogy * plag.	pyx.	amph.	biot.	Reference
Taupo Eruption	1.8						
Taupo plin.		23	H	H	VL	–	7,9
Rotongaio		1.3	H	H	VL	–	7,9
Hatepe phreat.		2.5	H	H	VL	–	7,9
Hatepe plin.		6	H	H	VL	–	7,9
Initial ash		0.02	H	H	VL	–	7,5,9
Mapara	2.2	2	H	H	VL	–	2,9
Whakaipo	2.8	1.5	H	H	VL	–	2,9
Waihimia	3.2	29	H	H	VL	–	2,5,9
Hinemaiaia	4.5	4.7	H	H	VL	–	3,4,9
Opepe	8.8	5	H	H	VL	–	2,4,9
Poronui	9.5	3.5	H	H	VL	–	2,4,9
Karapiti	9.9	5	H	H	VL	–	1,9
Oruanui	22.6	150	H	H	M	VL	8,10,11
Okaia	22	3.5**	H	H	M	VL	8,6,9
Tihoi	45	2.5**	H	H	M	VL	6,9

H=high abundance
M=medium abundance
L=low abundance
VL=very low abundance
– =absent

* The absolute crystal contents vary from about 3 to 15 %, and the abundances gven in the table represent relative abundances of different phenocrysts types.

** Represent magma volumes.

Table 2-2. Major plinian silicic tephra units from the Okataina Volcanic Center. References: 1) Froggatt, 1982a; 2) Lowe, 1986; 3) Nairn, 1980 4) Nairn, 1981; 5); Wilson and Walker, 1985; 6) Wilson et al., 1988; 7) Topping and Kohn, 1973 8) Howorth, 1976. Volumes are of in situ tephra. The "Vent Area" refers to the portion of the Okataina volcano from which the tephra was erupted, T for the Tawarewa area and H for the Haroharo area (from Nairn, 1981)

OKATAINA CENTER

Eruptive Unit	Age (ka BP)	Volume (km3)	Mineralogy * plag.	pyx.	amph.	biot.	Vent Area	reference
Kaharoa	0.93	5	H	L	L	M	T	1,3
Whakatane	4.8	10	H	M	M	-	H	5,1,3
Mamaku	7.5	6	H	M	M	L	H	2,1,3
Rotoma	9	12	H	M	M	L	H	1,7
Waiohau	11	13.8	H	M	M	L	T	1,4,3
Rotorua	13.8	7	H	M	M	L	T	3
Rerewhakaaitu	14.7	7	H	M	M	M	T	1
Okareka	17	8	H	L	M	M	?	1,7
Te Rere	20.5	9	H	M	M	-	H	6,1,3
Omataroa	26	18	H	M	M	-	H	1,4,8
Awakeri	30	2	H	L	L	-	H	1,4,8
Mangaone	31	16	H	M	M	-	H	1,8

H=high abundance
M=medium abundance
L=low abundance
VL=very low abundance
- =absent

* The absolute crystal contents vary from about 3 to 15 %, and the abundances gven in the table represent relative abundances of different phenocrysts types.

1980, 1981; Vucetich and Howorth, 1976; Vucetich and Pullar, 1969, 1973; Wilson et al., 1980, 1984). The tephra generally consists of pumice containing 3 to 5% phenocrysts, free crystals, obsidian fragments, and lithic fragments. The phreatoplinian deposits commonly contain little recognizable pumice, due to their fine grain size, but all other components are present.

Although many of the <20 ka tephra units from the TVC and OVC have been studied in this project, the ones that were examined in the most detail are from the 2 ka BP Taupo eruptive sequence, which erupted from the TVC, and culminated in the Taupo ignimbrite (Wilson and Walker, 1985). This plinian sequence consists of a phreatoplinian initial ash, the Hatepe plinian pumice deposit, the Hatepe phreatoplinian ash, the Rotongaio phreatoplinian ash, and finally the Taupo plinian pumice that was interpreted by Walker (1980) as the product of the most powerful plinian eruption yet documented (Wilson and Walker, 1985). This well exposed and mapped sequence was emplaced over an approximately 2 week interval (Wilson and Walker, 1985).

Volumes of Tephra

Volume, age, source, crystal content and other details for each tephra unit are also given in Tables 2-1 and 2-2. Vucetich and Pullar (1973), calculated a number of volumes for the TVC tephra, applying the formula $13ab^2$, where "a" is the thickness of tephra at source, and "b" is the distance over which tephra thickness is halved. Nairn (1981) has determined volumes for the OVC, presumably by the same method. Froggatt (1982a) compared 4 different volume determination methods, and estimated average volumes for the TVC and OVC tephra deposits. Walker (1981c) reported volumes for several tephra units from the TVC, using the crystal concentration method. This method is based on the assumption that the crystal to glass ratio in pumice clasts is representative of that for the magma as a whole. The entire volume of an eruption can therefore be estimated from the measured crystal content of a pumice-bearing tephra unit. This method yields much higher values than all others, but Walker explained that a high percentage of material is lost as fine dust and is neglected in normal volume calculations (Walker, 1981b).

Although eruption rates for the TVC and OVC over the last 50 and 20 ka, respectively, are similar (0.27 m^3/s), the frequency and relative size distribution of eruptions are different (Wilson et al., 1984) (Fig. 2-4). TVC eruptions were either large or small in volume, and clustered through time, whereas most OVC eruptions were of moderate volume, and occurred at relatively constant time intervals. The OVC maintained a steady state of

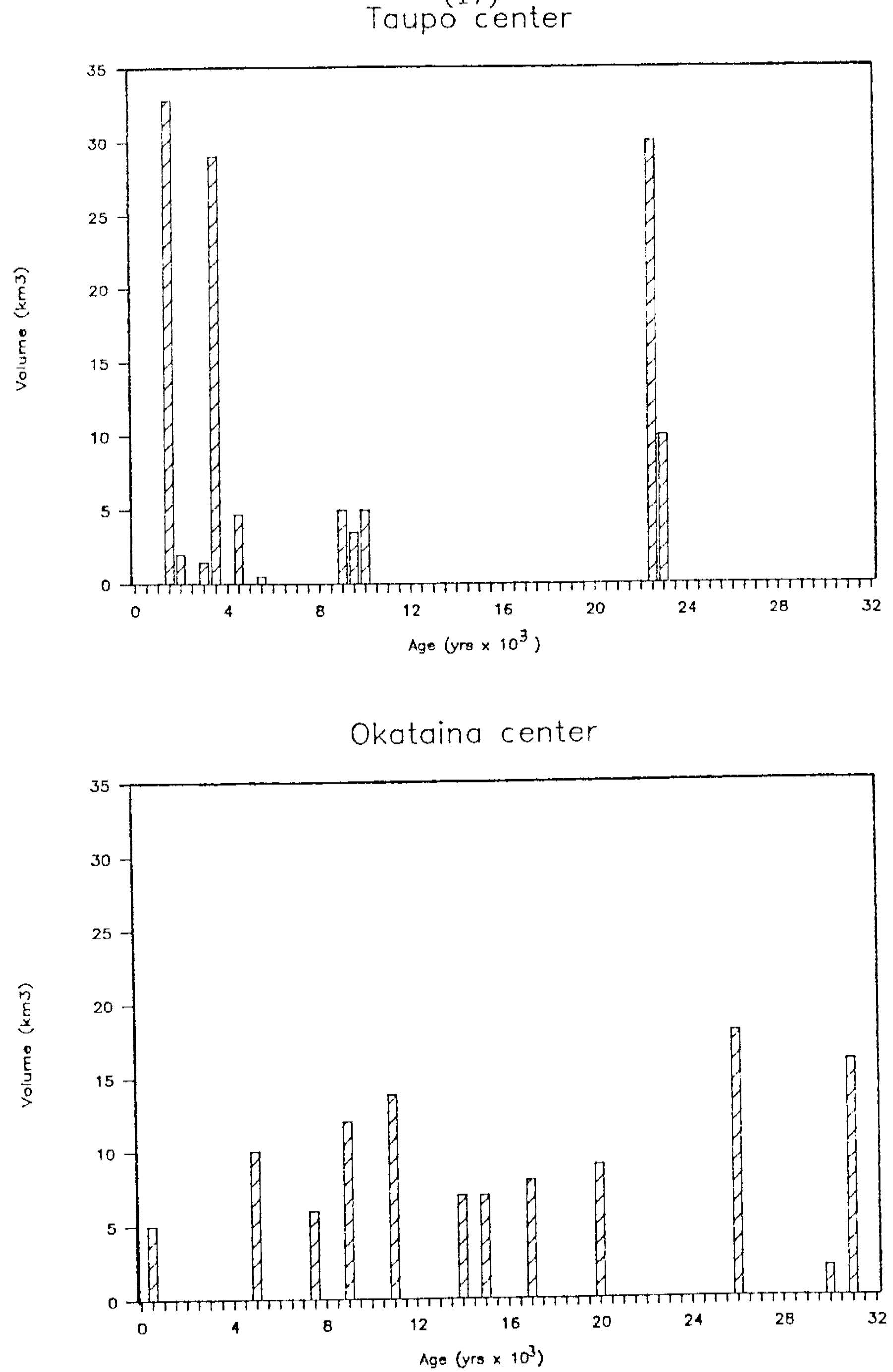

Figure 2-4. Volumes of tephra erupted through time from the TVC and OVC, showing the different eruptive patterns for the two centers. Eruptions from the OVC are uniform in size and evenly distributed through time, whereas TVC eruptions are of diverse sizes and are clustered in time (see Tables 2-1 and 2-2 for references to data).

magma eruption whereas the TVC followed a step function (Froggatt, 1982a). The combined volume of rhyolitic material erupted from the TVC and OVC over the last 50 ka is probably about 350 km^3 (Froggatt, 1982a).

Mineralogy and chemistry

Tephra from the TVC and OVC are composed of pumice, glass fragments, lithic fragments, and some, or all of the following phenocryst phases: plagioclase, quartz, pyroxene, amphibole, rare biotite, magnetite, and ilmenite (Froggatt, 1982b). The mineralogy of individual sampled units is shown in Tables 2-1 and 2-2. There is a significant change in mafic mineralogy after the large (155 km^3 magma) Oruanui eruption at 22.6 ka (Froggatt, 1982b; Wilson et al., 1988). Oruanui and pre-Oruanui tephras from the TVC contain significant amphibole, biotite and pyroxene as mafic silicate phases, whereas those after the Oruanui contain dominantly pyroxene. These phenocryst differences indicate some change in magma composition between these eruptive sets, possibly a difference in magmatic H_2O content.

Previous studies of mineral phase equilibria by Ewart (1963), and Ewart et. al. (1971, 1975), suggest that TVZ rhyolitic magmas began crystallization under saturated conditions, where $P_{H2O} = P_{total}$. They determined that the vapor pressure in the magma chamber was 2000 to 3000 kg/cm^2 and confining pressure of the magma chamber was 2.5 kb, corresponding to depths of between 5 and 7 km.

Chemically, the rocks of the TVZ fall on a calc-alkaline trend. The chemistry of a typical TVZ rhyolite is given in Table 2-3 (Reid, 1983). The rhyolite chemistry is in the I-type classification of Chappell and White (1974). The chemistry and textures of phenocryst show no evidence of magma mixing or disequilibrium after the onset of crystallization (Ewart and Taylor, 1969). However, pre-eruptive magma mixing is evident in the Waihimia eruption, based on the presence of mixed pumice. Walker (1981c) suggested that a small amount of basalt was mixed with the rhyolite melt prior to the Waihimia eruption.

The major element chemical composition of TVZ magma and phenocrysts are very constant, although there are slight differences through time. The main chemical variation seen is a slight change in major element composition after the Oruanui eruption (22.6 ka). There is no evidence of significant major element chemical zonation in the TVC magma chamber within or between eruptions (Ewart, 1963; Froggatt, 1982b)

Table 2-3. Average major element composition of TVZ rhyolite (from Reid, 1983)

Major element oxide	Wt %
SiO_2	73.73
TiO_2	0.29
Al_2O_3	13.30
FeO	1.82
MnO	0.06
MgO	0.36
CaO	1.67
Na_2O	4.28
K_2O	3.17
P_2O_5	0.06

* Total Fe as FeO

Volatile Determinations

Ewart et al. (1975), and Rutherford and Heming (1978), have suggested H_2O contents of between 5 and 8 wt% for some TVZ magmas, based on phenocryst assemblages. No other estimates of pre-magmatic volatile contents have been made for these magmas.

3. ANALYTICAL METHODS

Samples and sample preparation

TVC and OVC tephra were collected in Dec.-Jan., 1983/84 and 1985/86, mainly from roadcuts in sections where exposure was good, and units could be easily identified. Exposed tephra was cleared away with a spade, and 2 to 3 kg samples of fresh bulk tephra were then collected in large plastic bags. Where a tephra unit was <40 cm thick, a single sample was taken, otherwise samples were collected stratigraphically over 40-50 cm intervals. The bulk tephra samples consisted of pumice, obsidian, lithic fragments and free crystals. If a tephra unit contained a layer unusually rich in obsidian or free crystals, a sample of the layer was taken. In obsidian-rich units, some samples of pure obsidian were hand-picked at the outcrop. Samples were then sun- or oven-dried (100^{o}C) and stored in double plastic bags. Sample numbers and detailed locations are listed in Appendix A.

Obsidian fragments and crystals were separated from bulk samples for chemical analysis. A portion of the bulk sample was sieved to remove large pumice and fine dust, and the 0.5 to 2 mm fraction was used for hand-picking most of the obsidian and crystals. The mineralogy of free crystals matched that of crystals included in pumice, so free crystals were assumed to be co-genetic with the bulk of the tephra, and not xenocrystic material. The largest blocks of pumice from representative samples were also removed for trace element analysis.

Obsidian was found in most units, although the abundance varied widely from unit to unit. The obsidian fragments were generally angular and conchoidally fractured, ranging from ~1 cm to 0.5 mm in diameter. Obsidian color was constant in some samples, but in some cases a complete spectrum from clear to black was present. Approximately 50-100 fragments of obsidian were separated from each sample, depending on fragment size and obsidian abundance. The separated fragments were washed in distilled H_2O and oven-dried at $100^{o}C$. About half of the grains were ground to <75 mesh in an agate mortar and pestle, using acetone as a grinding solvent. The ground samples were dried overnight in at $100^{o}C$, and stored in glass vials for volatile analysis.

Polished obsidian grain mounts from at least 1 sample of each unit were prepared for microprobe analysis and optical observation. These grain mounts were ground with steel plates, and polished with diamond powder in order to avoid major element contamination.

Phenocrysts of plagioclase and pyroxene were separated from all units. In some cases, quartz and amphibole were also present. About 100 phenocrysts were hand picked from each sample. In most units, about half of the picked crystals were plagioclase and the other half pyroxene, but quartz and amphibole were also picked if they were present. These phenocrysts were generally euhedral, up to 3 mm in length, and often had rhyolite glass adhering to their exteriors. A hand magnet was used to separate phenocrysts containing magnetite inclusions. This technique usually yielded sufficient magnetite and ilmenite pairs for temperature analysis. Polished grain mounts were prepared of crystals from each unit, using the same technique used for obsidian. These sections were used for optical observations and electron microprobe analysis. In addition, ion microprobe mounts were prepared with crystals from several units. These mounts are 1/4" brass plugs, which contain 10-15 phenocrysts mounted in epoxy. The plugs are polished with diamond powder suspended in distilled H_2O. Doubly polished chips of plagioclase from a few samples were also prepared for high-temperature-stage geothermometry.

The pumice separated from the bulk samples was finely ground in a WC TEMA mill, and pressed into boric-acid backed pellets for trace element analysis. In addition, polished thin sections of pumice for each unit were prepared for optical and microscope analysis.

Analytical Techniques

A number of analytical techniques and procedures were used to complete this study. These techniques are discussed briefly here, with particular attention to several specialized techniques that were used for analysis of melt inclusions.

Four main types of analyses were done in this study: chemical composition, volatile analyses, isotopic analyses and geothermometry. Details of all analytical techniques used, including theory, procedures, standards and estimated errors are given in Appendix B. The analytical techniques used for chemical composition were x-ray fluorescence (XRF), instrumental neutron activation analysis (INAA), and electron and ion microprobe analysis. Analytical techniques for volatile analyses include Karl-Fischer titration (KFT), electron and ion microprobe analysis. Isotopic analyses were made by mass spectrometry. Geothermometry measurements were made with a high-temperature stage and with Fe-Ti oxide chemistry determined by electron microprobe.

<u>Chemical composition</u>

Analyses were done using XRF, INAA, and electron microprobe, as detailed in Appendix B. Electron microprobe was used to analyse 9 major element oxides: SiO_2, TiO_2, Al_2O_3, FeO, MgO, MnO, K_2O and Na_2O in pumice, obsidian and melt inclusions. XRF was used to analyse 7 trace elements: Pb, Th, Rb, Sr, Y, Zr, and Nb in ground pumice. INAA was used to analyse 2 major elements (Na, Fe) and a number of trace elements (Sc, Co, Zn, As, Rb, Sb, Cs, Ba, La, Ce, Sm, Eu, Tb, Yb, Lu, Hf, Ta, Th, and U) in individual obsidian fragments and ground pumice. In addition, some trace element analyses in melt inclusions were made by ion microprobe, which is a less common technique. The ion microprobe is discussed later in this chapter.

<u>Volatile composition</u>

The H_2O compsition of obsidian was determined by Karl-Fischer titration (Westrich, 1987). This technique involves titrating the unknown quantity of H_2O in a pyridine-methanol solution containing iodide ion (I^-) and SO_2 as principle components. The following reaction occurs:

$$I_2 + SO_2 + H_2O \Rightarrow 2HI + SO_2 \qquad (4.1)$$

The amount of H_2O introduced to the system is determined by the amount of I_2 that must be regenerated to keep the system in equilibrium. Individual fragments of obsidian, or crushed obsidian powders can be run by this technique, as the sample is heated to 1000°C in a furnace until all of the H_2O has been driven off and transfered to the iodine solution.

Two microbeam techniques, the ion and electron microprobes, were used to analyse volatile contents of melt inclusions due to their ability to analyse small sample areas. The electron microprobe was used to determine Cl and S, and the ion microprobe for H_2O and F. The electron microprobe is a widely used technique, but slight modifications in the procedure are necessary for volatile analysis (Devine et al., 1984). The beam must be broadened to at least 20 microns and the beam current reduced to avoid migration of volatile elements. Also, the counting times on peak and background must be increased (to 150 sec. and 75 sec. respectively) in order to accumulate sufficient counts of these low-abundance elements. This technique was applied to Cl and S analyses of obsidian, as well as to melt inclusions.

The second microbeam technique, the ion microprobe, is less widely applied than the electron microprobe, but has the advantage of being able to analyse low-atomic number elements, such as H. This technique involves bombarding a 20u diameter area of the sample with primary $^{16}O^-$ ions which are generated in a duoplasmatron. The beam is mass analysed to eliminate the H ions present in the duoplasmatron. Each primary ion that impinges on the sample ejects 1 to 10 atoms from the sample surface. Between 0.1 and 10% of these atoms are ionized and accelerated into a mass spectrometer and then counted. The ion microprobe was mainly applied to the analysis of H_2O and F in melt inclusions, but was also used to analyse P_2O_5, Rb, Ba, La, Ce, Sm, and Hf in some samples. Molecular species that interfer with the heavier trace elements can be filtered out with an energy filter (Shimuzu et al., 1978).

Isotopic analysis

Stable hydrogen and oxygen isotopic abundances were analysed on bulk obsidian powders and obsidian fragments. Hydrogen is extracted from obsidian as H_2O, by melting under vacuum. Complete degassing was required because hydrogen isotopes fractionate during the degassing process. The resultant vapor was analysed by mass spectrometry to determine the δD value.

Oxygen isotopic compositions of obsidian were determined on CO_2 that is formed using oxygen released from the sample by fluorination of the bulk sample. The

CO_2 was analysed by mass spectrometry to determine the $\delta^{18}O$ of the sample.

Geothermometry

The temperature of the Taupo magma chamber was determined by 2 techniques: Fe-Ti oxide geothermometry and high-temperature-stage melt inclusion analysis. Fe-Ti oxide geothermometry, as originally described by Buddington and Lindsley (1969) involves chemical analysis of co-existing non-exsolved magnetite and ilmenite pairs. Determination of the temperature and oxygen fugacity (fO_2) represented by this pair was calibrated by experimental studies. Temperatures and oxygen fugacities were calculated using the recalulation technique and calibration values of Anderson and Lindsey (1985).

High-temperature-stage analysis of melt inclusions involves heating doubly polished chips of crystals that contain melt inclusions, and observing their behavior. This technique has been widely applied to the study of fluid inclusions in ore deposits, but has not been used as extensively in inclusions from igneous systems (Roedder, 1984). Two main parameters can be observed: the temperature at which the inclusion glass melts (T_m) and the temperature at which all phases in the inclusion homogenize (T_h). The T_h of melt inclusions will more closely represent the actual magmatic temperature, as long as the inclusion contents were trapped as a single phase (Roedder, 1984).

4. CHEMISTRY OF TAUPO VOLCANIC ZONE ERUPTIVES

Major and trace element composition, and temperature and oxygen fugacity values of TVC and OVC tephras were analysed for several reasons. First, to evaluate chemical zonation in the magma chambers from which these sequential tephra units were derived, and compare these with volatile zonations. Second, by analysing pumice, the initial melt compositions of each tephra could be determined and then compared with the compositions of melt inclusions and obsidian. Also, solubility of volatile components in melts are dependent on melt composition, and to a lesser degree, temperature. As published trace element and T/fO_2 data is not available for all of the tephra units in the TVC and OVC, an internally consistent set of analyses was made. Only limited major element analyses of bulk rock and glass were made as many TVC and OVC units have been previously analysed (Ewart, 1966; Ewart et al., 1969, 1975; Froggatt, 1982b; Howorth, 1976).

The trace element and temperature/oxygen fugacity portion of this study have been compiled into the following manuscript "Evidence for limited silicic magma chamber zonation, Taupo Volcanic Zone, New Zealand" (p. 33

to 51) which has been submitted to "Geology". Although this paper has several authors, the first author was primarily responsible for the analytical work, and conclusions drawn from the data, and therefore feels justified in including the manuscript in this thesis. The major element data was not included in this manuscript because major element zonations are generally not as marked as trace elements (Hildreth, 1981). However, the major element composition of the TVC and OVC eruptives are briefly discussed following the manuscript. The few major element analyses were made mainly in order to verify that melt inclusions were chemically similar to pumice and obsidian from the same eruptions, or to address specific problems, such as possible chemical dependence of obsidian color.

Detailed analyses of major and trace elements, magnetite and ilmenite chemistry and T/fO_2 calculations are given in Appendices C and E.

Evidence for limited zonation in silicic magma systems, Taupo Volcanic Zone, New Zealand

Nelia W. Dunbar
Philip R. Kyle
Department of Geoscience
New Mexico Institute of Mining and Technology
Socorro, New Mexico, 87801

Colin J.N. Wilson
Earth Sciences, University of Cambridge
Cambridge CB23EQ, England

Abstract

Smith (1979) suggested that all pyroclastic eruptions that exceed 1 km^3 will show pronounced systematic compositional zonation. Since then, chemical and thermal zonation in large silicic magma bodies has become the expected condition in rhyolitic magma bodies. However, trace element chemistry and Fe-Ti oxide geothermometry of Quaternary rhyolitic Plinian tephras from two volcanic centers in the Taupo Volcanic Zone, New Zealand, suggest that no strong systematic chemical or thermal zonation was present in either magma system. Of the Plinian tephra units erupted over the past 50 ka from the Taupo and Okataina volcanoes, 28 were sampled, and most were analyzed for Th, Pb, Rb, Sr, Y, Zr, and Nb, as well as Fe-Ti oxide composition. Taupo volcano tephras erupted over the past 10 ka have uniform compositions for all elements except Sr, and all these samples fall on the same $\underline{T}/\underline{f}_{O}$ buffer trend. However, pre-22 ka Taupo tephras are mineralogically and chemically distinct from the younger group and fall on a different $\underline{T}/\underline{f}_{O}$ buffer trend. This may be a result of the large eruption (>155 km^3 of magma) from the Taupo Volcano at 22.5 ka, and subsequent reequilibration of the magmatic system.

The Okataina volcano tephras erupted over the past 31 ka show slight systematic and considerable nonsystematic trace element variation, but all fall on a single $\underline{T}/\underline{f}_{O}$ buffer trend. This may indicate slight preeruptive alteration of a single Okataina magma body.

INTRODUCTION

Chemical and thermal zonation in large silicic magma chambers is a well-accepted phenomena, and has become the expected condition of rhyolitic magma bodies. Smith (1979) suggested that all pyroclastic eruptions that exceed 1 km^3 will show pronounced systematic compositional zonation. Zonation is often seen in trace elements, temperature, phenocryst content, and isotopic composition (Hildreth, 1981). Major elements can also be zoned, but generally less strongly than trace elements.

A reconnaissance study has been undertaken of the chemical composition and temperature/oxygen fugacity ($\underline{T}/\underline{f}_O$) of some tephra units erupted in the Taupo Volcanic Zone over the last 50 ka. The objective was to characterize the Taupo and Okataina volcanic centers and search for differences between the two. The Taupo and Okataina magma chambers produced a number of small to medium-sized sequential eruptions over the past 50 ka, rather than single large ones. Tephras which showed evidence of magma mixing were not examined.

TAUPO VOLCANIC ZONE

The Taupo and Okataina caldera volcanoes have produced silicic tephras since before 50 ka and 250 ka respectively (Nairn, 1981; Wilson et al., 1984, 1986) (Fig. 1). Most of these volcanic products are high-silica rhyolites, and are virtually indistinguishable by major element chemistry (Ewart, 1963; Froggatt, 1982b). Although the two centers are within the same volcanic field and are compositionally similar, their eruptive behaviors differ. Eruptions from the Okataina volcano tend to be more evenly spaced through time (although this may be a function of poor age control), whereas those from Taupo volcano are clustered and episodic. Taupo eruptions also show greater variability in size, and have a higher ratio of pyroclastics to lavas than Okataina eruptions (Wilson et al., 1984).

METHODS

Samples were analyzed from most of the young tephra units (younger than 45 ka old) from the Taupo and Okataina volcanoes (Table 1 and 2). Individual pumice clasts separated from bulk samples were crushed and analyzed for Pb, Th, Rb, Sr, Y, Zr, and Nb by X-ray fluorescence (Norrish and Chappell, 1977).

Magnetite and ilmenite inclusions in silicate phenocrysts were analyzed by electron microprobe using the Bence and Albee (1968) method of correction. Temperature and oxygen fugacity were calculated using Stormer's (1983) modification of the Buddington and Lindsley (1964) geothermometer. Calibration constants were those of Andersen and Lindsley (1985).

RESULTS

Temperature and oxygen fugacity

Estimates of the average temperature and oxygen fugacity (Table 1 and 2) of 23 tephra units from the Taupo and Okataina volcanoes are plotted in Figure 2.

Ten tephras erupted from Taupo volcano over the past 10 ka range in temperature from 800 to 850 ^{o}C; corresponding log f_O values are between -13.1 and -14.4, respectively (Table 1), and units define a buffer trend which lies about 1 log unit above the QFM buffer. All these young tephras are phenocryst-poor (<5% crystals).

Tephras erupted from Taupo volcano prior to and during the major Oruanui eruption at 22.5 ka give temperatures between 786 and 798 ^{o}C, and generally have log f_O one log unit above the younger Taupo eruptives in terms of log f_O. These tephras contain moderate crystal contents (e.g. 12%-14% in the Oruanui, Self, 1983) in contrast to the younger deposits.

Okataina tephras erupted over the past 31 ka (Table 2) range in between 767 and 839 ^{o}C and log f_O from -14.8 to -12.1. These data define a trend on the T/f_O plot (Fig. 2) that is similar to the older Taupo trend, but distinct from the younger Taupo trend.

Geochemistry

Young (<10 ka) Taupo tephras show only minor variations in trace element compositions (Table 1). Pb, Th, and Nb are similar, within analytical error, throughout the sequence. Three samples, listed in stratigraphic order, from the Taupo plinian phase of the 1.8 ka eruption (23 km^3 of tephra) show no evidence of chemical zonation (Table 1). Within the six analyzed units representative of the whole 1.8 ka Taupo eruption, there appears to be a slight systematic decrease in Rb. However, excluding the Taupo ignimbrite value, which was analyzed at a different lab (C.J.N. Wilson and I.S.E. Smith, 1988, unpublished data) and is therefore not directly comparable on the ppm level, the Rb variation is within analytical error ($\pm$4 ppm). There is also a slight Sr increase in the Taupo plinian tephra compared to the three older tephra. This may reflect a slight increase in feldspar content within the lower part of the erupted magma chamber. The Sr of the Taupo ignimbrite is similar to the three older tephras. Sr increases and Zr decreases slightly following the large 3.4 ka Waihimia eruption (29 km^3 of tephra). There is evidence for mixing of an andesitic magma in the rhyolitic tephra from the Waihimia eruption (Blake et al. in prep.), therefore no trace element data are reported here. This mixing does not appear to have disturbed the overall geochemical features of the larger, long-term Holocene Taupo magmatic system.

Pumice from the Okaia and Tihoi tephras have distinctly lower Y and Zr content (Table 1) compared to the post-10 ka tephras. Analyses of tephra from the Oruanui eruption by C.J.N. Wilson and I.S.E. Smith suggest that it is similar to the two older tephras (Table 1).

Pumice from the Okataina volcano show greater variations in some trace elements than those erupted from the Taupo (Table 2). Within analytical error, Pb and Nb contents are uniform. Pumice from the three oldest tephra have almost identical trace element contents; only Zr shows an increase with decreasing age, from 191 to 210 ppm. In contrast, pumice from the three youngest tephra show a progressive increase in Pb, Th and Rb and marked decrease in Sr and Zr.

DISCUSSION

Pumice in tephra erupted over the past 10 ka from the Taupo volcano show nearly uniform trace element compositions. During this period, there is no evidence for the development of significant zonation within this body. The small variations seen in Sr and Zr content are consistent with minor differences in feldspar and zircon content of sampled pumices. In contrast, some rhyolitic systems (e.g. Bishop and Bandelier Tuffs) show two-fold variations in trace elements within single eruptions (Smith, 1979; Hildreth, 1981).

The overall uniformity of trace elements suggests derivation of all post-10 ka tephra in the Taupo volcano from the same magma body. However, the magmas that produced these tephras may represent discrete melting events from a homogeneous source. This possibility is less likely, but is supported by the lack of geophysical evidence for a Taupo magma chamber.

Trace element zonation is also virtually absent within the six pyroclastic phases of the 1.8 ka Taupo eruption sequence, which implies an absence of zonation in volatile elements. Water, the main volatile component in rhyolitic magmas, behaves like an incompatible element such as Rb or Nb (Hildreth, 1981). A fluid-rich roof zone probably did not form in the 1.8 ka Taupo eruption magma chamber. This is supported by ion microprobe analyses of water in melt inclusions trapped in phenocrysts for the Hatepe and

Taupo plinian tephras (Dunbar et al., in press). Eruptions at Taupo volcano need not have been initiated solely by the development of a volatile-rich roof zone which became oversaturated and began vesiculating. Tectonic activity within the Taupo Volcanic Zone, which is undergoing rapid back-arc extension (Stern, 1987), may also play an important role.

The clear contrast in trace element contents between the post-10 ka and pre-22 ka tephras marks a distinct change in the magmatic system. Eruption of the voluminous 22.5 ka deposits, which together represent a minimum volume of about 155 km^3 of magma (Self, 1983) may have effectively emptied the magma chamber, and the 12 ka eruptive hiatus following the Oruanui eruption may represent the recharge time necessary for the development of a new magma batch and associated intrusive system.

Pumice in tephra erupted from the Okataina volcano show greater trace element variations than Taupo pumices. The three youngest tephras, which span about 6.5 ka, show evidence for the development of trace element zonation. The decreasing Sr and Zr content in the pumice suggest that fractionation of feldspar and zircon may be largely responsible for the development of the zonation. If the three tephra are samples from a large evolving magmatic system, then future eruptions from the Okataina volcano may be marked by greater enrichment of incompatible elements Pb, Rb, Y, and Nb, and probably volatile enrichment as well. Therefore, if the magmatic system responsible for the three youngest tephra was to erupt again, the magma would be richer in volatiles, and a higher proportion of tephra to lava could result. However, the Okataina volcano is composed of two distinct centers; the Kaharoa tephra is erupted from the Tawarewa center, whereas Whakatane and Mamaku tephras were erupted from the Haroharo center (Nairn, 1981). It is not known if the Tawarewa and Haroharo centers represent two vents for a single plumbing system, or two separate magmatic systems. If the latter was the case, the zoning seen among the three youngest tephras would be coincidental.

Trace element zonations opposite to those displayed by the three youngest Okataina tephras are shown by pumice from the Rotorua (13.8 ka), Rerewhakaaitu (14.7 ka) and Okareka (17 ka) tephra. Pb, Th, and Rb decrease with decreasing age whereas Sr and Zr increase. Such zonation is difficult to acheive by progressive evolution over time by a fractionating rhyolitic magma. Mixing of a more mafic magma could account for the changes. A minor volume of basalt (though no mixed magmas) was erupted in the Okareka event. However, the zonation more likely existed prior to the Okareka eruption, and subsequent eruptions tapped less fractionated magma. Alternatively, the magma may represent separate independent batches derived from their source in the lower crust.

The three oldest Okataina tephras have pumice with nearly identical trace element contents. It is likely that all three tephra were erupted from the same magma body which was not evolving significantly by fractionation.

The magnetite-ilmenite-derived temperature and oxygen fugacity data indicate at least two different rhyolitic magma types (Fig. 2) in the Taupo Volcanic Zone. Younger (<10 ka) Taupo volcano tephras are higher in temperature and have a lower $\underline{f}_O$ than Okataina and older (>22 ka) Taupo volcano tephra. Older Taupo (>22 ka) tephra fall on a buffer trend similar to Okataina samples. The $\underline{T}$ and $\underline{f}_O$ of the rhyolites are reflected in the mineralogy of the magmas. The younger (<10 ka) and higher temperature Taupo rhyolites have low phenocryst contents, and contain orthopyroxene as the dominant ferromagnesian silicate, whereas the older (>22 ka), cooler, Taupo rhyolites contain amphibole, and occasional biotite as well as pyroxene. The Okataina rhyolites typically contain pyroxene, amphibole and biotite. The mineralogies of these groups are consistent with the observed oxygen buffer trends. The presence of hydrous phases is consistent with the overall lower magmatic temperatures observed for the Okataina and >22 ka Taupo volcano melts (Naney, 1983). There appears to be a slight, but inconsistent temperature zonation within the younger than 10 ka tephras from the Taupo volcano. However, as the temperature range is within the analytical error of estimates, no significance can be attached to the variation.

CONCLUSIONS

In recent years, much attention has been drawn to the existence of zoned magma chambers (Hildreth, 1981). Zoned magmatic systems are obviously common, however this does not preclude the existence of relatively homogeneous magmatic systems. We have shown the existence of long-term homogeneous rhyolitic magma compositions for the Taupo volcano and only weak to insignificant zonation for the Okataina volcano. There are several possible explanations but they require further study. For example, convection of the magma chamber may have inhibited development of any gradient, or the time between eruptions represented by the systems we have studied may be insufficient to allow a significant gradient to develop (see Smith, 1979 Fig. 12). We emphasize that although zoned magmatic systems are common, there are rhyolitic volcanoes that seem to have been derived from unzoned magma bodies.

REFERENCES CITED

Andersen, D.J., and Lindsley, D.H., 1985, New (and final) models for the Ti-magnetite/ilmenite geothermometer and oxygen barometer [abs.]: EOS (Transactions of the Americal Geophysical Union), v. 66, p. 416.

Bence, A.E., and Albee, A.L., 1968, Empirical correction factors for the electron microanalysis of silicates and oxides: Journal of Geology, v. 76, p. 382-403.

Buddington, A.F., and Lindsley, D.H., 1964, Iron-titanium oxide minerals and synthetic equivalents: Journal of Petrology, v. 5, p. 310-357.

Dunbar, N.W., Hervig, R.L., and Kyle, P.R., 1988, Determinations of pre-eruptive H_2O, F and Cl contents of silicic magmas using melt inclusions, examples from Taupo Volcanic center, New Zealand. Bulletin of Volcanology, in press.

Ewart, A., 1963, Petrology and petrogenesis of the Quaternary pumice ash in the Taupo area, New Zealand: Journal of Petrology, v. 4, p. 392-431.

Froggatt, P.C., 1981, Karapiti Tephra Formation: A 10,000 year B.P. rhyolitic tephra from Taupo: New Zealand Journal of Geology and Geophysics, v. 24, p. 96-98.

--------------, 1982a, Review of methods of estimating rhyolitic tephra volumes; applications to the Taupo Volcanic Zone, New Zealand: Journal of Volcanology and Geothermal Research, v. 14, p. 301-318.

--------------, 1982b, A study of some aspects of the volcanic history of the Lake Taupo area, North Island, New Zealand [Ph.D. thesis]: Wellington, New Zealand, Victoria University,.

Hildreth, W., 1981, Gradients in silicic magma chambers: Implications for lithospheric magmatism: Journal of Geophysical Research, v. 86, p. 10153-10152.

Lowe, D.J., 1986, Revision of the age and stratigraphic relationships of Hinemaiaia tephra and Whakatane ash, North Island, New Zealand, using distal occurrences in organic deposits: New Zealand Journal of Geology and Geophysics, v. 29, p. 61-73.

Michael, P.J., 1983, Chemical differentiation of the Bishop Tuff and other high-silica magmas through crystallization processes: Geology, v. 11, p. 31-34.

Nairn, I.A., 1981, Some studies of the geology, volcanic history, and geothermal resources of the Okataina volcanic center, Taupo volcanic zone, New Zealand: [Ph.D. thesis]: Wellington, New

Zealand, Victoria University, .

Naney, M.T., 1983, Phase equilibria of rock-forming ferromagnesian silicates in granitic systems: American Journal of Science, v. 283, p. 993-1033.

Norrish, K., and Chappell, B.W., 1977, X-ray fluorescence spectrometry, in Zussman, J., ed., Physical methods in determinative mineralogy: Academic Press, London, 210-273.

Self, S., 1983, Large-scale phreatomagatic silicic volcanism: A case study from New Zealand: Journal of Volcanology and Geothermal Research, v. 17, p. 433-469.

Smith, R.L., 1979, Ash flow magmatism, In Chapin, C.E. and Elston, W.E., eds., Ash flow tuffs: Geological Society of America Special Paper v. 180, p. 5-27.

Stern, T.A., 1987, Asymmetric back-arc spreading, heat flux and structure associated with the Central Volcanic Region of New Zealand: Earth and Plantary Science Letters, v. 85, p. 265-276.

Stormer, J.C., 1983, The effects of recalculation on estimates of temperature and oxygen fugacity from analyses of multicomponent iron-titanium oxides: Americal Mineralogist, v. 68, p. 586-594.

Vucetich, C.G., and Pullar, W.A., 1973, Holocene tephra formations erupted in the Taupo area, and interbedded tephras from other volcanic sources: New Zealand Journal of Geology and Geophysics, v. 16, p. 745-780.

Walker, G.P.L., 1981, The Waihimia and Hatepe Plinian deposits from the rhyolitic Taupo Volcanic Center: New Zealand Journal of Geology and Geophysics, v. 24, p. 305-325.

Wilson, C.J.N., and Walker, G.P.L., 1985, The Taupo eruption, New Zealand I. General aspects: Royal Society of London Philosphical Transactions, v. 314, p. 199-228.

Wilson, C.J.N., Rogan, A.M., Smith, I.E.M, Northey, D.J., Nairn, I.A., and Houghton, B.F., 1984, Caldera volcanoes of the Taupo Volcanic Zone, New Zealand: Journal of Geophysical Research, v. 89, p. 8463-8484.

Wilson, C.J.N., Houghton, B.F., and Lloyd, E.F., 1986, Volcanic history and evolution of the Maroa-Taupo area, cental North Island: Royal Society of New Zealand, Bulletin 23, p. 194-223.

Wilson, C.J.N., Switsur, V.R., and Ward, A.P., 1988, A new date for the Oruanui eruption, New Zealand: Geological Magazine, v. 125, p. 297-300.

Acknowledgments: Dunbar was supported by the Department of the Interior's Mineral Institute Program, administered by the Bureau of Mines, allotment grant G1164135. Kyle is supported by the National Science Foundation Division of Polar Programs. Wilson was supported by the Royal Society of London. Thanks to J. Stormer and J. Ratte for helpful reviews.

Figure Captions

Figure 1. Map of the North Island of New Zealand and the Taupo Volcanic Zone (after Wilson et al., 1984) showing locations of Taupo and Okataina volcanoes in the central, rhyolite dominant portion of the TVZ (shown in striped pattern).

Figure 2. Average temperature and oxygen fugacity values for Taupo and Okataina volcanoes as determined by iron-titanium oxide geothermometry (see text). One trend is seen for Taupo center tephra younger than 22 ka (closed circles), and nearly coincident trends for Taupo tephra older than 22 ka (open circles), and all Okataina tephra (closed triangles). Q = quartz, M = magnetite, F = fayalite. Chemical analyses of magnetite and ilmenite used to determine temperature and oxygen fugacity values are available on request from the first author.

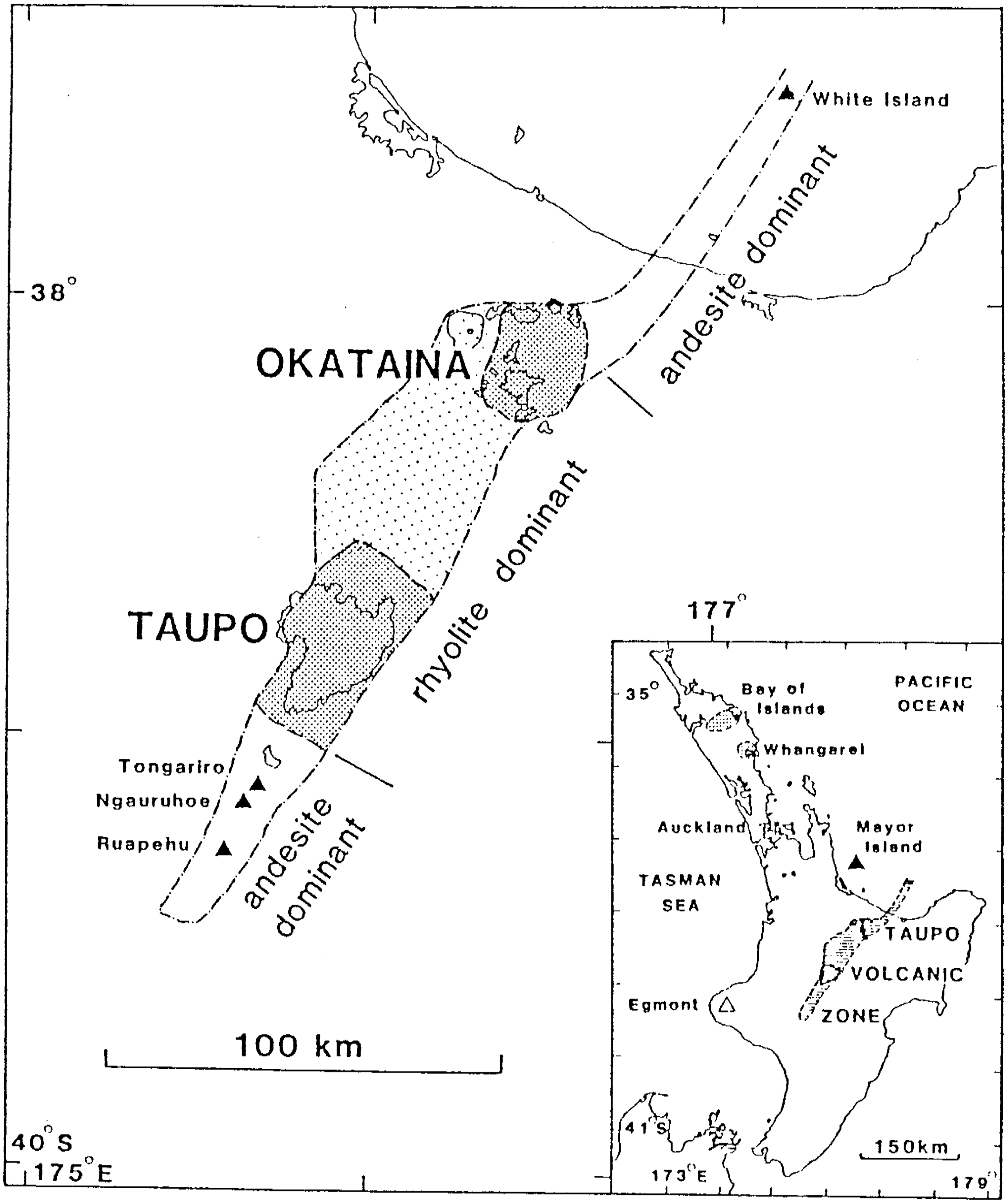
White Island
andesite dominant
38°
OKATAINA
rhyolite dominant
TAUPO
Tongariro
Ngauruhoe
Ruapehu
andesite dominant
100 km
40°S
175°E
177°
35°
Bay of Islands
PACIFIC OCEAN
Whangarei
Auckland
Mayor Island
TASMAN SEA
TAUPO
VOLCANIC
ZONE
Egmont
41°S
150km
173°E
179°

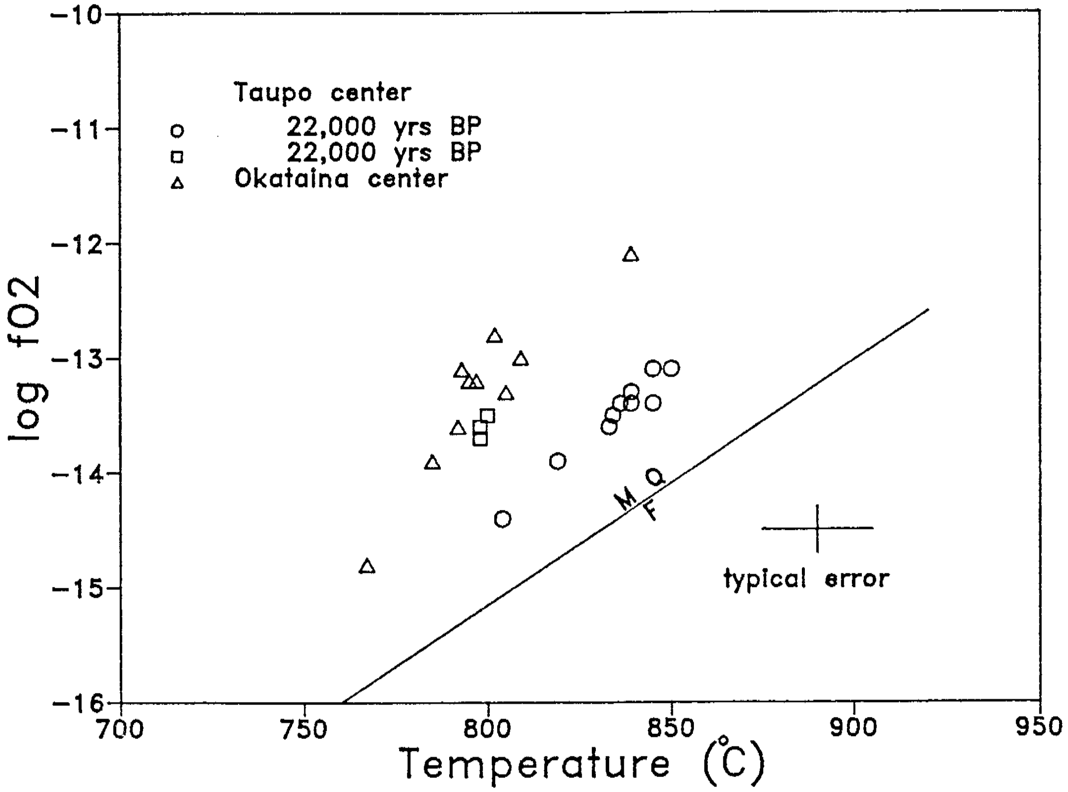
Taupo center
22,000 yrs BP
22,000 yrs BP
Okataina center
log fO2
Temperature (°C)
typical error
MQF
-10
-11
-12
-13
-14
-15
-16
700
750
800
850
900
950

Table 1. Iron-titanium oxide temperatures and trace element contents of major silicic plinian tephra units from the Taupo Volcano, New Zealand. Average errors of determination for temperature and oxygen fugacity are +30 degrees C, and +0.4 log units. Average errors of trace element analyses based on x-ray fluorescence repeat analyses to 1 sigma are as follows (in ppm): Pb +3 Th + 2, Rb +4, Sr +4, Y +2, Zr +4 Nb +1. Concentrations are given in ppm, and number of analyses are given as (n). Three samples are shown for the Taupo plinian tephra, and are listed in stratigraphic order. References refer to age and volume estimates only. Volume is given as in situ tephra volumes, unless marked with an asterix in which case volumes are of magma. References: 1) Froggatt, 1981; 2) Froggatt, 1982a; 3) Lowe, 1986 4) Vucetich and Pullar, 1973; 5) Walker, 1981; 6) Wilson et al., 1986; 7) Wilson and Walker, 1985; 8) Wilson et al., 1988, 9) Self, 1983; 10) Wilson, C.J.N, and Smith, I.S.E., unpublished data

TAUPO VOLCANO

Eruptive Unit	Age (ka BP)	Volume (km3)	Temp. C	-log fO_2	n	Pb	Th	Rb	Sr	Y	Zr	Nb	n	References
Taupo Eruption		1.8												
Taupo ignimbrite		30				19	15	93	152	33	221	8	6	10
Taupo plin.		23	850	13.1	5	22	12	97	166	36	222	10	2	7
						20	10	97	166	35	223	10	2	
						22	13	98	165	35	223	10	2	
Rotongaio		1.3												
Hatepe phreat		2.5				22	12	99	156	36	222	10	4	7
Hatepe plin.		6	839	13.3	5	21	11	100	156	36	222	10	5	7
Initial ash		0.02	845	13.1	5	22	13	101	156	35	222	10	1	7,5
Mapara	2.2	2	839	13.4	4	20	11	100	162	36	223	10		2
Whakaipo	2.8	1.5	845	13.4	4	21	12	104	126	36	223	10	2	2
Waihimia	3.4	29	804	14.4	2									2,5
Hinemaiaia	4.5	4.7												3,4
Motutere	5.4	0.5	836	13.4	4	20	12	93	133	36	235	10	2	2
Opepe	8.8	5	834	13.5	7	19	12	97	140	33	233	9	7	2,4
Poronui	9.7	3.5	833	13.6	6	19	12	97	139	33	243	9	2	2,4
Karapiti	9.9	5	819	13.9	3	20	13	100	137	31	233	9	5	1
Oruanui	22.6	180	798	13.7	5	21	18	96	117	22	159	7	7	8,9
Okaia	23-24	3.5*	798	13.6	4	16	11	100	140	23	151	8	4	8,6
Tihoi	45-50	2.5*	786	14.2	4	17	12	94	151	25	164	9	3	6

* Magma volume

Table 2. Iron-titanium oxide temperatures and trace element contents of major silicic plinian tephra units from the Okataina Volcano, New Zealand. Chemical analyses are done by x-ray fluorescence, and are given in ppm. Average errors are the same as in Table 1. References refer to age and volume estimates only. References: 1) Froggatt, 1982a; 2) Lowe, 1986; 3) Nairn, 1981; 4) Wilson et al., 1988. Volume are of in situ tephra. Number of analyses is listed as (n).

OKATAINA VOLCANO

Eruptive Unit	Age (ka BP)	Volume (km3)	Temp. C	-log fO_2	n	Pb	Th	Rb	Sr	Y	Zr	Nb	n	references
Kaharoa	0.93	5	805	13.3	2	18	14	125	54	29	88	10	2	3
Whakatane	4.8	10	785	13.9	6	17	13	107	96	27	123	9	4	,3
Mamaku	7.5	6	792	13.6	6	16	11	103	110	26	140	9	4,3	3,1
Rotoma	9	12	793	13.1	4	17	10	94	105	27	121	9	4	3
Waiohau	11	13.8	797	13.2	5								3	
Rotorua	13.8	7	839	12.1	4	15	9	90	160	26	222	9	5	3
Rerewhakaaitu	14.7	6				16	12	110	123	22	134	9	2	2,3
Okareka	17	4.8	767	14.8	2	17	13	113	82	27	125	9	1	1,3
Te Rere	20.5	9	795	13.2	3	20	12	89	110	31	166	11	1	4
Omataroa	26	17				17	9	87	130	37	210	10	4	3
Awakeri	30	1.8	809	13.0	5	16	9	86	128	39	204	10	2	3
Mangaone	31	16.5	802	12.8	3	16	9	85	127	36	191	10	4	3

Major elements

Based on the major element chemical analyses done in this study, the TVC and OVC magmas were high-silica, metaluminous rhyolites as shown in Table 4-3 and 4-4 (Carmichael et al., 1974). In general, tephras from the OVC are more silicic and potassic, and less sodic that <22 ka TVC tephras, although this is not always true. The same trend is seen between the <22 ka and >22 ka tephra from the TVC. The TVC trend is similar to those noted by Froggatt (1982b), however our analyses are not detailed enough to draw any definite conclusions.

The main purpose of major element analyses done in this study is to assess the pristine nature of melt inclusions, and assess the composition of obsidian. These problems will be discussed in the following chapters.

Table 4-3. Major element composition of melt inclusions, obsidian and pumice from the Taupo Volcanic Center as analysed by electron microprobe, reported as major element oxides. Analyses are recalculated to a 100% volatile-free composition and are normalized to 4.0 wt.% Na_2O. Total Fe is given as FeO.

Unit		Oxide (wt.%)							
		SiO_2	TiO_2	Al_2O_3	FeO^*	MgO	CaO	Na_2O	K_2O
Taupo plinian									
	melt incl.	76.2	0.3	12.6	2.4	0.2	1.4	4.0	2.8
	obsidian	76.2	0.3	13.0	1.8	0.2	1.4	4.0	3.0
	pumice	76.8	0.1	12.8	1.8	0.2	1.6	4.0	2.8
Rotongaio									
	pumice	78.2	0.2	12.0	1.4	0.1	1.2	4.0	3.0
Hatepe phreato.									
	melt incl.	76.6	0.4	12.8	2.2	0.2	1.1	4.0	2.9
	obsidian	76.5	0.2	12.8	1.9	0.2	1.3	4.0	2.9
	pumice	76.8	0.2	12.9	1.7	0.2	1.4	4.0	2.8
Hatepe plinian									
	melt incl.	76.0	0.3	12.5	2.7	0.3	1.4	4.0	2.9
	obsidian	77.0	0.2	12.7	1.6	0.2	1.2	4.0	3.1
	pumice	77.5	0.2	12.7	1.7	0.2	1.2	4.0	2.6
Initial ash									
	melt inlc.	76.0	0.3	12.5	2.6	0.2	1.4	4.0	2.9
Mapara									
	melt incl.	76.0	0.2	13.0	2.3	0.2	1.4	4.0	2.8
	obsidian	76.3	0.3	12.8	1.9	0.3	1.5	4.0	2.9
	pumice	76.6	0.2	12.8	1.5	0.2	1.6	4.0	3.1
Whaikapo									
	melt incl.	77.6	0.2	12.2	1.8	0.2	1.0	4.0	3.1
	obsidian	76.8	0.2	12.7	1.4	0.2	1.2	4.0	3.3
Waihimia									
	obsidian	76.1	0.2	13.1	2.0	0.2	1.4	4.0	2.8
Motutere									
	obsidian	76.7	0.2	12.7	1.7	0.2	1.3	4.0	3.2
	pumice	76.7	0.2	13.0	1.9	0.2	1.3	4.0	2.7
Opepe									
	melt incl.	76.3	0.3	12.9	1.9	0.2	4.0	2.1	3.0
	obsidian	75.4	0.4	12.8	2.2	0.3	1.6	4.0	3.3
	pumice	78.2	0.2	12.1	1.5	0.1	1.0	4.0	2.9
Poronui									
	melt incl.	75.2	0.2	13.5	1.7	0.1	1.4	4.0	3.4
	pumice	75.8	0.1	13.5	2.0	0.2	1.5	4.0	2.8
Karapiti									
	obsidian	76.5	0.2	12.8	1.7	0.2	1.5	4.0	3.1
	pumice	76.2	0.3	13.0	2.1	0.3	1.6	4.0	2.7

Oruanui									
	melt incl.	77.5	0.2	12.3	1.5	0.1	0.8	4.0	3.0
Okaia									
	melt incl.	79.4	0.2	11.0	1.7	0.1	0.8	4.0	3.0
	obsidian	76.0	0.3	13.6	1.8	0.2	1.5	4.0	2.8
Tihoi									
	melt incl.	77.5	0.1	12.2	1.3	0.1	0.9	4.0	4.1

* Total Fe given as FeO

Table 4-4. Major element composition of melt inclusions, obsidian pumice from the Okataina Volcanic Center as analysed by electron microprobe, reported as major element oxides. Analyses are recalculated to a 100% volatile-free composition and are normalized to 4.0 wt.% Na_2O.

Unit		Oxide (wt.%)							
		SiO_2	TiO_2	Al_2O_3	FeO^*	MgO	CaO	Na_2O	K_2O
Kaharoa									
	obsidian	78.2	0.1	12.0	0.7	0.1	0.7	4.0	4.0
Whakatane									
	melt incl.	78.2	0.1	12.2	1.1	0.1	0.7	4.0	3.6
	obsidian	77.5	0.2	12.8	1.2	0.2	1.0	4.0	2.9
Mamaku									
	melt incl	77.9	0.2	12.2	1.5	0.1	0.8	4.0	3.4
	obsidian	78.3	0.1	12.1	0.9	0.1	0.8	4.0	3.7
Rotoma									
	obsidian	78.5	0.1	12.2	0.9	0.1	0.8	4.0	3.5
Waiohau									
	melt incl.	78.6	0.1	11.9	1.3	0.0	1.7	4.0	3.5
Rotorua									
	melt incl.	77.1	0.9	12.0	1.7	0.2	1.0	4.0	3.3
	pumice	78.2	0.1	12.7	1.1	0.2	0.8	4.0	2.9
Te Rere									
	obsidian	78.1	0.1	12.4	1.0	0.2	0.9	4.0	3.2
	pumice	77.2	0.2	13.1	1.2	0.2	1.3	4.0	2.8
Mangaone									
	obsidian	78.4	0.1	12.3	0.8	0.1	0.7	4.0	3.6

* Total Fe given as FeO

Strontium isotopes

The $^{87}Sr/^{86}Sr$ ratios of the Taupo plinian, Hatepe plinian, Hatepe phreatomagatic, Initial ash (all 2 ka B.P.), and Okaia (~23 ka BP) tephras were measured in order to evaluate the zonation in the younger units, and the composition of the older units relative to the younger. The results are shown in Table 4-5. Each sample was only run once.

The differences between the $^{87}Sr/^{86}Sr$ values for the 2 ka tephra units are within analytical error. The $^{87}Sr/^{86}Sr$ composition of the 2 ka tephra sequence is unusually homogeneous, and shows no evidence of systematic compositional zonation. The Okaia tephra, however, shows an $^{87}Sr/^{86}Sr$ ratio which is significantly different from the younger tephras. This is consistent with the earlier-drawn conclusion that this tephra is derived from a different magma body.

Table 4-5. $^{87}Sr/^{86}Sr$ composition of tephras from Taupo center tephras. Each value represents one analysis (Analyst: P. Kyle).

Sample Number	Unit	(age ka)	Rb	Sr	$^{87}Sr/^{86}Sr$	2 sigma error
015A	Taupo plin.	(2)	95.9	166.5	0.706031	± .000013
027A	Hatepe plin.	(2)	98.5	155.6	0.706009	± .000008
002A	Hatepe phrea.	(2)	97.4	153.4	0.706023	± .000013
044	Initial ash	(2)	100.5	154.2	0.706039	± .000009
047	Okaia	(23)	101.4	139.7	0.705615	± .000008

*Rb and Sr analysed by x-ray fluorescence at NMIMT. $^{87}Sr/^{86}Sr$ measured at Royal Holloway and Bedford New College by VG 354 mass spectrometer using standard separation techniques. During the period of analysis the Sr standard SRM 987 has an $^{87}Sr/^{86}Sr$ = 0.710243±18 (2) n=8.

5. ANALYSIS OF OBSIDIAN

Introduction

Obsidian clasts in rhyolitic tephra deposits, if co-genetic with the bulk of the erupted magma, may contain some portion of the pre-eruptive volatile contents of the parental magma (Eichelberger and Westrich, 1981). These primary obsidian can therefore be used to investigate eruptive degassing processes, and, in some cases, to make an estimate of the minimum pre-eruptive volatile content of the melt.

Some obsidian in tephra deposits may not be co-genetic with the erupting magma, but may be lithic fragments derived from pre-existing rocks which are picked up during eruption. Several methods can be used to distinguish between primary and secondary obsidian in tephra deposits. These include H_2O release spectra, isotopic composition and trace element chemical analysis of the obsidian compared to that of bulk rock. The first two methods mentioned are applicable because the H_2O contained in lithic obsidian may not be magmatic, but may be meteoric H_2O added during hydration (Friedman and Long, 1976). Obsidian from a young tephra deposit with a high content of meteoric H_2O is probably lithic material, because obsidian hydrates gradually over time. However, it is difficult to assess whether an obsidian deposit of a given age will be hydrated because rates of hydration are dependent on temperature and availability of meteoric H_2O. The concentration of mobile elements, such as Na and K, can be altered during the hydration process (Jezek and Noble, 1978), so it is likely that volatile elements are also mobilized. Means for distinguishing between magmatic and secondary H_2O include optical, chemical, and isotopic analyses as well as investigation of the temperature spectrum at which H_2O release from the obsidian.

In this study, we have investigated the origin and mode of formation of rhyolitic obsidian fragments from the TVZ, New Zealand, and the degassing systematics of the volatile components of the system. This was done by analysing the H_2O and Cl contents, and δD and $\delta^{18}O$ values of obsidian fragments from a number of explosive plinian eruptions from the TVC and OVC. Trace element chemical analyses were made for certain units in order to determine whether the obsidian was co-genetic with the bulk of erupted tephra. The pre-eruptive H_2O and Cl contents of certain eruptions from the TVZ have been determined independently by melt inclusion analysis.

Samples

The most detailed analyses in this study were done on the 2 ka Taupo eruptive sequence, which includes the Taupo plinian tephra, deposited by the highly explosive "ultraplinian" eruption (Walker, 1980). This sequence was erupted over ~2 weeks, and consists of the following tephra units (from first to last erupted): the phreatoplinian initial ash (0.005 km^3 magma volume {MV}), the Hatepe plinian pumice (1.4 km^3 MV) the Hatepe phreatoplinian ash (1.0 km^3 MV), the Rotongaio ash (0.7 km^3 MV), the Taupo plinian pumice (5.1 km^3 MV), and finally, the Taupo Ignimbrite (10 km^3 MV) (Wilson and Walker, 1985, Wilson, 1985). This eruptive sequence is well suited to detailed study because all of the tephras contain obsidian, the sequence is very young, reducing the chances of alteration, and both plinian and phreatoplinian tephras are present.

Water analyses

Water in bulk obsidian samples and individual obsidian fragments was analysed by Karl-Fischer titration (Westrich, 1987). Prior to analysis, samples were oven-dried at 100°C overnight, and stored in sealed vials. Samples were also dried in the furnace connected to the titration device after being weighed for analysis in order to remove any adsorbed H_2O introduced during the weighing process. The H_2O count rate was monitored during this time, and the analysis was not begun until H_2O counts had fallen to background levels. Duplicate or triplicate analyses were made of most bulk samples. At least 1 individual obsidian fragments were also analysed from each tephra unit. This was problematic for units with low H_2O contents, because an individual fragment of obsidian which contains <0.3 wt% H_2O will generally not vesiculate and fully degas.

The temperature release spectrum of H_2O was also determined. Samples were dried in the furnace, and then the heat was increased incrementally during analysis, generally by 100^{o}C steps, and the amount of H_2O released over each step was measured. This type of analysis was done for bulk obsidian samples and individual obsidian fragments from the TVZ, and also for samples of coarsely ground hydrated dome obsidian from the Grefco perlite mine in Socorro, New Mexico, in order to compare the H_2O release spectra of these 3 sample types.

Results

General observations

Obsidian occurs in most TVC and OVC tephra units sampled as light grey to black angular or conchoidally fractured, translucent fragments, generally 0.5 to 5 mm in diameter. Obsidian color is consistent within some samples and ranges in other samples from light grey to black. Fragments of obsidian are generally hard and do not show the many small fractures characteristic of secondary glass hydration (Jezek and Noble, 1978). In thin section, the obsidian fragments appear clear, and lack strain-related birefringence typical of hydrated glass (Friedman and Smith, 1960). The color of obsidian appears to be dictated by the abundance of microphenocrysts in the obsidian, with more microphenocrysts in the darker glass. The orientation of microphenocrysts in some samples indicates laminar flow and shear in the melt prior to quenching (Fig. 5-1). No evidence of vesiculation was seen in the obsidian fragments.

Major and trace element composition

Major element composition of obsidian generally agree well with composition of bulk rock and melt inclusions from the same sample (Fig. 5-2). These analyses support but do not prove the co-genetic nature of obsidian and bulk rock. Furthermore, these analyses suggest that the obsidian has not been severely hydrated because no migration of K has occurred (Jezek and Noble, 1978).

Obsidian and pumice from several TVC and OVC tephras were analysed for trace elements. The TVC units

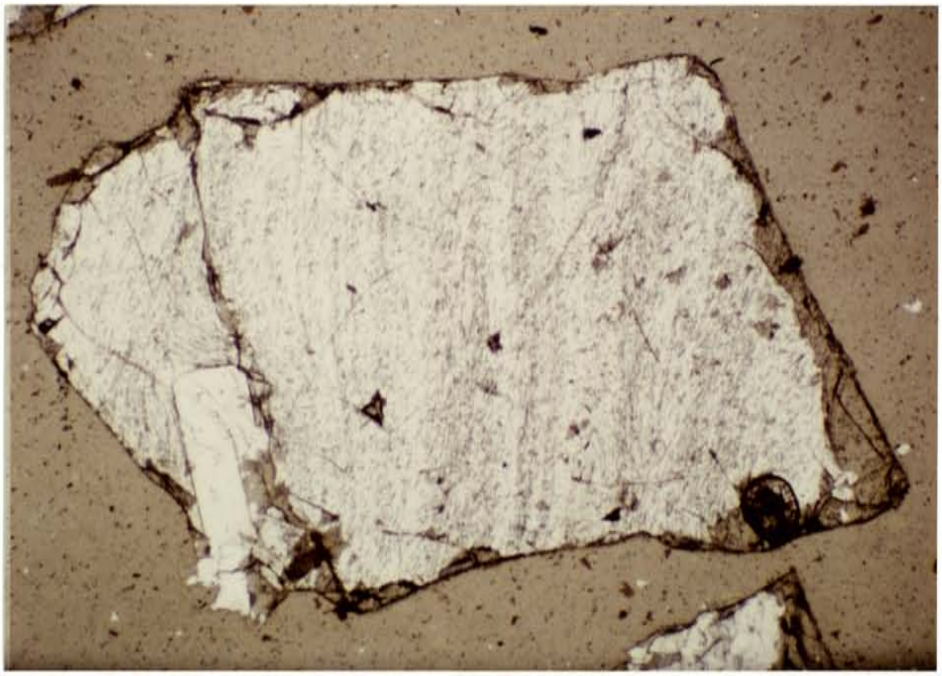

Figure 5-1. Photomicrograph of obsidian fragment showing evidence of laminar flow and shear as evidenced by pattern of microphenocrysts.

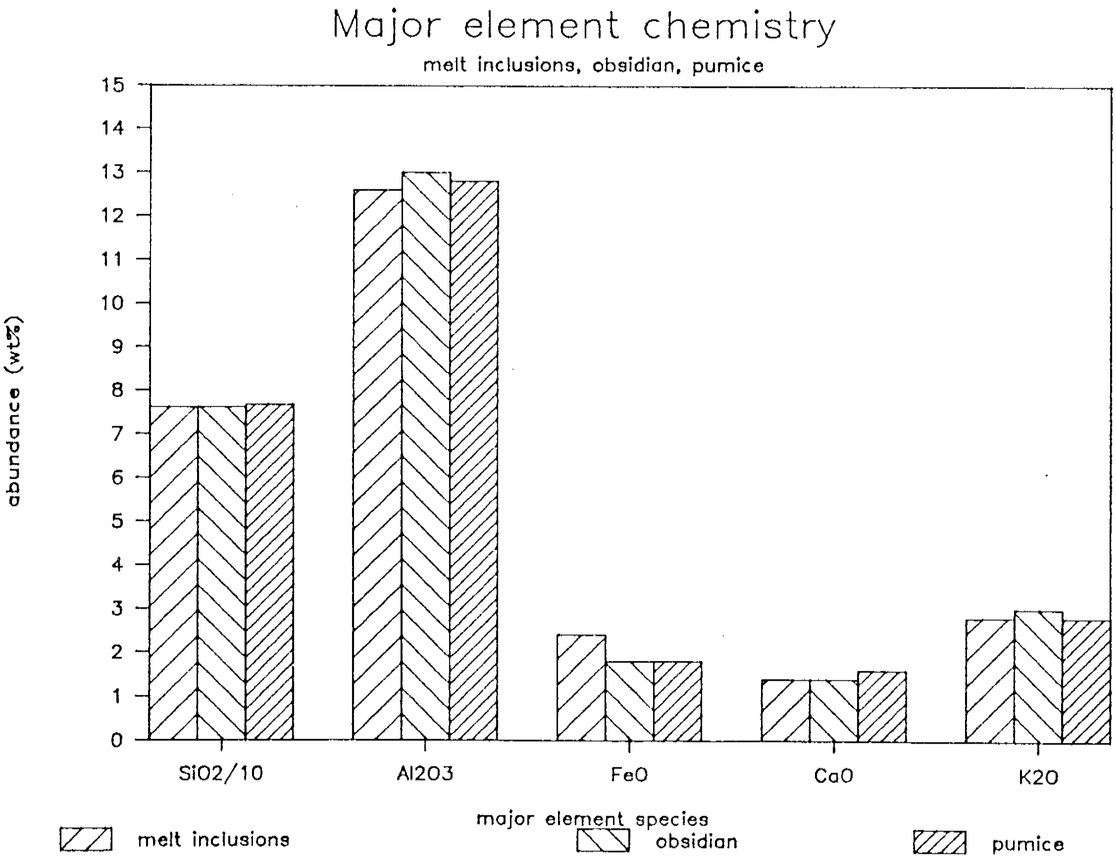

Figure 5-2. Representative major element chemistry of obsidian, melt inclusions and pumice from the Taupo plinian tephra as analysed by electron microprobe. Analytical errors to 1σ based on machine counting statistics (in wt%) are: SiO_2 $\pm$0.6, Al_2O_3 $\pm$0.4, FeO $\pm$0.2, CaO $\pm$0.1, K_2O $\pm$0.4.

analysed were the Taupo and Hatepe plinian tephras, and OVC tephras were the Mamaku and Kaharoa. About 10 samples of obsidian were analysed for each unit, each sample containing either single, or multiple obsidian fragments. The data for these analyses is included in Appendix C. In general, the trace element compositions of the obsidian samples are very similar to the bulk rock. The variations seen in some cases are probably due to slight differences in the content of trace-element-bearing phenocryst phases, as individual fragments are not large enough to represent a truely homogeneous sample. The trace element composition of obsidian normalized to the bulk rock analyses for the Kaharoa tephra are shown in Fig. 5-3. The normalized obsidian values generally cluster around 1, indicating that they are similar to bulk rock composition. The anomylously high Hf content of one sample may be due to a grain of zircon in the obsidian.

Water

Water was analysed in bulk obsidian samples, and also in individual obsidian fragments. The mean values for bulk samples and the range shown by individual fragments is shown in Table 5-1 and 5-2, and detailed H_2O analyses are given in Appendix D. In many cases, the bulk sample value is outside the range of values for

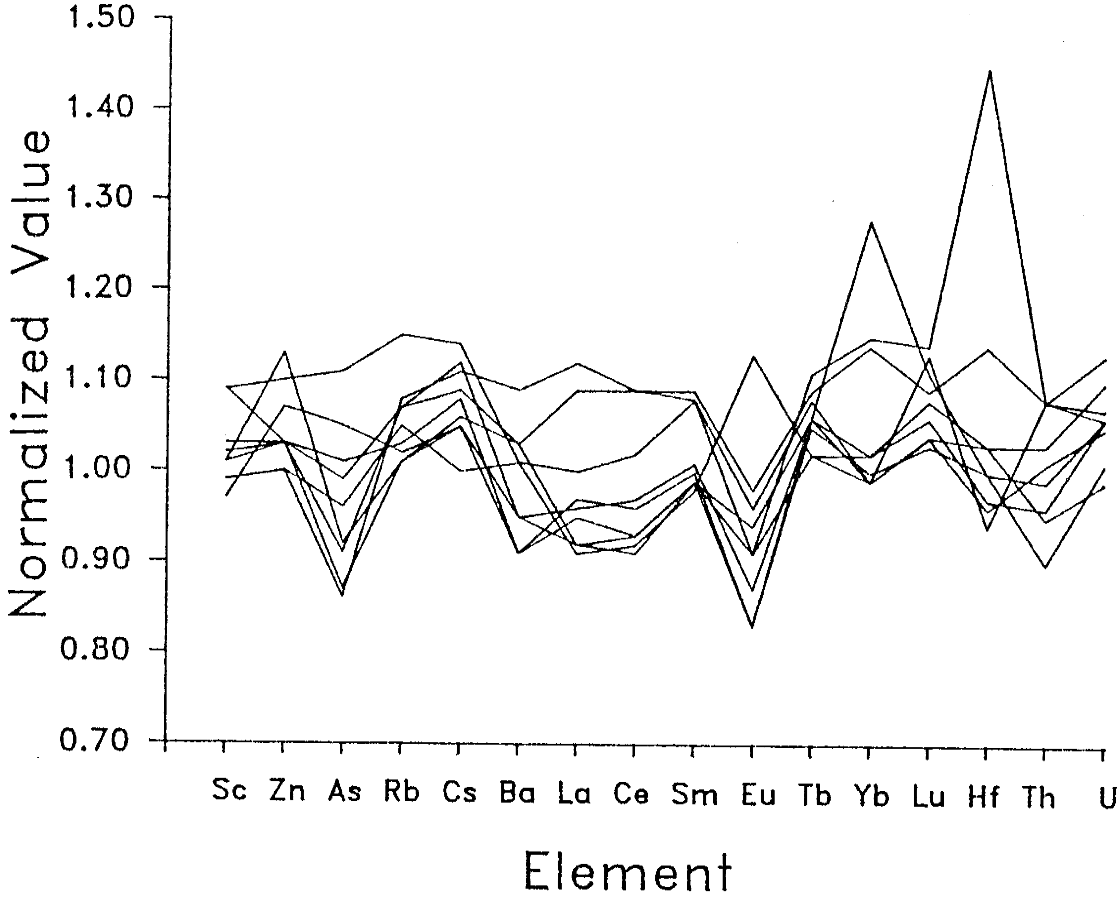

Figure 5-3. Trace element composition of obsidian normalized to bulk rock (pumice) compositions from the Kaharoa tephra. analysis. The normalizing factors used on the diagram (pumice composition, in ppm) are: Sc 3.3, Zn 32, As 4.5, Rb 128, Cs 5.7, Ba 951, La 23.7, Ce 50.9, Sm 4.1, Eu 0.5, Tb 0.7, Yb 3.2, Lu 0.5, Hf 3.4, Ta 0.8, Th 11.8, U 3.0. Analyses made by neutron activation.

Table 5-1. Water and chlorine contents of obsidian in TVC tephra. Samples of single tephra units are listed in stratigraphic order. Number of samples for each type of analysis is listed as "n". Error in water determinations is approximately ±2.5%, and for Cl ±130 ppm.

Unit	Age x1000	strat. pos.	bulk water content	n	range of individual fragment	n	Chlorine content wt%	n
Taupo plinian	2	top	0.35	2				
		inter	0.16	1				
		inter	0.24	2			0.140	4
		inter	0.13	1				
		base	0.30	2				
Rotongaio	2	top	0.24	1	0.32-0.58	4		
		inter	0.21	1				
		inter	0.23	1				
		inter	0.23	1	0.26-0.41	3		
		inter	0.34					
Hatepe phreato.	2	top	0.46	4				
		inter	0.45	4	0.61-1.94	5	0.131	9
		inter*	1.44	2	1.75-2.20	7		
		inter	1.55	2	2.08-2.23	3		
		inter	0.98	1	0.89-2.14	6		
		inter	1.26	1	1.26-2.10	3		
		inter	0.97	1	0.68-2.44	5		
		base	1.00	3	1.66	1		
Hatepe plinian	2	top	0.19	1				
		inter	0.19	1			0.121	11
		inter	0.17	1				
		inter	0.10	1				
		base	0.48	1	0.26-1.67	3		
Initial ash	2	top	0.26	3				
		base	0.38	3			0.120	4
Mapara	2.2	top	0.95	2	0.25-0.26	2		
		inter	0.65	1			0.136	6
		base	0.70	4				
Whaikapu	2.8	all	1.64	2	0.88-1.36	3	0.160	5

Table 5-1 con't

Waihimia	3.2	top	0.41	1	0.68-1.30	2	0.129	9
		inter	0.16	1				
		base	0.21	1				
Motutere	5.4	all	1.60	1	0.68-1.44	5	0.157	3
		all	0.81	1	0.79-2.76	5		
Opepe	8.8	top	1.10	2			0.141	9
		inter	1.02	1				
		base	1.00	1	0.70-1.43	3		
Porunui	9.5	top	0.36	1	0.88-1.22	5		
		base	0.71	3	0.51-1.22	9	0.143	7
Karapiti	9.8	top	0.90	4				
		base	1.15	2	0.82-1.50	9	0.138	5
Oruanui	20	top	1.20	2				
		inter	1.10	2	0.53-0.79	4	0.153	6

Table 5-2. Water and chlorine contents of obsidian in OVC tephra. Samples of single tephra units are listed in stratigraphic order. Number of samples for each type of analysis is listed as "n". Error in water determinations is approximately ±2.5%, and for Cl ±130 ppm.

Unit	Age x1000	strat. pos.	bulk water content	n	individual water contents	n	Chlorine content wt%	n
Kaharoa	0.65	top	1.06	1	0.91-1.37	5		
		inter	0.38	1				
		inter	0.45	1			0.137	8
		base	1.02	1	0.59-2.49	5		
Whakatani	5	near top	0.65	2			0.159	6
Mamaku	7	top			0.46-0.66	7		
		inter	0.82	2			0.149	7
		base	0.73	2				
Rotoma	9	top	0.67	1			0.162	10
		inter	0.76	2				
		base	0.52	1				
Waiohau	11	top	0.56	1				
		inter	0.89	1	1.28-2.53	5	0.165	7
		base	1.13	1	0.91-1.44	5		
Rotorua	13	top	0.39	1				
		inter	0.64	3				
		inter	1.13	2				
		inter	1.24	1			0.168	3
		inter	1.10	2				
		base	1.08	1				
Rerewhaikatu	14.7	top	0.51	1				
		base	0.87	2				
Okareka	17	inter	0.70	1				
Terere	19	top	0.40	1	0.21-0.38	2	0.119	6
		inter	0.52	3				
		base	0.68	2				
Omateroa	28	inter	1.66	1				

Table 5-2 con't

Awakeri	30	all	1.24	2	0.37-1.91	10	0.155	3
Mangaone	31	top	1.48	1				
		base	1.49	1			0.141	10

individual fragments. There are two reasons for this discrepency. First, the number of analysed fragments may be too few to provide a representative mean. Secondly, and more important, fragments which have H_2O contents of <0.3 wt% generally do not vesiculate, so cannot be analysed and are excluded from the range. Therefore, many individual samples with low water contents do not appear in the sample range, but are nevertheless included in the bulk ground sample.

Although the H_2O contents of obsidian vary widely among different units, stratigraphic variations within individual units are generally limited. This is even true for individual units within the rapidly-erupted Taupo eruptive sequence (2 ka). There does not appear to be any systematic variations of H_2O contents of obsidian from the base to the top of individual units, unlike variations seen elsewhere in other studies (Eichelberger and Westrich, 1981). In addition, the H_2O contents of individual obsidian fragments do not show any relation to the size or color of the fragment.

The results of step-wise heating runs for H_2O analysis for ground TVZ obsidian, individual TVZ obsidian fragments and coarsely ground Grefco perlite (hydrated obsidian) are shown in Fig. 5-4, and data is given in Appendix D. There are distinct differences between the three sample types; hydrated Grefco perlite begins to

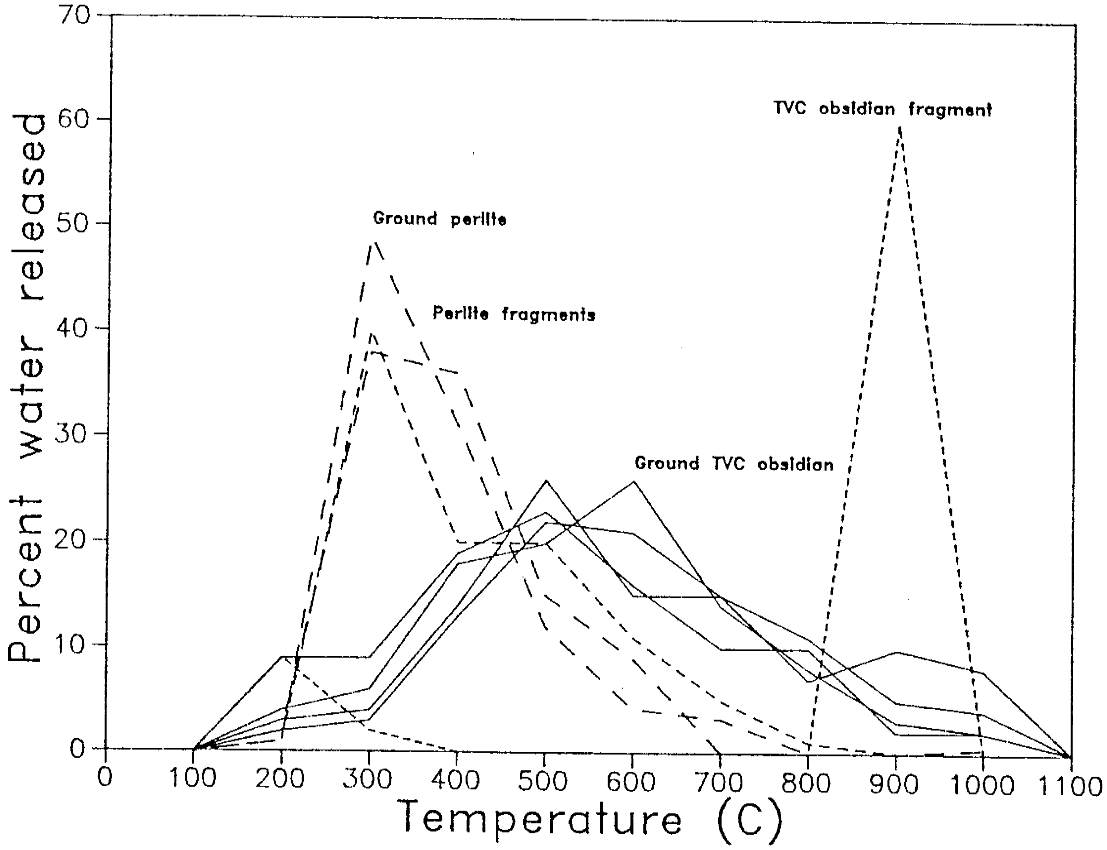

Figure 5-4. Degassing spectra of ground obsidian from the TVC (Hatepe phreatoplinian, Waiohau and Awakeri tephras), a single obsidian fragment from the TVC (Motutere tephra), fragments and coarsely ground samples of hydrated obsidian (Grevco perlite), as analysed by Karl-Fischer titration, showing the different behavior of these four sample types. Heating increment of 100°C used.

degas at low temperatures (~200^{o}C) and loses most of its H_2O content by <500^{o}C, whereas ground TVZ obsidian begins significant degassing at higher temperatures (~400^{o}C) and continues degassing up to 900^{o}C. Individual fragments of TVC obsidian do not degas significantly until 800^{o}C then all the H_2O is instantaneously released by vesiculation of the fragment. A single fragment of hydrated Grefco perlite show the same degassing behavior as coarsely ground Grefco perlite.

Chlorine

Chlorine was analysed by electron microprobe in obsidian from single samples of most units. Mean Cl contents of obsidian are shown in Tables 5-1 and 5-2, and detailed data are given in Appendix D. Chlorine contents of obsidian range from mean values of 0.119 wt% to 0.168 wt%. The range of Cl contents of obsidian from the TVC and OVC are similar, and there does not appear to be any systematic variations of Cl contents of obsidian from either center, stratigraphically within single units, or between sequential units. There is no systematic variation of Cl from the core to rim of individual fragments.

Isotopic analyses

Preliminary isotopic analyses for δD and $\delta^{18}O$ were made on bulk obsidian samples from a number of units. The methods of analysis are discussed in Appendix B. The $\delta^{18}O$ values are listed in Table 5-3. The values cluster around a value of +7 permil. The δD values are listed in Tables 5-4 and 5-5 and shown on Figs. 5-5, 5-6 and 5-7. There are some rough trends noted in these figures, but as the data was collected on bulk obsidian samples rather than individual obsidian fragments, the trends are not well defined. Future isotopic analyses should clarify this problem. Furthermore, two sets of isotopic analyses were made with two different reduction furnaces, one which was uranium and the other zinc, and obsidian standards run with both sets do not agree. However, mineral standards give correct values. Therefore, the δD values may not be correct or comparable between runs.

Discussion

Cogenetic nature of obsidian and tephra deposits

Chemical analyses of obsidian in plinian tephras from the TVC and OVC suggest that most obsidian is co-genetic with pumice in the tephra and it is not incidental lithic material. Major element compositions of obsidian and bulk rock from each eruption are identical, consistent with a co-genetic origin. This

Table 5-3. Oxygen isotope values for bulk obsidian fragments from the Taupo Volcanic Center. Stratigraphic position of samples is marked on the table. Age of tephra units can be determined from Table 1. All $\delta^{18}O$ values are positive.

Unit	stratigraphic position	$\delta^{18}O$
Taupo plinian	top	7.34
	base	7.38
Hatepe phreato.	inter	7.23
	inter	7.38
	base	7.21
Hatepe plinian	inter	7.46
	inter	7.35
Initial ash	base	6.95
Mapara	top	7.28
	inter	7.37
Motutere	all	7.39
Opepe	inter	7.49
	base	7.69
Karapiti	inter	6.72

Table 5-4. Preliminary hydrogen isotopic composition of obsidian from Taupo volcanic zone tephras. Those indicated in bold face and marked by an asterix (*) were analysed in July, 1985, and the others were analysed in Dec, 1985 (see text).

Unit and Sample Number	Stratigraphic Position	H_2O content (wt%)	Delta D (permil)
Taupo Plinian			
016	top	0.35	-35.2
014	inter	0.39	-39.5
022	base	0.73	-31.3
Rotongaio			
041	inter	0.63	-46.8
Rot./Taupo plin. transition			
013		0.34	-29.2
Hatepe phreatomagmatic			
***005**	**top**	**1.23**	**-74.9**
***023**	**inter**	**1.33**	**-57.7**
006	inter	1.41	-47.2
***003**	**inter**	**0.74**	**-76.7**
002	base	0.57	-36.3
Hatepe plinian			
007	all	0.20	-38.7
045	all	0.91	-57.0
***045b**	**1 obs. frag**	**0.18**	**-100.7**
Initial Ash			
044	top	0.28	-44.7
***043**	**base**	**0.58**	**-100.1**
Mapara			
026	top	0.55	-31.2
025	inter	1.01	-55.1
024	base	0.87	-66.5
Waihimia			
***018**	**base**	**1.40**	**-78.1**
020	inter	0.28	-74.7
Motutere			
008	all	0.65	-99.3
Opepe			
030	top	1.04	-32.3
031	inter	1.01	-44.5
032	base		-44.5
Poronui			
***009**	**all**	**0.70**	**-85.0**

Table 5-4 con't

Karapiti			
012	top	0.72	-36.5
*011	inter	1.31	-77.8
*034	top	1.35	-77.0
Obsidian flow			
*DOBS		0.14	-103.8
DOBS		0.10	-70.3
061		0.23	-76.7

Table 5-5. Preliminary hydrogen isotopic composition of obsidian from Okataina volcanic zone tephras. Those indicated in bold face were analysed in July, 1985, and the others were analysed in Dec, 1985 (see text).

Unit and Sample Number	Stratigraphic Position	H_2O content (wt%)	Delta D (permil)
Rotoma			
064	top	0.90	-51.3
063	inter	0.85	-71.9
062	base	0.71	-70.5
Rotorua			
091	top	0.31	-60.1
088	**inter**	**0.50**	**-95.6**
085	inter	1.16	-47.9
087	inter	1.21	-66.4
086	base	1.36	-54.9
Rerewhakaaitu			
079	**top**	**0.62**	**-92.2**
078	base	0.88	-55.8
Te Rere			
060	**top**	**0.31**	**-101.0**
057	base	0.60	-67.9

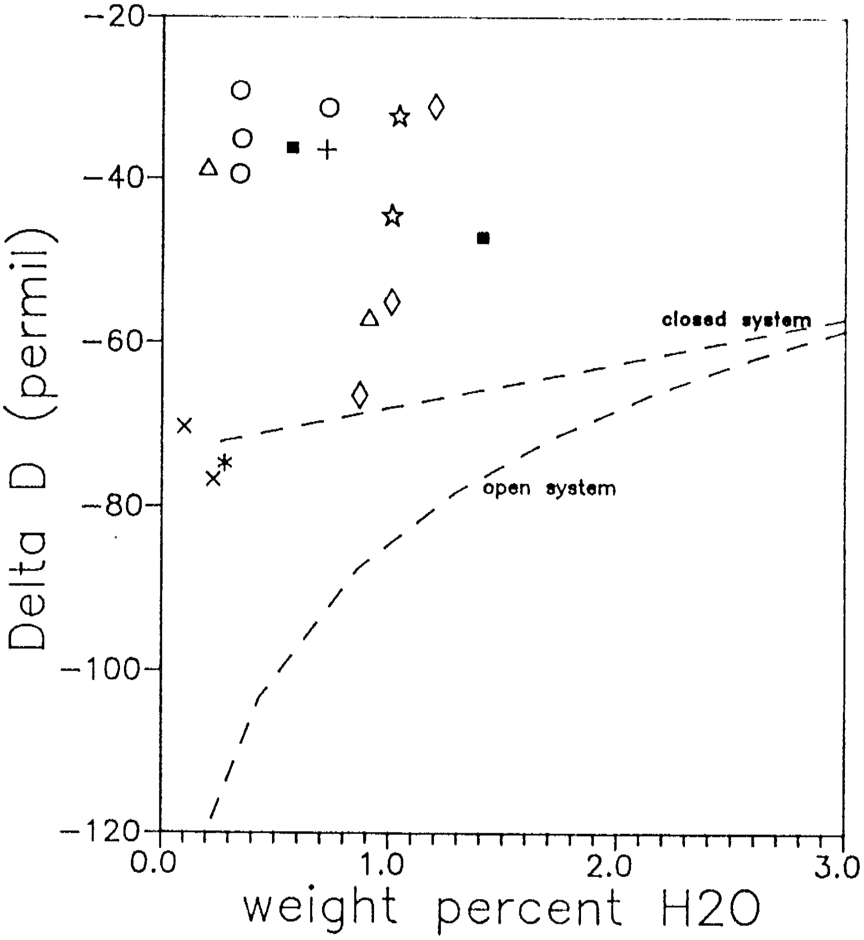

Figure 5-5. Hydrogen isotopic composition of bulk samples of TVC obsidian versus water content (samples analysed in Dec., 1985). Dotted line represents a calculated open and closed system degassing fractionation trends for a magma with an initial H_2O content of 4.3 wt.% and and initial delta D of -50 permil. Symbols: open circles-Taupo plinian; closed squares-Hatepe phreatomagmatic; open triangles-Hatepe plinian; open squares-Initial Ash; open diamonds-Mapara; asterix-Waihimia; star-Opepe; cross-Karapiti; ex-Obsidian flow.

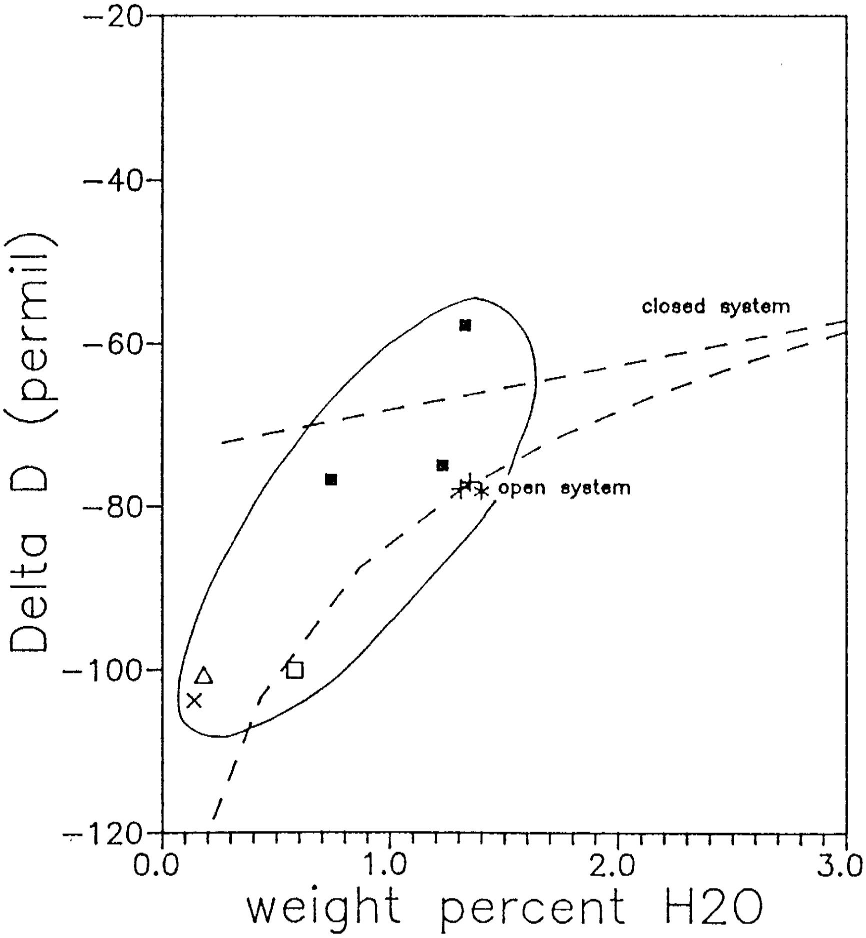

Figure 5-6. Hydrogen isotopic composition of bulk samples of Taupo center obsidian versus water content (samples analysed in July, 1985). Dotted line represents a calculated open and closed system degassing fractionation trends for a magma with an initial H_2O content of 4.3 wt.% and and initial delta D of -50 permil. Symbols: closed squares-Hatepe phreatomagmatic; open triangles-Hatepe plinian; open squares-Initial Ash; asterix-Waihimia; cross-Karapiti; ex-Obsidian flow.

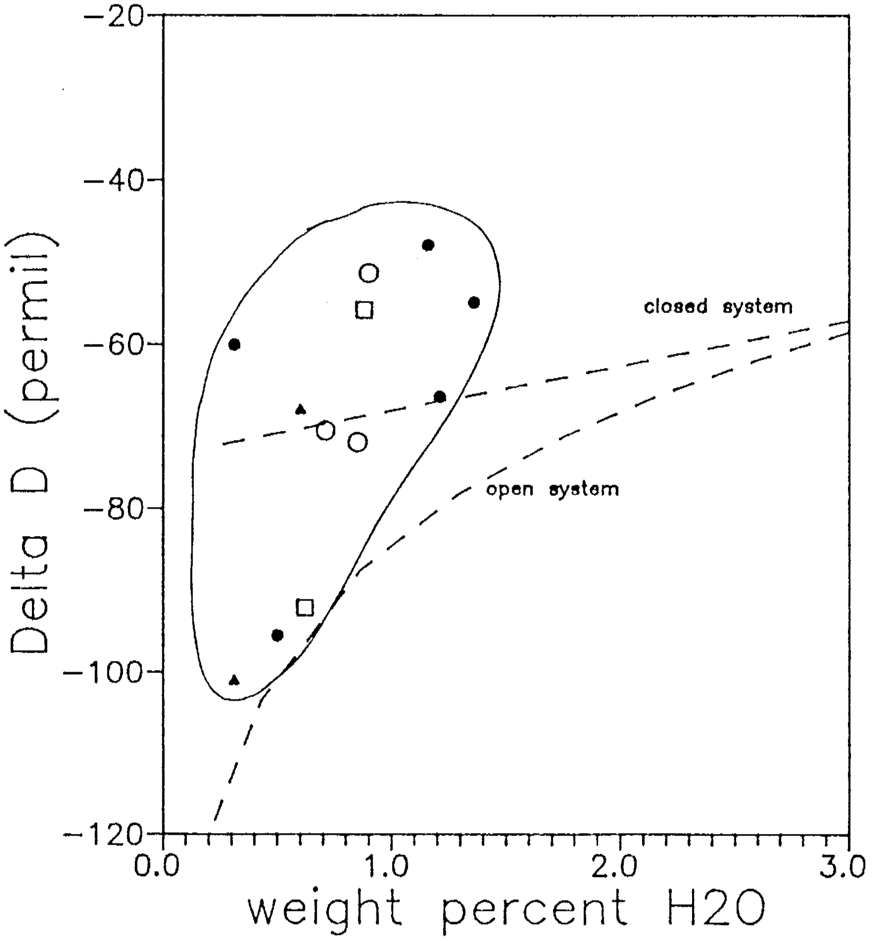

Figure 5-7. Hydrogen isotopic composition of bulk samples of OVC obsidian versus water content (samples analysed in July and Dec., 1985). Dotted line represents a calculated open and closed system degassing fractionation trends for a magma with an initial H_2O content of 4.3 wt.% and and initial delta D of -50 permil. Samples with solid symbols analysed in July, those with open symbols analysed in December. Symbols: open circles-Rotoma; closed circles-Rotorua; open squares-Rerewhakaaitu; closed triangles-Te Rere.

cogenetic origin is also strongly supported by the close agreement between obsidian and bulk rock trace element compositions. Trace elements, particularly rare earth elements (REE), can be analysed accurately to very low abundances, and are generally unique for a single magma chamber, or even for magma erupted at different times from a single magma chamber (Hildreth, 1981). Therefore, lithic obsidian fragments incorporated into a tephra at the time of eruption would be unlikely to have trace element composition similar to bulk tephra.

A possible exception to the generally co-genetic nature of obsidian in tephra deposits is in the Terere tephra (OVC). There is an anomalously high obsidian content in the lower part of this tephra unit, interpreted by Nairn (1981) to represent a disrupted obsidian dome. The H_2O and Cl contents of this glass are relatively low, although not all fragments are fully degassed This obsidian may represent a dome/near-surface conduit system in a pre-existing vent, which was incorporated into the Terere eruption. The obsidian derived from the conduit would have quenched at greater than atmopheric pressure, and would have slightly elevated H_2O contents. Major element chemistry of the obsidian is similar to bulk rock of the tephra deposit, but trace elements have not been analysed.

Origin of water in obsidian

A number of lines of evidence suggest that the H_2O contained in most primary obsidian fragments is juvenile, not a result of post-eruptive hydration processes. First, the obsidian does not appear hydrated, as the fragments are generally glassy and clear, lacking hydrated-related cracks and cloudiness, and does not show strain-related birefringence (Friedman and Smith, 1960; Jezek and Noble, 1978). Second, major element chemistry of obsidian does not show evidence of migration of alkali elements, as can occur when glass hydrates (Jezek and Noble, 1978). Third, as shown in Fig. 5-8 and 5-9, there is no correlation between the H_2O or Cl content of the obsidian and the age of the tephra deposits, as would be expected if the obsidian underwent progressive hydration with age. Fourth, the oxygen isotopic composition of the glass is similar to magmatic values ($\delta^{18}O$ ~+7 permil), and does not show evidence of contamination with the local groundwater, ($\delta^{18}O$ ~ −10 permil) (Table 5-3). Finally, the degassing spectra of obsidian analysed from some TVC and OVC eruptions is significantly different than degassing spectra of obsidian hydrated by meteoric H_2O (perlite) (Fig. 5-4). The hydrated perlite degasses at low temperature (from about 200 to 500°C) whereas obsidian containing magmatic H_2O degasses from about 400 to 800°C. The interpretation of the higher

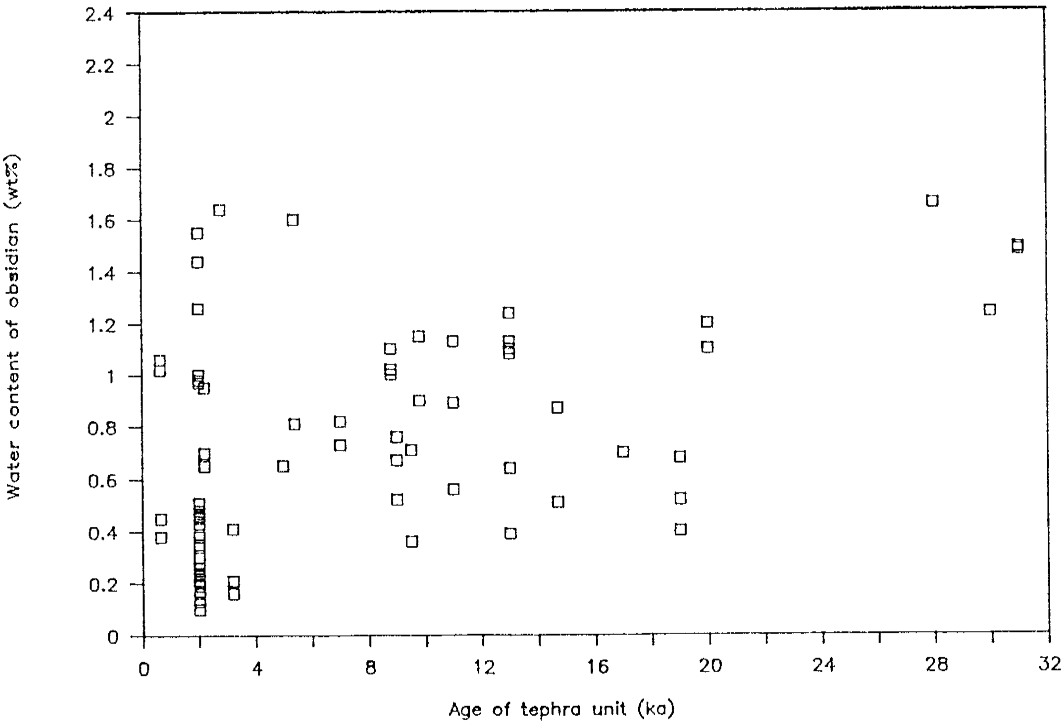

Figure 5-8. H_2O contents of bulk obsidian samples from the TVC and OVC versus age of the tephra deposit from which the obsidian was derived. Analyses are made by Karl Fischer titration.

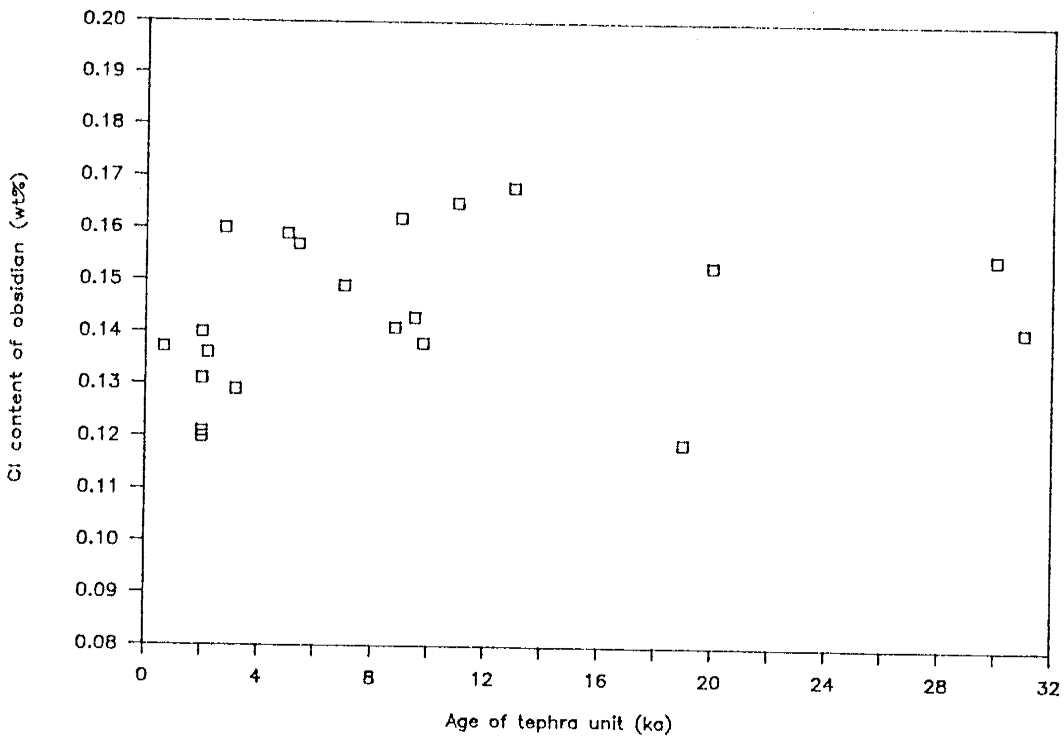

Figure 5-9. Mean Cl contents of bulk obsidian samples from the TVC and OVC versus age of the tephra deposit from which the obsidian was derived. Analyses are made by electron microprobe.

release temperatures of H_2O in TVC and OVC tephra is that the magmatic H_2O is homogeneously incorporated into, and strongly bonded with the structure of the glass, and must escape by chemical diffusion. However, secondary H_2O is adsorbed into the glass, loosely bonded, and is able to escape rapidly from the glass by the same fractures along which it entered, and is able to do so at lower temperatures.

Formation of obsidian

A model for obsidian formation during TVC and OVC tephra eruptions has been formulated, based on the features shown by obsidian in these tephras, such as elevated and variable H_2O contents, and shear structures in the glass, and the fact that some fragments of obsidian are seen to grade into pumice. This model incorporates features of Taylor et al. (1983) and Eichelberger et al. (1986) models. During the eruption, as the melt rises in the conduit and vesiculates it forms an expanded foam through which gas is readily mobile (Eichelberger et al., 1986). During ascent, a small portion of the partially degassed foam collapses and quenches along the walls of the conduit, due to shear caused by magma flow and cooler temperatures of the conduit walls. This type of vesicle collapse is seen in obsidian flows (Eichelberger et al., 1986). The amount of H_2O retained in the glass would be roughly a function of the depth at which quenching occurred, as the solubility of H_2O in the melt is essentially pressure dependent. The obsidian is removed from the walls by later stages of the eruption and incorporated into the eruption column. The point in time during the eruption when the obsidian forms is not clear, but the generally uniform distribution of obsidian throughout the tephra suggests that formation and incorporation of obsidian is an ongoing process.

The variability in H_2O contents of obsidian clasts within tephra suggests that quenching occurred after variable amounts of degassing, possibly corresponding to different quenching depths. The solubility of H_2O in a TVZ melt has been calculated following Burnham (1975, 1979a and b) and the resultant solubility curve is shown in Fig. 5-10. If the H_2O contents of obsidian represent the maximum solubility of H_2O at the point where they were quenched, then the depth of quenching can be determined from this solubility curve. This rests on the assumption that at near-magmatic temperatures, the kinetics of gas diffusion through the melt will not significantly inhibit degassing. In some cases, quenching took place at pressures as high as ~0.5 kb, (1.75 km depth). However, most glass didn't quench until it has reached near-surface pressures, as H_2O contents

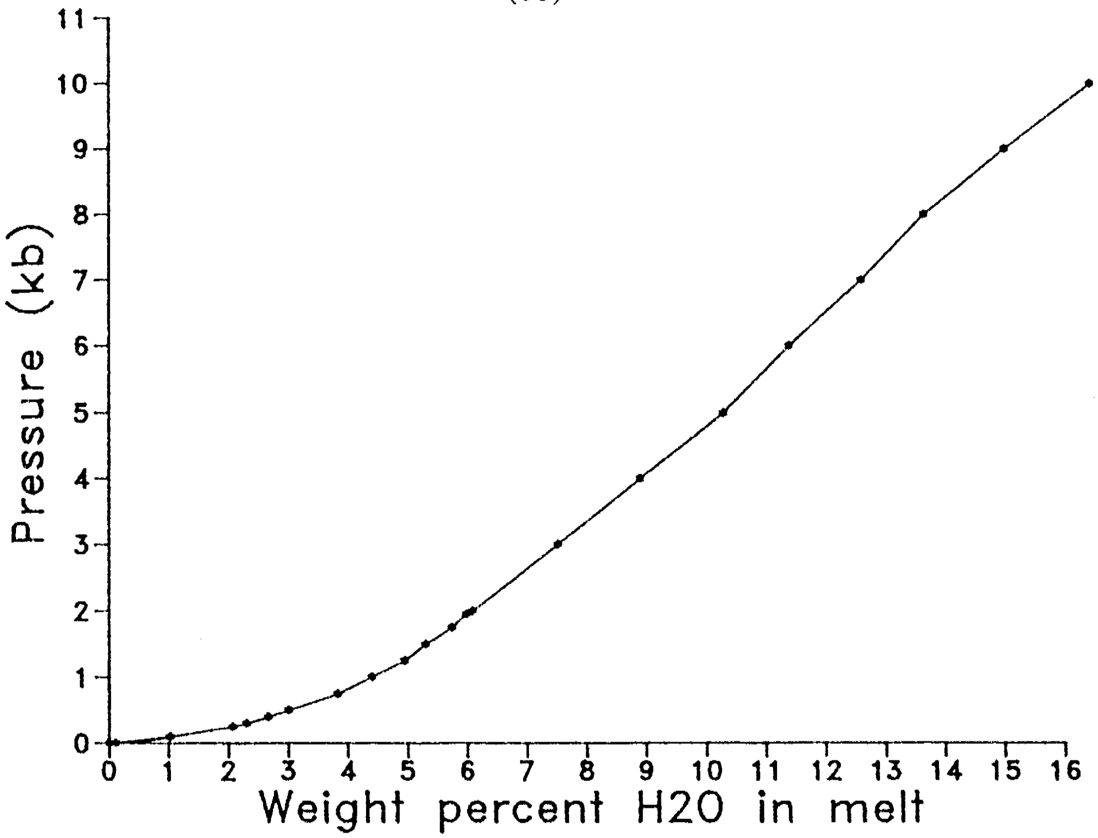

Figure 5-10. Calculated solubility curve of H_2O for an average TVZ rhyolite at 750°C. Calculated following Burnham (1975, 1979a and b). Calculations are shown in Appendix F.

of <1 wt.% (<0.1 kb) are more common.

The wide variation among the mean H_2O contents of obsidian from different tephra units may be related to the style of eruption which generated the tephra. Obsidian from two tephra deposits, the Taupo plinian and Waihimia tephras, have low mean H_2O contents (0.13-0.41 wt%). These two deposits were produced by extremely powerful explosive eruptions (Walker, 1981c), and perhaps the velocity of the magma within the conduit inhibited quenching of obsidian. Two phreatoplinian eruptions, the Hatepe phreatomagmatic and the Oruanui (Wilson and Walker, 1985; Wilson et al., 1988) have relatively high mean H_2O contents in obsidian. The phreatoplinian eruption process may have promoted quenching of magma to obsidian at depth (< 1.3 km). This interpretation is speculative, however, because other tephra units which do not show a strong phreatoplinian characteristics also contain obsidian with high H_2O contents. The mean H_2O content of the obsidian may be related to a number of factors, such as temperature of the conduit wallrock, viscosity of the melt, as well as velocity of magma within the conduit.

The Rotongaio phreatoplinian ash, a distinctive unit in the Taupo eruptive sequence (~0.2 ka) is composed almost entirely of fragmented obsidian (Wilson and Walker, 1985). The mean H_2O contents of bulk obsidian samples are uniform, and range from 0.21 to 0.34 wt%. The highest H_2O content measured in a single fragment was 0.58 wt.%. Wilson and Walker (1985) speculated that this deposit was produced by fragmentation of magma which was extruded during a break in the explosive activity of the Taupo eruptive sequence. However, the H_2O contents of the glass suggest that the obsidian quenched at depths of up to 350 m, so it may actually represent a still-hot conduit-filling plug or a cryptodome which subsequently fragmented by contact with external H_2O.

Chlorine in obsidian

The Cl contents of obsidian fragments also supports the hypothesis that obsidian represents partially degassed melt. For each eruption, the Cl contents of obsidian are invariably lower than that of melt inclusions (Fig. 5-11). The "near" equilibrium value of Cl for these melts at atmospheric pressure is not well known, however, old dome obsidian from the TVZ contains ~0.110 wt.% Cl, which suggests that the Cl is incompletely degassed from obsidian fragments in tephra.

The mean Cl and H_2O contents of obsidian from all tephra units show a rough correlation of increasing Cl with increasing H_2O (see Ch. 6 Fig. 5). This correlation seems to represent coupled degassing of H_2O and Cl.

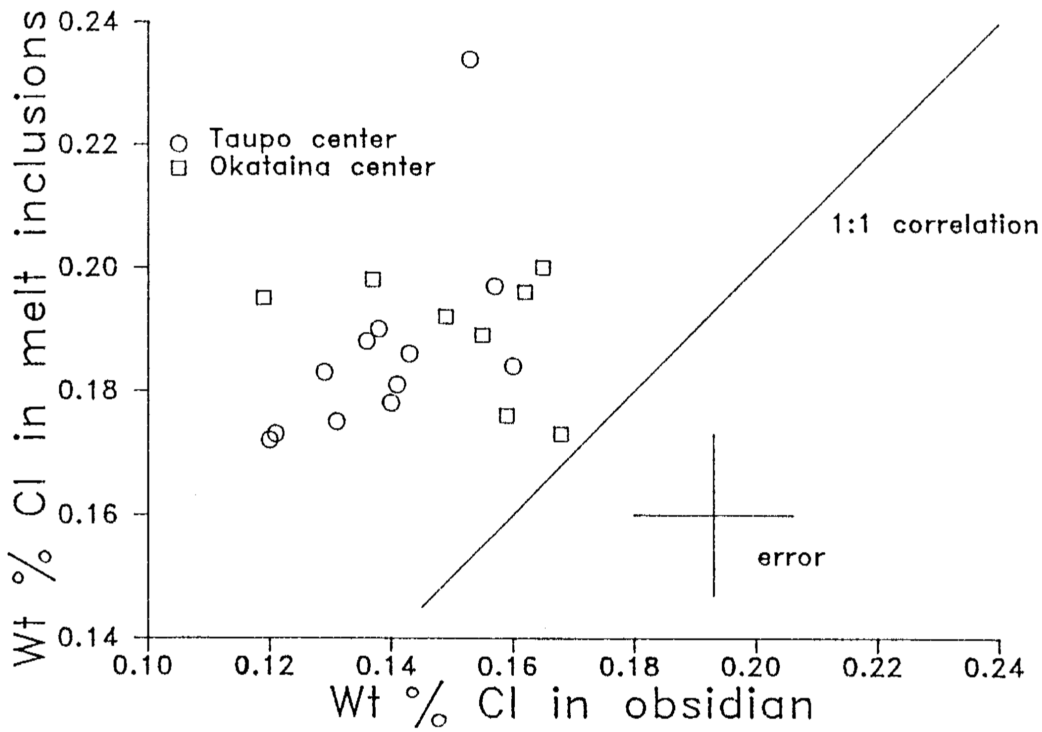

Figure 5-11. Cl contents of melt inclusions and obsidian from TVC and OVC tephra units as analysed by electron microprobe. A 1:1 correlation curve is shown. The average analytical error for the electron microprobe based on replicate analyses of standards (±0.013 wt%) is shown by error bars of figure.

Probably the degassing of Cl is dependent on H_2O degassing as there is a strong partitioning of Cl into a H_2O vapor phase (Kilinc and Burnham, 1972), and the Cl would partition into the H_2O-rich vapor phase. The partition coefficient of Cl between the melt and the H_2O-rich vapor phase can be calculated (wt % Cl in vapor/ wt % Cl in melt), and is 6 for the H_2O:Cl correlation seen in the Taupo volcanic center obsidian (see Ch. 6 Fig. 5). Webster and Holloway (1988) have shown experimentally that the partition coefficient of Cl between a melt and an H_2O-rich vapor phase is dependent on the melt composition, initial concentration of H_2O and Cl in the melt, and run time duration of the experiment, but that the partition coefficent for average rhyolites is generally between 2 and 10. Therefore, the co-efficients determined for TVC magmas are within reason. The true partition coefficient of Cl between TVC melts and a H_2O-rich vapor phase may be higher than that determined in this study, because time scale over which the degasssing occurred was the time of an explosive eruption, and is therefore relatively short.

The H_2O and Cl contents of obsidian from the OVC tephras alone do not define a curve which passes through the TVC melt inclusion points. This may be because the intial H_2O:Cl ratio of the OVC magmas is probably less homogeneous than that of the TVC magmas, based on the inhomogeneous versus homogeneous trace element chemistry of these two magma groups. If this were the case, and the Cl degasses from the OVC magmas with roughly the same partition coefficients as the TVC magmas, then the Cl and H_2O contents of the degassed OVC obsidian would be scattered, and not all fall along a roughly similar line.

The H_2O and Cl contents of melt inclusions from several Taupo Volcanic Center tephra units extend the obsidian H_2O:Cl data and fall on the same H_2O:Cl curve defined by obsidian (see Ch. 6 Fig. 5). The Okaia magma chamber (5.9 wt.% H_2O, 0.21 wt.% Cl) may have been at greater depth, and therefore higher pressure than the magma chamber from which the two less hydrous and younger tephras (Taupo and Hatepe plinian, 4.3 wt.% H_2O and 0.17 wt% Cl). This would imply that the magmas which produced these three tephras were near vapor saturation with respect to H_2O and Cl, but this is difficult to verify because there are no independent estimates of TVC magma chamber depths. However, experimental work on Cl solubility in silicic melts by Webster and Holloway (1988) suggests that the Cl contents determined for TVC melts represent approximate saturation values given that H_2O is saturated (pressure estimates of H_2O saturation made following Burnham (1975, 1979a and b)). In contrast, F contents of melt inclusions from these three tephras is invariant, and is far below saturation at around 400 ppm (Bailey, 1977). Based on the H_2O:Cl correlation and the known solubility curve for H_2O, a solubility curve for Cl in TVZ rhyolitic melts can be calculated, and is shown in Fig. 5-12.

Hydrogen isotopic composition of obsidian

In some cases, it is possible to evaluate degassing and other processes which occurred in a rhyolitic melt during eruptive degassing from the H isotopic composition of juvenile obsidian (Fig. 5-13). These processes include isotopic fractionation of H isotopes between a melt and vapor phase during degassing, high temperature equilibrium exchange between a melt and external H_2O, and low temperature alteration of a glass by external H_2O. Taylor et al. (1983) showed, based on H isotopic systematics, that the residual magmatic H_2O in obsidian was controlled by progressive in situ degassing during the eruptive process (Fig 5-14). Furthermore, their data suggest that this degassing occurred in an open, rather than closed system environment.

The same approach has been used for obsidian from the TVZ. However, due to the questionable nature of the data, interpretation of the results is difficult. Nevertheless, some trends can be discerned within samples run during individual analytical sessions. In general, there is a trend of decreasing δD values with

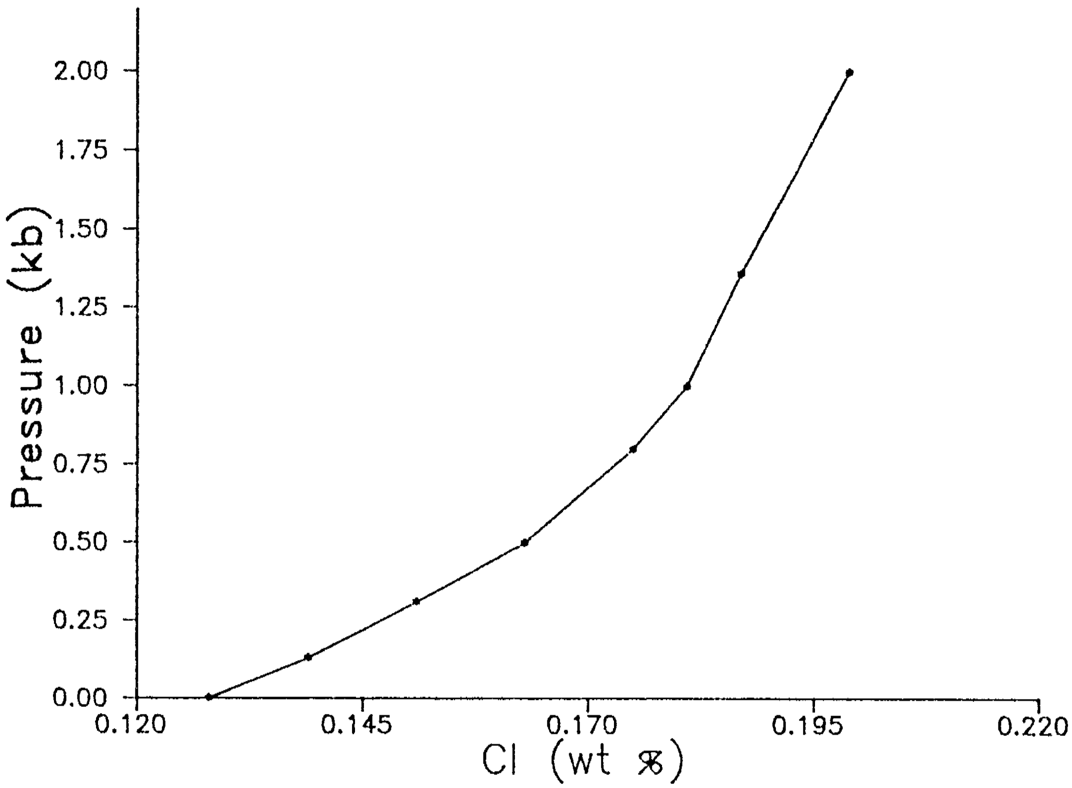

Figure 5-12. Cl solubility in an average TVZ rhyolite at 850°C. Calculations made by determining the quantity of Cl present at given H_2O contents from the Cl:H_2O correlation (Fig. 5-8), and then determining the pressure from the H_2O solubility curve calculated (Fig. 5-10).

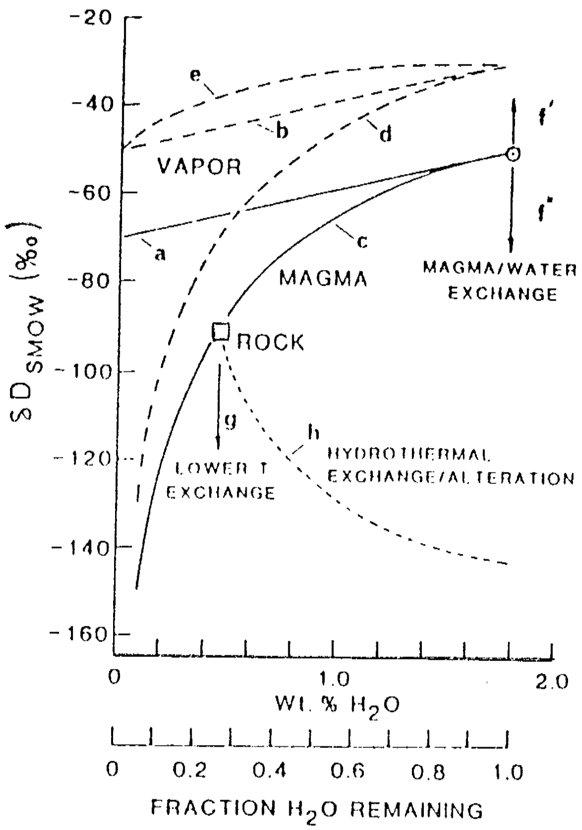

Figure 5-13. Variation of hydrogen isotopic compositions of vapor, melt and magmatic glass as a result of varying exchange and contamination processes. Curves a and b: closed system degassing. Curves c and D: open system degassing curves. Curves f and f': contamination/exchange; vapor-saturated magma contaminated with isotopically heavier H_2O (f') and with lighter (f). Curve g: low temperature exchange. Curve h: hydrothermal exchange/alteration. (From Taylor, 1986)

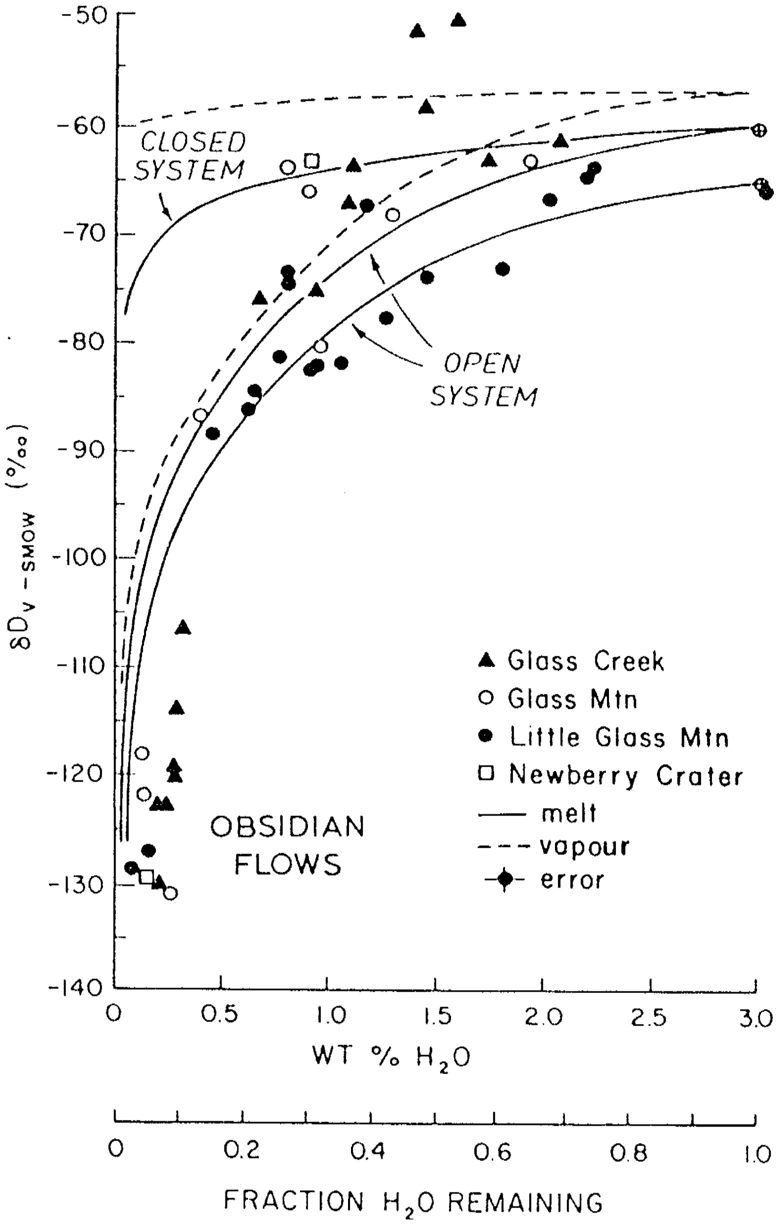

Figure 5-14. Hydrogen isotopic variation as a function of water contents for obsidian from eruptions in the Western U.S. Decrease in delta D can be seen with decreasing wt.% H_2O. Open and closed Raleigh distillation curves are shown for comparison, with initial delta D of -60 or -65 permil and 3 wt.% H_2O. Dashed lines indicate the compostion of exsolved water in the open and closed system cases. (From Taylor et al., 1983).

decreasing H_2O content of a glass (Fig. 5-5 to 5-7) which suggests Raleigh fractionation of hydrogen isotopes between the H_2O dissolved in the magma and a vapor phase occurred during degassing, prior to glass quenching (see general trends on Fig. 5-14, and specific open and closed system degassing trends calculated for Taupo magmas on Figs. 5-5 to 5-7). The shape of the trends seem closer to open system degassing than closed system, but as bulk obsidian samples were analysed rather than individual fragments, each point represents a mean of a number of individual H_2O and hydrogen isotopic values, so the curves are not well defined. Additional isotopic analysis, specifically of individual obsidian fragments, should clarify these problems, and allow defenite conclusions to be made.

7. ANALYSIS OF MELT INCLUSIONS

Melt inclusions are small samples of magma trapped in growing magmatic phenocrysts. These inclusions represent the best available samples of non-degassed magma prior to eruption (Roedder, 1984). Detailed analyses for major elements, some trace elements, H_2O, F and Cl were made of melt inclusions in phenocrysts from the Taupo eruptive sequence (2 ka BP) and the older Okaia tephra (>22 ka BP). These data are discussed in the following manuscript (p100 to 131) which has been submitted to Bulletin of Volcanology. Although this paper has several authors, the first author was primarily responsible for the analytical work, and conclusions drawn from the data, and therefore feels justified in including the manuscript in this thesis. General background on melt inclusions is given in this manuscript, and in Appendix G.

In addition to these analyses, melt inclusions from many other tephra units sampled were analysed for major elements and/or volatile element Cl. High-temperature-stage geothermometry was also performed on several melt inclusions from the Taupo plinian tephra. These data will be discussed following the melt inclusion manuscript.

Determination of pre-eruptive H_2O, F and Cl contents of silicic magmas using melt inclusions, examples from Taupo volcanic center, New Zealand

Nelia W. Dunbar[1]

Richard L. Hervig[2]

Philip R. Kyle[1]

[1]Department of Geoscience, New Mexico Institute of Mining and Technology, Socorro, NM 87801 USA

[2]Center for Solid State Science, Arizona State University Tempe, AZ 85287-1604 USA

Accepted by Bulletin of Volcanology

ABSTRACT

Water, F, and Cl contents of melt inclusions in phenocrysts from the 2-ka-old Taupo and Hatepe plinian tephras, and the ~22-ka-old Okaia tephra from the Taupo volcanic center, New Zealand, were measured by electron and ion microprobe. Major and trace element chemistry of the inclusions is similar to that of bulk rock, supporting our assumption that volatile contents of inclusions are representative of the magma in which the crystals grew. Inclusions in the 2 ka Taupo plinian tephra contain a mean of 4.3 wt% H_2O, 450 ppm F, and 1700 ppm Cl; from the Hatepe plinian tephra 4.3 wt% H_2O, 430 ppm F, and 1700 ppm Cl; and from the Okaia tephra 5.9 wt% H_2O, 470 ppm F, and 2100 ppm Cl. Sulfur was below the detection limit of 200 ppm. The constant H_2O, F and Cl from a number of stratigraphic horizons in the tephra deposits suggest that the Taupo and Hatepe plinian tephra (> 8.2 km^3 magma volume) were derived from a magma body that did not contain a strong volatile gradient. By inference, there is no pre-eruptive volatile difference between these plinian eruptions and a phreatoplinian eruption which occurred between the two. Virtually no major element zonation is seen in this eruptive sequence. Although the Okaia tephra was also erupted from the Taupo volcanic center, probably from a similar vent area, its higher volatile contents and distinct composition as

compared to the Taupo tephras show that it was derived from a different, and possibly deeper, magma body.

INTRODUCTION

Volatile components such as H_2O, Cl, and F strongly influence many properties of silicic melts, including crystallization temperatures, viscosity and density. However, the pre-eruptive volatile content of silicic magmas is difficult to estimate quantitatively, due partly to the lack of non-degassed volcanic material which can be analysed by conventional techniques. A number of approaches have been taken to estimate the pre-eruptive volatile content of melts, and have met varying degrees of success, as summarized by Clemens (1984).

Water, the dominant volatile in silicic systems, is also one of the most difficult to determine. Water in magmas is thought to strongly affect the eruption dynamics of the systems (Wilson et al., 1980), and is therefore an important parameter to determine accurately. Previous estimates of pre-eruptive magmatic water contents involve indirect methods, such as thermodynamic calculations or laboratory studies of mineral stabilities. The best available samples of non-degassed magma are melt inclusions in magmatic phenocrysts. These represent small samples of melt trapped during crystal growth (Roedder, 1984). If unaltered, the inclusions may be representative of the major, trace and volatile element chemistry of pre-eruptive magma. Only a few attempts at direct measurements of H_2O in melt inclusions have been made (Anderson, 1974; Harris, 1981; Rutherford et al., 1985; Sommer and Schramm, 1983).

Gradients of H_2O and halogens are thought to develop in many silicic magma chambers greater than 1 km^3, resulting in density gradients that affect magma chamber eruption dynamics (Hildreth, 1981; Blake and Ivey, 1986). Formation of volatile gradients and oversaturation of the uppermost regions of magma chambers may be a mechanism for triggering explosive eruptions (Blake, 1984). Although the mechanism which creates volatile gradients is not firmly established, it may be similar to that which generates trace element zonation (Hildreth, 1981).

The objective of this study was to estimate volatile contents of rhyolitic magmas that produced a series of explosive eruptions. Based on these determinations, pre-eruptive volatile zonation within the rhyolitic magma chambers in the Taupo area, New Zealand was assessed, and the volatile contents of the melts related to the nature of the eruptions which they produced. We determined H_2O and F by ion microprobe, and Cl by electron microprobe in melt inclusions within magmatic phenocrysts from these rhyolites.

BACKGROUND

Taupo Volcanic Zone

The central portion of the Taupo Volcanic Zone, in the North Island of New Zealand, is composed of 7 or more caldera-like structures (Wilson et al., 1986). One of the calderas, the Taupo volcanic center (TVC) (Fig. 1) has produced numerous explosive, rhyolitic eruptions over the last 50 thousand years (ka) (Wilson et al., 1984). In this study, we have sampled melt inclusions from three plinian tephras erupted from the TVC (Fig. 2). The first two, the Taupo and Hatepe plinian tephras, are part of the eruptive sequence which occurred 2 ka ago (Fig. 2). This sequence consists of the Initial ash, having a magma volume (MV) of 0.005 km^3, the Hatepe plinian pumice (1.4 km^3 MV), the Hatepe phreatoplinian ash (1.0 km^3 MV), the Rotongaio ash (0.7 km^3 MV) and the Taupo plinian pumice (5.1 km^3 MV) (Wilson and Walker, 1985) (Fig. 2). These were followed by eruption of the Taupo Ignimbrite (10 km^3) (Wilson and Walker, 1985). Between the beginning of the Hatepe plinian phase and the end of the Taupo plinian phase approximately 8.2 km^3 of magma were erupted.

The third unit studied, the Okaia tephra, was erupted at about 22-24 ka ago from the Taupo volcanic center and has an estimated magma volume of approximately 3.5 km^3 (Wilson et al., 1986). Although the vent position for this eruption is not precisely located, it is thought to be within Lake Taupo (Fig. 1) (Wilson et al., 1984). The trace element composition of the Okaia tephra is different from the younger units, and the phenocryst assemblage of the Okaia tephra contains quartz and amphibole as well as pyroxene and plagioclase, which are dominant phenocrysts in the Taupo and Hatepe plinian tephras (Howorth, 1976; Froggatt, 1982). Thus, the Okaia tephra was derived from a chemically distinct magma (Dunbar et al., in prep.). The Okaia was examined because the occurrence of amphibole can imply higher water pressure (Naney, 1983).

ANALYTICAL METHODS

Sample preparation

The tephra units from the TVC and stratigraphic position of relevant samples are shown in Fig. 2. Phenocrysts were hand-picked from bulk tephra samples collected at various stratigraphic horizons of the tephra. The phenocrysts were mounted in epoxy and polished with diamond grit. Samples were examined with reflected light to determine if inclusions were exposed.

Electron microprobe

Major element analyses of melt inclusions were performed using a JEOL-733 microprobe with accelerating voltage of 15 kV, beam current of 8 nA, and data reduction techniques of Bence and Albee (1968), and a defocussed beam (20 microns) to reduce to insignificance the problem of Na migration from the glass.

Electron microprobe analyses of Cl were made using the instrumental settings described above, but a different data reduction technique. Extended counting times were used on the peak (150 s.) and two background positions (75 s.). Standards used were natural comendite and pantellerite glasses: KN-18 (Cl=3100 ppm) and KE-12 (Cl=3400 ppm) (H.Sigurdsson, pers. comm., 1984). The estimated standard deviation for Cl analysis is $\pm$130 ppm, based on replicate analyses of a single Cl standard (n=26). Some of this variability may be due to inhomogeneity of the standard because replicate analyses of melt inclusions gave analytical precision as good as $\pm$0.005 wt%.

Ion microprobe

The technique of ion microprobe analysis of melt inclusions for volatile components H_2O and F, and trace elements is described in detail in Hervig et al. (1988) A Cameca IMS 3f ion microprobe was operated at constant conditions, using both negative and positive ions. Primary

$^{16}O^-$ ions were generated in the Cameca duoplasmatron, and mass analysed to eliminate H ions. The primary beam was focussed to a spot approximately 20 microns in diameter, striking the sample with 17 keV impact energy.

Standards with compositions similar to the Taupo rhyolites were selected to reduce the problem of matrix effects. These included hydrous rhyolite glass synthesized at Sandia National Laboratory and at Arizona State University, an A-type granite which had been ground, melted and quenched to a glass, and material from the Macusani lava flow in Peru. These standards have been been well analysed for H_2O, F, and/or trace element concentrations (London et al., 1987; Stanton et al., 1985; Westrich, 1987).

A typical calibration curve from an ion microprobe analytical session, in this case for H_2O, is shown in Fig. 3. Estimated total errors based on replicate analyses are $\pm$0.5 wt % for H_2O, $\pm$100 ppm for F, and $\pm$15-20% for trace elements.

Results

General observations

In the TVC tephra, inclusions are most abundant in pyroxene phenocrysts, but also occur in plagioclase, quartz, magnetite and, rarely, in amphibole. The largest inclusions are about 100 microns in diameter, but commonly range from 40 to 60 microns. The inclusions generally have a negative crystal shape, and contain clear to light-brown glass. Inclusions that contain shrinkage bubbles are rare, and were avoided in the analyses because it is possible for melt volatiles to partition into these void spaces. However, because bubbles can be polished away during sample preparation, the contents of some bubbles were examined by crushing inclusion-bearing phenocrysts in oil. No release of vapor was detected. Back-scattered electron imaging shows that inclusions are homogeneous, and the crystal/glass interface is sharp, without signs of recrystallization or resorption (Fig. 4).

Major element chemistry

The pristine nature of melt inclusions has been confirmed by comparing their major and trace element compositions with pumice, thought to represent bulk magma composition. Over 100 major element analyses of melt inclusions from a number of tephra units were made. The close agreement of representative inclusion analyses (Table 1) suggest that the inclusions reflect the pre-eruptive melt composition at the level in the magma chamber from which the pumice was extracted. Major element compositions of inclusions in pyroxene and magnetite host crystals from the Hatepe plinian tephra (pyroxene and magnetite) are nearly indistinguishable from the bulk pumice composition

(Table 1). The difference between the Ba contents of pumice and melt inclusions in pyroxene may be due to removal of Ba from the melt by crystallization prior to pyroxene crystallization. This is difficult to test as the Ba content of the plagioclase is not known. Post-entrapment crystallization of host crystal has not occurred on the inclusion walls, because it would lead to divergent glass compositions in different phenocryst types (Watson, 1976). The phenocryst content of the magmas is low (~3-5 %), suggesting that the volatile content remained constant throughout crystallization.

Volatile chemistry

Inclusions in pyroxene, plagioclase or quartz were analysed for H_2O, F and Cl in each of the tephra units. Sulfur was also analysed, and values were all below the electron microprobe detection limits of 200 ppm. Sulfur was determined to be ~50 ppm by Palais and Sigurdsson (1988). Additional samples from the Taupo and Hatepe plinian units were analysed only for Cl.

Results of H_2O, F and Cl analyses are given in Table 2. Stratigraphic unit mean values are listed as well as values for individual samples. The mean values for the Taupo plinian tephra are 4.3 wt% H_2O and 450 ppm F and for the Hatepe plinian tephra are 4.3 wt% H_2O and 430 ppm F. These values are identical within the estimated analytical error of

~0.5 wt% H_2O and 100 ppm F. Melt inclusions in the Okaia tephra contain 5.9 wt% H_2O and 470 ppm F. The H_2O value is statistically higher than the two younger tephras, although the F content is similar.

The Cl values (Table 2) are listed as mean values for individual samples within the three tephra units. There does not appear to be any systematic variation in Cl within or between the Taupo and Hatepe plinian tephra units within the analytical error of ~7%. Values range between 1680 and 1770 ppm Cl, and the mean value for both units is 1700 ppm Cl. Melt inclusions in 2 other tephras from the Taupo sequence, the Initial ash and the Hatepe phreatoplinian ash, were also analysed for Cl, and both contain 1700 ppm Cl. The mean Cl content of melt inclusions in the Okaia tephra, however, is 2100 ppm, statistically higher than that of the younger tephras. In the Okaia tephra Cl content of melt inclusions in pyroxene and quartz were similar; 2100 and 2010 ppm respectively.

In some cases the variation of H_2O and F contents of inclusions within a single crystal, or even of two points within a single inclusion, was greater than the analytical reproducibility seen for replicate analyses of standards. The variation in H_2O content of inclusions may be due to small-scale volatile inhomogeneities, or to post-entrapment phenomenon. Low H_2O and F values, particularly in the case of small inclusions, could be caused by overlap of the ion beam onto the host crystal. There did not appear to be any systematic gradients of H_2O, F or Cl within crystals, such as higher volatile contents in inclusions located in the core or the rim of a crystal. No Cl gradients were seen within individual inclusions (systematic core to rim analyses within a single inclusions were only possible with the electron probe).

Discussion

Volatile contents and gradients

The H_2O contents of rhyolitic magmas, which produced these three explosive eruptions, are 4.3, 4.3 and 5.9 wt%. The H_2O determinations are similar to H_2O saturation values determined for a rhyolitic melt by Naney (1983) based on their phenocryst assemblages and Fe-Ti oxide temperatures. The rhyolite in Naney's experiment was of similar composition and temperature to Taupo and was subjected to 2 kb pressure, which is close to the pressure of the Taupo magma chamber (Ewart et al., 1975). These determinations are also compatible with other direct estimates of volatile contents in rhyolitic melts which have produced explosive eruptions (Druitt et al., 1982, Devine et al., 1984, Sommer and Schramm, 1983, Taylor et al, 1983), as well as to experimental and analytical determined H_2O contents of Mount St. Helens dacite (Rutherford et al., 1985). Estimates of

H_2O in a Taupo magma based on phenocryst assemblages are between 5 and 8 wt% (Ewart et al., 1975).

There appears to be no difference in mean H_2O, F, and Cl content of the magma which produced the Taupo plinian (5.1 km^3 DRE) and Hatepe plinian tephras (1.4 km^3 DRE). Detailed Cl analyses for a number of stratigraphic horizons of these two tephra show no systematic variation. Melt inclusions from two other tephra from the same eruptive sequence, the Initial ash and the Hatepe phreatoplinian ash, contain 1700 ppm Cl. The similarity between all of these values indicates a lack of large-scale Cl zonation. Similarly, the analysed H_2O and F contents of melt inclusions from the Taupo and Hatepe plinian tephra show no evidence for strong compositional zonation with stratigraphic height, although less data are available. Water and Cl have been analysed in obsidian clasts (Dunbar et al., in prep) which are thought to represent partially degassed melt (Taylor et al., 1983). When these data are combined with the inclusion analyses, they show a correlation between H_2O and Cl (Fig. 4). The correlation of the obsidian data alone has a similar "m" value to that shown in Fig. 4, although the "r" value is lower. Using the correlation we can infer the H_2O contents in TVC rhyolitic magmas using measured Cl contents. Homogeneity of Cl from detailed analyses from the 2 ka Taupo eruptive sequence indicate a lack of strong H_2O zonation, consistent with their uniform trace element concentrations

(Dunbar et al., in prep).

Our conclusion that no steep volatile zonation was present in the 2 ka Taupo eruption magma chamber rests on two assumptions. First, a volatile zonation in the magma chamber did not develop after the entrapment of inclusions. If a volatile gradient formed after crystal entrapment, the volatiles would be concentrated in the upper part of the magma chamber, leading to crystal resorption. However, phenocrysts in the Taupo tephras show no evidence of resorption, so we consider that no post-crystallization volatile gradient developed. Secondly, we assume that the small variation of volatile contents of melt inclusions within a single stratigraphic horizon do not represent a volatile gradient which was disturbed during the eruption. The variation in volatile contents between melt inclusions in a single crystal are as large as the variation between melt inclusions in different crystals. This does not support the existence of a steep volatile gradient which was disturbed during eruption.

The Okaia tephra has higher melt H_2O and Cl, but similar F contents compared to the two younger tephras. Pumice from the Okaia tephra differs from the Taupo and Hatepe plinian tephras in trace element composition, temperature and oxygen fugacity (Dunbar et al., in prep). The different H_2O and Cl contents of the Okaia melt inclusions reflect a different source for this older magma.

A minimum depth can be estimated for the two magma chambers using Burnham's (1975, 1979) solubility model of H_2O versus pressure for a typical Taupo rhyolite. H_2O saturation depth of the Taupo and Hatepe plinian magmas would be at ~4 km whereas for Okaia tephra it would be ~2 km deeper, at ~7 km, using a magma density of 2.3 g/cm^3. However, no geophysical evidence is available to constrain these depth estimates to anything better than a minimum value.

Volcanological implications

A number of volcanological implications can be drawn from this study, particularly regarding eruption dynamics and volatile outputs during the eruptions.

The lack of a strong volatile gradient in the 2 ka eruption magma contrasts with that postulated for many magma chambers (Hildreth, 1981). Furthermore, the lack of a volatile gradient in this magma indicates that the 2 ka Taupo eruption was probably not initiated solely by the development of a volatile-rich roof zone which became oversaturated and began to vesiculate. Tectonic activity within the Taupo volcanic zone magma have played an important role.

In the Taupo eruptive sequence, there appears to be no difference in pre-eruptive volatile contents of melts that produce plinian or phreatoplinian eruptions, based on the Cl contents of these melts. The Taupo and Hatepe plinian tephras bracket the 1-km^3-MV Hatepe phreatoplinian ash. The pre-eruptive magmatic Cl contents of the Taupo and Hatepe plinian tephras, and the Hatepe phreatoplinian tephra were identical. By inference, the pre-eruptive H_2O content of the Hatepe phreatoplinian tephra was probably the same as well. This suggests that the eruptive difference between phreatoplinian and plinian tephras was not due to any differences in the pre-eruptive volatile content of their magmas, but rather entirely to magma/water interaction (Wilson, 1980).

Ignimbrite eruptions are generally thought to be initiated by the collapse of a plinian column, either due to a decrease of magmatic volatiles, or to changes in vent geometry (Wilson, 1980). Eruption of the Taupo ignimbrite (10 km^3 of magma) interrupted the eruption of the Taupo plinian tephra. The lack of evidence for a strong decrease in volatile contents towards the end of the Taupo plinian phase implies that the onset of the Taupo Ignimbrite was probably due to a change in vent geometry. This conclusion was also reached by Wilson and Walker (1985), based on other evidence.

Finally, the minimum eruptive output of the volatile components H_2O and Cl during the Taupo, Hatepe and Okaia tephra eruptions can be calculated based on the initial volatile content of the melt, the post-degassing volatile content of the tephra, and the mass of erupted material (Devine et al., 1984). In this case, the H_2O content of the degassed pumice is assumed to be the near atmospheric equilibrium value of H_2O in rhyolitic glass, 0.2 wt% (Eichelberger and Westrich, 1981, Eichelberger et al., 1986). No information is available on atmospheric equilibrium content of Cl in rhyolitic glass, so the intercept from Fig. 5 is used (1290 ppm Cl). Values are shown in Table 3. The mass of H_2O and HCl output for the Taupo plinian tephra are respectively 4.9×10^{14}g and 4.0×10^{12}g, for the Hatepe plinian 1.3×10^{14}g and 1.8×10^{12}g, and for the Okaia tephra 4.6×10^{14}g H_2O and 6.5×10^{12}g Cl.

The climatic impact of the 2 ka Taupo eruption sequence was probably minor because the emission of acid aerosols was small. The S contents of melt inclusions is low (<200 ppm) thus precluding significant production of H_2SO_4 in the atmosphere. The Taupo and Hatepe plinian eruptions together produced about 6×10^6 tonnes of HCl, insignificant when compared to estimates of 220×10^6 tonnes of HCl produced by the 1815 eruption of Tambora (Devine et al., 1984).

Conclusions

Determinations of volatile components in melt inclusions from the Taupo and Hatepe plinian, and Okaia tephras erupted from the Taupo Volcanic Zone yield mean H_2O contents of 4.3, 4.3, and 5.9 wt%, F contents of 450, 430, and 470 ppm; and Cl contents of 1700, 1700, and 2100 ppm for the three units respectively. These values are thought to represent direct measurements of the volatile composition of Taupo magmas. The mean volatile contents of the Taupo and Hatepe plinian melts are identical within analytical uncertainty, and stratigraphic samples through these two units show no systematic variation with respect to Cl. Thus, there is no support for the presence of a steep volatile zonation in the 8.7 km^3 of magma erupted from the beginning of the Hatepe plinian eruption to the end of the Taupo plinian eruption. The higher volatile content of the Okaia tephra may indicate derivation from deeper crustal levels.

Acknowledgements

Thanks to C.J.N. Wilson for assistance in the field and continued discussion, to K. Palmer and J. Gamble for use of the microprobe facility at Victoria University, Wellington, N.Z., to H. Sigurdsson for a number of microprobe standards, and to J. Eichelberger, P. Sylvester, and H. Westrich for helpful reviews. This research was in part supported by the Department of the Interior's Mineral Institutes program administered by the Bureau of Mines under allotment grant number G1164135.

Table 1. Major and trace element composition, expressed as oxides, of melt inclusions (MI) in pyroxene, and magnetite as compared to pumice from the Hatepe plinian tephra. Analyses are normalized to 100%, setting Na_2O content to 4 wt% due to the volatilization problems encountered with hydrous glass. Average counting errors to 1 sigma are as follows (wt% for major elements, ppm for trace elements): SiO_2 $\pm$0.9, Al_2O_3 $\pm$0.4, FeO $\pm$0.2, TiO_2 $\pm$0.1, CaO $\pm$0.1, K_2O $\pm$ 0.4, Rb $\pm$9, Ba $\pm$40, La $\pm$0.3, Ce $\pm$1.1, Sm $\pm$0.1.

	Oxide (wt%)							Element (ppm)				
Sample	SiO_2	TiO_2	Al_2O_3	FeO	CaO	Na_2O	K_2O	Rb	Ba	La	Ce	Sm
MI in pyx.	76.2	0.3	12.7	2.3	1.3	4.0	2.8	99	380	26	62	6
MI in magn.	76.8	0.7	12.5	2.0	0.9	4.0	3.0					
pumice	76.2	0.3	13.0	1.8	1.4	4.0	3.0	93	580	24	55	6

Note: Major elements for all samples are analysed by electron microprobe, trace elements in pumice are analysed by neutron activation, and trace elements in melt inclusion are analyed by ion microprobe.

Table 2. H_2O and F and Cl contents of the Taupo plinian, Hatepe plinian and Okaia eruptions as analysed by ion and electron microprobe. Samples are listed in correct stratigraphic order (see Fig. 1). In one case two different phenocryst types are listed under a single sample number. Value of "n" is the same for H_2O and F. The standard deviation of the number of analyses ("n") is given as S.D. Average errors are discussed in text.

Sample #	H_2O		F			Cl		
	wt.%	S.D.	ppm	S.D.	n	wt.%	S.D.	n
Taupo plinian								
157	3.9	0.3	500	80	3	0.17	.014	6
155						0.18	.014	5
154						0.17	.015	8
015	4.5	0.8	430	140	10	0.18	.006	6
total mean	**4.3**	**0.8**	**450**	**60**	**13**	**0.17**	**.013**	**25**
Hatepe phreatomagmatic								
003						**0.18**	**.007**	**4**
Hatepe plinian								
112	4.9	1.0	430	10	3	0.17	.025	6
110						0.17	.016	6
108	4.1	0.5	430	130	5	0.18	.006	4
027						0.17	.005	2
total mean	**4.3**	**0.8**	**430**	**140**	**8**	**0.17**	**.016**	**18**
Initial ash								
044						**0.17**	**.010**	**6**
Okaia								
047 pyx	5.6	0.8	460	120	3	0.21	.024	7
047 qtz	6.1	0.5	480	120	5	0.20	.020	5
total mean	**5.9**	**0.6**	**470**	**110**	**8**	**0.20**	**.022**	**12**

Table 3. Atmospheric input of H_2O and Cl for the Taupo, Hatepe and Okaia tephra eruptions. Density of the melt in calculations is 2.3 g/cm^3. Degassed H_2O values are the atmospheric equilibrium value of H_2O in rhyolite glass (Eichelberger et al., 1981). Degassed Cl values are the Cl content of obsidian from these eruptions.

Tephra unit	Volume (DRE) (cm^3)	Mass (g)	Initial H_2O (wt%)	Degassed H_2O (wt%)	Initial Cl (wt%)	Degassed Cl (wt)	Output H_2O (g)	Output HCl (g)
Taupo plinian	$5.1x10^{15}$	$1.2x10^{16}$	4.3	0.2	0.173	0.129	$4.9x10^{14}$	$5.5x10^{12}$
Hatepe plinian	$1.4x10^{15}$	$3.2x10^{15}$	4.3	0.2	0.173	0.129	$1.3x10^{14}$	$1.5x10^{12}$
Okaia	$3.5x10^{15}$	$8.1x10^{15}$	5.9	0.2	0.207	0.129	$4.6x10^{14}$	$6.5x10^{12}$

Figure Captions

1. Map of the Taupo center. Symbol 1 represents the caldera margins as mapped by surface geology. The vent indicated on the figure is the vent for the 2 ka Taupo eruption. The vent for the Okaia eruption is thought to be within the lake area, but is not precisely located. After Wilson et al., 1984.

2. Plinian and phreatoplinian tephra units of the Taupo center plotted versus age, including a detailed representation of the Taupo sequence, erupted at 0.2 ka. The indicated thickness in the detailed representation of the Taupo sequence is proportional to the magma volume of that unit. Sample numbers and stratigraphic position of samples are indicated on the detailed Taupo sequence and the Okaia tephra. Volumes indicated are dense rock equivalent.

3. Ion microprobe calibration curve for H_2O (positive H^+ ions) in experimentally hydrated rhyolitic glasses. Secondary H^+ ion are normalized to count rates for doubly charged ^{28}Si.

4. Electron-backscatter-image photo of melt inclusion in pyroxene from the Taupo plinian tephra. Grey level intensity indicates different mean atomic number of the sample surface. The consistent shade throughout the inclusion indicates consistent composition. Scale: 8 mm on photo represents 10 microns.

5. Cl versus H_2O for melt inclusions from the Taupo, Hatepe, and Okaia plinian tephras and obsidian from the Taupo volcanic center. H_2O in obsidian was determined by Karl Fischer titration (Westrich, 1987). Analytical errors shown on figure are based on standard deviations from multiple analyses of standards. Cl in both obsidian and melt inclusions was determined by electron microprobe. H_2O in melt inclusions was determined by ion microprobe. Obsidian data is from Dunbar (unpublished).

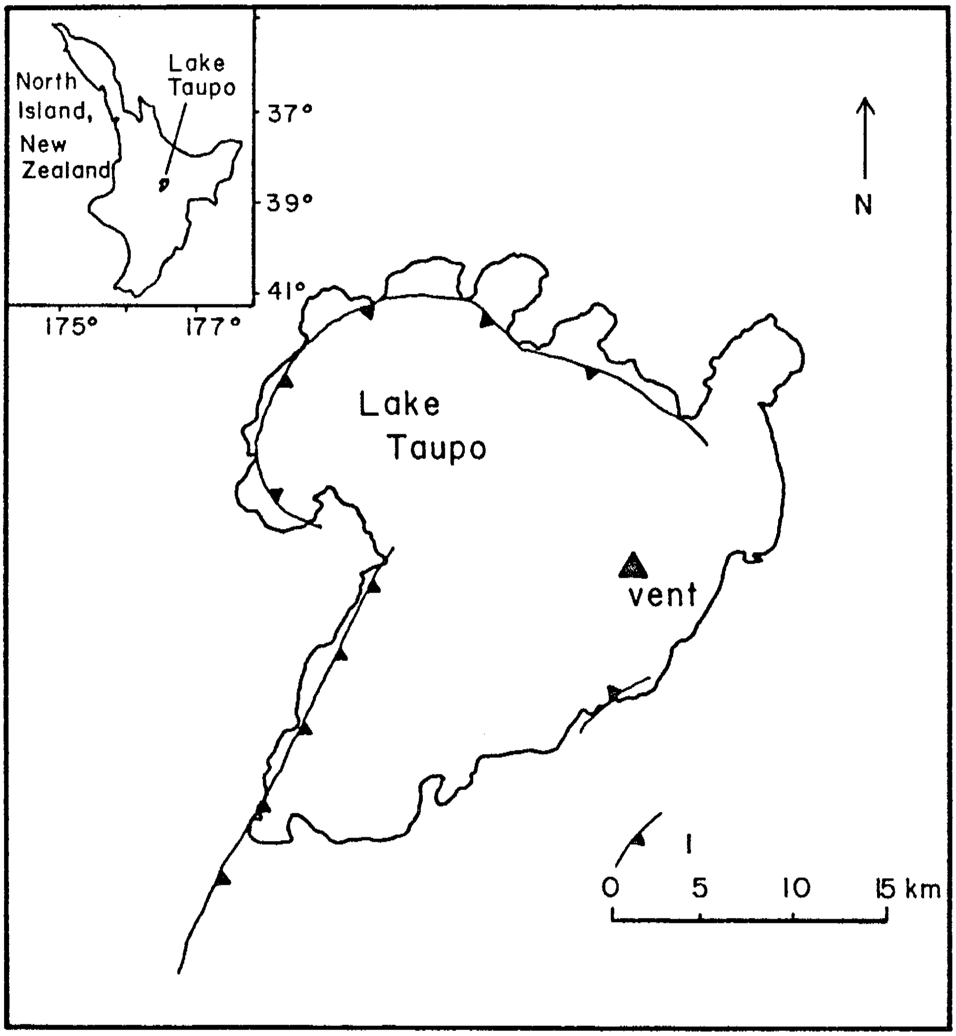
North Island, New Zealand
Lake Taupo
37°
39°
41°
175°
177°
N
Lake Taupo
vent
1
0 5 10 15 km

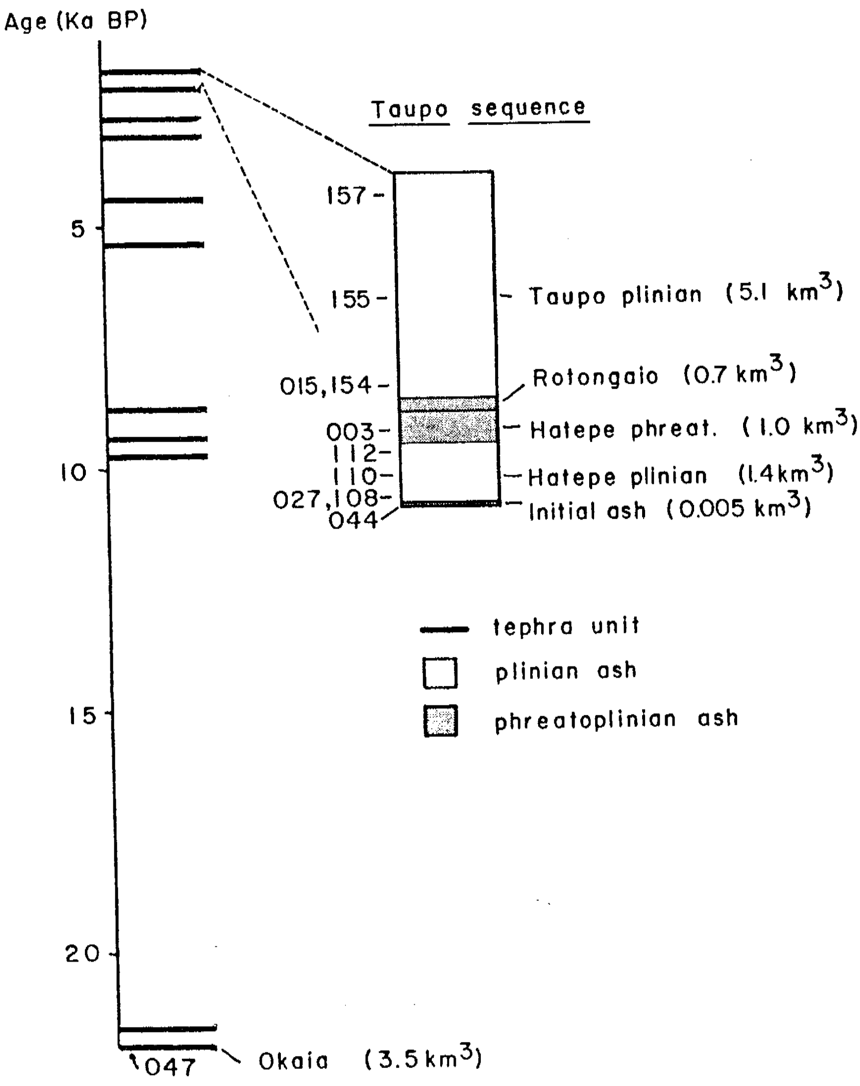
Age (Ka BP)
5
10
15
20
047
Okaia (3.5 km3)
Taupo sequence
157
155
015,154
003
112
110
027,108
044
Taupo plinian (5.1 km3)
Rotongaio (0.7 km3)
Hatepe phreat. (1.0 km3)
Hatepe plinian (1.4km3)
Initial ash (0.005 km3)
tephra unit
plinian ash
phreatoplinian ash

Fig. 2

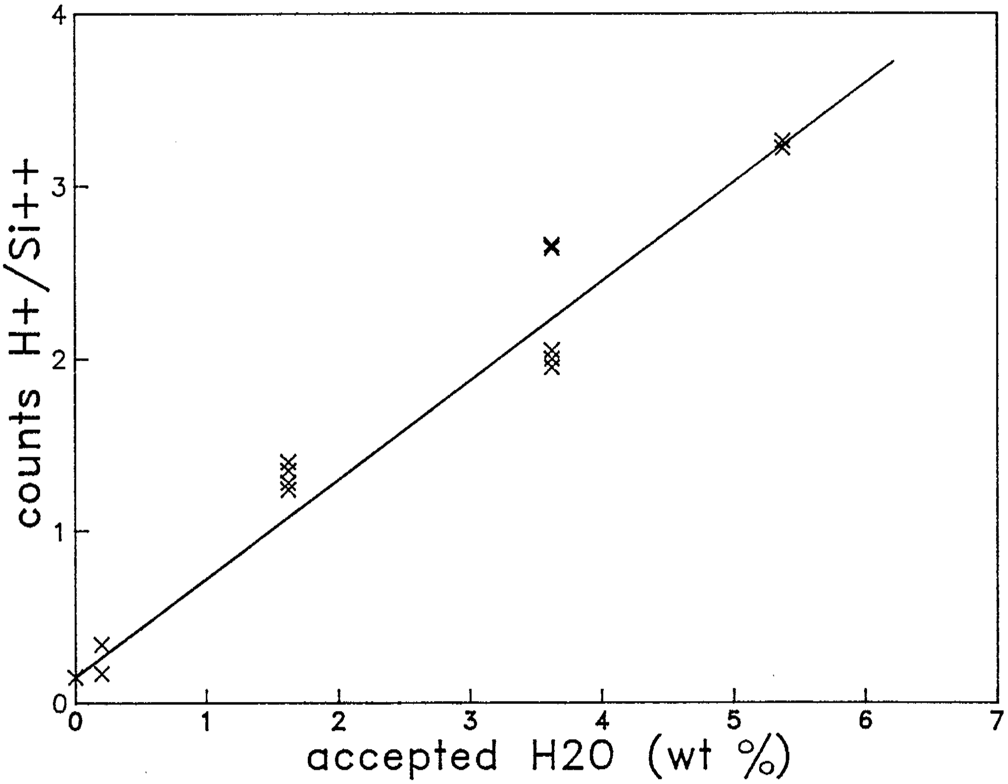
counts H+/Si++
accepted H2O (wt %)
0
1
2
3
4
5
6
7
0
1
2
3
4

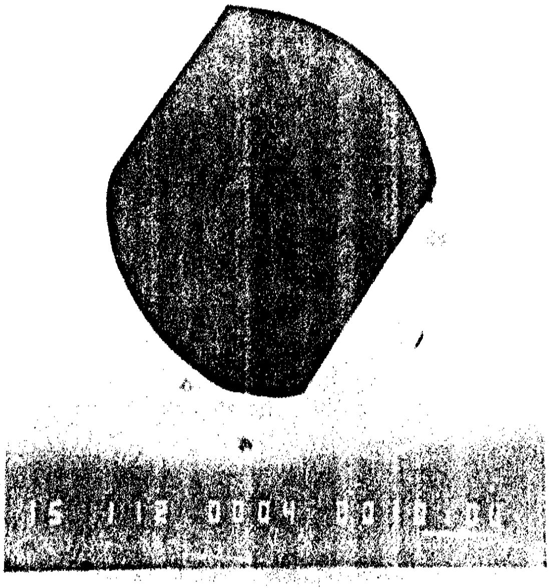

Fig. 4

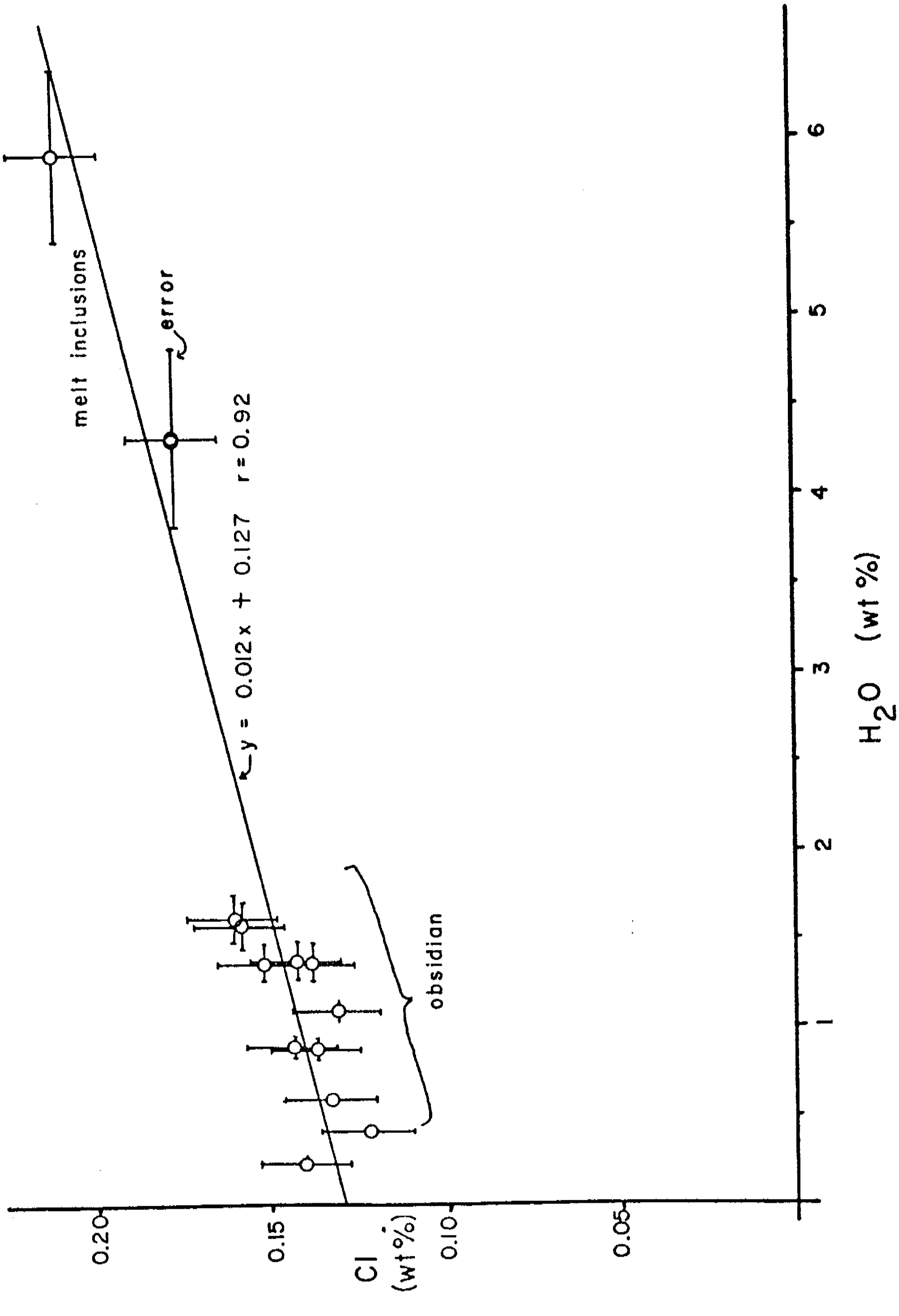
melt inclusions
error
y = 0.012x + 0.127   r = 0.92
obsidian
Cl (wt %)
0.20
0.15
0.10
0.05
H_2O (wt %)
1
2
3
4
5
6

References Cited

Anderson, A.T. (1974) Chlorine, sulfur and water in magmas and oceans. Geol Soc Bull 85: 1485-1492

Blake, S. (1984) Volatile oversaturation during evolution of silicic magma chambers as an eruption trigger. J Geophys Res 89, B10: 8237-8244

Blake, S., and Ivey, G.N. (1986) Density and viscosity gradients in zoned magma chambers, and their influence on withdrawal dynamics. J Volcanol Geotherm Res 30: 201-230

Bence, A.E., and Albee, A.L. (1968) Empirical correction factors for the electron microanalysis of silicates and oxides. J Geol 76: 382-403

Burnham, C.W. (1975) Water and magma; a mixing model. Geochim Cosmochim Acta 39: 1077-1084

Burnham, C.W. (1979) Importance of volatile constituents. In: Evolution of igneous rocks, 50 anniversary perspectives (H.D. Yoder, ed). Princeton Univ. Press, Princeton, N.J. pp 439-482

Clemens, J.D. (1984) Water contents of silicic to intermediate magmas. Lithos 17: 273-287

Devine, J.D., Sigurdsson, H., and Davis, A.N. (1984) Estimates of sulfur and chlorine yield to the atmosphere from volcanic eruptions and potential climatic effects. J Geophys Res 89: 6309-6325

Druitt, T.H., Anderson, A.T., and Nagle, F. (1982) Water in rhyolitic magma, Bishop, California. EOS 63: 451

Dunbar, N.W., and Kyle, P.R., and Wilson, C.J.N. Evidence for non-zoned silicic magma chambers, Taupo Volcanic Zone, New Zealand. (MS in prep)

Eichelberger, J.C., Carrigan, C.R., Westrich, H.R., and Price R.C., 1986. Non-explosive silicic volcanism. Nature, 323, 589-602.

Eichelberger, J.C. and Westrich, H.R. (1981) Magmatic volatiles in explosive rhyolitic eruptions. Geophys Res Let 8: 757-760

Ewart, A., Hildreth, W., and Carmichael, I.S.E. (1975) Quaternary acid magma in New Zealand. Contr Mineral Petrol 51: 1-27

Froggatt, P.C. (1982) A study of some aspects of the volcanic history of the Lake Taupo area, North Island, New Zealand. Ph.D. thesis, Victoria University of Wellington, New Zealand

Harris, D.M. (1981) The microdetermination of H_2O, CO_2, and SO_2 in glass using a 1280°C microscope heating stage, cryopumping, and vapor pressure measurements from 77 to 273 K. Geochim Cosmochim Acta 45: 2023-2036

Hervig, R.L., Dunbar, N.W., Westrich, H., and Kyle, P.R. (1988) Pre-eruptive water content of some rhyolitic magmas as determined by ion microprobe analyses of melt inclusions in phenocrysts. J Volcanol Geotherm Res (in press)

Hildreth, W. (1981) Gradients in silicic magma chambers: Implications for lithospheric magmatism. J Geophys Res 86, B11: 10153-10152

Howorth, R. (1976) Late Pleistocene tephras of the Taupo and Bay of Plenty regions. Ph.D. thesis, Victoria University, Wellington, New Zealand

London, D., Morgan, G.B., and Hervig, R.L (1987) Element partitioning and fractionation trends in volatile and LILE-rich rhyolite. Eos 68: 450

Naney, M.T. (1983) Phase equilibria of rock-forming ferromagnesian silicates in granitic systems. Am J Sci 283: 993-1033

Palais, J. and Sigurdsson, H. (1988). Petrologic evidence of volcanic emissions from major historic and pre-historic eruptions. Contributions of Geophysics to Climate change studies (eds. A. Berger and R. Dickenson) AGU Geophys Mono 15: in press

Roedder, E. (1984) Fluid Inclusions. Reviews in Mineralogy (ed. Paul H. Ribbe). Am Mineral Soc 12: 473-502

Rutherford, M.J., Sigurdsson, H., Carey, S., and Davis, A. (1985) The May 18, 1980 eruption of Mount Saint Helens 1. Melt compositon and experimental phase equilibria. J Geophys Res 90: 2929-2947

Sommer, M.A. and Schramm, L.S. (1983) An analysis of the water concentrations in silicate melt inclusions in quartz phenocrysts from the Bandelier Tuff, Jemez Mountains, New Mexico. Bull Volcanol 46: 299-320

Stanton, T.R., Holloway, J.R., Hervig, R.L., and Stolper, E. (1985) Isotope effect on water diffusivity in silicic melts: an ion microprobe and infrared analysis Eos 66: 1131

Taylor, B.E., Eichelberger, J.C., and Westrich, H.R. (1983) Hydrogen isotopic evidence of rhyolitic magma degassing during shallow intrusion and eruption. Nature 306: 541-544

Watson, E.B. (1976) Glass inclusions as samples of early magmatic liquid: determinative method and application to a South Atlantic basalt. J Volcanol Geotherm Res 1: 73-84

Westrich, H.R. (1987) Determination of water in volcanic glasses by Karl Fischer titration. Chem Geol 63: 335-340

Wilson, C.J.N., Houghton, B.F., and Lloyd, E.F. (1986) Volcanic history and evolution of the Maroa-Taupo area, Central North Island. Royal Society of New Zealand, Bull 23: 194-223

Wilson, C.J.N., Rogan, A.M., Smith, I.E.M., Northey, D.J., Nairn, I.A., and Houghton, B.F. (1984). Caldera volcanoes of the Taupo Volcanic Zone, New Zealand. Jour Geophys Res 89: 8463-8484.

Wilson, C.J.N., and Walker, G.P.L. (1985) The Taupo Eruption, New Zealand, I. General Aspects. Phil Trans R Soc Lond A314: 199-228

Wilson, L. (1980) Relationships between pressure, volatile content and ejecta velocity in three types of volcanic eruptions. J Volcanol Geoth Res 8: 297-313

Wilson, L., Sparks, R.S.J., and Walker, G.P.L. (1980) Explosive volcanic eruptions - IV. The control of magma properties and conduit geometry on eruption column behavior. Geophys J R Astr Soc 63: 117-148

Results

Major element chemistry

The major element composition of melt inclusions in some tephras was analysed by electron microprobe. Mean major element composition are shown in Table 6-4 and detailed analyses are included in Appendix C. The major element chemistry of melt inclusions remains generally constant within eruptive centers, although there is a chemical break following the Oruanui eruptions from the TVC.

Analyses from core to rim of some inclusions were made, in order to verify that no chemical zonation is present within inclusions, and the results of these analyses are shown in Fig. 6-6 a and b. These analyses were made with a 1 micron electron beam, so, due to loss of alkali elements, the analyses do not represent a true chemical composition, but comparison of relative differences between points is valid. The composition of inclusions from core to rim is generally constant.

Chlorine chemistry

Chlorine analyses of melt inclusions from most tephra were also made by electron microprobe, and are listed in Table 6-4. Detailed analyses are listed in Appendix D. The Cl contents of melt inclusions vary slightly between

Table 6-4. Average major element chemistry and chlorine contents of melt inclusions from the Taupo and Okataina volcanic centers as analysed by electron microprobe.

Unit	SiO_2	TiO_2	Al_2O_3	FeO	MgO	CaO	Na_2O	K_2O	Cl
Taupo center									
Taupo plinian	76.2	0.3	12.7	2.3	0.2	1.3	4.0	2.8	0.174
Hatepe phreato.	76.6	0.4	12.8	2.2	0.2	1.1	4.0	2.9	0.175
Hatepe plinian	76.0	0.3	12.5	2.7	0.3	1.4	4.0	2.9	0.173
Initial ash	76.0	0.3	12.5	2.6	0.2	1.4	4.0	2.9	0.172
Mapara	76.0	0.2	13.0	2.3	0.2	1.4	4.0	2.8	0.188
Whaikapu	77.2	0.2	12.6	1.9	0.1	1.0	4.0	3.1	0.184
Waihimia									0.183
Motutere									0.197
Opepe	76.3	0.3	12.9	1.9	0.2	1.4	4.0	3.0	0.181
Porunui	75.2	0.2	13.5	1.7	0.1	1.4	4.0	3.4	0.186
Karapiti									0.190
Oruanui	78.0	0.1	11.7	1.4	0.1	0.7	4.0	4.0	0.234
Okaia	79.4	0.2	11.0	1.7	0.1	0.8	4.0	3.0	0.211
Tihoi	77.5	0.1	12.2	1.3	0.1	0.9	4.0	4.1	0.224
Okataina center									
Kaharoa									0.198
Whakatani	78.2	0.1	12.2	1.1	0.1	0.7	4.0	3.6	0.176
Mamaku	77.9	0.2	12.2	1.5	0.1	0.8	4.0	3.4	0.192
Rotoma									0.196
Waiohau	78.6	0.1	11.9	1.3	0.0	1.7	4.0	3.5	0.200
Rotorua	76.5	0.3	12.6	1.9	0.2	1.6	4.0	2.9	0.173
Okareka									0.128
Terere									0.195
Omateroa									0.137
Awakeri									0.189
Mangaone									0.132

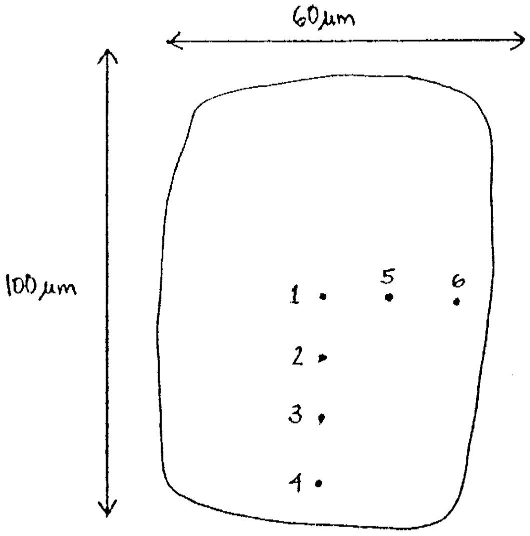

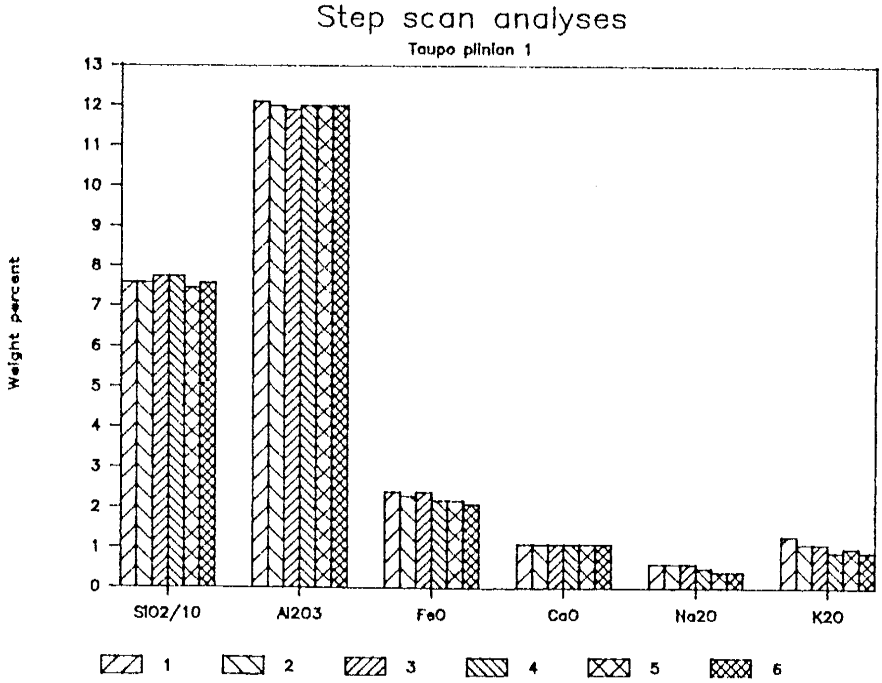

Figure 6-6 a . Major element compositions of points in a melt inclusion. The lack of systematic chemical zonation suggests that no significant post-entrapment crystallization has taken place. Analyses are made with an electron microprobe using a 1 micron beam, so absolute analyses of mobile elements are not accurate, but relative values should be correct.

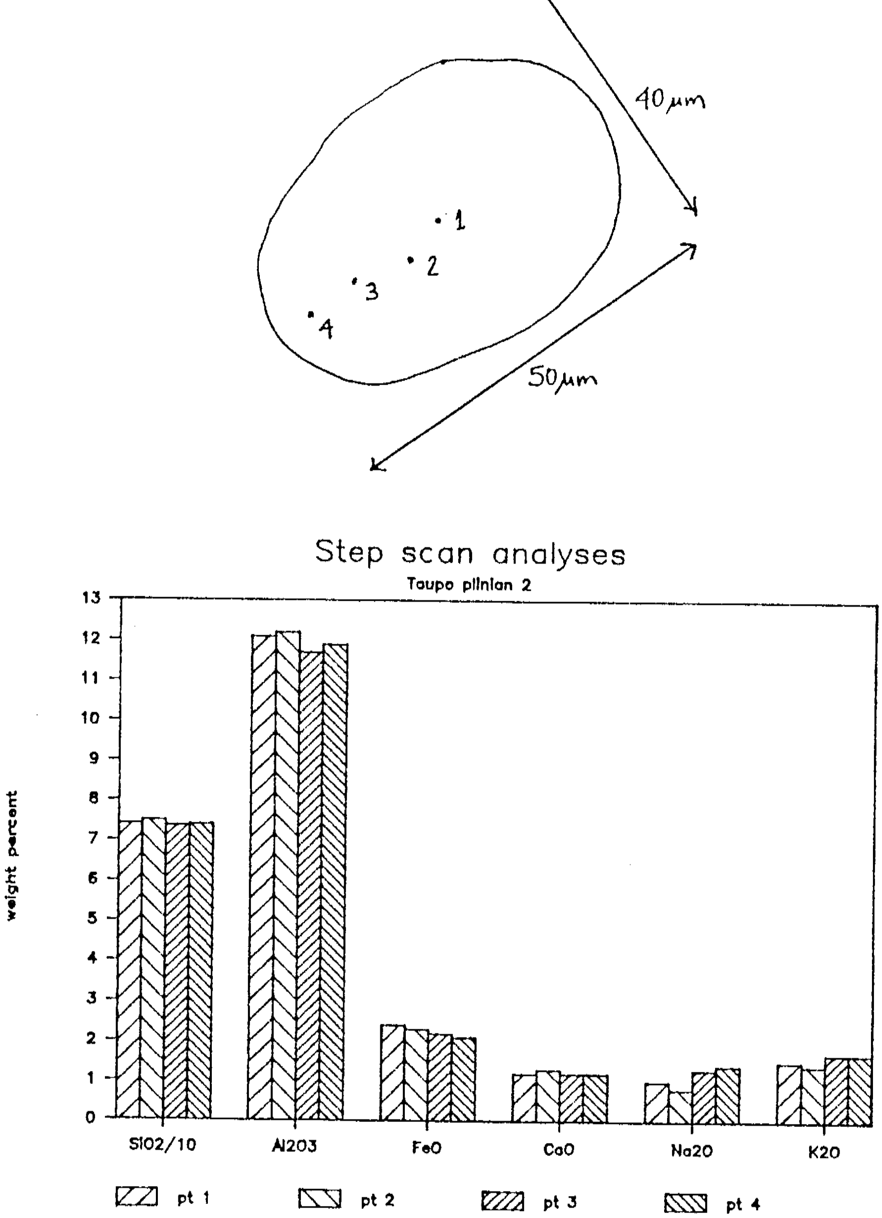

Figure 6-6 b. Major element compositions of points in a melt inclusion. The lack of systematic chemical zonation suggests that no significant post-entrapment crystallization has taken place. Analyses are made with an electron microprobe using a 1 micron beam, so absolute analyses of mobile elements are not accurate, but relative values should be correct.

the young tephra units (<22 ka) from the TVC, but no systematic variations are present. However, the Cl content of the pre-22 ka melts is significantly higher than the younger magmas. The Cl contents of OVC melts are slightly more variable than those from the TVC, but no systematic changes through time are present. Three OVC tephra units contain melt inclusions with consistently low Cl contents (~0.130 wt%).

Geothermometry

High-temperature-stage analyses were made of melt inclusions in plagioclase from the Taupo plinian tephra. Attempts were made to determine the melting and homogenization temperatures of these melt inclusions. Determined melting and decrepitation temperatures are listed in Table 6-5.

Melting points of the glass in these melt inclusions were difficult to pinpoint because of the similar appearance of molten and solid glass, and the regular shape of the vapor bubbles which did not deform when the glass melted. In some cases, melting could be detected by the nucleation of numerous small bubbles in the inclusion. This would give the maximum temperature of melting. The simultaneous nucleation of a large number of bubbles was seen in some cases, and could be due to a shock wave created when the first bubble formed and then

Table 6-5. Melt and decrepitation temperatures of melt inclusions in plagioclase crystals from the Taupo plinian tephra. Temperatures are reported in degrees C.

Inclusion	Melt temperature	Decrepitation temp.
Taupo 1	740	–
Taupo 2	740	850
Taupo 3	600*	–
Taupo 4	700	800
Taupo 5	700	–

* This temperature is determined from very slight bubble size change and may denote the earliest first melt.

triggered nucleations of other bubbles (E. Roedder, pers. comm.). Another explanation could be that a nucleation threshold is crossed at that temperature, just as many ice crystals form simultaneously in supercooled water, but this is unlikely because dissolution kinetics in rhyolite melts are slow (Roedder, 1984).

Another possible way to determine melting was by the color of the inclusion glass. As heating progresses, the glass will darken in color, and will then lighten. In some cases, lightening was approximately simultaneous with the nucleation of vapor bubbles, and was used to estimate the melting temperature in cases where vapor bubbles did not nucleate. The color changes of the glass were probably due to chemical changes within the glass (Roedder, 1984).

Homogenization of Taupo melt inclusions were not attainable with a stage heating to 1000^{o}C. At 1000^{o}C, the inclusions did not homogenize, and instead the size of the vapor bubbles increased, rather than shrinking. However, two inclusions decrepitated at 800 and 850^{o}C, which correspond approximately with the magmatic temperatures as determined by Fe-Ti oxide geothermometry.

Discussion

Major elements

The major element chemistry of the melt inclusions suggest that the inclusions represent pristine rhyolitic melt which has not undergone post-entrapment crystallization. This conclusion is supported by the comparison of melt inclusion chemistry with that of obsidian fragments from the same eruptions (see Ch. 5). The compositions are generally similar for most melt inclusion/obsidian pairs. An exception to this is the major element Fe, which is generally higher in the melt inclusions than obsidian, possibly because magnetite was crystallized from the melt subsequent to inclusion entrapment.

The break in major element composition following the Oruanui eruption from the TVC has been noted by other workers (Froggatt, 1982b). The magma chamber may have been effectively emptied by the large Oruanui eruption (155 km^3), allowing a slightly different batch of magma to equilibrate. The major element chemistry of the OVC melts is slightly more variable than that from the TVC, as are the trace elements. As discussed in Ch. 5, these tephras were probably derived from a number of small magma batches which underwent some fractionation and/or contamination.

Chlorine

The Cl contents of melt inclusions follow generally the same trends as seen in major and trace elements. Chlorine contents in the <22 ka TVC melt inclusions are very consistent, with a major break following the Oruanui eruption. The Cl contents of the OVC tephra melt inclusions are variable, and are anomylously low in the case of several older OVC tephras, apparently reflecting low Cl contents of these magmas.

Geothermometry

The melt temperatures of glass obtained from these melt inclusions seem reasonable for the first melt of hydrous rhyolite (Carmichael, Turner and Verghoogen, 1974; Naney, 1983). However, these temperatures tell us little about the actual conditions in the Taupo magma chamber, because this temperature only represents the lowest possible temperature of the melt, not the actual melt temperature.

Homogenization temperatures of inclusions were not obtained, although the inclusions were heated to well above the magmatic temperature as indicated by Fe-Ti oxide geothermometry. There are two possible reasons for this behavior, both of which may be responsible to some extent. First, the dissolution kinetics of rhyolite melts are slow, so the run length may not have been sufficient to allow homogenization (Roedder, 1984). Second, the inclusion glass may have stretched the host crystal during the heating run, which would allow the volume of the vapor bubble to increase, and lead to erroneous homogenization temperature determinations (Roedder, 1984). Several inclusions decrepitated explosively at around 800^{o}C. This behavior suggests that the inclusion glass was rich in volatile elements. Chaigneau et al. (1980) suggested that the decrepitation temperature of inclusions may approximate the inclusions' trapping temperatures. The Taupo decrepitation temperatures agree with temperatures determined by Fe-Ti oxide geothermometry.

7. DISCUSSION

A. Eruption and degassing systematics of TVC magmas

The depths of initial vesiculation and fragmentation of rhyoltic magmas are generally poorly constrained, because the pre-eruptive volatile contents of such melts are poorly known. However, for TVC magmas, the pre-eruptive H_2O contents determined in this study allow these depths to be accurately calculated. Initial vesiculation occurs at approximately the depth where the melt is saturated with respect to H_2O, and fragmentation occurs where the vapor:melt ratio is 3:1 (Sparks, 1978). The saturation depths of H_2O in these TVC rhyolites has been calculated using the solubility model of Burnham (1975, 1979a) (Appendix F).

The factors which initiated the vesiculation resulting in the eruptions of the 2 ka Taupo magma and 23 ka Okaia magma are difficult to assess, as the crustal depths of the magma chamber depths are unknown. There are three possible explanations for the volatile oversaturation which intitated these explosive eruptions. First, if the magma chambers were near saturation at their crustal residence depth (near ~3.8 km, and ~7.5 km for the 2 ka Taupo and the 23 ka Okaia magmas respectively) a slow bouyant rise of the magma may have produced oversaturation in the upper portion of the chamber. Vesiculation would have begun at pressures of ~0.9 kb for the 2 ka Taupo magma, and at ~1.9 kb for the Okaia magma, ideally corresponding to depths of ~3.8 and ~7.5 km respectively, assuming crustal density of 2.5 g/cm^3 (Fig. 7-1). Once a vapor phase was present, the magma would increase in volume rapidly with decreasing pressure (Fig. 7-2), and may have caused overpressuring sufficient to rupture the magma chamber roof and allow a rapid rise of magma towards the earth's surface (Burnham, 1979b). The second possibililty is that tectonic activity in the TVZ initiated these eruptions. Tectonic activity may create zones of crustal weakness along which magma could move upwards, eventually reaching saturation depths, or alternatively could depressurize the magma chamber, allowing vesiculation to begin. Structural control of vent positions in the TVZ suggest that tectonics did play a role in these eruptions (Wilson and Walker, 1985). Finally, development of a volatile gradient in the magma chamber could have lead to volatile oversaturation and vesiculation. However, at least in the case of the 2 ka

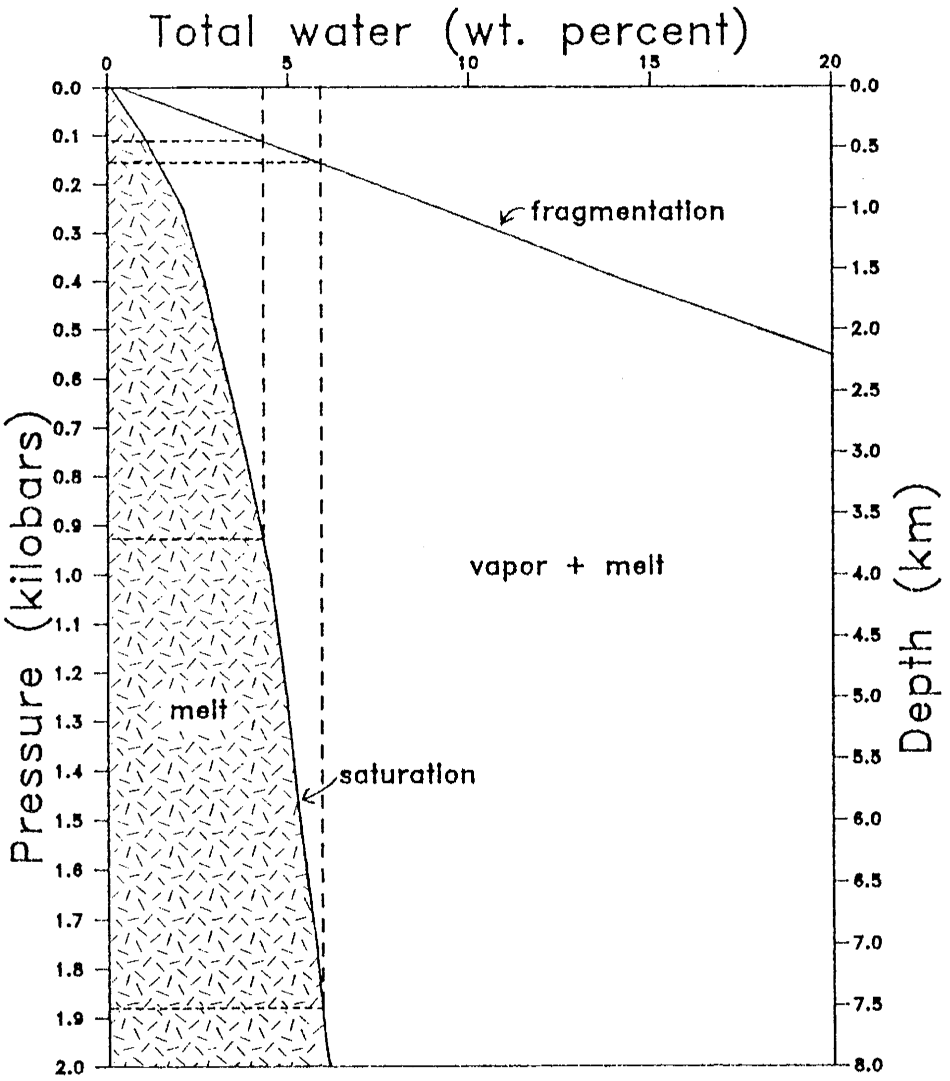

Figure 7-1 Pressure versus total water content for TVZ rhyolite at 750°C, using solubility relationships proposed by Burnham (1975, 1979a and b). The melt field is shown in a hachured pattern, saturation and fragmentation boundaries are shown. Fragmentation is assumed to be at a 3:1 vapor:melt volume ratio (ideal gas behavior is assumed). Pressure equilibrium between lithostatic load and vapor pressure is assumed for the pressure:depth relationship, and an average crustal density of 2.5 g/cm^3 is used. The dotted lines represent the path followed by magmas containing 4.3 and 5.9 wt.% respectively. Pressures of saturation and fragmentation are indicated.

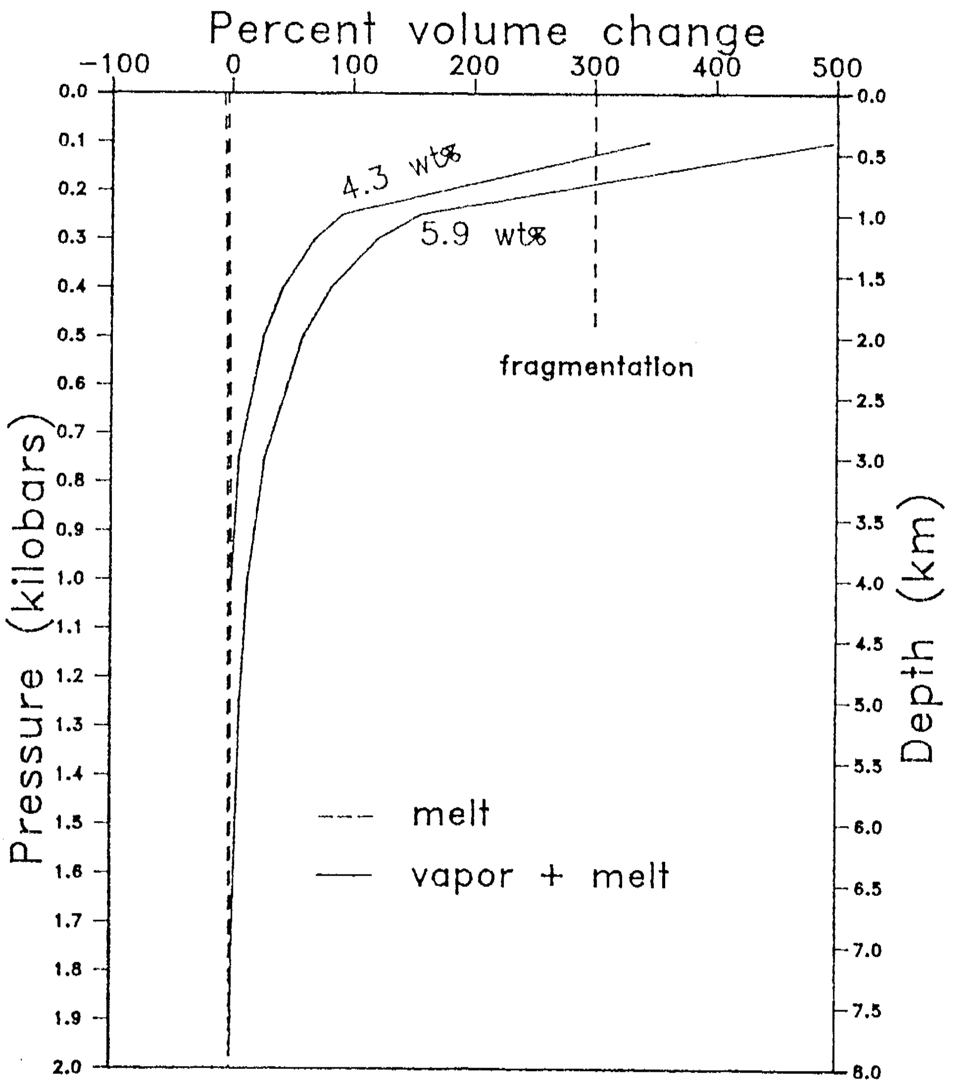

Figure 7-2. Volume change of a TVZ rhyolite at 750°C as a result of decreasing pressure (assuming ideal gas behavior) using solubility relationships proposed by Burnham (1975, 1979a and b). Two cases are represented, magmas intially containing 4.3 wt.% H_2O, and 5.9 wt.% H_2O respectively. Volatile elements other than H_2O are not considered as H_2O is dominant. Pressure equilibrium between lithostatic load and pressure is assumed for the pressure:depth relationship, and an average crustal density of 2.5 g/cm^3 is used.

Taupo eruption, this is unlikely, as no volatile gradient appears to be present. Once the eruption was underway, and overburden was removed, the saturation front may have migrated downwards.

Regardless of how the eruption was initiated, as the 2 ka Taupo and the 23 ka Okaia magmas rose from 3.8 and 7.5 km respectively towards the earth's surface, the progressive pressure decrease allowed more H_2O to exsolve from the melt, resulting in a greater degree of vesiculation. Also, as the pressure decreased, the molar volume of the vapor phase and the vapor:melt ratio increased rapidly, resulting in a foam of magma and vapor. Such a foam has been shown, by a combined analytical and numerical approach, to be permeable to vapor under eruptive conditions, particularly at above 60% porosity (Eichelberger et al., 1986). The hydrogen isotopic composition of some obsidian from TVZ eruptions suggest that open-system degassing, as would be expected from Eichelberger et al.'s (1986) degassing model, at above 60% porosity, may have occurred during magma ascent.

The explosive phase of an eruption will probably not begin until the vapor:melt ratio is ~3:1, at which point large bubbles rupture, and the magma becomes an incoherent mass of pumice, dust and gas (Sparks, 1978). Sparks (1978) suggests that nucleation and fragmentation can occur either in a magma chamber or in a conduit. Assuming that the confining pressure of the magmas was initially equal to the lithostatic load during ascent, fragmentation first occurred at slightly less than 500 m for the 2 ka Taupo eruption, and at slightly greater than 600 m for the Okaia melt (Fig. 7-1). The equilibrium residual water contents of the melts at these depths were ~1.0 and 1.2 wt.% respectively. Following initial fragmentation, the fragmentation surface may migrate downwards in the conduit, and possibly into the magma chamber, depending on the rate of upward magma flow (Sparks, 1978). Such fragmentation surface migration may have occurred in the TVC eruptions. A cartoon of the Taupo and Okaia magma chambers during eruption, with depths of saturation, fragmentation and obsidian formation is shown in Fig. 7-3.

Obsidian formation

An implication of the calculated fragmentation depths of the Taupo magma chambers is that most obsidian was quenched from fragmented magma. The calculated pressures at which fragmentation occurs are generally higher than the pressures at which obsidian is expected to form, based on water content (Fig 7-3). The fragmented magma is thought to be spattered against the

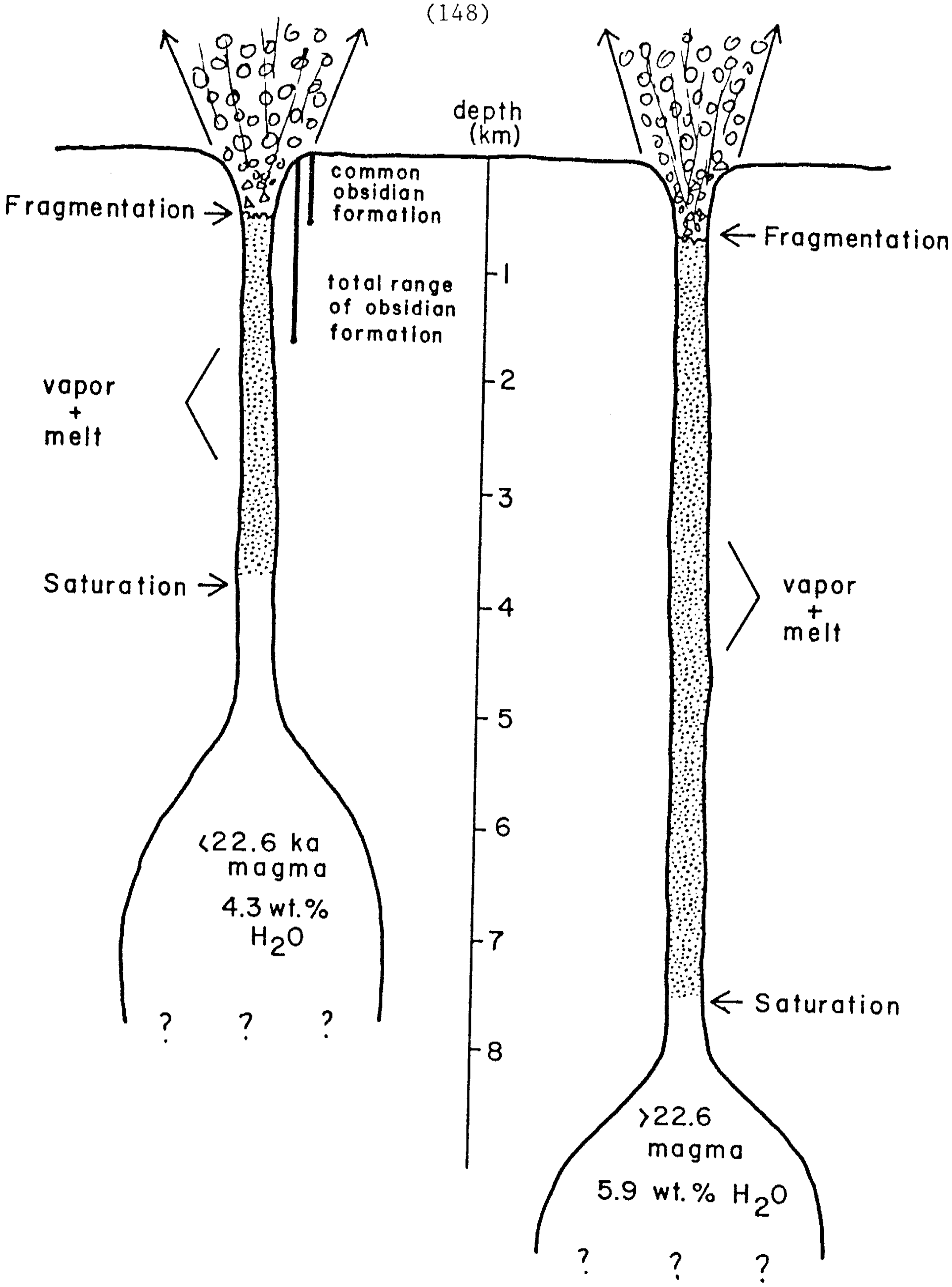

Figure 7-3. Cartoon of 2 ka Taupo and 23 ka Okaia magma chambers showing approximate depths of initial saturation and fragmentation (derived from Fig. 7-2). Approximate ranges of obsidian quenching are indicated (assuming pressure equilibrium between lithostatic load and vapor pressure, and an average crustal density of 2.5 g/cm^3).

walls of the conduit, where it would become welded and quench. The bubbles in the vesiculated melt would collapse during this process, leaving dense obsidian containing an amount of H_2O related to the pressure of quenching.

Obsidian from the Hatepe phreatoplinian tephra contains a larger amount of water (up to 2.5 wt.% H_2O) than obsidian from any other 2 ka Taupo tephra, or most other TVC tephras. Based on the solubility of water in these melts, obsidian containing 2.5 wt% H_2O must have quenched at ~0.35 kilobars, or close to 1.5 km depth. The meteoric water which was responsible for the phreatic nature of this eruption may also have influenced the deep quenching of the obsidian. This would suggest that meteoric water could have penetrated to 1.5 km, and interacted with an unfragmented magma at this depth, in order to cause a large phreatoplinian eruption.

B. Volcanological Implications- Eruptive processes of TVZ rhyolites

Magmatic water content is widely believed to be one of the strong controls on rhyolitic eruptive explosivity, eruption dynamics and consequent pyroclastic deposits (Wilson et al., 1980, Fisher and Schmincke, 1984). However, because there are few direct measurments of the H_2O content of rhyolitic melts, the relationship between water content and explosivity is not clearly understood.

"Ultraplinian" versus plinian eruptions

The exceptionally widely dispersed nature of the 2 ka Taupo plinian tephra and the unusually fine grain size, as compared to other plinian tephras led Walker (1980) to propose the "ultraplinian" classification for this eruption. The "ultraplinian" nature of the Taupo plinian tephra is thought to be a result of rapid rates of vesiculation, fragmentation and thermal energy transfer from the magma to the surrounding air. The Taupo plinian tephra contains 90% by weight of ash <1 mm in size, whereas in the associated Hatepe plinian tephra, 81% of the ash is <1 mm. Also, for the Taupo plinian eruption, the area enclosed by the 0.01-times-the-maximum-tephra-thickness isopach is $10^4 km^3$, whereas it is 10^3 for the Hatepe plinian tephra. Walker (1980) postulated that the gas content, temperature, and viscosity of a magma were important factors in the generation of this highly explosive eruption.

However, this study's ion microprobe analyses of melt inclusions indicate that there was no difference in pre-eruptive volatile contents between the Taupo plinian magma and the less-explosive Hatepe plinian magma at the time of crystal growth (Table 6-2). The lack of crystal resorption in the Taupo plinian further suggests that post-crystallization volatile enrichment did not occur. Also, Fe-Ti oxide geothermometry indicates that the temperature of the Taupo plinian melt was not significantly higher than that of the Hatepe plinian magma, or most of the other <10 ka magmas (Table 4-1).

Because the temperature, volatile content and major element compositions of the Taupo and Hatepe plinian magmas were virtually identical, their viscosities must also have been very similar, suggesting that viscosity did not play a role in controlling the difference between their eruptive styles. Furthermore, the magma that produced the Okaia tephra, which contained~1.6 wt % more H_2O than the Taupo magma, and was 50^oC cooler, would be less viscous (McBirney and Murase, 1984), but did not produce an eruption as explosive as the Taupo "ultraplinian" event.

Based on this evidence, it is unlikely that the Taupo "ultraplinian" event was a result of magmatic characteristics, but may instead reflect unusual eruptive conditions. Some possibilities include unusual vent configuration, or rapid downward migration of the vesiculation front by rapid removal of magma, as suggested by Wilson and Walker (1985) for the generation of the Taupo ignimbrite.

Plinian versus phreatoplinian eruptions

The Hatepe phreatoplinian eruption was bracketed in time by the Taupo and Hatepe plinian eruptions. The lack of H_2O gradient through the Taupo and Hatepe plinian tephras suggests that the pre-eruptive H_2O content of the Hatepe phreatoplinian tephra was also approximately 4.3 wt%. The consistent Cl contents through all three tephra units (Table 6-2) also suggests that the H_2O content was constant, based on the H_2O:Cl correlation noted in melt inclusions and partially degassed magma (Fig. 6-5). This suggests that the transition from plinian to phreatoplinian eruptive styles is a result of external water input, as suggested by most authors (eg. Self, 1983), and has no relation to the actual volatile content of the magma.

Initiation of eruptions

Blake (1984) suggests that oversaturation and critical overpressuring of a magma chamber due to the development of a volatile gradient is an important means of initiating explosive silicic eruptions. However, the lack of a volatile gradient in the 2 ka Taupo melt suggest that the eruption is unlikely to have been triggered by gradual, progressive volatile oversaturation in the uppermost portion of the magma chamber. Tectonic activity within the TVZ, which is undergoing rapid back-arc extension (Stern, 1987) may have played an important role. Tectonic activity may have initiated slight decompression of the magma chamber, which could have triggered rapid volatile oversaturation and eruption.

C. Petrological Implications- Magma chamber processes

The physical and chemical characteristics of magma chambers are fundamental problems in igneous petrology and volcanology. Until the early 1960's, when exhaustive studies of plinian and ignimbrite deposits were begun, little was known about silicic magma chambers. Plinian and ignimbrite tephra eruptions provide an insight into the magma chambers from which they were erupted as they represent large volumes of magma that preserve many magma chamber characteristics unchanged by crystallization and alteration. Petrological problems that can be addressed by the study of plinian tephras and ignimbrites include size, depth and temperature of magma chambers, as well as the nature and origin of magmatic chemical zonation. Some of these questions have been addressed in this study of magma chambers in the TVZ, New Zealand.

Magma chamber zonation

Chemical zonation has become the expected condition of silicic magma chambers and Smith (1979) suggests that any pyroclastic eruption of >1 km^3 magma volume will show compositional zonation. Zonation is thought to be a result of crystal fractionation, and/or liquid-state thermodiffusion (Hildreth, 1981). Incompatible elements, including volatile elements, will be concentrated upwards in the magma chamber. This chemical zonation leads to a density gradient in the magma chamber, which affects the eruption dynamics of the chamber, causing thin layers to be successively drawn off the top of the magma body (Blake and Ivey, 1986).

However, the major, trace and volatile element determinations for the TVC tephras indicate that there is no systematic chemical zonation in the parent magma chamber with respect to any of these elements (Tables 4-1, 6-2). The uniform Sr isotopic composition of the 2 ka Taupo eruption tephras re-enforce this conclusion (Table 4-5). The lack of systematic volatile zonation in the TVC eruptives can be seen in Fig. 7-4. The post-10-ka TVC tephras also show virtually identical major and trace element composition, with the exception of some variability in elements Sr and Zr, which could be due to slight differences in phenocryst content. These magmas are probably derived from the same magma chamber, as their vents are all supposed to lie within Lake Taupo (Wilson and Walker, 1985). Furthermore, the products of the 2 ka BP Taupo eruption, which represent ~19 km^3 of magma, show only the slightest evidence of chemical zonation (unp. data for Taupo Ignimbrite from C.J.N. Wilson and I.S.E. Smith). In addition to major and trace elements, the <10 ka TVC tephras show no systematic volatile zonation. Analyses of

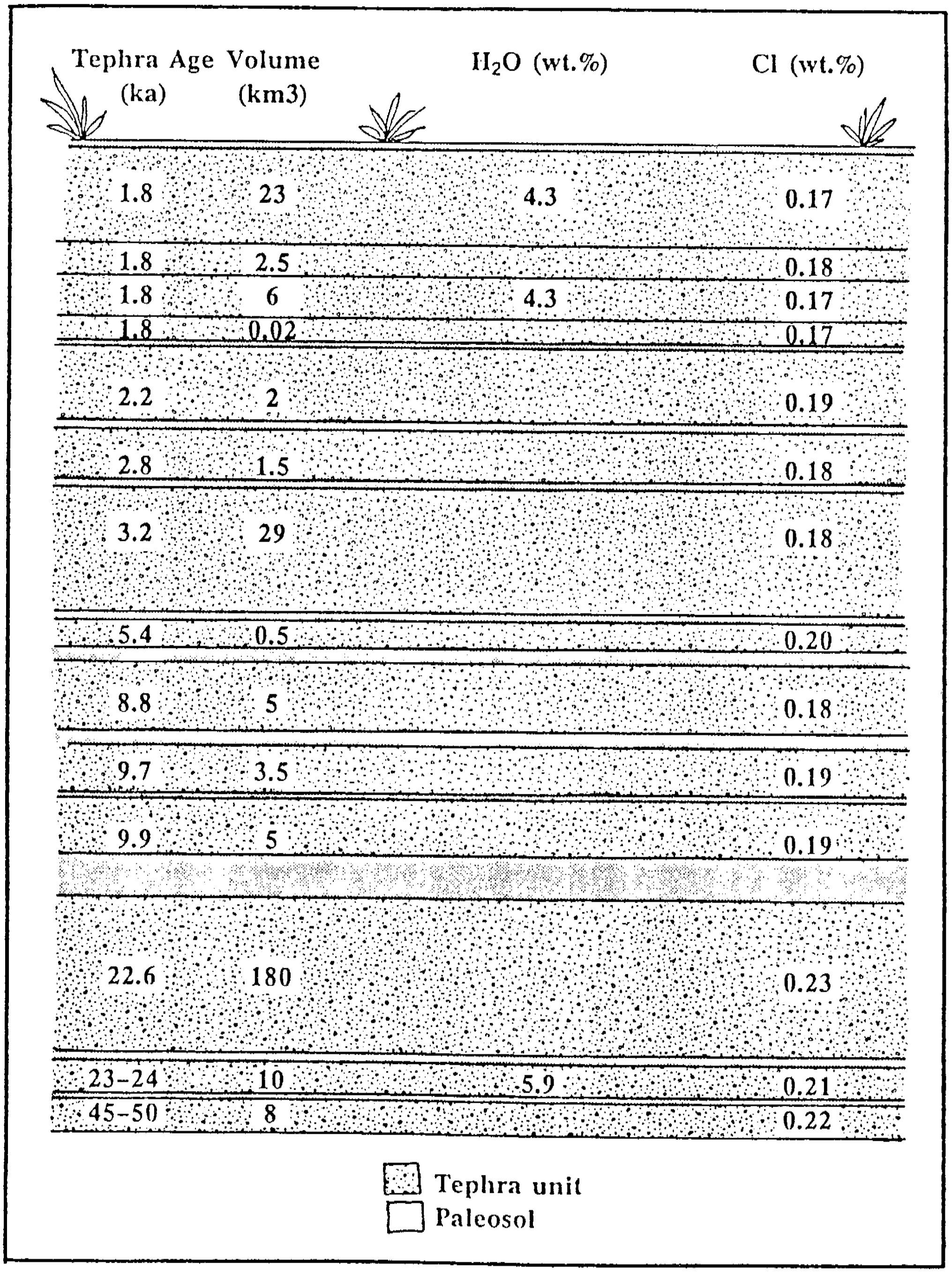

Figure 7-4. Systematic representation of tephra units from the T.V.C. showing analysed magmatic H_2O and Cl contents. Age and volume of tephra units are noted. Thicknesses of tephra units and paleosols do not represent true thicknesses.

H_2O from two units within the 2 ka Taupo eruption show identical H_2O contents, and the Cl contents of all tephra units are similar (Fig. 7-4). Temperature and oxygen fugacity, as determined by Fe-Ti oxide chemistry show slight variations among the <10 ka tephras, but all variations are within the error of the analytical technique. All <10 ka tephras fall on a single buffer trend, again supportive of derivation from a single magma chamber (see Fig. 4-2).

There are several possible reasons for the lack of systematic zonation in the <10 ka TVC magmas. Each <10 ka Taupo melt could be the result of a discrete partial melting episode of the greywacke crust. This may be a possible mechanism for the formation of rhyolitic magmas, as suggested by Huppert and Sparks (1988). However, although it is not possible to discount this mechanism of magma genesis, it seems unlikely for the TVC magmas view of the extremely homogeneous composition, the single temperture/oxygen fugacity trend, and the episodic nature of eruptions. If all of the magmas were derived from a single body, as is more likely, the magma must have remained homogeneous by some process such as rapid convection. Alternatively, the magmatic system may have been too young, or have erupted too frequently, to allow systematic zonation to evolve.

Size of magma chamber

Comparative chemical data for the pre- and post 22.6 ka TVC eruptions may allow an estimation of the size of a TVC magma chamber. Following the 22.6 ka Oruanui eruption or the TVC, which consisted of a plinian and ignimbrite eruption totalling 155 km^3 of magma (Self, 1983), the TVC magmas underwent a distinct chemical change. The major element chemistry remained essentially unchanged, as did certain trace elements (Th, Rb, Sr, Nb), but other trace elements (Y, Pb, Zr) underwent a distinct shift. Also, the mean H_2O and Cl contents of the magmas changed from ~5.9 to ~4.3 wt% and 2200 to 1800 ppm respectively, after the 22.6 ka eruption. The mean temperature became slightly higher, as did the oxygen fugacity, and the pre- and post-22.6 ka magmas define separate buffer trends. These changes suggest that the pre-22.6 ka magmas were not part of the same magma batch as the post-22.6, although the vents for all of the eruptions were within the Taupo caldera, probably within Lake Taupo.

A possible explanation for these changes is that the 22.6 ka Oruanui eruption emptied the magma chamber sufficiently to allow a chemically different magma to evolve. As the composition of the two magmas are not very different, the source from which the second melt evolved must have been chemically similar to the source of the first. Smith (1979) suggests that only 10% of a magma chamber can be emptied in any single eruption, and that subsequent eruptions represent deeper levels of a single chamber, but this does not appear to be the case in the TVC. An alternative explanation is that the chemical changes are due to mixing of residual post-Oruanui eruption magma with some amount of new melt. In view of the chemical trends seen, and the marked shift in the Fe-Ti oxide buffer trends, and the relatively short time (~12.6 ka) of the non-eruptive interval, mixing seems unlikely, although not impossible. Assuming that mixing did not occur, the TVC magma chamber, which produced the Oruanui eruption, probably contained several hundred km^3 of magma.

Mineral stabilities with magmatic water content

The H_2O content of a melt, among other factors, has an effect on the minerals that will crystallize from that melt (Luth, 1969). Experimental studies have been made on the effect of H_2O on mineral stabilities (Eggler, 1972; Esperanca and Holloway, 1986; Mertzbacher and Eggler, 1984; Naney, 1983), but few determinations have been made for actual magmatic systems. Naney (1983) showed that in a granitic melt at uniform pressure, hydrous ferromagnesian silicate phases are stable at higher H_2O contents and lower temperatures. This conclusion is apparently applicable to the Taupo system, where amphibole ($\pm$biotite) were stable in a melt that contained 5.9 wt% H_2O and was at 800°C, whereas pyroxene was the dominant ferromagnesian silicate phase in a chemically similar melt with 4.3 wt% H_2O at 845°C.

D. Implications to ore deposits: Estimates of volatiles and metals released during crystallization

Plutonic systems, particularly subduction-related magma chambers, can play a major role in the formation of certain types of ore deposits, particularly mineralized porphyry systems. Magmas can provide the metals which form ore deposits, the complexing agents (Cl, S) for transport of these metals and the principle volatile phase in which the ore metals are transported (generally H_2O) (Burnham, 1981).

The types of ore deposits in which a magmatic influence has been most clearly demonstrated are porphyry metal deposits, including copper (Cu), molybdenum (Mo), tin (Sn) and tungsten (W). This relationship has been shown by the spatial distribution of ore bodies and their relation to plutonic systems (Lowell and Guilbert, 1970; Gustafson and Hunt, 1975; Sillitoe et al., 1975) as well by isotopic systematics (Taylor, 1979). In general, porphyry Cu deposits are derived from granidioritic to dioritic melts, porphyry Mo deposits are derived from highly differentiated rhyolitic magmas, and porphyry Sn and W deposits are derived from granites (Brimhall and Crerar, 1987). All three of these magma types can be produced by subduction-related processes, either generated along a subduction front, or in a back-arc basin (Mitchell and Garson, 1982).

A magma body must meet a number of constraints in order to form a mineralized porphyry system. First, the magmatic H_2O content must be sufficient to produce extensive fracturing when it separates from the magma during crystallization (second boiling) (Burnham, 1979b). There must also be enough H_2O to transport the ore metals out of the magma into the surrounding country-rock where they will be deposited as ore minerals. Although the H_2O does not directly complex all ore-forming metals, it forms the vapor phase into which metals fractionate from the melt. Second, the magma must be sufficiently hot to rise to shallow levels in the crust without extensive crystallization (>800^{o}C) (Burnham, 1981). Third, the Cl and S content of the magma must be high enough, at least 0.05 and 0.2 wt% respectively, to efficiently complex ore metals, and also to cause extensive wall-rock alteration. Cl is a complex-forming ligand for metal transport, and is strongly partitioned into an aqueous phase out of a silicate melt. The partition coefficient of Cl between a silicate melt and an aqueous vapor phase is 43 at 2 kb (Kilinc and Burnham, 1972). S may have similar partition coefficients (Brimhall and Crerar, 1987). Cl is important in the transport of many metals, except Mo and W, and S is important in the transport of Cu (Burnham, 1981; Candela and Holland, 1984; Brimhall and Crerar, 1987). Molybdenum may be transported as molybdic acid (H_2MoO_4) (Burnham, 1981). Finally, the metal content of the melt must be sufficient to form an economic mineral deposit. It is difficult, however, to put any specific numbers to the minimum metal content.

Although these parameters are important in the ore deposition process, many are unknown in actual ore-forming magmatic systems. In the course of the present study, some of these parameters, specifically the volatile content, size, and metal content of a rhyolitic magma body, have been determined for the TVC magma chamber in the TVZ. Although the TVC magma chambers considered in these calculations has erupted repeatedly, rather than crystallizing, and will therefore not generate ore deposits from the magmas analysed in this study, it has some similarities to other ore-deposit-generating magmatic systems. The data obtained in this study can therefore be applied to other systems, and used as an aid in modelling formation of porphyry ore deposits. The TVC is located in a back-arc subduction-related basin, and the rhyolite magmas are generated from partial melts of crustal sediments (Stern, 1985; Cole, 1979), as is typical of porphyry ore deposits elsewhere (Brimhall and Crerar, 1987).

Estimates of volatiles and metals released during crystallization

In the case of the TVC, accurate estimates can be made of the quantity of H_2O, Cl, and F which would have been released if the magma had crystallized. This can be done by estimating the size of the magma chamber, and by calculating the percent of total magma volatiles (as determined by ion microprobe and electron microprobe analyses) which would have exsolved from the melt during crystallization. The amount of volatile components which exsolve during crystallization of a pluton is considered to be independent of magma depth as the pluton crystallized fully and drives out all volatile phases not incorporated in hydrous phenocrysts. Once the quantity of volatiles released by the melt is calculated, the amount of Cu and Mo carried in the volatile phase can be calculated using experimental partitioning coefficients of Candela and Holland (1984, 1986). Estimates of Sn released can also be made.

In order to determine the abundances of volatiles and metals released during crystallization, the TVC rhyolitic magmas must be broken into 2 groups: those older than 22.6 ka, and those younger. The major Oruanui eruption at 22.6 ka B.P. appears to have effectively emptied the TVC magma chamber, and the chemistry of the subsequent magma was subtly changed. The calculated outputs of H_2O, Cl and F from these two magma batches per cubic km of magma are given in Table 7-1. The final H_2O and Cl values are average values of these components in crystalline granites (Hurlbut and Klein, 1977; Krauskopf, 1979). Because the F content of granites is variable, the final F content for the Taupo is simplistically estimated at 10% (40 ppm) of the original magmatic content, similar to the estimated remaining fractions of H_2O and Cl.

The Cu and Mo contents of the volatile phase released per cubic km of these melts can be calculated using partition coefficients experimentally determined by Candela and Holland (1984, 1986) for melts similar to Taupo rhyolite. The partition coefficients are expressed as "E", which represents the percent of the metal removed from the melt into the vapor phase. The E values for Cu and Mo are 70% and 60%, and 60% and 50% for the >22.6 ka and <22.6 ka magmas respectively, based on the H_2O and Cl contents of the melts (Candela and Holland, 1986). The Mo coefficient is mainly dependent on the initial water content of the melt,

Table 7-1. H_2O, Cl, F, Cu, Sn, and Mo released per cubic km for <22.6 ka and >22.6 ka magmas from the TVC. Calculations are explained in text. Final H_2O and Cl values are average contents in granites from Krauskopf (1979). Final F is estimated as 10% of initial F. Initial Cu and Sn are back-calculated based in degassed values in TVC pumice determined by atomic absorbtion analysis. Initial Mo is back-calculated from the Mo content of an average granite (Krauskopf, 1979). The "E" value represents the percentage of Cu, Mo, and Sn released from the given melt during crystallization.

	Magma >22.6 ka	Magma <22.6 ka
Mass of 1 km^3 of magma	$2.3x10^{15}$ g	$2.3x10^{15}$ g
Mean initial H_2O	5.9 wt.%	4.3 wt.%
Final H_2O	0.5 wt.%	0.5 wt.%
H_2O released per km^3	**$1.2x10^{14}$ g**	**$8.7x10^{13}$ g**
Mean initial Cl	0.22 wt.%	0.18 wt.%
Final Cl	0.02 wt.%	0.02 wt.%
Cl released per km^3	**$4.6x10^{12}$ g**	**$3.7x10^{12}$ g**
Mean initial F	0.047 wt.%	0.044 wt.%
Final F	0.004 wt.%	0.004 wt.%
F released per km^3	**$9.9x10^{11}$ g**	**$9.3x10^{11}$ g**
Mean initial Cu	3 ppm	3 ppm
Total Cu in melt	$1.1x10^{12}$ g	$3.8x10^{11}$ g
"E"	70%	60%
Cu released per km^3	**$4.8x10^9$ g**	**$4.2x10^9$ g**
Mean initial Mo	2 ppm	2 ppm
Total Mo in melt	$7.4x10^{11}$ g	$2.5x10^{11}$ g
"E"	60%	50%
Mo released per km^3	**$2.7x10^9$ g**	**$2.4x10^9$ g**
Mean initial Sn	3 ppm	3 ppm
Total Sn in melt	$1.1x10^{12}$ g	$3.8x10^{11}$ g
"E"	60%	50%
Sn released per km^3	**$4.1x10^9$ g**	**3.5x10x^9 g**

whereas the Cu coefficient is dependent on the initial Cl content of the melt as well as H_2O. No partition coefficients for Sn were found for magmas similar to Taupo rhyolites, so an E value equal to that for Mo is assumed. The Cu and Sn contents of TVC rhyolitic pumice were determined by atomic absorbtion. These values represent the abundances of Cu and Sn in the rhyolitic magmas after eruptive degassing, which may have removed much of the Cu and Sn from the melt. Therefore, the initial Cu and Sn content of the melt is back-calculated using the "E" value of Candela and Holland (1986). The initial Mo content of the magma is also back-calculated from the final composition using the "E" values given above, but as Mo was not analysed the final content is assumed to be equal to the Mo content of an average fully crystallized granite (Krauskopf, 1979). The abundance of metals released per cubic km of <22.6 ka and >22.6 ka magmas are shown in Table 7-1.

Based on the estimates of metal outputs per cubic km of magma, total outputs for magma chambers of various sizes can be calculated, and compared to the sizes of large porphyry ore deposits (Table 7-2) (Hollister, 1978). The metal outputs of hypothetical >22.6 ka and <22.6 ka magma chambers are also included in Table 7-2. The volume of the older deposits from

Table 7-2. Outputs of Cu, Mo, and Sn from various size magma chambers of <22.6 ka and >22.6 ka TVC compositions. Range of amount of metals estimated for large Cu, Mo, and Sn ore deposits are noted on table (data from Hollister, 1978).

Magma chamber size	Cu (g)	Mo (g)	Sn (g)
5 km^3			
>22.6 ka composition	$2.4x10^{10}$	$1.4x10^{10}$	$2.1x10^{10}$
<22.6 ka composition	$2.1x10^{10}$	$1.2x10^{10}$	$1.8x10^{10}$
50 km^3			
>22.6 ka composition	$2.4x10^{11}$	$1.4x10^{11}$	$2.1x10^{11}$
<22.6 ka composition	$2.1x10^{11}$	$1.2x10^{11}$	$1.8x10^{11}$
500 km^3			
>22.6 ka composition	$2.4x10^{12}$	$1.4x10^{12}$	$2.1x10^{12}$
<22.6 ka composition	$2.1x10^{12}$	$1.2x10^{12}$	$1.8x10^{12}$
>22.6 ka TVC magma chamber (161 km^3)	$7.7x10^{11}$	$4.4x10^{11}$	$6.6x10^{11}$
<22.6 ka TVC magma chamber (55 km^3)	$2.3x10^{11}$	$1.3x10^{11}$	$1.9x10^{11}$
Known ore deposits	$10^{10}-10^{14}$	$10^{10}-10^{12}$	$10^{10}-10^{12}$

the TVC (Okaia, Tihoi, Oruanui) represent approximately 161 km^3 of magma. The younger tephras represent a volume of 55 km^3 of magma, but this is a minimum volume for the magma chamber, as there is no apparent evidence for emptying the magma chamber. These volumes are determined by adding the magma volume of all erupted tephra deposits.

The amount of Cu, Sn, and Mo released by the Taupo magma chambers has implications for the formation of porphyry ore deposits. The Taupo magmas are in the range of typical rhyolites in terms of size, temperature and composition, but would nevertheless been capable of forming a porpyry ore deposit under certain depositional conditions.

E. Atmospheric impact of TVZ eruptions

Volatile components emitted from magmas during volcanic eruptions undoubtedly affect atmospheric conditions of the earth (Rampino and Self, 1984). The major recognized climatic effect of volcanic eruptions is due to injection into the stratosphere (15-50 km) of SO_2 which interacts with solar and thermal radiation. The results of this process is to cool the earth's surface and the troposhere (0-15 km) and to warm the stratosphere (Rampino et al., 1985). The major volcanic contributors of SO_2 to the atmosphere tend to be basaltic or andesitic eruptions, as they usually contain more S than silicic magmas (Devine et al., 1984).

However, another atmospheric effect of volcanic eruptions which has not been widely addressed is the destruction of stratopheric ozone (O_3) by volatile components such as H_2O and HCl (Wang et al., 1986). The reaction sequence for Cl is as follows (from Turco, 1985):

$$HCl + OH \rightarrow Cl + H_2O$$

$$Cl + O_3 \rightarrow ClO + O_2$$

$$ClO + O \rightarrow Cl + O_2$$

---

net $$O + O_3 \rightarrow 2O_2$$

For H_2O, the reaction sequence is slightly more involved. First, H_2O is converted to OH as follows (from Turco, 1985):

$$O\ (D^1) + H_2O \rightarrow 2OH$$

where O (D^1) is an electronically excited oxygen atom.

Then OH reacts with O_3 in two ways:

a)

$$OH + O_3 \rightarrow HO_2 + O_2$$
$$HO_2 + O_2 \rightarrow OH + O_2$$

net $$O + O_3 \rightarrow 2O_2$$

b)

$$OH + O_3 \rightarrow HO_2 + O_2$$
$$HO_2 + O_3 \rightarrow OH + 2O_2$$

net $$O + O_3 \rightarrow 2O_2$$

The Cl reaction process is very effective at destroying ozone because a single Cl atom may be cycled through the process hundreds of times before becoming inert HCl (Turco, 1985). The destruction of O_3 by H_2O is also a cyclic process because the HO_2 radical is not changed by the conversion of O_3 to O_2. However, the cycle will be terminated when HO_2 is converted to stable H_2O and H_2 molecules (Turco, 1985). Ozone depletion by OH is comparativly not as effective, per molecule, as by Cl (Turco, 1985). However, both reaction processes are considered significant sources of ozone depletion (Wang et al., 1986).

Based on evidence that HCl and H_2O can destroy stratospheric ozone, it is possible that some volcanic eruptions may result in significant stratospheric ozone depletion. High-silica magmas, such as those examined in this study, are considered most likely as they contain relatively more Cl and H_2O than mafic melts (Devine et al, 1984; Fisher and Schminke, 1984). Also, silicic melts tend to be highly explosive and would be likely to generate stratosphere-penetrating eruption column allowing H_2O and HCl to react with stratospheric ozone.

Petrological estimates of the amount of HCl and H_2O emitted by some TVC and OVC eruptions have been made, and are shown in Table 7-3 and Fig. 7-5. The technique used to make these estimates involves determining the difference between the pre-eruptive volatile content of the melt and that of fully degassed magma, thereby determining the

Table 7-3. Atmospheric input of HCl and H_2O by eruptions from rhyolitic plinian tephra eruptions of the TVC and OVC. Atmospheric equilibrium value for H_2O used is 0.2 wt%, and for Cl 0.129 wt%.

Unit	Age (ka)	Pre-eruptive Cl (wt%)	Pre-eruptive H_2O (wt%)	Mass of tephra (gm)	Cl lost (wt%)	H_2O lost (wt %)	HCl output (tonnes)	H_2O output (tonnes)
Taupo plinian	1.8	0.174	4.3	1.2E+16	0.045	4.1	5.4E+06	4.9E+08
Hatepe phreato	1.8	0.175		2.3E+15	0.046		1.1E+06	
Hatepe plinian	1.8	0.173	4.3	3.2E+15	0.044	4.1	1.5E+06	1.3E+08
Initial ash	1.8	0.172		2.6E+14	0.043		1.2E+05	
Mapara	2.2	0.188		2.3E+15	0.059		1.4E+06	
Whaikapu	2.8	0.184		1.8E+15	0.055		1.0E+06	
Waihimia	3.2	0.183		3.2E+16	0.054		1.8E+07	
Motutere	5.4	0.197		6.9E+14	0.068		4.8E+05	
Opepe	8.8	0.181		5.8E+15	0.052		3.1E+06	
Poronui	9.5	0.186		4.1E+15	0.057		2.4E+06	
Karapiti	9.9	0.190		5.8E+15	0.061		3.6E+06	
Oruanui	22.6	0.234		1.7E+17	0.105		1.9E+08	
Okaia	23	0.211	5.9	8.0E+15	0.082	5.7	6.8E+06	4.6E+08
Tihoi	45	0.224		5.8E+15	0.095		5.6E+06	
Kaharoa	0.93	0.198		5.8E+15	0.069		4.1E+06	
Whakatani	4.8	0.176		1.2E+16	0.047		5.6E+06	
Mamaku	7.5	0.192		6.9E+15	0.063		4.5E+06	
Rotoma	9	0.196		1.4E+16	0.067		9.5E+06	
Waiohau	11	0.200		1.6E+16	0.071		1.2E+07	
Rotorua	13.8	0.173		8.0E+15	0.044		3.6E+06	
Okareka	17	0.128		9.2E+15	0		0	
Terere	20	0.195		1.0E+16	0.066		7.0E+06	
Omateroa	26	0.137		2.1E+16	0.008		1.7E+06	
Awakeri	30	0.189		2.3E+15	0.060		1.4E+06	
Mangaone	31	0.132		1.8E+16	0.003		5.7E+05	

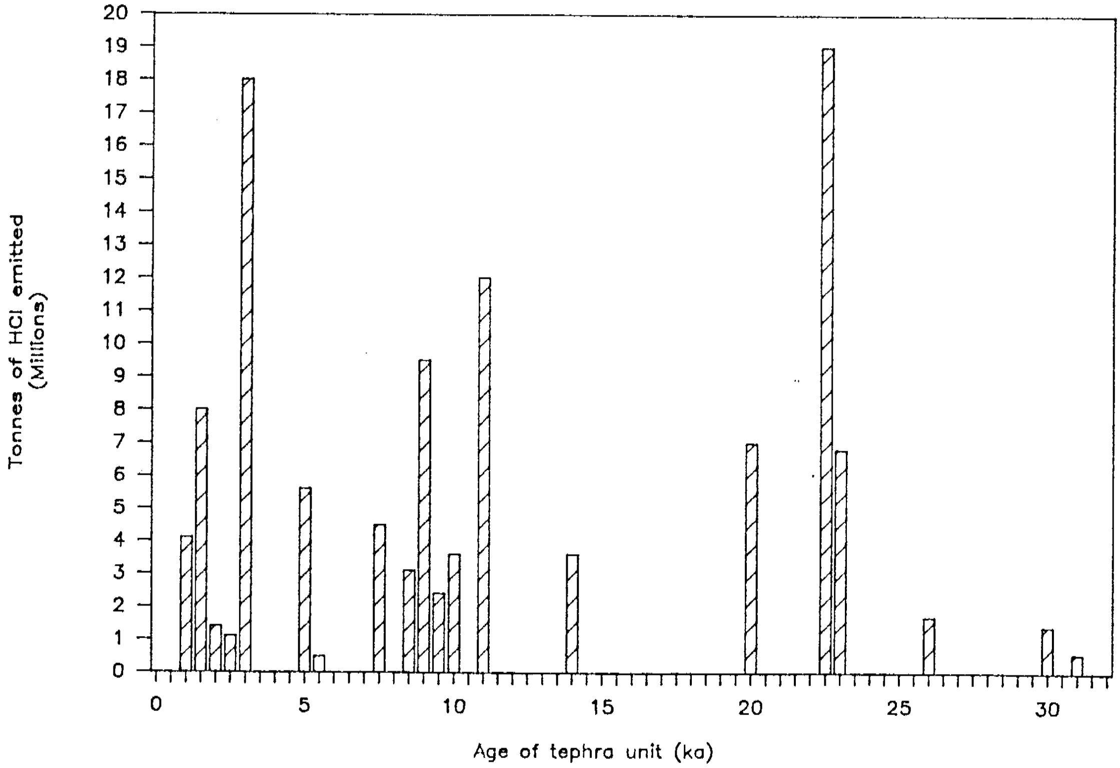

Figure 7-5. Graphic representation of Cl outputs to the atmosphere from each of the analysed TVC and OVC tephra eruptions, as determined by petrological estimates.

weight percent of the volatile compontent which degasses during eruption. This percent of degassed volatiles is multiplied by the total mass of the erupted material in order to determine the absolute amount of the volatile component which is input to the atmosphere. In this study, the concentration of H_2O in degassed magma used is 0.2 wt% (Eichelberger and Westrich, 1981), and is 0.129 wt% for Cl, which is the amount of Cl corresponding to 0.2 wt% H_2O on the H_2O:Cl correlation curve shown in Ch. 6 (Fig. 6-5).

The production of HCl by many of the TVC and OVC eruptions may be comparable to recent global anthropogenic production of HCl (~$4x10^6$ metric tonnes/yr)(Cadle, 1980; Symonds et al., 1988). The large-volume Oruanui eruption (22.6 ka) alone produced $1.9x10^8$ metric tonnes of HCl. This is among the largest outputs of HCl by a volcanic eruption for which the HCl output has been calculated (Palais and Sigurdsson, 1988).

The H_2O output has only been calculated for 3 eruptions from the TVC because they are the only ones in which the pre-eruptive H_2O contents have been directly determined in this study. The H_2O released to the atmosphere by this eruption is about 2 orders of magnitude higher than the HCl output, so may have a similar effect on the stratospheric ozone. An approximate H_2O output of the combined plinian phases of the 2 ka TVC eruption is approximately 0.5 km^3, whereas an estimate of the total H_2O

volume in the stratosphere is only 1 km^3 (Viė le Sage, 1983), so these eruptions could have a significant effect on total stratospheric H_2O. As with HCl, this amount of H_2O would be injected into a very small portion of the stratosphere, and could cause a substantial local ozone hole (Stolarski and Cicerone, 1974).

However although it appears, based on bulk H_2O and HCl output, that silicic eruptions from the TVZ could have a major impact on the stratospheric ozone layer, a number of essential factors remain unknown. Although the eruption column of the Taupo plinian tephra is approximately 50 km high (Wilson and Walker, 1985), and definitely penetrates well into the stratosphere, as many other TVZ eruptions columns are likely do as well, it is difficult to determine how much H_2O and HCl will remain in the stratosphere, and how much will rapidly return to the troposphere, adhered to larger ash particles. Johnston (1980) estimated that approximately 14 to 18% of the HCl emitted by the 1976 eruption of Augustine volcano reached the stratosphere, although the Augustine eruption column was only 12 to 14 km high. The Taupo plinian eruption, with a higher eruption column, may have transferred a greater percent of HCl and H_2O to the stratosphere. Many authors feel confident that volatile phases from volcanic eruptions would penetrate into, and remain in, the stratophere (Stolarski and Cicerone, 1974; Johnston, 1980; Turco, 1985), but no actual change in stratospheric ozone as a consequence of a volcanic eruption has been documented. However, a reason for this may be that no major silicic eruptions have occurred in the recent past, when direct observations of stratospheric ozone were possible, and no geologic or biologic record of past ozone variations have been recognized. In view of this, local or global stratospheric ozone depletions due to H_2O and Cl should be regarded as yet another volcanic hazard associated with major explosive rhyolitic eruptions.

8. CONCLUSIONS

In this project, the pre-eruptive conditions and eruptive processes of TVZ rhyolitic magmas have been investigated using a combination of approaches. The following conclusions have been reached:

Pre-eruptive magmatic compositions and compositional gradients. The pre-eruptive H_2O contents of a post-22.6 ka and pre-22.6 ka TVC magma, based on detailed melt inclusions analyses, were 4.3 and 5.9 wt.% respectively. Melt inclusion compositions also indicate that the pre-eruptive F for all magmas analysed was ~400-500 ppm, and the Cl ranged from 0.13 to 0.22 wt.%. Melt inclusion and bulk rock analyses together clearly indicate that there were no strong, systematic volatile, major or trace element compositional zonations in the magmas which produced TVC and OVC eruptions. Vigorous convection, and/or short residence time of magmas in the crust may account for their compositional homogeneity. Furthermore, compositional changes in the TVC magma at 22.6 ka suggest that the TVC magma chambers were relatively small, not more than several hundred cubic km in volume, and were not highly differentiated magmatic cupolas capping a larger, more mafic magmatic system.

<u>Initiation of eruptions</u> The compositional homogeneity of the TVC magmas suggest that the oversaturation of volatile phases in the melt (primarily H_2O) which triggered the eruptions was not caused by the development of a volatile gradient, but was initiated by another process, such as bouyant rise of the magma through the crust, or tectonic depressurization of the magma chamber. The similarity in water contents of magmas which produced the Taupo "ultraplinian" event and another less explosive eruption suggest that the degree of explosivity of the eruptions from the TVC was not soley controlled by the pre-eruptive volatile content of the melt, but was probably dependent on withdrawal dynamics of the magma from the chamber.

<u>Eruptive processes and degassing</u> During the eruptive process, obsidian quenched from primary melt, probably along the conduit walls, retaining a volatile content proportional to the pressure at which it quenched. Based on the water content of obsidian and calculations of fragmentation depths, most obsidian must have quenched from fragmented magma (bubble volume:melt volume of 3:1). Hydrogen isotope systematics suggest that degassing of magma during eruptions was primarily an open-system process, at least in the pressure range where obsidian

formed. As evidenced by volatile composition of obsidian, degassing of H_2O and Cl during the eruptions were coupled, probably due to the strong partitioning of Cl into a H_2O-rich vapor phase.

Volatile and metal outputs of TVZ magmas Calculations suggest that the stratospheric ozone budget could have been significantly affected by H_2O and Cl released during explosive TVZ eruptions, if the eruption columns penetrated into the stratosphere, which is likely. Also, calculations of the total H_2O, Cl, Cu, Sn, and Mo which could have been released by a non-eruptive, crystallizing, TVC magmatic system suggest that even small-volume, average-composition rhyolitic systems have the potential to form porphyry ore deposits under certain geological conditions.

APPENDICES

APPENDIX A

Table A-1. List of samples from Taupo center.

Number	Unit	Locality	Type	Comments
83-001	Rotongaio	19	B	
83-002	Hatepe phr.	"	B	basal 12 cm.
83-003	" "	"	B	next 12 cm.
83-004	" "	"	B	next 12 cm.
83-005	" "	"	B	top 12 cm.
83-006	" "	"	B	obs. rich layer 38-40 cm from base.
83-007	Hatepe pl .	"	O	
83-008	Motutere	"	B	
83-009	Poronui	"	B	lower 12 cm. of plinian
83-010	Karapiti	"	B	lower 8 cm.
83-011	" "	"	B	base of upper 13 cm.
83-012	" "	"	B	upper 13 cm.
83-013	Rot/Taupo pl.	27	B	transition between 2 units
83-014	Taupo pl.	"	B	basal 15 cm.
83-015	" "	"	B	next 50 cm.
83-016	" "	"	O	top of unit (top of sample 15)
83-017	" "	"	P	top 20 cm.
83-018	Waihimia	31	O	from 1 m. above base
83-019	" "	"	P	from 1 to 2 m. above base
83-020	" "	"	B	from crystal rich layer
83-021	" "	"	P	mixed pumice from 2 m below top
83-022	Taupo pl.	32	O	in gulley fill
83-023	Hatepe phr.	"	B	plinian layer 80 cm. up from base of phreatomagmatic
83-024	Mapara	1	B	basal 15 cm.
83-025	" "	"	B	31 cm., 39 cm up from base
83-026	" "	"	B	top 10 cm.
83-027	Hatepe pl.	"	B	
83-028	Groundlayer	"	B	
83-029	Whaikapo	"	B	bottom 15 cm., lithic rich
83-030	Opepe	"	B	22 cm., 114 cm. up from base
83-031	" "	"	B	50 cm., 65 cm. up from base
83-032	" "	"	B	basal 65 cm.
83-033	" "	"	P	top of unit
83-034	Karapiti	"	B	bottom 50 cm.

Table A-1 con't

Number	Unit	Stop	Type	Comments
83-035	" "	"	B	top 50 cm.
83-036	" "	"	P	top of unit
83-037	Groundlayer	24	O	
83-038	" "	"	O	one large chunk
83-039	Rotongaio	"	B	0-10 cm. from base
83-040	" "	"	B	10-20 cm. from base
83-041	" "	"	B	20-30 cm. from base
83-042	" "	"	B	30-70 cm. from base
83-043	Initial ash	"	B	lower 30 cm.
83-044	Hatepe pl./I.A	"	B	8 cm. between Hat. pl. and Initial Ash
83-045	Hatepe pl.	"	O	
83-046	Hatepe pl.	"	P	
83-047	Okaia	10	B	top 85 cm.
83-048	Okaia	"	B	basal 20 cm.
83-049	Oruanui	"	B	layer 1, 20 cm.
83-050	" "	"	B	layer 2, 4 cm.
83-051	" "	9	B	layer 3
83-052	" "	"	B	basal airfall
83-053	" "	10	B	layer 1, 22 cm.
83-054	Tihoi	"	B	top 57 cm.
83-055	" "	"	B	top 40 cm.
83-056	Okaia	33-b	B	
83-082	Oruanui	46	B	unit 1
86-108	Hatepe pl.	26	B	0-45 cm.
86-109	" "	"	B	45-90 cm.
86-110	" "	"	B	90-135 cm.
86-111	" "	"	B	135-180 cm.
86-112	" "	"	B	180-220 cm.
86-113	Poronui	19	B	0-22 cm.
86-114	"	"	B	22-44 cm.
86-115	Motutere	19	B	20 cm.
86-116	Waihimia	31	B	0-106 cm.
86-117	"	"	B	106-212 cm.
86-118	"	"	B	212-320 cm.
86-119	"	"	B	320-460 cm.
86-120	"	"	B	460-600 cm.
86-121	Initial Ash	46	B	0-12 cm.
86-122	" "	"	B	12-40 cm.
86-123	Tau. pl./Rot.	46	B	0-9 cm.
86-124	" " "	"	B	9-23 cm.
86-125	" " "	"	B	23-39 cm.
86-126	Pl. w/in T.Ig	46	B	
86-127a	Whaikapo	1	B	0-33 cm.
86-133	Lithic Obs.	46	O	
86-134	Rotongaio	46	B	0-50 cm.
86-135	"	"	B	50-100 cm.
86-136	"	"	B	100-150 cm.
86-137	"	"	B	150-200 cm.
86-138	"	"	B	200-250 cm.

Table A-1 con't

Number	Unit	Stop	Type	Comments
86-139	"	"	B	250-300 cm.
86-140	"	"	B	275-285 cm.
86-141	"	"	B	300-350 cm.
86-142	"	"	B	350-400 cm.
86-143	"	"	B	400-450 cm.
86-144	"	"	B	450-500 cm.
86-145	"	"	B	500-545 cm.
86-146	"	"	B	545-560 cm.
86-147	Hatepe Phr.	26	B	0-100 cm.
86-148	" "	"	B	100-200 cm.
86-149	" "	"	B	200-300 cm.
86-150	" "	"	B	300-400 cm.
86-151	" "	"	B	400-500 cm.
86-152	" "	"	B	500-675 cm.
86-153	" "	"	B	675-775 cm.
86-154	Taupo Pl.	27	B	0-32 cm.
86-155	" "	"	B	32-64 cm.
86-156	" "	"	B	64-96 cm.
86-157	" "	"	B	96-128 cm.
86-158	" "	"	B	128-160 cm.
86-159	" "	"	P	from top 80 cm.
86-160	" "	"	P	from bottom 80 cm.
DOBS	Ben Lomond Obs.	4	O	obsidian flow

B = bulk sample
P = pumice picked at outcrop
O = obsidian picked at outcrop

Abbreviations: (in order of occurrence)
phr: phreatomagmatic
pl: plinian
Rot: Rotongaio
IA: Initial Ash
Tau: Taupo
T. Ig: Taupo Ignimbrite
Obs: obsidian

Table A-2. List of samples from Okataina center.

Number	Unit	Locality	Type	Comments
83-057	Te Rere	35	B	basal 10 cm.
83-058	" "	"	B	next 11 cm.
83-059	" "	"	B	next 10 cm.
83-060	" "	"	B	top 15 cm.
83-061	------	36		glassy skin of lava flow
83-062	Rotoma	37	B	coarse layer 30-70 cm from base
83-063	" "	"	B	next 60 cm.
83-064	" "	"	B	top 140 cm.
83-065	Mamaku	38	B	55-65 cm. from base
83-066	" "	"	B	165-175 cm. from base
83-067	" "	"	B	30 cm. layer above 1st ignimbrite
83-068	Whakatane	39	B	fine layer 3m. above base
83-069	" "	"	P	pumice from base
83-070	Mangaone	40	B	basal 39 cm.
83-071	" "	"	B	next 24 cm.
83-072	Awakeri	"	B	
83-073	Omataroa	41	P,O	1 m. above base
83-074	" "	"	O	4.5 m. above base
83-075	" "	"	O	2 m. above base
83-076	Okareka	42	B	60-100 cm. up from base
83-077	" "	"	P	16-43 cm. up from base
83-078	Rerewhai.	43	B	0-38 cm. from base
83-079	" "	"	B	42 -65 cm. from base
83-080	Kaharoa	44	B	60 cm. up from base
83-081	Waiohau	45	B	Obs. rich layer 40 cm. up from base
83-083	Rotorua	34	O	coarse bed 1.5 m. from base
83-084	" "	"	P	coarse bed 1.5 m. from base
83-085	" "	"	B	1 m. above base
83-086	" "	"	O	base
83-087	" "	"	O	1 m. above base
83-088	" "	"	O	2.5 m. above base
83-090	" "	"	P	2.5 m. above base
83-091	" "	"	B	2.5 m. above base
86-127b	Waiohau	45	B	0-29 cm.
86-128	"	"	B	29-62 cm.
86-129	Kaharoa	44	B	0-45 cm.
86-130	"	"	B	45-90 cm.
86-131	"	"	B	90-135 cm.
86-132	"	"	B	135-180 cm.

Table A-2 con't

B = bulk sample

P = pumice picked from outcrop

O = obsidian picked from outcrop

Table A-3. List of sample localities listed in Tables A-1 and A-2

Locality number	Location
1	DeBretts Section. Highway 5, 0.25 km. west of junction with Crown Rd. NZMS 1 N94/579353
4	Poihipi Rd., 2.5 km. southwest of junction with Whangamata forestry Rd. NZMS 1 N93/435050
9	Whangamata Rd., 2 km. southwest of junction with Waihora Rd. NZMS 1 N93/312456
10	Whangamata Rd. 0.5 km. southeast of junction with Otake Rd. NZMS 1 N93/374457
19	Mission Bay Rd. NZMS 1 N103/491076
24	Unnamed forest rd. 1.5 km southeast of Highway 1. NZMS 1 N103/493158
27	Highway 5, 0.75 km. northwest of Opepe monument NZMS 1 N103/680280
31	High Level Rd., 2 km. southwest of junction with Mere Rd. NZMS 1 N103/689190
32	High Level Rd., 3.5 km. southwest of junction with Mere Rd. NZMS 1 N103/677184
34	Quarry on Tawarewa-Okareka loop Rd. NZMS 152 793002
35	Highway 30 at Huaparu Bay. NZMS 152 877148
36	Unnamed forest rd., 1.5 km. south of Highway 30. NZMS 152 915130

Table A-3 con't

Locality number	Location
37	Unnamed forest rd., 4 km. south of Highway 30. NZMS 152 925110
38	NZMS 1 N77/919105
39	NZMS 1 N77/956075
40	NZMS 1 N77/181093
41	NZMS 1 N77/184015
42	NZMS 1 N77/131943
43	NZMS 1 N86/995825
44	NZMS 1 N86/971868
45	NZMS 1 N85/897820
46	NZMS 1 N85/726661

Kilometer distances are estimates.

APPENDIX B

1. CHEMICAL COMPOSITION

Major element analysis

Nine major element oxides, SiO_2, TiO_2, Al_2O_3, FeO, MgO, MnO, K_2O, and Na_2O were analysed by electron microprobe in pumice, melt inclusions, and obsidian. Although the errors associated with this technique are higher than some other techniques used for major element analysis, a microbeam technique is essential for analysis of melt inclusions due to their small size.

Electron microprobe analysis involves bombarding a sample with a focussed beam of electrons generated by a tungsten filament. The electron beam strikes the sample surface, and causes some inner-shell electrons from constituent elements to be ejected. Outer shell electrons then cascade down to take the place of the ejected electrons, and these electronic transformations emit x-rays of characteristic energies, and therefore characteristic wavelengths. These x-rays are then diffracted by specifically prepared crystals of known d-spacing, and the intensities of specific elemental x-rays are measured. Several methods of relating raw counts to elemental abundances are available, and in this study, the empirical correction technique proposed by Bence and Albee (1968) was used. A variety of characterized minerals were used as end-member standards.

The electron microprobe used for this portion of the study was a JEOL-733 superprobe at Victoria University, Wellington, NZ. Operating conditions were as follows: 15 kV accelerating voltage, $8x10^{-9}$ amps beam current, and beam defocussed to 20 um. These conditions are specific for glass analysis, to reduce the migration and volatilization of Na during analysis. Counting times were generally 20 sec. on peak, repeated 3 times, and 20 sec. on background, repeated once. Variations on these conditions were sometimes used. A peak search was generally performed on every third analysis.

A number of standards were analysed as unknowns to ensure that the electron microprobe analysis were accurate. The most frequently used were comenditic obsidian KN-18, and a pantelleritic obsidian KE-12, provided by H. Sigurdsson. These standards were run at the beginning, and at intervals throughout the analytical sessions. Average analysed values for these standards compared with the accepted values are shown in Table B-1-1.

The average errors for electron microprobe analyses of major elements can be determined from the number of counts generated for a specific element. The counting error to 1 sigma confidence is equal to the square root of the number of counts per second generated by a specific element. The average counting errors of specific elements for samples KN-18, KE-12, and an average Taupo sample are given in Table B-1-1. The counting errors for KN-18 and KE-12 are generally similar to, or slightly higher than, the standard deviations shown for the repeat runs of these samples.

Table B-1-1. Comparison of determined and accepted values for two electron microprobe standards, KE-12 and KN-18. Accepted values were provided by H. Sigurdsson (pers comm., 1984). Also given are the standard deviations for replicate analyses of standards (st. dev.) and counting errors to a 1 sigma confidence level for standards and an average Taupo composition (1 sigma error). All values are given in wt %.

Element	KN-18				KE-12				Average Taupo
	accepted	mean	st. dev.	1 error	accepted	mean	st. dev.	1 error	error
to 1									
SiO2	74.60	75.0	0.9	0.9	70.30	70.9	1.5	0.9	0.9
TiO2	0.18	0.2	0.1	0.1	0.33	0.3	0.1	0.1	0.1
Al2O3	10.53	10.4	0.4	0.4	7.62	7.4	0.1	0.3	0.4
FeO	3.45	3.4	0.3	0.5	8.36	8.4	0.3	0.9	0.2
MnO	0.06	*	*	*	0.26	0.3	0.1	0.2	*
MgO	0.01	*	*	*	0.02	*	*	*	*
CaO	0.15	0.1	0.1	0.1	0.35	0.3	0.1	0.1	0.2
Na2O	5.68	5.0	0.4	0.5	7.28	6.8	0.4	0.5	0.3
K2O	4.39	4.5	0.1	0.4	4.27	4.3	0.2	0.4	0.4
total	99.90	98.9			99.58	99.0			
n=		19				19			

Trace element analyses

X-Ray Fluorescence

X-ray fluorescence (XRF) analysis was used to determine 7 trace elements, Pb, Th, Rb, Sr, Y, Zr, and Nb in pumice samples. The pumice was ground with a TEMA swing mill, using a tungsten-carbide inner container. Approximately 7 g of powder were pressed into boric-acid-backed pellets, using 10 tons of pressure.

In x-ray fluorescence analysis, a beam of primary x-rays is produced in a rhodium tube to generate characteristic secondary x-rays from a sample. The secondary x-rays are characteristic of an element and have unique wavelengths. The intensity of x-rays emitted by a sample is proportional to the elemental abundance.

Analyses followed the procedure of Norrish and Chappell (1977), using a Rigaku 3062 instrument. Generator settings for the x-ray beam were 60 kV and 45 mA. Counting times for each element are shown in Table B-1-2. Standards used to produce the calibration curve include PCC-1, AGV-1, G-2, GSP-1, and BCR-1, MA-N, AN-G, BE-N, NIM-G, and JR-2. Absorption corrections were made using Rh compton peak determinations.

Multiple runs of standard JR-2 were made in order to assess the reproducibility of the XRF determinations.

In addition, the counting errors to 1 sigma for each element were determined using the method described in the previous section. In general, the counting errors were greater than the actual reproducibility of analyses, which indicates that these XRF determinations are more precise than would be indicated by counting statistics alone. Counting errors for an average Taupo sample are also given in Table B-1-2.

Table B-1-2. Counting times and error determinations for trace elements analysed by x-ray fluorescence. Mean determined values for 10 analyses of sample JR-2 are given, along with standard deviations of multiple analyses (st. dev.). Also, errors based on machine counting statistics to a 1 sigma confidence level are given for JR-2 and an average Taupo sample. All determinations and errors are given in ppm.

Element	counting time peak (s)	counting time bkg. (s)	JR-2 accepted* (ppm)	JR-2 mean (ppm)	JR-2 st. dev. (ppm)	JR-2 error to 1	Taupo counting error to 1 (ppm)
Pb	200	100	21.9	24	1	3	3
Th	200	100	32.2	36	1	4	2
Rb	100	100	297	304	3	6	3
Sr	100	40	8	8	1	1	4
Y	100	40	51	52	1	2	2
Zr	100	100	98.5	96	1	3	4
Nb	200	100	19.2	20	1	1	1
n=				10			

*From Ando et al., 1987

Neutron activation analysis

A number of trace elements, including Sc, Co, Zn, As, Rb, Sb, Cs, Ba, La, Ce, Sm, Eu, Tb, Yb, Lu, Hf, Ta, Th, and U were analysed by instrumental neutron activation analysis (INAA) (Jacobs et al., 1977). Two major elements, Na and Fe were also determined by this technique. Individual fragments of obsidian and bulk pumice samples from 4 units were analysed by INAA.

INAA involves irradiating samples, thereby converting some stable isotopes to radioactive nuclides. These nuclides decay and some emit gamma particles which have characteristic energies. The intensity of gamma particles of certain energies can be related to the abundance of their parent elements.

Approximately 20 to 100 mg of sample were packed in ultrapure quartz vials and irradiated at the University of Missouri research reactor for approximately 40 hrs at a flux of 2.23×10^{13} $N \cdot cm^{-2} \cdot s^{-1}$. Samples were counted for 2 to 3 hrs each at 7 days and 40 days after irradiation using 2 high-purity germanium detectors. Data was reduced using a Nuclear Data 6620 system and TEABAGS (Korotev and Lindstrom, 1985). An NBS fly ash standard (reference material 1633a) was used for calibration (Korotev, 1987). Counting errors to 1 sigma are calculated for each analysed sample and are listed with the chemical analyses.

2. VOLATILE ANALYSES

Water Analyses

Karl Fischer Titration

The main method used for water analyses was Karl Fischer titration (Westrich, 1987). This technique involves titrating the unknown quantity of water in a pyridine-methanol solution containing iodide ion (I^-) and SO_2 as principle components. The following reaction occurs:

$$I_2 + SO_2 + H_2O = 2HI + SO_2 \qquad (B.2.1)$$

As this reaction proceeds, iodide ion is generated by electrolysis at the anion. The H_2O/I_2 reaction always occurs in 1:1 proportions, so the amounts of H_2O introduced to the solution (H_2O content of the sample) is directly proportional to the amount of electric current necessary to regenerate the I_2.

The apparatus consists of a furnace and a Karl-Fischer titration cell. The furnace used was a platinum-wound cylindrical furnace with a solid-state proportional controller, calibrated by a Pt/Pt^- 10% Rh thermocouple. The water vapor emitted from the sample was transported to the Karl-Fischer (COSA Instruments Inc., model CA-05) titration cell by dry helium. The titration cell is controlled by an automated electrolysis current control system.

The sensivity of this technique has been evaluated by the manufacturer at 0.1 micrograms of H_2O, and the precision is ± 3 micrograms for a sample size of between 10 and 1000 micrograms of H_2O, or about a 3% error for a typical sample size of 1000 micrograms H_2O used in this study. Although this may be true under ideal conditions for perfectly homogenous samples, precision of the analyses done so far have been lower. My results suggest that precision is often this high for some samples, but that multiple runs of other samples do not fall within these limits, probably due to inhomogeneity of natural samples (Table B-2-1). Samples run on different days tend to show lower precision, probably due to differences in atmospheric humidity or drying conditions. Westrich (1987) estimated average standard deviations of this method at $< 5\%$ for samples with low H_2O contents of ~ 0.1 wt%, and $< 2.5\%$ for samples with H_2O contents of > 1.5 wt%.

The basic technique for extraction of the water from the obsidian is as follows:

1) Prepare samples, either by grinding obsidian fragments to 75 mesh with an agate mortar and pestle, using acetone as a grinding medium, or by cleaning obsidian fragments in an ultrasonic bath.

2) Dry in a 100^{o} C oven overnight.

Store in dried vials.

3) Load sample into a tin sample boat. A wide range of weights are acceptable, but it is best to use more than 10 mg.

4) Place sample in furnace, and heat to ~200^{o} C for approximately 2 mins, to drive off any H_2O adsorbed during weighing. Then heat to 950^{o} C for 10-15 mins., and begin titrating at 250^{o}C. Heating may be required for longer than 15 minutes if titration is still continuing at that point.

Duplicate or triplicate runs were done of ground samples. Obsidian fragments were analysed from selected samples, generally 1 sample per tephra unit. Approximately 10-15 individual fragments were analysed per sample, although not all yield water content values because some do not vesiculate.

The water contents of 4 geochemical standards were analysed by Karl Fischer titration, and the results are shown in Table B-2-2. The accepted and analysed values do not agree well, and the Karl Fischer titration analyses invariably indicate a lower water content than the accepted values. The probable reason for the discrepancy is that in Karl Fischer titration analysis, the sample is pre-dried in the analytical furnace, and is not re-exposed

Table B-2-1. Replicate analyses of powdered obsidian samples listed in order of increasing H_2O content. The number of replicate runs is indicated by "n".

Sample	Mean H_2O content	n	% variance about mean
017	0.21	2	14
148	0.40	2	13
028	0.47	2	2
059	0.52	2	4
056	0.61	2	5
037	0.62	2	3
068	0.66	2	2
057	0.70	2	4
024	0.70	4	4
078	0.87	2	1
034	0.88	2	5
026	0.95	2	5
150	0.97	3	2
032	1.10	2	0
011	1.13	2	4
029	1.25	2	2
072	1.27	2	2

Table B-2-2. Water contents of standards analysed by Karl Fischer titration.

Standard	Accepted Water (wt.%)	Analysed Water (wt.%)	Drying Temp. degrees C
G-2		0.273	200
		0.287	200
BCR		0.265	200
		0.268	200
		0.433	100
AGV-1		0.376	200
		0.438	150
		0.504	100
NBS-278		0.270	220
		0.300	190
		0.330	180
		0.330	160

to air prior to analysis. This eliminates the problem of analysing adsorbed water which can be introduced into a fine-grained sample in a very short time of exposure to the air, while the sample is being weighed for analysis (Westrich, 1987). Furthermore, drying to 200^{o}C may be more effective than drying to 100^{o}C, as can be seen in Table B-2-2, although at this temperature a small amount of magmatic water may be removed as well as adsorbed water.

The main advantage of this technique is that the accuracy is good at low quantities of H_2O, so it is possible to analyse individual obsidian fragments. Also, it is possible to do stepwise heating runs of samples, and to determine the H_2O output over each heating step. This allows detailed analyses of the degassing spectrum of natural samples. Other advantages are that each analysis is quick, and because the technique is direct, not relative, there is no need for standardization.

Analyses from the Karl Fischer titration method compare favorably with another technique of water analysis, the Dupont Moisture Analyser. However, with the Dupont Moisture analyser it is not easy to dry the sample in the furnace just prior to analysis, and this is can be a problem for samples with low water concentration. Values for samples run by both methods are shown in Table B-2-3.

Table B-2-3. Comparison of water values from the Dupont Moisture Analyser (DMA) and Karl Fischer Titration (KFT).

Sample	H_2O by KFT (wt.%)	H_2O by DMA (wt.%)	Difference (wt.%)
002	0.46	0.42	0.04
003	0.58	0.56	0.02
004	1.56	1.55	0.01
005	1.12	1.07	0.05
006	1.26	1.59	0.33
014	0.45	0.43	0.02
015	0.23	0.24	0.01
016	0.52	0.49	0.03
026	0.90	1.20	0.30
030	1.00	1.16	0.16
031	1.02	1.41	0.39
032	1.10	1.44	0.33
057	0.73	0.78	0.05
059	0.54	0.60	0.06
070	1.49	1.52	0.03
071	1.48	1.68	0.20
DOBS	0.29	0.10	0.19

Ion Microprobe

The ion microprobe is a microbeam technique which has been applied to analysis of H_2O in melt inclusions. The basic theory of the ion microprobe is discussed in Ch. 3. The instrument used in this study was at Arizona State University, and consists Cameca IMS 3f with a Cameca duoplasmatron to generate primary ions. The primary beam was accelerated to 12.5 keV, and mass analysed to eliminate H ions present in the duoplasmatron. To determine H_2O, either positive or negative secondary H ions can be analysed. Operating currents for negative secondary ions were 2-4 nA, and 8-12 nA for positive secondary ions. Positive H ion were normalized to Si^{++} in the sample, and negative H ions normalized to O^-. The beam was focussed to approximately 20 um and was positioned on the area of interest using an optical microscope. The sample was held at a current of either + or - 4500 eV depending on whether negative or positive secondary ions were analysed.

Secondary ions were generated from the sample by the impinging primary ion beam. A fraction of the secondary ions were accelerated at 4500 eV into a mass spectrometer. There, they were passed through an energy filter and magnet into the counting system.

The effect of sample composition on ion microprobe analyses is not well understood or quantitatively resolved, so the best approach is to use standards which are as compositionally similar to the samples as possible. The main standards used in the analysis of H_2O in this study are hydrous rhyolitic glasses prepared by H. Westrich at Sandia National Labs, containing 0.2, 1.62 and 3.62 wt% H_2O. A synthetic albite containing 5.38 wt% H_2O was also used. A calibration curve for H_2O analysed as positive H ($H^{=}$) ions is shown in Fig. B-2-1. An anhydrous feldspar is used as a blank for H analyses.

The error of this technique is approximately ± 0.5 wt% H_2O based on replicate analyses of standards. The actual error is higher than it should be based on count rate statistics. This may be due to variable charging of the samples during analysis.

Chlorine Analyses

Electron microprobe analysis of chlorine in melt inclusions requires longer counting times than are normally used due to the low concentrations of Cl. Therefore, the full suite of major elements are not analysed and usual calibration techniques are not possible. Instead, two standards of similar chemical composition as Taupo rhyolites are analysed as unknowns,

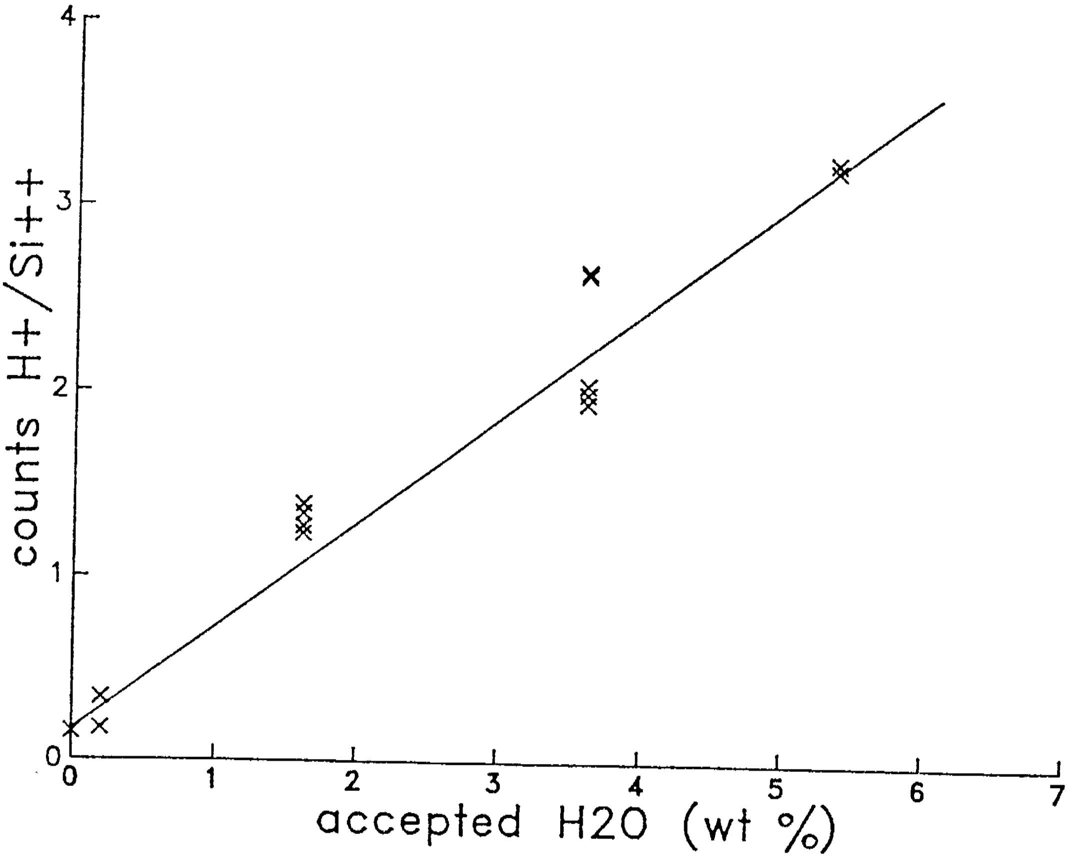

Figure B-2-1. Ion microprobe calibration curve for H^+.

and a calibration factor is calculated. This factor is then applied to the analytical results in order to determine true values.

Chlorine in glass inclusions and obsidian was analysed using the method described by Devine et al (1984). Analyses were made using a JEOL-733 superprobe at Victoria University, N.Z., with the operating conditions described for major element analysis. The Cl analyses each involved a peak search and then three 50 second counts on the peak and one 75 second count on each background.

This analytical method is applicable to elements such as Cl, S, and F, which are not normally analysed by electron microprobe. An average correction factor of 1.45 was used. Calibration curves for analyses done in other years are slightly different. The lack of matrix correction could be a problem, but the standards used to determine the calibration factor have similar chemistry to the TVZ samples. The detection limit for Cl by this method is approximately 200 ppm. The error of analyses for Cl is determined by the standard deviation of replicate standard analyses, shown in Table B-2-4.

Sulfur was also analysed by this technique, but was below detection limits of 200 ppm for all Taupo samples.

Table B-2-4. Accepted and analytical values for Cl standards. for electron microprobe analyses done in Jan., 1988. The "n" column represents the number of analyses.

standard	accepted Cl value (wt. %)	n	stand. dev.
KN-18	0.37	21	0.018
KE-12	0.33	23	0.012

Fluorine analyses

Fluorine was analysed by ion microprobe by the same technique used to analyse H_2O (described earlier in this section). The standards used for F analyses include an A-type granite (GI-1), a rhyolitic obsidian (Los Posos rhyolite) and macusanite glass from Peru (Westrich, 1987; London et al., 1987). A calibration curve for F in these standards is shown in Fig. B-2-2. The error for F determinations are approximately $\pm$100 ppm, based on replicate analyses of the standards.

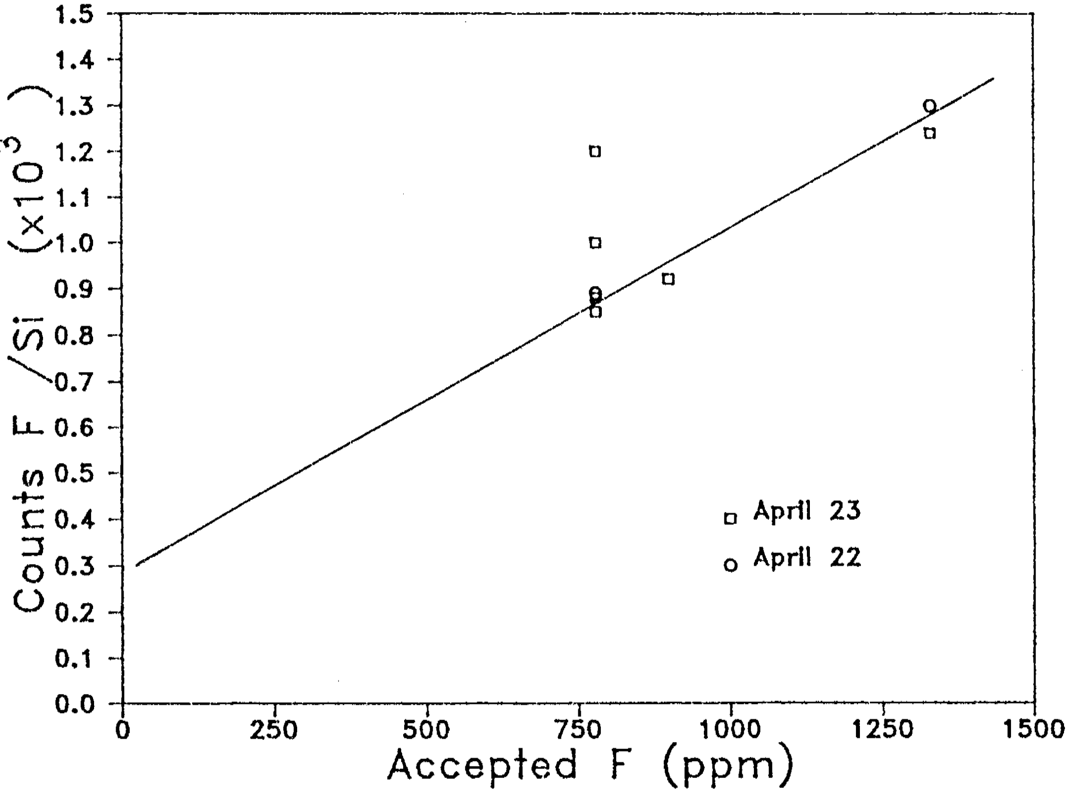

Figure B-2-2. Ion microprobe calibration curve for F.

3. GEOTHERMOMETRY

Magnetite/ilmenite geothermometry

The composition of magnetite and ilmenite from Taupo and Okataina tephras were determined by electron microprobe analysis.

Polished thin sections were prepared from crystals separated with a hand magnet, and polishing was done using only diamond grit, so as not to introduce any contaminants. Large crystals containing both magnetite and ilmenite inclusions were found using a reflected light microscope with crossed polarizers, where magnetite is isotropic and ilmenite shows reflective pleiochroic behavior. Grains containing both species were photographed and circled with a thin ink line for easy location during analysis. Slides were then carbon coated.

Most microprobe analyses were made using an ARL microprobe at the University of New Mexico. Some analyses of Fe-Ti oxides were also made on a JEOL-733 superprobe at Victoria University, NZ, and operating conditions are discussed in part B-1. Operating conditions for the ARL were: 15 kV accelerating voltage, 1.2×10^{-8} amps beam current; 1 micron beam size, and count times of 10 seconds. Raw data correction was done with the Bence and Albee (1968) method, using known mineral standards. Known standards of magnetite and ilmenite were also used as checks to ensure that the calibration was maintained. Three or four grains were analysed per sample, and 2 to 6 points of magnetite and ilmenite each were analysed per grain, as many as possible on different magnetite and ilmenite blebs.

Once the data had been accumulated, temperature and oxygen fugacity were calculated based on the method established by Buddington and Lindsley (1964), using a computer program written by Stormer (1983). The program initially converts total iron determined by the microprobe into divalent and trivalent species, for both magnetite and ilmenite, then calculates temperature and oxygen fugacity by methods proposed by Stormer (1983). This program was slightly modified to include recent changes in some thermodynamic data (Anderson and Lindsley, 1985). Errors of determinations are given in the table of temperature and oxygen fugacity values in Appendix E.

Melt Inclusion analyses

The basic technique used to determine melt (T_m)

and homogenization (T_h) temperatures of melt inclusions was to heat the inclusion on a carefully controlled microscope heating stage. During heating, the behavior of the inclusion was observed, noting changes in the inclusion's appearance, and the temperatures at which they occur.

The crystals containing inclusions used for analyses were doubly polished in order to assure good visibility of the inclusions, especially at high temperatures where optics become distorted. The thickness of the chip is not very important for transparent minerals such as quartz and feldspar, in fact, thicker chips are often desirable because more inclusions will be present in a given chip.

Measurements used a Linkham 1500 stage connected to an automated power supply which allowed heating rate adjustments, monitored temperature with a thermocouple. The outer jacket of the stage was H_2O cooled, and the inner portion cooled by circulating air. The standards used for calibration are shown in Table B-3-1. The calibration curve prepared from this data is shown in Fig. B-3-1. Once calibrated, the stage remained quite stable, although the maximum attainable temperature constantly dropped due to corrosion problems with the connection between the power supply and the heating element. Before running samples, a bracketing high and

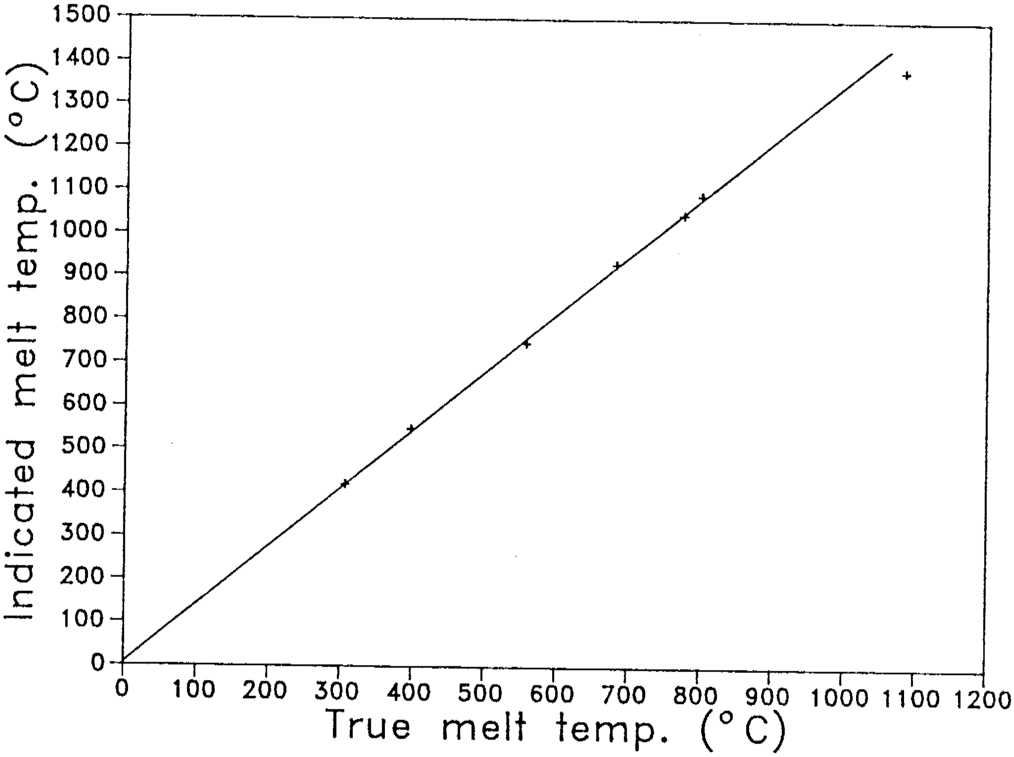

Figure B-3-1. Calibration curve for high-temperature stage

Table B-3-1. True melt temperature and indicated melt temperature for a number of pure standards as determined by high-temperature-stage analysis.

Compound	True Melt Temp. (°C)	Indicated Melt Temp. (°C)
$NaNO_3$	307	420
$K_2Cr_2O_7$	398	550
AgI	558	748
KI	683	932
KCl	776	1048
NaCl	801	1093
Cu	1083	topped out at 1385

low standard were run to ensure that the calibration had been maintained.

The sample was heated quickly (~100°C/min) to the melting point. Once melting was attained, heating proceeded more slowly, leaving samples at higher temperatures for 5 to 30 minutes, because homogenization requires dissolution of gas into melt and kinetics of melt/gas reactions are slow. Because so few inclusions were analysed, no standard post-melting procedure was established.

The melting point of silicate melt inclusions from the Taupo Volcanic Zone are often not easy to pinpoint, because the appearance of the inclusion does not change much. Some changes which indicate melting include: subtle movement of the vapor bubble, simultaneous nucleation of a number of small bubbles, change in vapor bubble size, or color change of the glass. All of these criteria, except color change, are definite indications that the glass has melted, but show maximum melt temperature, because the glass may be molten for some time before any of these changes occur.

The T_h is easier to pinpoint than the T_m, but may not be representative of true trapping temperature of the inclusion because dissolution kinetics of melts can be slow, and heated inclusion glass can cause the host crystal to stretch, or even decrepitate during the heating process (Roedder, 1979). A problem encountered with the Taupo inclusions is that they would commonly decrepitate, rather than homogenize. The decrepitation temperature may approximate the trapping temperature, and decrepitation of heated inclusions may indicate that the volatile content of the melt was high (Chaigneau et al., 1980).

4. ISOTOPIC ANALYSES

Oxygen isotopes

The oxygen isotopic composition was measured on CO_2 made from oxygen released from obsidian by fluorination of samples with ClF_3 at 575°C in nickel reaction tubes. Oxygen was converted into CO_2 by reaction with a graphite rod held in a Pt wire coil. Analyses were performed on a modified Nuclide 6", 60° double collecting ratio mass spectrometer.

Hydrogen isotopes

Hydrogen (as water) was extracted from bulk obsidian samples by melting in vacuum, after degassing the samples at 150°C in vacuum for 2 hours. The non-condensible portion of the sample was exposed to CuO at 450°C in order to insure that all hydrogen was in the form of H_2O. Analyses were performed with a modified Varian GD 150 double collecting ratio mass spectrometer.

APPENDIX C

Major and trace element composition of melt inclusions, obsidian and bulk rock

Table C-1. Major element oxide composition of melt inclusions, obsidian and pumice from the Taupo volcanic center as analysed by electron microprobe, reported as major element oxides. Melt inclusions analyses marked with an asterix were done in 1985, and those without in 1986. Analyses are normalized to 4 wt% Na_2O.

Unit		Oxide (wt.%) SiO_2	TiO_2	Al_2O_3	FeO	MgO	CaO	Na_2O	K_2O	total
Taupo plinian										
melt incl.	1	72.8	0.2	12.1	2.4	0.2	1.3	3.4	2.8	95.2
	2	72.8	0.3	11.6	1.9	0.2	1.3	3.4	2.5	94.1
	3	73.0	0.2	11.9	2.4	0.2	1.3	3.3	2.8	95.4
	4	73.9	0.3	12.6	2.3	0.2	1.4	3.5	2.8	97.2
mean		73.1	0.3	12.1	2.3	0.2	1.3	3.4	2.7	95.4
stand. dev.		0.5	0.1	0.4	0.2	-	0.1	0.1	0.2	1.3
recal. to 100%		76.6	0.3	12.7	2.4	0.2	1.4	3.6	2.8	100.0
to 4 wt.% Na_2O		76.2	0.3	12.6	2.4	0.2	1.4	4.0	2.8	100.0
melt incl.	1*	76.4	0.4	13.1	2.0	0.2	1.4	3.2	2.8	99.8
	2*	74.8	0.3	12.4	2.2	0.2	1.2	3.4	2.7	97.4
	3*	74.1	0.3	12.7	2.0	0.2	1.2	3.9	2.8	97.5
	4*	73.7	0.3	12.8	2.2	0.2	1.4	3.7	2.7	97.2
	5*	74.2	0.2	12.0	2.6	0.2	1.3	3.2	2.6	97.7
mean		74.3	0.3	12.6	2.2	0.2	1.3	3.5	2.7	97.7
stand. dev.		0.4	0.1	0.4	0.2	-	0.1	0.3	0.1	
recal. to 100%		76.5	0.3	12.9	2.3	0.2	1.3	3.6	2.8	100.0
to 4 wt.% Na_2O		76.2	0.3	12.7	2.3	0.2	2.3	4.0	2.8	100.0
obsidian	1a	74.9	0.3	13.0	1.8	0.2	1.5	4.3	3.3	99.7
	1b	74.9	0.3	12.5	1.6	0.2	1.5	4.4	3.2	98.8
	2	74.9	0.2	12.8	1.6	0.2	1.4	4.3	2.8	98.5
	3	75.2	0.3	12.7	2.0	0.2	1.3	4.3	2.9	98.4
	4	74.8	0.3	12.6	1.9	0.2	1.3	4.2	2.9	98.4
mean		74.9	0.3	12.7	1.8	0.2	1.4	4.3	3.0	98.8
stand. dev.		0.2	0.1	0.2	0.2	-	0.1	0.1	0.2	
recal. to 100%		75.9	0.3	12.9	1.8	0.2	1.4	4.4	3.0	100.0
to 4 wt.% Na_2O		76.2	0.3	13.0	1.8	0.2	1.4	4.0	3.0	100.0
pumice	1	74.0	0.0	12.2	1.7	0.2	1.5	2.5	2.6	94.9
	2	71.7	0.1	12.1	1.6	0.2	1.4	2.5	2.6	92.5
mean		72.8	0.1	12.2	1.7	0.2	1.5	2.5	2.6	93.7
stand. dev.		1.6	0.1	0.1	0.1	-	0.1	-	-	1.7
recal. to 100%		77.8	0.1	13.0	1.8	0.2	1.6	2.7	2.8	100.0

Table C-1 con't

Unit		Oxide (wt.%) SiO_2	TiO_2	Al_2O_3	FeO	MgO	CaO	Na_2O	K_2O	total
to 4 wt.% Na_2O		76.8	0.1	12.8	1.8	0.2	1.6	4.0	2.8	100.0
Rotongaio										
pumice	1	75.5	0.2	11.8	1.2	0.1	0.9	2.2	3.0	95.0
	2	75.3	0.1	11.5	1.3	0.1	1.1	2.2	2.9	94.7
	3	74.3	0.3	11.2	1.3	0.1	1.2	2.2	2.5	93.5
mean		75.0	0.2	11.5	1.3	0.1	1.1	2.2	2.8	94.4
stand. dev.		0.6	0.1	0.3	0.1	-	0.2	-	0.3	0.8
recal. to 100%		79.6	0.2	12.2	1.4	0.1	1.2	2.3	3.0	100.0
to 4 wt.% Na_2O		78.2	0.2	12.0	1.4	0.1	1.2	4.0	3.0	100.0
Hatepe phreatomagmatic										
melt incl.	1	73.4	0.3	12.3	2.0	0.2	1.1	3.5	2.6	95.7
	2	74.1	0.2	12.4	2.2	0.2	1.0	3.4	2.7	96.5
	3	72.4	0.7	11.8	2.0	0.2	0.8	1.9	2.8	92.8
mean		73.3	0.4	12.2	2.1	0.2	1.0	2.9	2.7	95.0
stand. dev.		0.9	0.3	0.3	0.1	-	0.2	0.9	0.1	1.9
recal. to 100%		77.3	0.4	12.9	2.2	0.2	1.1	3.1	2.9	100.0
to 4 wt.% Na_2O		76.6	0.4	12.8	2.2	0.2	1.1	4.0	2.9	100.0
melt incl.	1*	73.7	0.2	12.0	2.5	0.2	1.3	3.8	2.7	96.7
recal. to 100%		76.5	0.2	12.5	2.6	0.2	1.4	3.9	2.8	100.0
to 4 wt.% Na_2O		76.4	0.2	12.5	2.6	0.2	1.4	4.0	2.8	100.0
obsidian	1	77.0	0.2	12.9	1.7	0.2	1.2	4.1	3.0	100.7
	2	74.1	0.2	12.5	2.3	0.2	1.3	4.3	2.9	98.1
	3	75.3	0.2	12.6	1.7	0.2	1.3	4.3	2.9	98.7
mean		75.5	0.2	12.7	1.9	0.2	1.3	4.2	2.9	99.2
stand. dev.		1.5	-	0.2	0.3	-	0.1	0.1	0.1	1.4
recal. to 100%		76.3	0.2	12.8	1.9	0.2	1.3	4.3	2.9	100.0
to 4 wt.% Na_2O		76.5	0.2	12.8	1.9	0.2	1.3	4.0	2.9	100.0
pumice	1	76.5	0.2	12.7	1.7	0.2	1.3	4.1	2.9	99.6
	2	73.7	0.1	12.4	1.4	0.2	1.3	4.2	2.8	96.5
	3	70.8	0.2	12.3	1.6	0.2	1.2	3.9	2.9	93.5
	4	74.2	0.2	12.4	1.6	0.2	1.2	4.0	2.3	96.5
mean		73.8	0.2	12.5	1.6	0.2	1.3	4.1	2.7	96.5
stand. dev.		2.3	0.1	0.2	0.1	-	0.1	0.1	0.3	2.5
recal. to 100%		76.6	0.2	12.9	1.7	0.2	1.4	4.3	2.8	100.0
to 4 wt.% Na_2O		76.8	0.2	12.9	1.7	0.2	1.4	4.0	2.8	100.0

Table C-1 con't

Unit		Oxide (wt.%)								
		SiO_2	TiO_2	Al_2O_3	FeO	MgO	CaO	Na_2O	K_2O	total
Hatepe plinian										
melt incl.	1	74.2	0.3	11.6	2.8	0.4	1.1	3.8	2.9	98.1
	2	73.2	0.3	12.0	2.5	0.2	1.4	3.3	2.8	95.8
	3	72.9	0.2	12.4	2.4	0.2	1.3	3.3	2.7	95.5
mean		73.4	0.3	12.0	2.6	0.3	1.3	3.5	2.8	96.5
stand. dev.		0.7	0.1	0.4	0.2	0.1	0.2	0.3	0.1	1.4
recal. to 100%		76.3	0.3	12.5	2.7	0.3	1.4	3.6	2.9	100.0
to 4 wt.% Na_2O		76.0	0.3	12.5	2.7	0.3	1.4	4.0	2.9	100.0
obsidian	1	75.4	0.2	12.8	1.6	0.2	1.4	3.9	3.2	98.9
	2	73.8	0.2	12.6	1.7	0.2	1.4	3.8	2.9	96.7
	3	75.8	0.1	13.0	1.4	0.2	1.5	3.9	2.9	98.9
	A	76.0	0.1	12.1	1.7	0.1	1.0	3.9	3.0	98.3
	B	75.6	0.2	11.9	1.5	0.1	1.0	3.9	3.0	97.5
	C	75.8	0.1	11.9	1.7	0.2	1.0	3.9	2.9	97.9
mean		75.4	0.2	12.4	1.6	0.2	1.2	3.9	3.0	98.0
stand. dev.		0.8	0.1	0.5	0.1	0.1	0.2	0.0	0.1	0.9
recal. to 100%		77.0	0.2	12.7	1.6	0.2	1.2	4.0	3.1	100.0
to 4 wt.% Na_2O		77.0	0.2	12.7	1.6	0.2	1.2	4.0	3.1	100.0
pumice	1	75.4	0.1	12.3	1.5	0.2	1.3	2.2	2.6	95.8
	2	75.9	0.2	12.1	1.7	0.2	1.2	2.1	2.4	96.1
	3	75.0	0.4	12.5	1.6	0.1	1.3	2.2	2.5	95.9
mean		75.4	0.2	12.3	1.6	0.2	1.3	2.2	2.5	95.9
stand. dev.		0.5	0.2	0.2	0.1	0.1	0.1	0.1	0.1	0.2
recal. to 100%		78.8	0.2	12.9	1.7	0.2	1.2	2.3	2.6	100.0
to 4 wt.% Na_2O		77.5	0.2	12.7	1.7	0.2	1.2	4.0	2.6	100.0
Initial ash										
melt incl.	1	72.5	0.2	11.5	2.7	0.2	1.3	3.7	2.9	96.1
	2	72.5	0.3	11.3	2.3	0.2	1.2	3.6	2.6	94.3
	3	71.6	0.3	12.5	2.2	0.3	1.3	2.8	2.6	93.7
mean		72.2	0.3	11.8	2.4	0.2	1.3	3.4	2.7	94.7
stand. dev.		0.5	0.1	0.6	0.3	0.1	0.1	0.5	0.2	1.2
recal. to 100%		76.6	0.3	12.5	2.6	0.2	1.4	3.6	2.9	100.0
to 4 wt.% Na_2O		76.0	0.3	12.5	2.6	0.2	1.4	4.0	2.9	100.0

Table C-1 con't

Unit		Oxide (wt.%)								
		SiO_2	TiO_2	Al_2O_3	FeO	MgO	CaO	Na_2O	K_2O	total
Mapara										
melt incl.	1*	74.5	0.2	12.9	2.1	0.2	1.4	4.0	2.8	98.6
	2*	73.2	0.0	12.6	2.2	0.2	1.5	3.7	2.7	96.2
	3*	73.9	0.3	12.6	2.2	0.2	1.3	3.8	2.6	97.1
mean		73.9	0.2	12.7	2.2	0.2	1.4	3.8	2.7	97.3
stand. dev.		0.7	0.2	0.2	0.1	–	0.1	0.2	0.1	1.2
recal. to 100%		76.1	0.2	13.0	2.3	0.2	1.4	3.9	2.8	100.0
to 4 wt.% Na_2O		76.0	0.2	13.0	2.3	0.2	1.4	4.0	2.8	100.0
obsidian	1a	74.9	0.3	12.7	2.6	0.4	1.9	4.3	2.6	99.9
	1b	74.5	0.4	12.8	3.0	0.6	2.4	4.2	2.1	100.8
	2a	77.5	0.2	12.8	1.4	0.1	1.1	4.2	3.1	100.5
	2b	76.7	0.2	12.8	1.6	0.2	1.3	4.2	3.1	100.4
	3	76.9	0.2	12.9	1.2	0.2	1.3	4.3	3.0	100.2
	4	76.9	0.2	12.8	1.8	0.2	1.2	4.2	3.4	100.9
mean		76.2	0.3	12.8	1.9	0.3	1.5	4.2	2.9	100.5
stand. dev.		1.2	0.1	0.1	0.7	0.2	0.5	0.1	0.5	0.4
recal. to 100%		76.1	0.3	12.8	1.9	0.3	1.5	4.2	2.9	100.0
to 4 wt.% Na_2O		76.3	0.3	12.8	1.9	0.3	1.5	4.0	2.9	100.0
pumice	1	72.2	0.2	12.0	1.3	0.2	1.4	3.7	3.0	94.2
	2	72.9	0.2	12.2	1.3	0.2	1.5	3.8	2.8	95.2
	3	73.5	0.1	12.3	1.5	0.2	1.5	3.8	2.9	96.4
mean		72.8	0.2	12.2	1.4	0.2	1.5	3.8	2.9	95.3
stand. dev.		0.7	0.1	0.2	0.1	–	0.1	0.1	0.1	1.1
recal. to 100%		76.6	0.2	12.8	1.5	0.2	1.6	4.0	3.1	100.0
to 4 wt.% Na_2O		76.6	0.2	12.8	1.5	0.2	1.6	4.0	3.1	100.0

Table C-1 con't

Unit		Oxide (wt.%) SiO_2	TiO_2	Al_2O_3	FeO	MgO	CaO	Na_2O	K_2O	total
Whaikapo										
melt incl.	1	74.9	0.2	12.1	1.7	0.1	1.0	2.3	2.9	95.4
	2	75.7	0.2	11.4	1.6	0.2	0.9	3.8	3.1	96.9
mean		75.3	0.2	11.8	1.7	0.2	1.0	3.1	3.0	96.2
stand. dev.		0.6	-	0.5	0.1	0.1	0.1	1.1	0.1	1.1
recal. to 100%		78.2	0.2	12.3	1.8	0.2	1.0	3.2	3.1	100.0
to 4.0 wt.% Na_2O		77.6	0.2	12.2	1.8	0.2	1.0	4.0	3.1	100.0
melt incl.	1*	72.1	0.2	12.3	1.8	0.1	1.1	3.3	2.8	94.1
	2*	77.7	0.2	12.2	1.8	0.1	0.9	3.7	3.1	99.8
	3*	75.6	0.2	12.0	1.8	0.1	1.1	3.8	3.2	98.0
mean		75.1	0.2	12.2	1.8	0.1	1.0	3.6	3.0	97.3
stand. dev.		2.8	-	0.2	-	-	0.1	0.3	0.2	2.9
recal. to 100%		77.4	0.2	12.6	1.9	0.1	1.0	3.7	3.1	100.0
to 4.0 wt.% Na_2O		77.2	0.2	12.6	1.9	0.1	1.0	4.0	3.1	100.0
obsidian	1	76.6	0.2	12.5	1.3	0.1	1.0	4.2	3.2	99.3
	2	75.8	0.2	12.7	1.5	0.2	1.2	4.3	3.0	99.2
	3	75.7	0.2	12.6	1.4	0.2	1.2	3.7	3.8	98.9
mean		76.0	0.2	12.6	1.4	0.2	1.2	4.1	3.3	99.0
stand. dev.		0.5	-	0.1	0.1	0.1	0.1	0.3	0.4	0.4
recal. to 100%		76.8	0.2	12.7	1.4	0.2	1.2	4.1	3.3	100.0
to 4.0 wt.% Na_2O		76.8	0.2	12.7	1.4	0.2	1.2	4.0	3.3	100.0
Waihimia										
obsidian	1	75.4	0.2	12.9	1.7	0.2	1.4	4.2	2.8	99.2
	2	74.9	0.3	13.1	2.1	0.3	1.4	4.3	2.8	99.6
	3	74.3	0.2	12.8	2.3	0.1	1.5	4.2	2.8	98.5
mean		74.9	0.2	12.9	2.0	0.2	1.4	4.2	2.8	99.1
stand. dev.		0.6	0.1	0.2	0.3	0.1	0.1	0.1	-	0.6
recal. to 100%		75.9	0.2	13.1	2.0	0.2	1.4	4.3	2.8	100.0
to 4.0 wt.% Na_2O		76.1	0.2	13.1	2.0	0.2	1.4	4.0	2.8	100.0
pumice	1	71.3	0.1	11.3	1.7	0.1	2.9	7.2	2.5	97.2
recal to 100%		73.4	0.1	11.6	1.8	0.1	3.0	7.4	2.6	100.0
to 4.0 wt.% Na_2O										

Table C-1 con't

Unit		SiO_2	TiO_2	Al_2O_3	FeO	MgO	CaO	Na_2O	K_2O	total
Motutere										
obsidian	1	73.3	0.3	12.6	2.0	0.3	1.4	4.2	2.9	97.2
	2	76.6	0.2	12.3	1.7	0.2	1.1	4.4	3.0	99.7
	3	76.1	0.2	12.6	1.7	0.1	1.3	4.3	3.0	99.5
	4	75.3	0.1	12.3	1.3	0.1	1.3	3.7	3.6	97.8
mean		75.3	0.2	12.5	1.7	0.2	1.3	4.2	3.1	98.6
stand. dev.		1.5	0.1	0.2	0.3	0.1	0.1	0.3	0.3	1.2
recal. to 100%		76.5	0.2	12.7	1.7	0.2	1.3	4.3	3.2	100.0
to 4.0 wt.% Na_2O		76.7	0.2	12.7	1.7	0.2	1.3	4.0	3.2	100.0
pumice	1	74.4	0.3	12.7	1.9	0.2	1.4	4.1	2.7	98.0
	2	74.7	0.0	12.6	1.6	0.1	1.3	4.2	2.8	97.6
	3	74.8	0.3	12.8	1.7	0.3	1.1	3.9	2.2	97.5
	4	74.4	0.3	12.7	1.9	0.2	1.2	4.0	2.7	97.8
mean		74.6	0.2	12.7	1.8	0.2	1.3	4.1	2.6	97.7
stand. dev.		0.2	0.2	0.1	0.2	0.1	0.1	0.1	0.3	0.2
recal. to 100%		76.5	0.2	13.0	1.9	0.2	1.3	4.2	2.7	100.0
to 4.0 wt.% Na_2O		76.7	0.2	13.0	1.9	0.2	1.3	4.0	2.7	100.0
Opepe										
melt incl.	1	71.9	0.2	11.9	1.6	0.2	1.2	1.7	2.8	91.7
	2	73.4	0.3	12.6	1.9	0.1	1.3	2.2	2.7	94.7
mean		72.7	0.3	12.3	1.8	0.2	1.3	2.0	2.8	93.2
stand. dev.		1.1	0.1	0.5	0.2	0.1	0.1	0.4	0.1	2.1
recal. to 100%		77.8	0.3	13.1	1.9	0.2	1.4	2.1	3.0	100.0
to 4.0 wt.% Na_2O		76.3	0.3	12.9	1.9	0.2	4.0	2.1	3.0	100.0
obsidian	1	75.7	0.2	12.2	1.4	0.2	1.1	4.2	3.1	98.3
	2a	73.9	0.5	13.1	2.0	0.2	1.9	4.4	3.2	99.6
	2b	74.7	0.5	12.3	2.3	0.4	1.6	3.9	3.2	98.9
	3	72.6	0.5	12.6	3.1	0.5	1.9	3.9	3.5	99.1
mean		74.2	0.4	12.6	2.2	0.3	1.6	4.1	3.3	98.9
stand. dev.		1.3	0.2	0.4	0.7	0.2	0.4	0.2	0.2	0.5
recal. to 100%		75.2	0.4	12.8	2.2	0.3	1.6	4.2	3.3	100.0
to 4.0 wt.% Na_2O		75.4	0.4	12.8	2.2	0.3	1.6	4.0	3.3	100.0
pumice	1	77.6	0.2	12.2	1.6	0.1	1.0	3.6	2.9	99.5
	2	77.9	0.2	11.7	1.5	0.1	1.1	3.5	2.7	98.9
	3	76.8	0.1	12.1	1.5	0.1	1.0	3.2	3.0	98.2
mean		77.4	0.2	12.0	1.5	0.1	1.0	3.4	2.9	98.9
stand. dev.		0.6	0.1	0.3	0.1	–	0.1	0.2	0.2	0.7
recal. to 100%		78.6	0.2	12.2	1.5	0.1	1.0	3.5	2.9	100.0
to 4.0 wt.% Na_2O		78.2	0.2	12.1	1.5	0.1	1.0	4.0	2.9	100.0

Oxide (wt.%)

Table C-1 con't

Unit		Oxide (wt.%) SiO_2	TiO_2	Al_2O_3	FeO	MgO	CaO	Na_2O	K_2O	total
Poronui										
melt incl.	1	72.1	0.2	12.2	1.8	0.1	1.3	3.3	2.9	94.3
	2	70.3	0.2	13.3	1.8	0.1	1.4	2.8	3.6	94.3
	3	70.4	0.2	12.7	1.9	0.0	1.2	4.0	3.0	93.5
mean		70.9	0.2	12.7	1.8	0.1	1.3	3.4	3.2	94.0
stand. dev.		1.0	-	0.6	0.1	0.1	0.1	0.6	0.4	0.5
recal. to 100%		75.9	0.2	13.6	1.7	0.1	1.4	3.6	3.4	100.0
to 4.0 wt.% Na_2O		75.2	0.2	13.5	1.7	0.1	1.4	4.0	3.4	100.0
pumice	1	75.5	0.1	13.4	2.0	0.2	1.5	3.8	2.8	100.5
recal. to 100%		76.0	0.1	13.5	2.0	0.2	1.5	3.8	2.8	100.0
to 4.0 wt.% Na_2O		75.8	0.1	13.5	2.0	0.2	1.5	4.0	2.8	100.0
Karapiti										
obsidian	1	74.8	0.2	12.8	1.8	0.2	1.5	4.1	3.0	98.8
	2	75.3	0.2	12.4	1.5	0.1	1.4	3.8	3.0	97.9
	3a	75.9	0.3	12.6	1.6	0.2	1.4	3.9	3.0	99.3
	3b	75.2	0.1	12.8	1.7	0.2	1.5	3.9	3.2	98.8
	3c	75.9	0.2	12.7	1.6	0.2	1.4	3.8	3.2	99.2
	4	75.1	0.1	12.5	1.7	0.2	1.6	3.9	3.2	98.5
mean		75.4	0.2	12.6	1.7	0.2	1.5	3.9	3.1	98.8
stand. dev.		0.4	0.1	0.2	0.1	0.0	0.1	0.1	0.1	0.5
recal. to 100%		76.5	0.2	12.8	1.7	0.2	1.5	4.0	3.1	100.0
to 4.0 wt.% Na_2O		76.5	0.2	12.8	1.7	0.2	1.5	4.0	3.1	100.0
pumice	1	75.1	0.3	12.9	2.0	0.3	1.5	2.0	2.6	97.3
recal. to 100%		77.7	0.3	13.3	2.1	0.3	1.6	2.1	2.7	100.0
to 4.0 wt.% Na_2O		76.2	0.3	13.0	2.1	0.3	1.6	4.0	2.7	100.0

Table C-1 con't

Unit		Oxide (wt.%)								
		SiO_2	TiO_2	Al_2O_3	FeO	MgO	CaO	Na_2O	K_2O	total
Oruanui										
melt incl.	1	72.3	0.0	11.2	1.4	0.1	0.6	2.5	3.7	91.9
	2	71.6	0.4	11.8	1.8	0.2	0.9	2.2	3.9	92.7
	3	72.7	0.3	11.3	1.1	0.1	0.6	3.4	2.6	92.5
mean		72.2	0.2	11.4	1.4	0.1	0.7	2.7	3.4	92.4
stand. dev.		0.6	0.2	0.3	0.4	0.1	0.2	0.6	0.7	0.4
recal. to 100%		78.4	0.2	12.4	1.5	0.1	0.8	2.9	3.7	100.0
to 4.0 wt.% Na_2O		77.5	0.2	12.3	1.5	0.1	0.8	4.0	3.0	100.0
melt incl.	1*	74.5	0.0	11.7	0.9	0.0	0.7	3.6	3.5	95.1
	2*	73.9	0.1	10.7	1.4	0.1	0.5	1.8	4.6	93.3
	3*	74.2	0.1	11.0	1.5	0.1	0.8	2.6	3.2	93.8
mean		74.2	0.1	11.1	1.3	0.1	0.7	2.7	3.8	94.1
stand. dev.		0.3	0.1	0.5	0.3	0.1	0.2	0.9	0.7	0.9
recal. to 100%		78.9	0.1	11.8	1.4	0.1	0.7	2.9	4.0	100.0
to 4.0 wt.% Na_2O		78.0	0.1	11.7	1.4	0.1	0.7	4.0	4.0	100.0
Okaia										
melt incl.	1	72.9	0.2	10.1	1.5	0.1	0.7	2.3	2.7	90.7
recal. to 100%		80.6	0.2	11.2	1.7	0.1	0.8	2.5	3.0	100.0
to 4.0 wt.% Na_2O		79.4	0.2	11.0	1.7	0.1	0.8	4.0	3.0	100.0
pumice	1	72.9	0.3	12.5	1.8	0.2	1.2	3.8	2.6	95.8
	2	74.1	0.4	12.5	1.7	0.2	1.4	4.1	2.7	97.5
	3	72.4	0.2	13.9	1.6	0.2	1.6	4.7	2.7	97.9
mean		73.1	0.3	13.0	1.7	0.2	1.4	4.2	2.7	97.1
stand. dev.		0.9	0.1	0.8	0.1	–	0.2	0.5	0.1	1.1
recal. to 100%		75.7	0.3	13.5	1.8	0.2	1.5	4.4	2.8	100.0
to 4.0 wt.% Na_2O		76.0	0.3	13.6	1.8	0.2	1.5	4.0	2.8	100.0

Table C-1 con't

Unit		Oxide (wt.%)								
		SiO_2	TiO_2	Al_2O_3	FeO	MgO	CaO	Na_2O	K_2O	total
Tihoi										
melt incl.	1	72.8	0.1	11.2	1.2	0.1	0.7	3.1	3.5	92.7
	2	70.7	0.2	11.1	1.3	0.1	0.6	2.5	4.6	91.1
	3	72.0	0.1	11.5	1.5	0.1	0.6	2.7	3.9	92.6
mean		71.8	0.1	11.3	1.3	0.1	0.6	2.8	4.0	92.1
stand. dev.		1.1	0.1	0.2	0.2	–	0.1	0.3	0.6	0.9
recal. to 100%		78.0	0.1	12.3	1.4	0.1	0.7	3.0	4.4	100.0
to 4.0 wt.% Na_2O		77.2	0.1	12.2	1.4	0.1	0.7	4.0	4.4	100.0
melt incl.	1*	74.8	0.1	11.4	1.1	0.1	0.8	2.7	3.9	95.2
	2*	71.2	0.1	12.5	1.4	0.1	0.9	2.7	3.8	93.0
	3*	73.4	0.1	10.7	1.1	0.1	0.8	2.6	3.8	92.8
mean		73.1	0.1	11.5	1.2	0.1	0.8	2.7	3.8	93.7
stand. dev.		1.8	–	0.9	0.2	–	0.1	0.1	0.1	1.3
recal. to 100%		78.4	0.1	12.3	1.3	0.1	0.9	2.9	4.1	100.0
to 4.0 wt.% Na_2O		77.5	0.1	12.2	1.3	0.1	0.9	4.0	4.1	100.0

Table C-2. Major element oxide chemistry of melt inclusions, obsidian and pumice from the Okataina Volcanic center as analysed by electron microprobe. Melt inclusion analyses marked with an asterix (*) were done in 1985 and those without in 1986. Analyses are normalized to 4 wt% Na_2O

Unit		Oxide (wt.%)								
		SiO_2	TiO_2	Al_2O_3	FeO	MgO	CaO	Na_2O	K_2O	total
Kaharoa										
obsidian	1	76.7	0.1	12.1	0.7	0.0	0.8	3.7	4.1	98.7
	2	76.7	0.2	11.6	0.8	0.1	0.7	4.0	3.8	98.0
	3	77.4	0.1	11.8	0.7	0.1	0.7	3.5	3.8	98.6
	4	76.4	0.1	11.7	0.7	0.1	0.7	3.9	3.3	97.1
	5	75.9	0.1	11.8	0.5	0.1	0.7	2.7	5.6	97.7
	6	76.9	0.2	12.1	1.1	0.2	0.9	4.3	3.1	100.6
	7	77.9	0.1	11.8	0.6	0.1	0.7	3.8	3.7	98.7
mean		76.8	0.1	11.8	0.7	0.1	0.7	3.7	3.9	98.5
stand. dev.		0.7	-	0.2	0.1	-	0.1	0.5	0.8	1.1
recal to 100%		77.9	0.1	11.9	0.7	0.1	0.7	3.8	3.9	100.0
to 4.0 wt.% Na_2O		77.7	0.1	11.8	0.7	0.1	0.7	4.0	3.9	100.0
Whakatane										
melt incl.	1	77.4	0.1	12.0	1.1	0.0	0.7	3.8	3.6	98.7
	2	79.2	0.1	12.3	1.0	0.1	0.7	3.8	3.6	100.8
mean		78.3	0.1	12.2	1.1	0.1	0.7	3.8	3.6	99.8
stand. dev.		1.3	-	0.2	0.1	0.1	-	-	-	1.5
recal to 100%		78.4	0.1	12.2	1.1	0.1	0.7	3.8	3.6	100.0
to 4.0 wt.% Na_2O		78.2	0.1	12.2	1.1	0.1	0.7	4.0	3.6	100.0
obsidian	1	75.5	0.2	12.5	1.2	0.2	1.0	4.1	2.9	97.8
	2	75.0	0.2	12.5	1.1	0.2	0.9	3.9	2.8	96.9
	3	74.3	0.2	12.2	1.1	0.2	1.0	4.0	2.9	96.1
	4	74.7	0.2	12.4	1.3	0.2	1.0	4.0	2.8	96.9
	5	74.3	0.2	12.4	1.2	0.2	1.0	4.0	2.8	96.5
mean		74.8	0.2	12.4	1.2	0.2	1.0	4.0	2.8	96.8
stand. dev.		0.5	-	0.1	0.1	-	0.1	0.1	0.1	0.6
recal to 100%		77.4	0.2	12.8	1.2	0.2	1.0	4.1	2.9	100.0
to 4.0 wt.% Na_2O		77.5	0.2	12.8	1.2	0.2	1.0	4.0	2.9	100.0

Table C-2 con't

Unit		Oxide (wt.%)								
		SiO_2	TiO_2	Al_2O_3	FeO	MgO	CaO	Na_2O	K_2O	total
Mamaku										
melt incl.	1	74.2	0.1	11.0	1.4	0.1	0.8	3.1	3.0	93.6
	2	71.4	0.2	11.7	1.3	0.1	0.6	3.0	3.3	91.9
mean		72.8	0.2	11.4	1.4	0.1	0.7	3.1	3.2	92.7
stand. dev.		2.0	0.1	0.5	0.1	–	0.1	0.1	0.2	1.2
recal to 100%		78.4	0.2	12.3	1.5	0.1	0.8	3.3	3.4	100.0
to 4.0 wt.% Na_2O		77.9	0.2	12.2	1.5	0.1	0.8	4.0	3.4	100.0
melt incl.	1*	75.2	0.1	11.8	1.0	0.1	0.7	3.6	3.3	96.0
	2*	72.9	0.2	11.5	0.9	0.1	0.6	3.7	3.5	93.7
	3*	72.4	0.1	11.2	1.3	0.1	0.7	3.6	3.6	93.3
	4*	75.3	0.2	11.7	1.2	0.1	0.7	3.6	3.1	95.9
mean		73.9	0.2	11.6	1.1	0.1	0.7	3.6	3.4	94.7
stand. dev.		1.5	0.1	0.3	0.2	–	–	–	0.2	1.4
recal to 100%		78.1	0.2	12.3	1.2	0.1	0.7	3.8	3.6	100.0
to 4.0 wt.% Na_2O		77.9	0.2	12.3	1.2	0.1	0.7	4.0	3.6	100.0
obsidian	1a	77.6	0.2	12.1	0.9	0.2	0.9	3.5	3.6	99.3
	1a	77.9	0.1	12.2	0.9	0.1	1.0	3.7	3.6	99.8
	2a	77.1	0.1	12.0	0.8	0.1	0.8	3.9	3.6	98.5
	2b	76.8	0.1	11.8	0.8	0.1	0.7	3.7	3.6	97.7
	3a	77.0	0.1	11.9	1.0	0.1	0.8	3.8	3.6	98.6
	3b	76.6	0.2	11.8	0.8	0.1	0.8	3.6	3.5	97.6
	4a	77.2	0.1	11.9	0.8	0.1	0.7	3.9	3.5	98.4
	4b	77.0	0.1	11.8	0.9	0.1	0.7	3.7	3.7	98.3
mean		77.1	0.1	11.9	0.9	0.1	0.8	3.7	3.6	98.5
stand. dev.		0.4	0.0	0.2	0.1	–	0.1	0.1	0.1	0.7
recal to 100%		78.5	0.1	12.1	0.9	0.1	0.8	3.8	3.7	100.0
to 4.0 wt.% Na_2O		78.3	0.1	12.1	0.9	0.1	0.8	4.0	3.7	100.0

Table C-2 con't

Unit		Oxide (wt.%)								
		SiO_2	TiO_2	Al_2O_3	FeO	MgO	CaO	Na_2O	K_2O	total
Rotoma										
obsidian	1a	76.9	0.1	11.9	0.8	0.1	0.7	3.8	3.2	97.9
	1b	77.3	0.1	12.0	0.8	0.1	0.8	3.9	3.2	98.3
	2a	76.7	0.1	11.7	0.9	0.1	0.7	3.6	3.4	97.4
	2b	76.9	0.1	11.8	0.8	0.1	0.7	3.9	3.4	97.9
	3a	76.8	0.1	11.9	0.8	0.1	0.8	3.8	3.3	97.9
	3b	77.1	0.2	12.0	0.9	0.1	0.8	3.9	3.3	98.4
	4a	76.8	0.1	12.0	0.9	0.1	0.8	3.7	3.8	98.5
	4b	77.0	0.1	11.9	0.9	0.1	0.8	3.7	3.7	98.4
mean		76.9	0.1	11.9	0.9	0.1	0.8	3.8	3.4	98.1
stand. dev.		0.2	-	0.1	0.1	-	0.1	0.1	0.2	0.4
recal to 100%		78.6	0.1	12.2	0.9	0.1	0.8	3.9	3.5	100.0
to 4.0 wt.% Na_2O		78.5	0.1	12.2	0.9	0.1	0.8	4.0	3.5	100.0
Waiohau										
melt incl.	1	74.9	0.1	11.6	1.4	0.1	0.6	3.1	3.6	95.6
	2	74.9	0.2	11.2	1.2	0.0	0.8	2.6	3.3	95.1
	3	75.8	0.1	11.4	1.1	0.0	0.8	3.0	3.0	95.3
mean		75.2	0.1	11.4	1.2	0.0	0.7	2.9	3.3	95.3
stand. dev.		0.5	0.1	0.2	0.1	-	0.1	0.3	0.3	0.3
recal to 100%		79.3	0.1	12.0	1.3	0.0	1.7	3.1	3.5	100.0
to 4.0 wt.% Na_2O		78.6	0.1	11.9	1.3	0.0	1.7	4.0	3.5	100.0

Table C-2 con't

Unit		Oxide (wt.%)								
		SiO_2	TiO_2	Al_2O_3	FeO	MgO	CaO	Na_2O	K_2O	total
Rotorua										
melt incl.	1	74.5	0.1	11.2	1.3	0.1	0.8	3.0	2.8	93.9
	2	70.5	0.1	11.0	1.6	0.2	0.8	1.6	3.4	89.4
	3	72.0	1.5	10.9	2.0	0.2	0.9	2.7	2.7	91.6
	4	71.2	1.5	11.7	1.3	0.2	0.9	1.8	2.9	90.7
mean		72.1	0.8	11.2	1.6	0.2	0.9	2.3	3.0	91.4
stand. dev.		1.7	0.8	0.4	0.3	0.1	0.1	0.7	0.3	1.9
recal to 100%		78.3	0.9	12.2	1.7	0.2	1.0	2.5	3.3	100.0
to 4.0 wt.% Na_2O		77.1	0.9	12.0	1.7	0.2	1.0	4.0	3.3	100.0
melt incl	1*	75.9	0.3	12.6	1.6	0.2	1.6	3.7	2.7	98.9
	2*	72.1	0.2	11.8	1.9	0.2	1.3	4.0	2.8	94.7
mean		74.0	0.3	12.2	1.8	0.2	1.5	3.9	2.8	96.8
stand. dev.		2.7	0.1	0.6	0.2	–	0.2	0.2	0.1	2.9
recal to 100%		76.5	0.3	12.6	1.9	0.2	1.6	4.0	2.9	100.0
to 4.0 wt.% Na_2O		76.5	0.3	12.6	1.9	0.2	1.6	4.0	2.9	100.0
pumice		73.9	0.1	11.9	1.0	0.2	0.8	4.2	2.7	95.6
recal to 100%		77.9	0.1	12.6	1.1	0.2	0.8	4.4	2.9	100.0
to 4.0 wt.% Na_2O		78.2	0.1	12.7	1.1	0.2	0.8	4.0	2.9	100.0
Te Rere										
obsidian	1	77.8	0.1	12.4	1.0	0.2	0.7	4.1	3.3	99.8
	2	75.2	0.1	12.1	1.0	0.1	0.9	4.3	2.9	96.8
	3	77.1	0.1	12.2	1.0	0.1	0.9	3.9	3.4	99.1
	4	77.8	0.2	12.3	1.0	0.2	1.1	3.8	3.3	98.8
	5a	77.4	0.0	12.2	1.0	0.2	0.8	4.1	2.9	98.8
	5b	77.9	0.1	12.4	1.0	0.2	0.8	3.9	3.2	99.5
mean		77.2	0.1	12.3	1.0	0.2	0.9	4.0	3.2	98.8
stand. dev.			0.1	0.1	–	0.1	0.1	0.2	0.2	1.1
recal to 100%		78.1	0.1	12.4	1.0	0.2	0.9	4.0	3.2	100.0
to 4.0 wt.% Na_2O		78.1	0.1	12.4	1.0	0.2	0.9	4.0	3.2	100.0
pumice	1	72.6	0.1	12.3	1.1	0.2	1.1	4.0	2.6	94.7
	2	71.9	0.3	12.3	1.0	0.2	1.2	3.9	2.6	93.7
mean		72.3	0.2	12.3	1.1	0.2	1.2	4.0	2.6	94.2
stand. dev.		0.5	0.1	–	0.1	–	0.1	0.1	–	0.7
recal to 100%		77.0	0.2	13.1	1.2	0.2	1.3	4.3	2.8	100.0
to 4.0 wt.% Na_2O		77.2	0.2	13.1	1.2	0.2	1.3	4.0	2.8	100.0

Table C-2 con't

Unit		Oxide (wt.%)								
		SiO_2	TiO_2	Al_2O_3	FeO	MgO	CaO	Na_2O	K_2O	total
Mangaone										
obsidian	1	77.8	0.1	12.2	0.8	0.1	0.7	4.1	3.5	99.4
	2	77.6	0.2	12.2	0.9	0.1	0.7	4.1	3.6	99.5
	3	76.9	0.1	12.0	0.8	0.1	0.6	3.8	3.7	98.4
mean		77.4	0.1	12.1	0.8	0.1	0.7	4.0	3.6	99.1
stand. dev.		0.5	0.1	0.1	0.1	-	0.1	0.2	0.1	0.6
recal to 100%		78.3	0.1	12.3	0.8	0.1	0.7	4.1	3.6	100.0
to 4.0 wt.% Na_2O		78.4	0.1	12.3	0.8	0.1	0.7	4.0	3.6	100.0

Table C-3. X-Ray Fluorescence analyses of Taupo Volcanic Center tephra All analyses are given in ppm. Multiple analyses with the same sample number represent individually prepared aliquots of a single bulk sample

Unit and Number	Pb	Th	Rb	Sr	Y	Zr	Nb	Rb/Sr
Taupo plinian								
014A	21.9	13.7	97.8	167.0	35.2	222.8	9.3	0.6
014B	22.5	11.8	97.6	163.6	35.7	223.5	10.1	0.6
015A	19.5	10.1	95.9	166.5	35.2	222.3	9.7	0.6
015B	20.3	10.7	98.1	164.9	35.0	223.1	9.9	0.6
017A	22.1	11.4	96.1	166.7	35.8	221.4	9.8	0.6
017B	21.1	13.4	97.7	165.4	36.4	221.7	10.2	0.6
Hatepe phreatomagmatic								
002A	21.6	11.8	97.4	153.4	34.9	217.3	9.6	0.6
002B	22.1	11.5	101.1	158.5	37.3	226.2	10.1	0.6
023A	20.9	12.1	98.0	153.2	35.6	220.9	9.7	0.6
023B	21.2	11.8	99.8	157.9	36.4	225.3	10.1	0.6
Hatepe plinian								
027A	19.8	12.0	100.0	156.2	36.2	222.5	9.9	0.6
027B	20.2	9.4	98.5	155.6	36.9	221.1	9.4	0.6
046A	21.4	9.8	99.5	156.1	36.3	222.3	9.9	0.6
046B	21.7	12.1	99.3	154.9	35.9	220.5	9.8	0.6
046C	21.1	12.9	100.4	156.3	35.8	221.9	10.2	0.6
Initial Ash								
044	22.2	12.7	100.5	154.2	35.4	222.2	9.4	0.7
Mapara								
024A	20.1	12.1	100.3	160.7	36.1	220.5	9.6	0.6
024B	20.2	11.7	101.1	163.6	35.5	224.0	9.8	0.6
025A	19.6	10.5	99.6	162.0	36.4	223.5	10.2	0.6
025B	20.5	9.9	99.7	160.7	36.0	222.7	10.1	0.6

Table C-3 con't

Unit and Number	Pb	Th	Rb	Sr	Y	Zr	Nb	Rb/Sr
Whaikaipo								
029A	20.3	11.6	104.1	126.4	37.3	218.8	9.8	0.8
029B	21.2	12.2	103.5	126.8	36.7	219.5	9.8	0.8
Motutere								
008A	19.4	11.5	92.1	134.9	36.7	234.3	9.7	0.7
008B	21.2	12.2	92.9	131.4	36.5	239.4	10.1	0.7
Opepe								
030	20.1	12.9	100.1	139.7	32.8	228.8	9.3	0.7
031A	18.8	12.7	98.3	135.9	33.1	228.7	9.1	0.7
031B	18.5	10.5	97.7	134.0	33.3	226.1	8.3	0.7
032A	19.9	11.9	96.0	136.0	33.3	235.6	9.3	0.7
032B	19.0	11.5	98.8	138.4	32.8	232.8	8.7	0.7
033A	19.1	11.3	94.8	149.3	32.5	237.0	9.6	0.6
033B	20.3	12.1	90.2	146.7	35.2	245.4	10.1	0.6
Poronui								
009A	18.9	12.3	94.8	137.0	33.4	240.1	8.9	0.7
009B	19.4	11.6	98.5	141.2	33.1	247.4	8.6	0.7
Karapiti								
010	19.6	12.4	99.3	136.1	33.1	250.0	9.4	0.7
034A	20.5	13.2	101.5	134.5	30.9	232.0	8.8	0.8
034B	19.8	13.4	100.5	133.4	30.0	228.4	8.4	0.8
036A	20.7	12.3	99.7	141.3	31.6	230.0	8.8	0.7
036B	19.2	11.9	99.8	140.1	30.2	223.3	8.5	0.7
Okaia								
047	15.7	12.7	101.4	139.7	23.3	149.4	7.6	0.7
048	16.6	11.4	102.5	135.2	22.5	154.8	7.6	0.8
056A	14.3	10.1	96.5	136.5	22.7	145.8	7.1	0.7
056B	16.7	10.8	100.2	139.5	23.8	154.5	8.3	0.7
Tihoi								
054A	16.4	13.1	93.9	150.1	25.2	167.0	9.3	0.6
054B	16.8	11.6	94.9	151.8	24.4	157.2	8.4	0.6
055	16.3	10.5	93.3	151.2	26.3	167.0	8.7	0.6

Table C-4. X-Ray Fluorescence analyses of Okataina Volcanic Center tephra. All analyses reported in parts per million (ppm). Multiple analyses with the same sample number represent analyses of separate aliquots of a single bulk sample.

Unit and Number	Pb	Th	Rb	Sr	Y	Zr	N	Rb/Sr
Kaharoa								
080A	18.8	14.4	126.7	53.4	28.6	88.5	9.7	2.4
080B	17.9	13.8	124.3	55.2	28.6	88.7	9.8	2.3
Whakatane								
068A	17.8	11.7	103.1	110.8	26.5	140.0	9.4	0.9
068B	17.4	12.7	101.5	105.9	25.4	138.5	9.4	1.0
069A	17.4	11.8	111.2	83.3	27.2	108.8	9.0	1.3
069B	16.7	13.8	111.6	82.7	26.9	106.9	9.0	1.3
Mamaku								
066A	16.6	11.5	102.9	114.2	26.0	143.3	9.9	0.9
066B	15.9	11.5	103.9	107.5	26.1	137.2	9.0	1.0
067A	17.4	12.3	102.4	111.7	25.5	142.2	9.1	0.9
067B	14.7	9.8	107.7	107.7	26.4	139.1	9.2	1.0
Rotoma								
062	16.4	9.4	94.8	104.3	27.2	117.8	9.9	0.9
063	16.8	9.4	92.5	106.7	26.3	123.2	9.0	0.9
064A	17.2	12.2	95.9	107.1	26.2	121.9	8.6	0.9
064B	16.7	10.0	94.2	103.4	27.1	121.4	9.2	0.9
Rotorua								
084A	17.3	12.1	86.9	163.1	27.3	224.9	9.2	0.5
084B	15.5	10.1	84.7	160.8	26.8	231.0	9.1	0.5
084C	15.1	7.5	83.2	157.6	26.2	240.2	9.6	0.5
086A	13.4	8.0	109.7	146.3	23.7	187.2	8.7	0.7
086B	15.6	9.4	87.7	169.5	26.5	225.3	9.2	0.5
Rerewhakaaitu								
078A	16.3	10.9	110.0	128.7	21.5	135.9	9.1	0.9
078B	16.1	12.2	109.1	118.1	22.8	131.8	9.7	0.9

Table C-4 con't

Unit and Number	Pb	Th	Rb	Sr	Y	Zr	N	Rb/Sr
Okareka								
077	17.2	12.9	113.1	81.6	26.7	125.4	9.1	1.4
Te Rere								
059	19.5	11.7	89.2	110.4	30.8	166.4	10.9	0.8
Omataroa								
073A	17.5	9.9	88.3	130.2	37.4	211.4	9.9	0.7
073B	16.0	8.8	85.9	128.9	36.1	203.4	9.9	0.7
074A	16.9	8.4	87.3	129.7	37.8	214.0	10.4	0.7
074B	17.0	8.4	87.7	129.9	36.6	211.8	10.1	0.7
Awakere								
072A	15.9	8.9	85.6	127.9	38.9	200.0	10.1	0.7
072B	16.6	9.9	86.2	127.7	39.8	208.3	10.3	0.7
Mangaone								
070A	15.7	7.9	85.8	124.9	35.4	183.9	10.7	0.7
070B	16.8	9.6	85.1	126.6	36.4	186.9	10.4	0.7
071A	16.6	9.2	84.8	123.2	34.2	184.3	9.8	0.7
071B	15.4	8.4	84.1	132.6	36.5	209.4	10.6	0.6

Table C-5. Trace and rare earth element compositions of obsidian and bulk rock (pumice) from 4 tephra units: Taupo plinian, Hatepe phreatoplinian, Kaharoa and Mamaku tephras. Analyses made by neutron activation. All elements are reported in ppm except for Fe and Na_2O which are in wt %. A description of each sample is included following the analytical results.

Taupo plinian tephra- samples 158 and 015B

Trace and rare earth element composition of obsidian fragments

sample number	FeO	Na_2O	Sc	Co	Zn	As	Rb
* 158-1	2.89	4.32	13.89	1.23	99	4.1	105
158-2	1.71	4.51	9.88	3.93	68	4.2	110
158-3	1.91	4.47	10.17	0.48	69	4.3	103
158-4	1.74	4.44	9.91	0.42	67	4.2	109
158-5	1.93	4.43	10.21	0.49	69	4.4	106
158-6	1.83	4.42	9.54	0.93	60	4.4	107
158-7	1.86	4.35	10.21	0.51	68	4.4	109
158-8	1.81	4.53	10.15	0.45	69	4.6	105
158-9	1.75	4.38	10.03	0.43	63	4.3	116
average error	0.03	0.05	0.12	0.03	3	0.4	9
corrected mean	1.82	4.44	10.01	0.53	67	4.4	108
standard dev.	0.08	0.06	0.2	0.18	3	0.1	4
bulk rock 015-B	2.16	4.28	10.95	20.1	72	3.8	93

sample number	Sb	Cs	Ba	La	Ce	Sm	Eu
* 158-1	0.28	5.03	586	25.56	56.3	5.91	1.08
158-2	0.31	5.16	622	25.31	56.3	5.67	1.05
158-3	0.31	5.19	637	25.04	54.5	5.65	1.07
158-4	0.29	5.36	655	25.08	55.5	5.57	1.06
158-5	0.29	5.18	630	25.38	56.3	5.75	1.07
158-6	0.28	5.21	663	24.06	53.3	5.42	1.02
158-7	0.35	5.21	643	25.32	56.1	5.69	1.08
158-8	0.31	5.33	615	25.61	57.2	5.76	1.07
158-9	0.31	5.27	714	25.06	56.2	5.73	1.02
average error	0.05	0.1	40	0.33	1.1	0.13	0.02
corrected mean	0.31	5.23	647	25.1	55.7	5.65	1.06
standard dev.	0.02	0.07	31	0.46	1.2	0.11	0.02
bulk rock 015-B	0.27	4.66	580	24.16	54.8	5.56	1.11

Table C-5 con't Taupo plinian tephra

sample number	Tb	Yb	Lu	Hf	Ta	Th	U
* 158-1	0.97	3.81	0.571	6.65	0.78	10.35	2.71
158-2	0.91	3.48	0.583	6.28	0.64	10.41	2.54
158-3	0.91	3.63	0.575	7.14	0.67	10.31	2.47
158-4	0.91	3.65	0.575	6.28	0.66	10.71	2.63
158-5	0.92	3.64	0.567	6.54	0.69	10.51	2.74
158-6	0.86	3.35	0.532	6.32	0.65	10.37	2.53
158-7	0.89	3.68	0.579	6.89	0.69	10.78	2.61
158-8	0.95	3.51	0.576	6.83	0.71	10.61	2.62
158-9	0.92	3.56	0.598	6.32	0.66	10.45	2.61
average error	0.03	0.12	0.02	0.18	0.03	0.2	0.3
corrected mean	0.91	3.56	0.573	6.56	0.67	10.52	2.6
standard dev.	0.03	0.11	0.02	0.33	0.02	0.17	0.08
bulk rock 015-B	0.92	3.45	0.537	6.01	0.82	9.9	2.4

* this sample has been removed from the "corrected mean"

Sample descriptions		Sample Mass (mg)
158-1	1 black fragment	29.70
158-2	1 black fragment	20.33
158-3	1 black fragment	27.22
158-4	2 black fragments	23.68
158-5	2 black fragments	24.83
158-6	2 black fragments	33.56
158-7	2 black fragments	27.34
158-8	2 black fragments	23.73
158-9	4 black fragments	35.38
015-B	pumice- bulk sample	120.23

Table C-5 con't

Hatepe phreatomagmatic tephra- samples 152 and 002A

sample number	FeO	Na_2O	Sc	Co	Zn	As	Rb
* 152-1	1.79	4.31	8.57	1.15	52	4.1	114
152-2	1.79	4.54	10.12	0.44	68	4.2	101
152-3	1.81	4.48	10.46	0.46	73	4.5	104
152-4	1.78	4.53	10.19	0.35	70	4.4	104
152-5	2.17	4.37	10.25	1.11	73	4.4	100
152-6	2.64	4.16	10.14	2.26	65	4.4	103
152-7	1.89	4.56	10.21	0.42	70	4.4	81
* 152-8	1.78	4.29	8.56	1.09	52	4.4	110
152-9	1.77	4.46	9.82	0.46	66	4.1	111
average error	0.03	0.05	0.1	0.04	3	0.4	10
corrected mean	1.97	4.44	10.17	0.54	69	4.3	104
standard dev.	0.3	0.1	0.2	0.28	3	0.2	4
bulk rock 002-A	2.11	4.26	10.84	54	75	4	98

sample number	Sb	Cs	Ba	La	Ce	Sm	Eu
* 152-1	0.28	5.71	642	24.41	53.3	5.1	0.88
152-2	0.31	5.26	659	25.55	57.2	5.7	1.08
152-3	0.38	5.12	723	25.28	57.1	5.8	1.13
152-4	0.28	4.93	619	25.16	54.9	5.8	1.13
152-5	0.32	5.03	655	24.11	54.3	5.4	1.11
152-6	0.31	5.21	655	24.43	55.4	5.3	0.91
152-7	0.22	5.15	645	25.48	56.6	5.7	1.09
* 152-8	0.34	5.36	655	24.41	54.1	5.1	0.94
152-9	0.28	5.22	715	24.71	55.1	5.6	1.09
average error	0.06	0.15	50	0.3	1.1	0.1	0.02
corrected mean	0.31	5.13	667	24.9	55.6	5.6	1.07
standard dev.	0.05	0.12	38	0.55	1.1	0.2	0.08
bulk rock 002-A	0.28	4.76	574	24.28	54	5.6	1.12

Table C-5 con't Hatepe phreatoplinian tephra

sample number	Tb	Yb	Lu	Hf	Ta	Th	U
* 152-1	0.86	3.26	0.601	7.19	0.96	11.1	2.86
152-2	0.91	3.69	0.581	6.51	0.71	10.8	2.39
152-3	0.93	3.78	0.599	6.63	0.77	10.4	2.32
152-4	0.95	3.62	0.586	6.21	0.65	10.1	2.32
152-5	0.91	3.46	0.551	6.93	0.72	10.1	2.32
152-6	0.86	3.46	0.568	7.11	0.67	10.6	2.71
152-7	0.93	3.73	0.567	6.53	0.77	10.5	2.69
* 152-8	0.85	3.42	0.534	6.26	1.02	10.7	2.81
152-9	0.93	3.58	0.573	6.64	0.84	10.6	2.55
average error	0.04	0.12	0.03	0.18	0.04	0.2	0.3
corrected mean	0.92	3.62	0.575	6.65	0.73	10.4	2.51
standard dev.	0.03	0.13	0.02	0.29	0.07	0.3	0.17
bulk rock 002-A	0.88	3.51	0.536	6.19	1.19	10.4	2.5

* These samples have been removed from the corrected mean

Sample descriptions		Sample mass (mg)
152-1	1 black fragment	19.76
152-2	1 black fragment	21.75
152-3	2 black fragments	23.10
152-4	2 black fragments	21.20
152-5	2 black fragments	22.42
152-6	2 black fragments	23.23
152-7	2 black fragments	21.36
152-8	3 black fragments	27.60
152-9	1 black fragment	35.26
002-A	pumice - bulk rock	108.15

Table C-5 con't
Kaharoa samples 129 and 80-A

sample number	FeO	Na_2O	Sc	Co	Zn	As	Rb
129-1	0.81	4.19	3.31	0.22	31	4.26	130
129-2	0.84	4.11	3.56	0.65	31	4.04	123
129-3	0.88	4.34	3.22	0.26	30	4.46	128
129-4	0.78	4.03	3.29	0.22	31	4.61	131
129-5	0.89	4.23	3.41	0.31	33	4.38	125
129-6	0.79	3.91	3.36	0.35	31	4.71	126
129-7	0.78	3.81	3.16	0.21	32	4.91	125
129-8	0.83	4.19	3.56	0.23	33	5.16	140
129-9	0.75	4.21	3.22	0.21	30	4.03	132
129-1	0.85	4.08	3.28	0.35	34	4.31	123
average error	0.02	0.05	0.06	0.01	2	0.45	8
corrected mean	0.82	4.11	3.31	0.3	32	4.48	128
standard dev.	0.05	0.16	0.15	0.14	1	0.36	5
bulk rock 80-A	0.82	3.92	3.26	19.9	30	4.66	122

sample number	Cs	Ba	La	Ce	Sm	Eu	Tb
129-1	5.73	981	23.81	52.1	4.31	0.53	0.71
129-2	5.57	982	20.18	44.5	3.93	0.51	0.69
129-3	5.24	963	19.93	43.9	3.91	0.61	0.66
129-4	5.89	908	20.95	46.1	4.01	0.47	0.69
129-5	5.61	957	46.21	87.8	5.84	0.63	0.75
129-6	5.67	869	21.25	45.7	3.98	0.45	0.69
129-7	5.49	867	20.66	44.5	3.94	0.45	0.68
129-8	6.01	965	21.86	48.6	4.29	0.49	0.72
129-9	5.82	1035	24.53	51.8	4.27	0.52	0.7
129-1	5.52	909	20.19	43.5	3.93	0.49	0.66
average error	0.08	50	0.4	0.8	0.11	0.01	0.02
corrected mean	5.67	951	23.66	50.9	4.24	0.51	0.7
standard dev.	0.19		7	13.3	0.58	0.06	0.03
bulk rock 80-A	5.25	953	21.83	47.7	3.97	0.54	0.65

Table C-5 con't Kaharoa tephra

sample number	Yb	Lu	Hf	Ta	Th	U
129-1	3.51	0.513	3.66	0.79	12.1	3.11
129-2	3.93	0.525	3.21	0.76	10.1	2.93
129-3	3.04	0.491	3.29	0.73	10.6	2.86
129-4	3.13	0.509	3.31	0.77	11.5	3.19
129-5	3.19	0.507	4.01	0.77	16.1	2.79
129-6	3.05	0.489	3.06	0.92	11.3	3.04
129-7	3.06	0.484	3.21	0.76	11.1	3.07
129-8	3.54	0.538	4.63	0.85	12.1	3.28
129-9	3.03	0.531	3.01	0.75	12.1	3.08
129-1	3.14	0.498	3.09	0.83	10.8	3.07
average error	0.12	0.03	0.1	0.02	0.2	0.3
corrected mean	3.17	0.508	3.44	0.79	11.8	3.04
standard dev.	0.19	0.02	0.5	0.06	1.6	0.15
bulk rock 80-A	3.07	0.471	3.2	0.99	11.2	2.9

Sample descriptions		Sample mass (mg)
129-1	1 clear fragment	46.33
129-2	1 clear fragment	40.58
129-3	1 clear fragment	48.50
129-4	1 clear fragment	30.38
129-5	1 clear fragment	21.87
129-6	2 clear fragments	26.75
129-7	2 clear fragments	28.44
129-8	2 clear fragments	20.13
129-9	3 clear fragments	33.88
129-10	3 clear fragments	24.78
80-A	pumice- bulk sample	80.29

Table C-5 con't

Mamaku tephra- sample 067

sample number	FeO	Na_2O	Sc	Co	Zn	As	Rb
*67-1	1.16	4.41	5.42	0.24	49	3.9	95
67-2	1.02	4.08	4.11	0.31	44	3.7	99
67-3	0.99	3.95	3.49	0.59	36	3.6	112
* 67-4	2.28	3.94	5.63	2.12	60	3.6	103
67-5	1.17	4.09	4.05	0.64	40	4.4	112
67-6	0.88	4.12	3.31	0.46	37	3.8	118
67-7	1.11	4.15	3.64	0.47	40	3.6	108
67-8	1.22	4.24	3.46	0.52	38	4.3	112
average error	0.01	0.06	0.05	0.02	2	0.5	7
corrected mean	1.07	4.11	3.67	0.51	39	3.9	110
standard dev.	0.13	0.1	0.33	0.12	2.6	0.36	6
bulk rock							
67-B	1.36	4.04	3.91	0.52	38	4.11	97

sample number	Sb	Cs	Ba	La	Ce	Sm	Eu
*67-1	0.09	3.69	821	25.63	57.1	5.54	1.02
67-2	0.16	4.18	816	24.19	55.3	4.82	0.91
67-3	0.19	4.91	872	24.19	49.7	4.01	0.62
* 67-4	0.17	4.45	849	22.39	48.8	3.91	0.65
67-5	0.16	4.91	884	23.91	51.1	4.06	0.67
67-6	0.26	5.17	912	24.35	50.9	4.08	0.65
67-7	0.12	4.73	904	24.11	51.4	4.26	0.69
67-8	0.18	4.79	964	23.59	49.7	4.03	0.68
average error	0.03	0.08	35	0.33	1	0.11	0.02
corrected mean	0.18	4.78	892	24.06	51.3	4.2	0.7
standard dev.	0.05	0.33	50	0.31	2.1	0.3	0.1
bulk rock							
67-B	0.18	4.43	862	21.65	46.4	3.73	0.75

Table C-5 con't Mamaku tephra

sample number	Tb	Yb	Lu	Hf	Ta	Th	U
*67-1	0.913	3.72	0.601	5.41	0.69	9.18	2.31
67-2	0.806	3.26	0.534	4.57	0.71	9.73	2.21
67-3	0.672	2.82	0.465	3.56	0.74	10.82	2.92
* 67-4	0.611	2.77	0.463	4.77	0.71	10.15	2.93
67-5	0.643	2.91	0.482	4.36	0.76	10.87	2.61
67-6	0.641	2.93	0.476	3.67	0.73	11.17	2.67
67-7	0.669	2.99	0.482	3.86	0.74	10.79	2.71
67-8	0.603	2.68	0.479	4.59	0.68	10.72	2.91
average error	0.02	0.08	0.02	0.13	0.03	0.2	0.25
corrected mean	0.66	2.93	0.486	4.1	0.73	10.68	2.67
standard dev.	0.07	0.19	0.02	0.5	0.03	0.5	0.26
bulk rock							
67-B	0.596	2.79	0.432	4.55	0.95	n.	2.6

* sample has been removed from the "corrected mean"

Sample descriptions		Sample weight (mg)
67-1	3 lt black fragments	30.23
67-2	3 black fragment	23.50
67-3	2 grey fragments	31.00
67-4	2 grey fragments	37.50
67-5	2 grey fragments	27.60
67-6	2 grey fragments	28.29
67-7	3 grey fragments	24.09
67-8	4 grey fragments	36.74
67-B	pumice- bulk sample	92.45

Table C-6. Step-scan analyses of melt inclusions done by electron microprobe. Position of analyses is shown on accompanying sketch. The analyses were made with a 1 micron beam, so absolute abundances of mobile elements, particularly Na_2O, are incorrect.

Taupo plinian inclusion 1

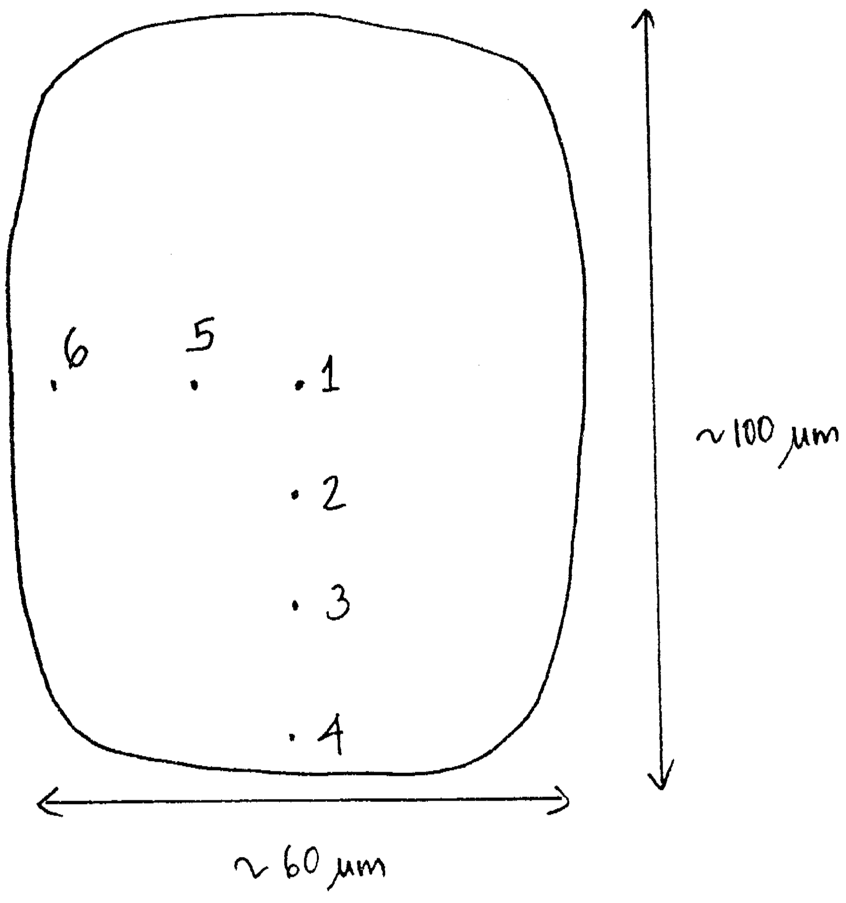

	SiO_2	TiO_2	Al_2O_3	FeO	MgO	MnO	CaO	Na_2O	K_2O	total
1	75.9	0.1	12.1	2.4	0.2	0.3	1.1	0.6	1.3	94.0
2	75.9	0.2	12.0	2.3	0.1	0.2	1.1	0.6	1.1	93.5
3	77.5	0.1	11.9	2.4	0.1	0.2	1.1	0.6	1.1	95.0
4	77.5	0.1	12.0	2.2	0.2	0.2	1.1	0.5	0.9	94.6
5	74.6	0.1	12.0	2.2	0.1	0.2	1.1	0.4	1.0	91.7
6	75.7	0.1	12.0	2.1	0.1	0.2	1.1	0.4	0.9	92.8

Table C-6 con't

Taupo plinian inclusion 2

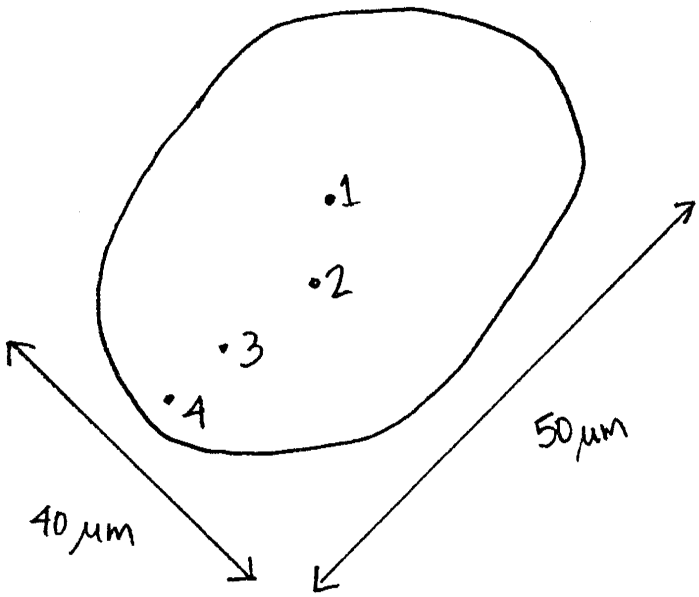

	SiO_2	TiO_2	Al_2O_3	FeO	MgO	MnO	CaO	Na_2O	K_2O	total
1	74.1	0.3	12.1	2.4	0.2	0.2	1.2	1.0	1.5	93.3
2	74.9	0.3	12.2	2.3	0.1	0.2	1.3	0.8	1.4	93.5
3	73.7	0.3	11.7	2.2	0.0	0.2	1.2	1.3	1.7	92.4
4	74.0	0.2	11.9	2.1	0.1	0.2	1.2	1.4	1.7	92.9

Table C-6 con't

Taupo plinian inclusion 3

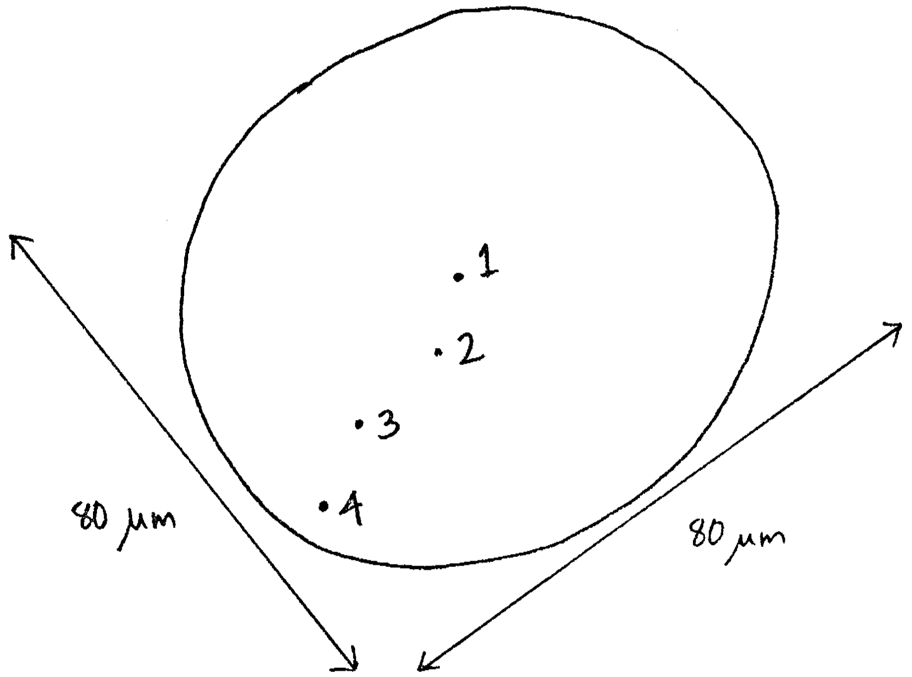

	SiO_2	TiO_2	Al_2O_3	FeO	MgO	MnO	CaO	Na_2O	K_2O	total
1	74.3	0.3	12.9	2.4	0.2	0.2	1.3	0.7	1.5	93.7
2	73.9	0.2	12.2	2.4	0.2	0.2	1.2	0.6	1.5	92.8
3	73.7	0.2	12.4	2.3	0.1	0.2	1.2	0.6	1.3	92.1
4	74.2	0.2	12.6	2.4	0.0	0.2	1.2	0.6	1.3	92.8

Table C-6 con't

Initial Ash inclusion 1

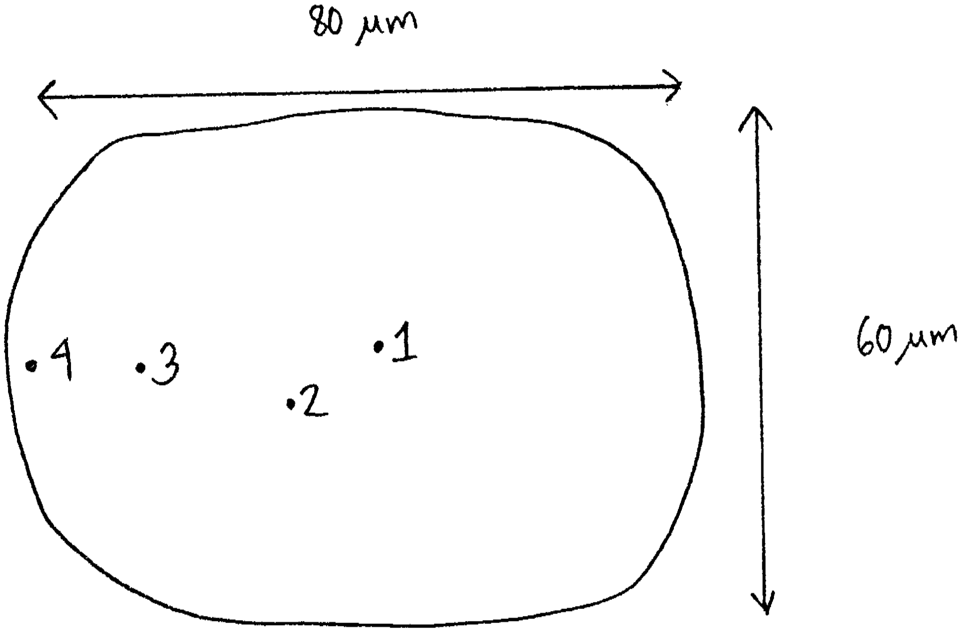

	SiO_2	TiO_2	Al_2O_3	FeO	MgO	MnO	CaO	Na_2O	K_2O	total
1	74.2	0.2	12.2	2.3	0.1	0.2	1.1	0.6	1.1	92.1
2	75.7	0.2	11.9	2.3	0.1	0.2	1.2	0.7	1.2	93.7
3	75.1	0.3	12.4	2.2	0.1	0.2	1.1	0.4	1.1	92.9
4	74.5	0.3	12.1	2.4	0.2	0.2	1.1	0.8	1.4	93.0

Table C-6 con't

Initial Ash inclusion 2

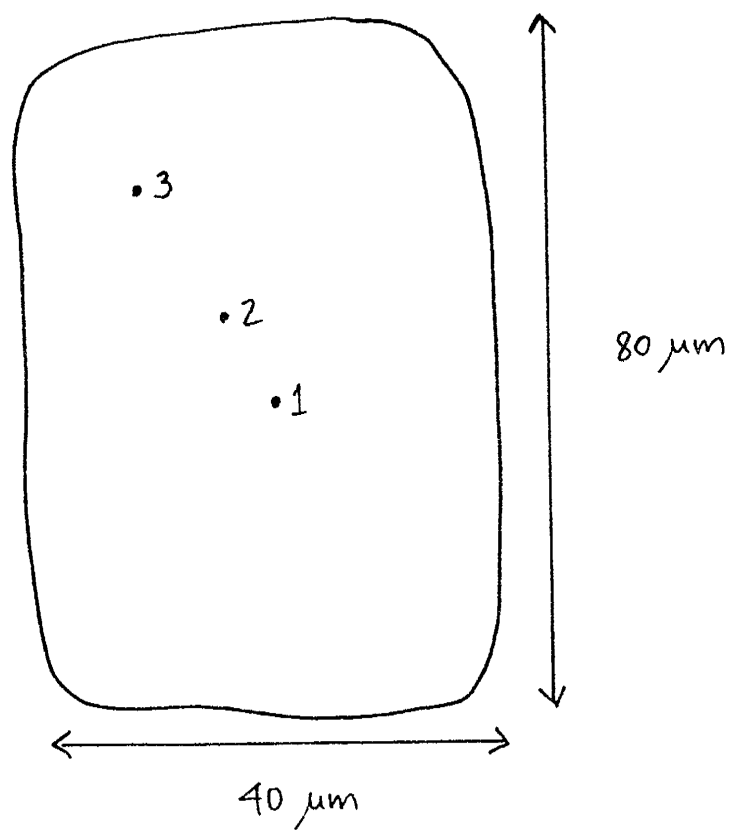

	SiO_2	TiO_2	Al_2O_3	FeO	MgO	MnO	CaO	Na_2O	K_2O	total
1	71.7	0.2	12.4	2.3	0.1	0.2	1.2	3.6	2.7	94.5
2	73.8	0.3	11.8	1.6	0.2	0.1	1.2	3.3	2.0	94.4
3	73.1	0.3	12.5	2.3	0.0	0.2	1.2	0.4	0.9	90.9

APPENDIX D

Volatile composition of melt inclusions and obsidian

Table D-1. Water contents of obsidian in tephra deposits from the Taupo Volcanic center as analysed by Karl-Fisher titration. Mean water contents are of bulk samples of crushed obsidian and each value is a mean of 2 to 4 determinations.
Individual water contents are of single obsidian fragments.
The comments refer to the single obsidian fragments, and describe the color and appearance of the fragment (bl=black; gr=grey; lt gr=light grey; sl ves=slightly vesicular).

Unit	Age x1000	Sample Number	Strat. Pos.	Mean Water Content	Individual water contents
Groundlayer of Taupo Ignimbrite	2	028	all	0.47	
		037	all	0.62	
		038	all	0.61	
Taupo plinian	2	016	top	0.52	
		022	inter	0.38	
		015	inter	0.23	
		014	base	0.43	
		158	top	0.17	
		157	inter	0.16	
		156	inter	0.24	
		155	inter	0.13	
		154	base	0.17	
T.P./Rot. trans.	2	125	top	0.51	
		124	inter	0.43	
		123	base	0.46	
		013	inter	0.39	
Rotongaio	2	041	inter	0.34	
		146	top	0.24	0.33 gr/bl cloudy
					0.32 gr/bl cloudy
					0.58 gr/bl
					0.52 bl
		140	inter	0.21	0.09 bl
		138	inter	0.23	
		137	inter	0.19	
		136	inter	0.23	0.26 bl
					0.41 bl
					0.33 bl

Table D-1 con't

Unit	Age x1000	Sample Number	Strat. Pos.	Mean Water Content	Individual water contents
Hatepe	2	002	top	0.46	0.40 8 bl frags
phreatomagmatic		003	inter	0.56	
		023	inter	1.44	2.14 bl
					1.91 bl
					1.75 bl
					1.80 dk gr
					1.85 bl
					1.86 gr
					2.20 bl
		004	inter	1.55	2.27 bl
					2.23 gr
					2.08 gr
		006	inter	1.26	1.26 bl
					2.01 gr
					2.10 gr
					0.06 crushed did not vesic.
		005	base	1.12	1.66
		153	top	0.46	
		152	inter	0.37	
		151	inter	0.38	1.65 gr/bl
					1.68 bl
					0.74 bl/gr
					1.94 bl/gr
					0.61 bl
		150	inter	0.98	0.99 bl/gr
					1.00 bl/gr
					0.89 bl/gr
					1.68 bl
					2.14 bl clear
					1.48 bl
		149	inter	0.97	1.79 bl/gr sl ves
					1.56 bl clear
					0.68 bl clear
					0.79 dull bl
					2.44 bl glassy
		148	inter	0.40	
		147	base	0.90	

Table D-1 con't

Unit	Age x1000	Sample Number	Strat. Pos.	Mean Water Content	Individual water contents
Hatepe plinian	2	007		0.20	
		027		0.38	
		045		0.44	
		112	top	0.19	
		111	inter	0.19	
		110	inter	0.17	
		109	inter	0.10	
		108	base	0.48	1.67 bl
					1.44 gr sl ves
					0.26 bl
Initial ash		044	top	0.21	
		043	base	0.41	
		122	top	0.31	
		121	base	0.33	
Mapara	2.2	026	top	0.95	0.25 bl/gr
					0.26 bl/gr
		025	inter	0.65	
		024	base	0.70	
Whaikapo	2.8	029		1.22	0.88 gr
					1.36 bl
					1.09 gr clear
		127a		0.51	
Waihimia	3.2	020	inter		1.33 bl
		018	base	1.05	
		120	top	0.41	1.30 bl
					0.68 bl sl ves
		119	inter	0.16	
		117	inter		1.72 lg bl
					1.87 same as above
		116	base	0.21	

Table D-1 con't

Unit	Age x1000	Sample Number	Strat. Pos.	Mean Water Content	Individual water contents
Motutere	5.4	008	all	1.60	1.39
					1.44 gr
					0.83 gr
					0.68 gr same as a
					0.69 ""
		115	all	0.81	0.78 bl clear
					2.76 bl/gr
					0.86 gr/bl
					0.79 gr/bl
					0.85 gr sl ves
Opepe	8.8	032	top	1.10	
		031	inter	1.02	
		030	base	1.00	1.43 bl
					0.90 gr
					0.70 bl
Poronui	9.5	009	base	0.75	1.16 gr
					0.97 gr
					0.51 gr
					1.08 gr
		114	top	0.36	0.85 gr/bl
					1.07 gr/bl
					1.04 bl clear
					1.22 bl
					0.88 bl/gr
		113	base	0.67	0.99 gr sl ves
					0.90 gr sl ves
					1.09 bl/gr
					0.89 bl
					1.15 gr/bl
Karapiti	9.8	012	top	1.02	
		034	top	0.84	
		011	base	1.15	0.95 gr
					0.82 gr
					1.35 gr
					0.78 bl
					1.29 bl
					1.50 bl
					0.45 gr
					1.29 bl
					1.09 gr

Table D-1 con't

Unit	Age x1000	Sample Number	Strat. Pos.	Mean Water Content	Individual water contents
Oruanui	20	082	top	1.02	
		050	inter	1.37	3.99 lt gr
					0.68 lt gr
					0.62 lt gr
					0.53 lt gr
					0.79 lt gr
		051	base	3.30	
Okaia	22	047	all	0.79	
		056	all	0.62	
Tihoi	38	055	base	1.49	

Table D-2. Water contents of obsidian in tephra deposits from the Okataina Volcanic center as analysed by Karl-Fisher titration. Mean water contents are of bulk samples of crushed obsidian and each value is a mean of 2 to 4 determinations. Individual water contents are of single obsidian fragments. The comments refer to the single obsidian fragments, and describe the color and appearance of the fragment (bl=black; gr=grey; lt gr=light grey; sl ves=slightly vesicular).

Unit	Age x1000	Sample Number	Strat. Pos.	Mean Water Content	Individual Water Contents
Kaharoa	0.65	080	inter	0.49	
		132	top	1.06	1.04
					1.37
					0.97
					0.91
					1.02
		131	inter	0.38	
		130	inter	0.59	
		129	base	1.02	0.59 gr
					1.36 gr
					1.01 gr
					2.49 bl
					1.19 gr
Whakatane	5	68	inter	0.65	
Mamaku	7	67	top		0.62 gr
					0.44 gr
					0.46 gr
					0.64 gr
					0.65 gr
					0.66 gr
					0.54 gr
		66	inter	0.82	
		65	base	0.73	
Rotoma	9	64	top	0.67	
		63	inter	0.76	
		62	base	0.52	

Table D-2 con't

Unit	Age x1000	Sample Number	Strat. Pos.	Mean Water Content	Individual Water Contents
Waiohau	11	128	top	0.56	
		127b	base	1.13	0.91 clear bl
					1.03 gr bl
					1.17 gr bl
					1.06 gr
					1.44 gr
		81	inter	0.89	1.28 cloudy gr
					2.00 gr
					2.26 bl glassy
					1.32 3 bl
					2.53 1 bl
Rotorua	13	91	top	0.39	
		88	inter	0.64	
		83	inter	1.13	
		85	inter	1.24	
		87	inter	1.10	
		86	base	1.08	
Rerewhakaaitu	14.7	79	top	0.51	
		78	base	0.87	
Okareka	17	76	inter	0.70	
Te Rere	19	60	top	0.40	0.21 bl
					0.38 clear bl
		59	inter	0.52	
		57	base	0.68	
Omataroa	28	74	inter	1.66	
Awakeri	30	72	all	1.24	0.51 gr
					0.95 bl
					1.13 lt gr
					0.69 lt clear gr
					0.46 cloudy gr
					0.37 clear gr
					1.91 lt gr
					0.45 lt gr
					0.98 clear gr
					0.64 clear gr
Mangaone	31	71	top	1.48	
			base	1.49	

Table D-3. Chlorine content of obsidian and melt inclusions from the Taupo Volcanic Center tephras as analysed by electron microprobe. Some samples were analysed by both ion microprobe and electron microprobe, and these are noted with the sample number. Analyses of individual inclusions which were analysed by electron and ion microprobes are noted with an asterix (*). The standard deviation of analyses is shown in column labeled "SD".

Unit and Sample number		Obsidian Cl (wt.%)	SD	Melt inclusions Cl (wt%)	SD
Taupo plinian					
015	mean	0.140	0.007	0.178	0.006
	individual	0.150		0.176	
		0.134		0.176	
		0.138		0.179	
		0.139		0.189	
				0.171	
				0.179	
015 ion probe plag.	mean			0.161	0.020
	individual			0.175*	
				0.147*	
155	mean			0.171	0.014
	individual			0.184	
				0.151	
				0.185	
				0.159	
				0.153	
				0.178	
				0.185	
				0.173	
154	mean			0.176	0.015
	individual			0.160	
				0.196	
				0.170	
				0.169	
				0.186	

Table D-3 con't

Unit	Sample Number	Obsidian Cl (wt.%)	SD	Melt inclusions Cl (wt%)	SD
157	mean			0.168	0.014
	individual			0.179	
				0.166	
				0.186	
				0.151	
				0.173	
				0.153	
157 ion probe	mean			0.162	0.011
	individual			0.175*	
				0.145*	
				0.162*	
				0.167*	
				0.159*	
Hatepe phreatomagmatic					
003	mean	0.131	0.008	0.175	0.007
	individual	0.125		0.174	
		0.129		0.176	
		0.089		0.166	
		0.165		0.182	
		0.139			
		0.141			
		0.131			
		0.130			
		0.122			

Table D-3 con't

Unit	Sample Number	Obsidian Cl (wt.%)	SD	Melt inclusions Cl (wt%)	SD
Hatepe plinian					
	mean	0.121	0.020	0.173	0.005
027					
	individual	0.119		0.176	
		0.145		0.169	
		0.109			
		0.099			
		0.118			
		0.126			
		0.131			
		0.141			
		0.079			
		0.111			
		0.153			
110	mean			0.171	0.016
	individual			0.170	
				0.170	
				0.199	
				0.175	
				0.152	
				0.160	
112	mean			0.173	0.025
	individual			0.214	
				0.144	
				0.167	
				0.173	
				0.184	
				0.153	
112	mean			0.136	0.020
ion probe					
	individual			0.107*	
				0.147*	
				0.147*	
				0.127	
				0.152	
108	mean			0.177	0.006
	individual			0.186	
				0.173	
				0.177	
				0.171	

Table D-3 con't

Unit	Sample Number	Obsidian Cl (wt.%)	SD	Melt inclusions Cl (wt%)	SD
108 ion probe	mean			0.163	0.019
	individual			0.159*	
				0.137*	
				0.158*	
				0.177	
				0.186	
108 ion probe plagioclase	mean			0.139	0.017
	individual			0.142*	
				0.142*	
				0.122	
				0.125	
				0.164*	
Initial ash					
044	mean			0.172	0.010
	individual			0.181	
				0.173	
				0.173	
				0.180	
				0.169	
				0.153	
045	mean	0.120	0.005		
	individual	0.122			
		0.115			
		0.126			
		0.118			
Mapara					
025	mean	0.136	0.006	0.188	0.009
	individual	0.146		0.189	
		0.129		0.205	
		0.130		0.180	
		0.139		0.186	
		0.134		0.183	
		0.135		0.183	

Table D-3 con't

Unit	Sample Number		Obsidian Cl (wt.%)	SD	Melt inclusions Cl (wt%)	SD
Whaikapo						
029		mean	0.160	0.012	0.184	0.006
	individual		0.180		0.181	
			0.160		0.180	
			0.150		0.193	
			0.150		0.181	
			0.162			
Waihimia						
020		mean	0.129	0.011	0.183	0.003
	individual		0.143		0.186	
			0.116		0.183	
			0.136		0.181	
			0.146		0.180	
			0.115			
			0.129			
			0.134			
			0.125			
			0.119			
Motutere						
008		mean	0.157	0.006	0.197	0.013
	individual		0.151		0.197	
			0.160		0.180	
			0.161		0.200	
					0.200	
					0.216	
					0.182	
					0.205	
Opepe						
032		mean	0.141	0.018	0.181	0.009
	individual		0.144		0.180	
			0.111		0.180	
			0.091		0.187	
			0.120		0.189	
			0.140		0.167	
			0.146		0.168	
			0.172		0.187	
			0.160		0.187	
			0.122			

Table D-3 con't

Unit	Sample Number	Obsidian Cl (wt.%)	SD	Melt inclusions Cl (wt%)	SD
Poronui					
009	mean	0.143	0.013	0.186	0.015
	individual	0.150		0.170	
		0.152		0.173	
		0.153		0.205	
		0.120		0.196	
		0.152		0.186	
		0.130			
		0.146			
Karapiti					
011	mean	0.138	0.016	0.190	0.012
	individual	0.131		0.180	
		0.159		0.180	
		0.129		0.200	
		0.121		0.200	
		0.148			
Oruanui					
050	mean	0.153	0.015	0.234	0.024
	individual	0.150		0.246	
		0.178		0.249	
		0.135		0.247	
		0.150		0.202	
		0.144		0.259	
		0.162		0.206	

Table D-3 con't

Unit	Sample Number	Obsidian Cl (wt.%)	SD	Melt inclusions Cl (wt%)	SD
!!					
Okaia					
047	mean			0.211	0.024
	individual			0.251	
				0.205	
				0.220	
				0.224	
				0.183	
				0.183	
				0.216	
047	mean			0.194	0.033
	individual			0.182	
				0.240	
				0.162	
				0.192	
047 ion probe	mean			0.174	0.025
	individual			0.175*	
				0.138*	
				0.207	
				0.163	
				0.185	
047 ion probe plag.	mean			0.201	0.020
	individual			0.234*	
				0.179*	
				0.199	
				0.197*	
				0.195*	
Tihoi					
054	mean			0.224	0.034
	individual			0.203	
				0.185	
				0.213	
				0.192	
				0.244	
				0.288	
				0.250	
					0.219

* Denotes an inclusion which was analysed by electron and ion microprobe

Table D-4. Chlorine content of obsidian and melt inclusions from the Okataina Volcanic Center tephras as analysed by electron microprobe.

Unit and Sample number		Obsidian Cl (wt.%)	SD	Melt inclusions Cl (wt%)	SD
Kaharoa					
080	mean	0.137		0.198	0.001
	individual	0.129		0.199	
		0.138		0.199	
		0.132		0.197	
		0.141			
		0.114			
		0.145			
		0.151			
		0.145			
Whakatane					
068	mean	0.159	0.011	0.176	0.011
	individual	0.152		0.190	
		0.156		0.180	
		0.178		0.153	
		0.152		0.196	
		0.152		0.159	
		0.167			
Mamaku					
066	mean	0.149	0.014	0.192	0.009
	individual	0.122		0.189	
		0.161		0.200	
		0.142		0.179	
		0.145		0.198	
		0.155			
		0.158			
		0.159			

Table D-4 con't

Unit and Sample number		Obsidian Cl (wt.%)	SD	Melt inclusions Cl (wt%)	SD
Rotoma					
064	mean	0.162	0.014	0.196	0.006
	individual	0.149		0.199	
		0.165		0.189	
		0.174		0.199	
		0.179			
		0.157			
		0.138			
		0.160			
		0.149			
		0.170			
		0.180			
Waiohau					
081	mean	0.165		0.200	0.012
	individual	0.182		0.200	
		0.170		0.202	
		0.158		0.220	
		0.189		0.196	
		0.151		0.183	
		0.178		0.196	
		0.127			
Rotorua					
085	mean	0.168	0.004	0.173	0.007
	individual	0.173		0.178	
		0.165		0.163	
		0.166		0.168	
				0.179	
				0.178	
Okareka					
076	mean			0.128	0.006
	individual			0.124	
				0.125	
				0.134	

Table D-4 con't

Unit and Sample number		Obsidian Cl (wt.%)	SD	Melt inclusions Cl (wt%)	SD
Te Rere					
060	mean	0.119	0.007	0.195	
	individual	0.109		0.195	
		0.125			
		0.116			
		0.118			
		0.115			
		0.130			
Omataroa					
075	mean			0.137	0.001
	individual			0.138	
				0.136	
				0.136	
Awakeri					
072	mean	0.155	0.006	0.189	0.060
	individual	0.151		0.263	
		0.152		0.159	
		0.162		0.129	
				0.206	
Mangaone					
071	mean	0.141	0.020	0.132	
	individual	0.111		0.124	
		0.121		0.140	
		0.108			
		0.160			
		0.141			
		0.146			
		0.154			
		0.142			
		0.155			
		0.172			

Tables D-5. Water release from obsidian at various temperatures as analysed by Karl Fischer titration.

Sample	Temperature (degrees C)	Wt% Water released	Percent Water released
115	100-200	0.07	8.8
Motutere	200-300	0.02	2.5
1 black chip	300-400	0	0
	400-500	0	0
	500-600	0.01	1.3
	600-700	0	0
	700-800	0	0
	800-900	0.70	87.5
115	250-450	0.02	2.6
Motutere	450-600	0.01	1.3
1 black chip	600-950	0.75	96.2
148	100-200	0.07	19.4
Hatepe phr.	200-300	0.05	13.9
powder	300-400	0.08	22.2
	400-500	0.06	16.7
	500-600	0.05	13.9
	600-700	0.03	8.3
	700-800	0.01	2.8
	800-900	0.01	2.8
127b	100-400	0.07	10.7
Waiohau	400-500	0.25	38.5
powder	500-600	0.12	18.5
	600-700	0.08	12.3
	700-1000	0.13	20.0
147	200-300	0.07	9.1
Hatepe phr.	300-400	0.16	20.8
powder	400-500	0.19	24.7
	500-600	0.15	22.1
	600-700	0.08	10.4
	700-800	0.09	11.7
	800-1000	0.03	3.9

Table D-5 con't

Sample	Temperature (degrees C)	Wt% Water released	Percent Water released
29 Whaikapo powder	200-300	0.05	4.5
	300-400	0.08	7.2
	400-500	0.18	16.2
	500-600	0.22	19.8
	600-700	0.28	25.2
	700-800	0.15	13.5
	800-900	0.09	8.1
	900-1000	0.06	5.4
72 Awakeri powder	200-300	0.06	5.7
	300-400	0.14	13.2
	400-500	0.23	21.1
	500-600	0.23	21.1
	600-700	0.16	14.7
	700-800	0.07	6.4
	800-900	0.12	10.3
	900-1000	0.08	8.0
149 Hatepe phr. powder	200-300	0.03	6.7
	300-400	0.07	15.5
	400-500	0.12	26.7
	500-600	0.07	15.6
	600-700	0.07	15.6
	700-800	0.05	11.1
	800-900	0.03	6.7
	900-1000	0.01	2.2
161 perlite powder	200-300	1.14	52.0
	300-400	0.62	28.3
	400-500	0.27	12.3
	500-600	0.11	5.0
	600-700	0.05	2.3
	700-900	0	0
	900-1000	0	0
163 perlite powder	200-300	1.06	49.1
	300-400	0.67	31.0
	400-500	0.26	12.0
	500-600	0.09	4.2
	600-700	0.07	3.2
	700-900	0	0
	900-1000	0.01	0.5

Table D-5 con't

Sample	Temperature (degrees C)	Wt% Water released	Percent Water released
161	200-300	1.08	39.3
perlite	300-400	0.56	20.4
powder	400-500	0.54	19.6
	500-600	0.29	10.5
	600-700	0.15	5.5
	700-900	0.09	3.3
	900-1000	0.04	1.5
161	200-300	1.12	39.0
perlite	300-400	1.05	36.2
chips	400-500	0.44	15.4
	500-600	0.25	8.7
	600-700	0	0
	700-900	0	0
	900-1000	0	0

Table D-6. Water, fluorine and trace element contents of melt inclusions as analysed by ion microprobe.

Taupo plinian melt inclusions

Sample Number	015	015	015	015	015
Host crystal	pyx	pyx	pyx	pyx	pyx
Date of analysis (m/d/yr)	5/10/86	5/10/86	5/10/86	10/10/86	10/10/86
H_2O (wt%)	3.7	3.4	5.4	5.4	4.8
F (ppm)	440	480	400	380	360
P_2O_5 (ppm)				220	190
Rb (ppm)	83	110	94		
Ba (ppm)	290	390	350		
La (ppm)	21	26	24		
Ce (ppm)	53	62	62		
Sm (ppm)	4	5	5		
Hf (ppm)					
Sr (ppm)	80	100	87		
Nd (ppm)	18	23	23		

Taupo plinian melt inclusions

Sample Number	015	015	157	157	157
Host crystal	pyx	pyx	pyx	pyx	pyx
Date of analysis (m/d/yr)	10/20/86	10/20/86	7/29/87	7/29/87	7/29/87
H_2O (wt%)	3.8	4.2	4.3	3.7	3.8
F (ppm)	420	420	580	500	420
P_2O_5 (ppm)			420	510	390
Rb (ppm)	89	104	56	70	58
Ba (ppm)	350	410	220	280	220
La (ppm)	25	25	13	13	12
Ce (ppm)	56	66	30	30	30
Sm (ppm)	7	7	3	3	3.3
Hf (ppm)			3.3	3.3	4
Sr (ppm)	79	97			
Nd (ppm)	24	29			

Table D-6 con't

Taupo plinian melt inclusions

Sample Number	154	154	154	015
Host crystal	pyx	pyx	pyx	plag
Date of analysis (m/d/yr)	7/29/87	7/29/87	7/29/87	7/29/87
H_2O (wt%)	3.5	6	6.2	5.2
F (ppm)	490	560	1460	400
P_2O_5 (ppm)	420	520	630	280
Rb (ppm)	68	82	108	83
Ba (ppm)	290	340	380	440
La (ppm)	16	19	21	22
Ce (ppm)	42	48	52	
Sm (ppm)	3.4	3.5	4.1	4.3
Hf (ppm)	5.1	4	5.6	5.8
Sr (ppm)				
Nd (ppm)				

Table D-6 con't

Hatepe plinian melt inclusions

Sample Number	108	108	108	112	112
Host crystal	pyx	pyx	pyx	pyx	pyx
Date of analysis (m/d/yr)	7/29/87	7/29/87	7/29/87	7/29/87	7/29/87
H_2O (wt%)	4.7	3.9	3.7	3.9	5.1
F (ppm)		326	395	420	440
P_2O_5 (ppm)		340	340	300	430
Rb (ppm)		48	50	48	68
Ba (ppm)		190	200	195	250
La (ppm)		10	10	12	15
Ce (ppm)		26	26	26	34
Sm (ppm)		2.8	2.6	2.4	3
Hf (ppm)		2.4	3.4	3.4	4.6
Sr (ppm)					
Nd (ppm)					

Hatepe plinian melt inclusions

Sample Number	112	108	108	108
Host crystal	pyx	plag	plag	plag
Date of analysis (m/d/yr)	7/29/87	7/30/87	7/30/87	7/30/87
H_2O (wt%)	5.9	4.4	3.6	6.5
F (ppm)		630	380	780
P_2O_5 (ppm)		350	300	300
Rb (ppm)		100	90	78
Ba (ppm)		640	620	410
La (ppm)		28	30	19
Ce (ppm)		72	74	48
Sm (ppm)		6	5.5	4.6
Hf (ppm)		6.8	6.6	4.5
Sr (ppm)				
Nd (ppm)				

Table D-6 con't

Okaia tephra melt inclusions

Sample Number	047	047	047	047	047
Host crystal	amph	pyx	pyx	qtz	qtz
Date of analysis (m/d/yr)	7/29/87	7/29/87	7/29/87	7/30/87	7/30/87
H_2O (wt%)	4.6	6.1	5.9	6.5	6.1
F (ppm)	468	570	334	440	690
P_2O_5 (ppm)	500	410	420	460	430
Rb (ppm)	278	148	90	156	160
Ba (ppm)	1100	360	340	800	560
La (ppm)	25	18	14	26	25
Ce (ppm)	56	37	34	72	62
Sm (ppm)	4.4	3.1	2.4	5.1	4.1
Hf (ppm)	4.2	3.7	2.2	5.6	3.6
Sr (ppm)					
Nd (ppm)					

Okaia tephra melt inclusions

Sample Number	047	047	047
Host crystal	qtz	qtz	qtz
Date of analysis (m/d/yr)	7/30/87	7/30/87	7/30/87
H_2O (wt%)	6.6	5.9	5.5
F (ppm)	440	380	460
P_2O_5 (ppm)	390	300	330
Rb (ppm)	140	110	130
Ba (ppm)	530	400	640
La (ppm)	23	16	24
Ce (ppm)	57	40	57
Sm (ppm)	3.2	2	3
Hf (ppm)	3.4	2.3	4.4
Sr (ppm)			
Nd (ppm)			

APPENDIX E
Composition of magnetite and ilmenite and temperature and oxygen fugacity determinations

Table E-1. Magnetite and ilmenite analyses from the Taupo and Okataina centers, analysed by an ARL electron microprobe. Each grain (A,B,C,D) represents a number (n) of analyses of magnetite and ilmenite in one silicate phenocryst. Samples marked with an asterix (*) were analysed on a JEOL-733 microprobe. Total Fe analysed as FeO.

TAUPO CENTER

Unit	grain	type of crystal	n	Ti_2O	FeO	MgO	Al_2O_3	MnO	total
Taupo plinian	A	mag.	3	13.7	78.1	1.0	1.8	0.8	95.4
	B	mag.	3	13.2	78.7	1.0	1.9	0.7	95.5
	C	mag.	3	13.8	79.2	1.0	1.9	0.8	96.7
	A*	mag.	1	13.3	77.2	1.1	1.9	0.8	94.3
	C*	mag.	1	13.7	77.5	1.1	2.0	0.8	95.1
	1*	mag.	2	12.9	78.5	1.0	1.9	0.8	95.1
	2*	mag.	1	12.9	77.0	1.0	1.9	0.8	93.6
	3*	mag.	2	13.7	78.1	1.1	1.8	0.8	95.5
	A	ilm.	3	45.7	47.1	2.0	0.3	1.3	96.4
	B	ilm.	4	44.5	47.6	1.8	0.3	1.2	95.4
	C	ilm.	4	45.0	47.3	1.8	0.3	1.2	95.6
	A*	ilm.	1	48.1	47.7	1.9	0.1	1.2	99.0
	B*	ilm.	1	48.6	47.2	1.9	0.1	1.2	99.0
	B*	ilm.	1	47.4	47.6	2.0	0.1	1.1	98.2
	4*	ilm.	1	48.5	47.5	1.9	0.1	1.1	99.1
	5*	ilm.	1	48.0	48.6	1.7	0.2	1.0	99.5
	6*	ilm.	1	47.6	48.1	1.9	0.2	1.2	99.0
	7*	ilm.	1	47.5	48.5	1.8	0.2	1.0	99.0
	8*	ilm.	1	47.4	48.6	1.8	0.2	1.1	99.1
	9*	ilm.	1	48.3	48.1	1.8	0.2	1.2	99.6
Hatepe plinian	A	mag.	4	13.5	78.2	1.2			92.9
	B	mag.	6	13.7	77.8	0.9			92.4
	C	mag.	5	13.1	77.4	0.9			91.4
	A*	mag.	1	12.2	78.6	1.0	1.8	0.8	94.4
	A*	mag.	1	14.0	78.6	1.0	1.8	0.9	96.3
	3*	mag.	1	13.5	78.2	1.0	1.8	0.9	95.4
	4*	mag.	1	14.0	78.1	0.9	1.8	0.9	95.7
	A	ilm.	11	47.3	46.9	2.0			96.2
	B	ilm.	2	47.4	46.6	1.8			95.8
	C	ilm.	5	47.6	47.1	2.1			96.8
	1*	ilm.	1	48.9	48.5	1.5	0.1	1.2	100.2

Table E-3 con't

Unit	grain	type of crystal	n	Ti_2O	FeO	MgO	Al_2O_3	MnO	total
Initial Ash	A	mag.	4	12.3	76.6	1.0	1.8	0.8	92.5
	B	mag.	4	11.6	76.8	0.9	1.8	0.8	91.9
	C	mag.	4	11.5	76.3	0.9	1.8	0.8	91.3
	*1	mag.	1	13.7	79.4	1.0	1.8	0.9	96.8
	*1	mag.	1	13.5	78.3	1.0	1.6	0.9	95.3
	*2	mag.	1	13.9	78.7	1.0	1.9	1.0	96.5
	A	ilm.	3	47.8	47.4	1.9	0.3	1.1	98.5
	B	ilm.	3	47.7	47.6	1.8	0.3	1.2	98.6
	C	ilm.	4	46.5	47.3	1.8	0.3	1.3	97.2
	*3	ilm.	1	48.3	48.9	1.7	0.2	1.3	100.4
Mapara	A	mag.	3	12.7	78.1	1.0	1.8	0.7	94.3
	B	mag.	3	12.7	77.3	0.9	1.7	0.8	93.4
	*B	mag.	1	13.4	77.0	0.8	1.8	0.8	93.8
	A	ilm.	2	47.4	47.5	1.5	0.3	1.2	97.9
	B	ilm.	2	46.9	46.6	1.9	0.3	1.1	96.8
	*A	ilm.	1	48.7	47.4	1.7	0.1	1.1	99.0
	*A	ilm.	1	47.9	47.1	1.8	0.1	1.1	98.0
	*B	ilm.	1	48.3	47.9	1.7	0.2	1.1	99.2
Whaikapo	A	mag.	4	13.9	79.8	0.8	1.9	0.9	97.3
	B	mag.	3	14.3	79.5	0.7	1.9	0.9	97.3
	1*	mag.	1	15.2	77.2	0.1	1.5	1.0	95.0
	2*	mag.	1	14.8	75.4	0.9	1.5	0.9	93.5
	A	ilm	2	46.5	46.4	1.2	0.2	1.2	95.5
	B	ilm	2	46.1	46.3	1.3	0.3	1.2	95.2
	1*	ilm	1	48.3	47.5	1.4	0.1	1.4	98.7
	2*	ilm	1	49.0	48.2	1.3	0.1	1.3	99.9
Waihimia	A	mag.	3	13.6	76.0	0.8			90.4
	C	mag.	2	13.8	76.1	0.7			90.6
	A	ilm.	6	47.7	47.0	1.5			96.2
	C	ilm.	2	47.9	47.4	1.6			96.9
Motutere	A	mag.	3	12.9	80.1	0.8	1.8	0.8	96.4
	B	mag.	4	13.0	77.7	0.8	1.7	0.9	94.1
	C	mag.	2	12.9	77.6	0.8	1.7	0.8	93.8
	D	mag.	2	13.4	77.8	0.7	1.8	0.7	94.4
	A	ilm.	3	47.8	46.9	1.4	0.4	1.2	97.7
	B	ilm.	2	46.6	46.7	1.8	0.4	1.3	96.8
	C	ilm.	2	46.9	46.4	1.6	0.4	1.2	96.5
	D	ilm.	3	46.7	47.0	1.5	0.4	1.3	96.9

Table E-1 con't

Unit	grain	type of crystal	n	Ti_2O	FeO	MgO	Al_2O_3	MnO	total
Opepe	A	mag.	2	13.7	79.3	0.8	1.7	0.5	96.0
	B	mag.	4	13.0	78.5	0.8	1.8	0.6	94.7
	C	mag.	2	12.3	77.5	0.8	1.9	0.6	93.1
	D	mag.	2	13.0	77.8	0.8	1.8	0.6	94.0
	1*	mag.	1	13.7	78.1	0.7	1.7	0.5	94.7
	A	ilm.	3	46.6	46.7	1.6	0.3	0.9	96.1
	B	ilm.	3	45.5	46.9	1.5	0.2	0.9	95.0
	C	ilm.	1	45.9	46.1	1.5	0.2	0.8	94.5
	D	ilm.	2	45.5	46.2	1.5	0.3	0.9	94.4
	1*	ilm.	1	47.4	46.5	1.4	0.1	1.0	96.4
	2*	ilm.	1	49.6	48.2	1.5	0.1	0.9	100.3
	3*	ilm.	1	49.0	48.6	1.4	0.1	0.9	100.0
Poronui	A	mag.	2	13.0	78.9	0.6	1.8	0.7	95.0
	B	mag.	3	13.7	77.5	0.7	1.7	0.7	94.3
	C	mag.	3	13.6	78.3	0.7	1.7	0.7	95.0
	D	mag.	3	13.6	78.6	0.7	1.8	0.6	95.3
	1*	mag.	1	13.4	79.7	0.6	1.5	0.6	95.8
	A	ilm.	2	45.5	47.7	1.3	0.3	0.8	95.6
	B	ilm.	2	46.2	46.4	1.3	0.3	0.8	95.0
	C	ilm.	3	47.9	47.0	1.5	0.4	0.8	97.6
	D	ilm.	6	45.1	46.9	1.3	0.4	0.9	94.6
	1*	ilm.	1	48.8	48.0	1.2	0.1	0.8	98.9
	2*	ilm.	1	49.3	48.3	1.7	0.1	0.6	100.0
Karapiti	A	mag.	3	13.6	78.0	0.6			92.2
	B	mag.	3	13.6	75.9	0.8			90.3
	C	mag.	3	13.7	76.3	0.5			90.5
	A	ilm.	1	40.8	41.1	1.4			83.3
	B	ilm.	4	45.0	45.1	1.3			91.4
	C	ilm.	5	45.5	45.8	1.3			92.6
Oruanui	A	mag.	5	10.2	81.0	0.5			91.7
	B	mag.	3	9.2	82.7	0.6			92.5
	C	mag.	4	8.5	83.0	0.8			92.3
	D	mag.	4	11.0	82.2	0.6			93.8
	*A	mag.	2	10.6	81.1	0.8	1.1	0.6	94.2
	A	ilm.	3	47.2	47.6	1.3			96.1
	B	ilm.	3	47.1	48.3	1.6			97.0
	C	ilm.	4	46.3	47.9	1.7			95.9
	D	ilm.	5	47.4	48.4	1.6			97.4
	*A	ilm.	1	47.3	48.9	1.4	0.8	1.0	99.4

Table E-1 con't

Unit	grain	type of crystal	n	Ti_2O	FeO	MgO	Al_2O_3	MnO	total
Okaia	A	mag.	3	9.3	80.9	0.5			90.7
	B	mag.	4	9.3	79.5	0.7			89.5
	C	mag.	2	8.6	78.7	0.6			87.9
	*A	mag.	1	10.1	80.2	0.2	1.5	0.6	92.6
	*B	mag.	1	9.5	81.1	0.1	1.4	0.6	92.7
	1*	mag.	1	9.6	81.0	0.1	1.5	0.6	92.8
	A	ilm.	5	45.5	45.9	1.3			92.7
	B	ilm.	5	44.5	45.8	1.5			91.8
	C	ilm.	6	43.4	45.5	1.9			90.8
Tihoi	A	mag.	6	9.9	80.0	0.5			90.4
	C	mag.	6	8.2	79.9	0.6			88.7
	*A	mag.	1	9.7	81.6	0.6	1.3	0.6	93.8
	*B	mag.	1	10.7	82.2	0.5	1.2	0.5	95.1
	A	ilm.	3	46.1	46.6	1.6			94.3
	C	ilm.	4	44.9	45.5	1.1			91.5
	*A	ilm.	1	48.0	48.6	1.4	0.0	1.0	99.0

Table E-1 con't
OKATAINA CENTER

Unit	grain	type of crystal	n	Ti_2O	FeO	MgO	Al_2O_3	MnO	total
Kaharoa	A	mag.	3	8.9	81.8	0.3	1.6	0.6	93.2
	B	mag.	3	8.4	79.2	0.9	2.2	0.9	91.6
	A	ilm.	4	44.7	49.4	1.0	0.2	1.4	96.7
	B	ilm.	3	45.9	44.5	1.9	0.2	4.0	96.5
Whakatane	A	mag.	3	8.1	82.4	0.6	1.4	0.8	93.3
	B	mag.	3	7.7	81.9	0.7	1.5	0.8	92.6
	C	mag.	4	8.0	82.5	0.6	1.4	0.8	93.3
	D	mag.	3	8.6	80.2	0.7	1.5	1.0	92.0
	*1	mag.	1	8.3	82.9	0.6	1.4	0.8	94.0
	*2	mag.	1	8.3	83.7	0.6	1.3	0.8	94.7
	A	ilm.	3	45.8	47.2	1.4	0.3	0.8	95.5
	B	ilm.	3	44.7	47.3	1.5	0.2	1.6	95.3
	C	ilm.	2	46.5	47.2	1.7	0.3	1.7	97.4
	D	ilm.	4	44.4	46.7	1.5	0.4	1.6	94.6
	*1	ilm.	1	47.3	47.3	1.4	0.2	1.7	97.9
	*2	ilm.	1	47.7	47.9	1.4	0.1	1.5	98.6
	*4	ilm.	1	48.3	48.5	1.4	0.1	1.6	99.9
Mamaku	A	mag.	3	7.5	82.7	0.6	1.5	0.8	93.1
	B	mag.	2	8.3	81.8	0.7	1.5	0.8	93.1
	C	mag.	4	8.3	82.5	0.6	1.4	0.8	93.6
	D	mag.	2	7.4	77.1	0.7	1.4	0.8	87.4
	*B	mag.	1	8.1	83.9	0.6	1.3	0.8	94.7
	*B	mag.	1	8.3	83.7	0.7	1.3	0.9	94.9
	A	ilm.	2	46.8	47.6	1.6	0.3	1.5	97.8
	B	ilm.	2	46.3	47.4	1.6	0.3	1.6	97.2
	C	ilm.	3	45.8	47.3	1.9	0.3	1.5	96.8
	D	ilm.	1	43.1	46.9	1.7	0.4	1.3	93.4
	*B	ilm.	1	47.1	49.3	1.5	0.1	1.4	99.4
	*B	ilm.	1	47.6	48.6	1.5	0.1	1.7	99.5
Rotoma	A	mag.	2	4.6	84.0	0.7	1.7	0.8	91.8
	B	mag.	2	7.2	80.8	0.7	1.6	0.9	91.2
	C	mag.	3	7.2	81.8	0.7	1.5	1.0	92.2
	D	mag.	4	7.6	81.4	0.7	1.7	0.9	92.3
	A	ilm.	2	43.9	48.6	1.7	0.2	2.0	96.4
	B	ilm.	3	44.8	47.7	1.6	0.2	1.6	95.9
	C	ilm.	3	43.5	47.7	1.7	1.5	1.0	95.4
	D	ilm.	2	44.0	47.9	1.7	0.2	1.6	95.4

Table E-1 con't

Unit	grain	type of crystal	n	Ti_2O	FeO	MgO	Al_2O_3	MnO	total
Waiohau	A	mag.	3	7.8	91.3	0.7	1.4	0.7	101.9
	B	mag.	2	7.5	92.3	0.8	1.4	0.7	102.7
	C	mag.	2	7.5	90.7	0.8	1.5	0.7	101.2
	*1	mag.	1	8.2	82.9	0.6	1.5	0.6	93.8
	*2	mag.	1	8.1	82.6	0.7	1.5	0.7	93.6
	*3	mag.	1	8.1	81.9	0.7	1.4	0.8	92.9
	A	ilm.	2	45.6	47.8	1.7	0.2	1.6	96.9
	B	ilm.	2	45.2	48.7	1.7	0.3	1.4	97.3
	C	ilm.	4	45.3	48.5	1.8	0.2	1.4	97.2
Rotorua	A	mag.	2	8.3	82.4	1.2	1.7	0.6	94.2
	B	mag.	3	8.3	82.2	1.1	1.7	0.6	93.9
	C	mag.	2	8.0	82.5	1.0	1.7	0.6	93.8
	A	ilm.	3	43.1	50.4	2.2	0.3	1.0	97.0
	B	ilm.	4	43.8	50.3	2.2	0.3	0.8	97.4
	C	ilm.	2	43.3	50.0	2.2	0.3	0.9	96.7
	*1	ilm.	2	44.3	52.1	2.1	0.2	0.9	99.6
	*2	ilm.	2	43.7	51.5	2.1	0.1	0.9	98.3
Okareka	*1	mag.	2	9.2	80.3	0.5	1.3	0.9	92.2
	*1	mag.	1	9.3	81.2	0.4	1.2	0.9	93.0
	*1	ilm.	2	48.5	47.6	1.1	0.1	2.0	99.3
Te Rere	A	mag.	3	7.5	74.9	0.9			83.3
	B	mag.	5	7.9	82.3	1.1			91.3
	C	mag.	4	7.9	82.5	0.8			91.2
	A	ilm.	2	42.3	46.8	1.9			91.0
	B	ilm.	4	43.8	47.3	2.0			93.1
	C	ilm.	2	43.4	46.5	1.9			91.8
Awakeri	A	mag.	3	8.4	80.5	0.9	1.5	0.8	92.1
	B	mag.	3	8.4	80.5	0.9	1.5	0.8	92.1
	C	mag.	3	8.4	80.3	0.9	1.5	0.9	92.0
	*B	mag.	1	9.1	81.6	0.8	1.6	1.0	94.1
	*B	mag.	1	9.0	82.2	0.9	1.6	0.9	94.6
	A	ilm.	4	46.0	48.1	2.1	0.2	1.5	97.9
	B	ilm.	3	45.8	48.1	1.9	0.3	1.5	97.6
	C	ilm.	4	45.2	47.8	2.0	0.3	1.6	96.9
	*B	ilm.	1	47.3	48.9	1.8	0.1	1.6	99.7
	*B	ilm.	1	46.6	49.7	2.0	0.1	1.4	99.8
Mangaone	A	mag.	2	7.7	92.4	1.0	1.6	0.9	103.6
	B	mag.	2	8.2	91.6	1.0	1.5	0.9	103.2
	C	mag.	3	8.2	92.4	1.0	1.6	1.0	104.2
	A	ilm.	3	44.2	48.7	2.1	0.3	1.6	96.9
	B	ilm.	3	44.7	48.5	2.1	0.2	1.5	97.0
	C	ilm.	2	44.1	49.1	2.0	0.2	1.5	96.9

Table E-2. Temperature/Oxygen fugacity values for Taupo and Okataina center tephras. The temperature and oxygen fugacity are calculated from the from average magnetite and ilmenite compositions the constants from Anderson and Lindsley (1985). The average error of temperature and oxygen fugacity estimates are ±30 degrees and ±0.7 log of fugacity units. The "grain" refers to the host crystal of the magnetite and ilmenite blebs (from Table E-1). If two grains are listed, the first hosts the magnetite and the second hosts the ilmenite.

Unit	grain	Temperature	-log oxygen fugacity
Taupo Plinian	A	890	-11.7
(017)	B	900	-11.3
	C	896	-11.6
	C* B*	834	-13.6
	5* 7*	869	-12.7
	5*	858	-12.9
	3* 9*	840	-13.3
Hatepe plinian	A	844	-13.9
	B	844	-14.5
	C	852	-13.6
	1*	812	-13.8
	4* 1*	841	-13.4
Initial Ash	A	833	-13.3
(044)	B	826	-13.3
	C	844	-12.7
	1*	860	-12.8
	3*	863	-12.8
Mapara	A	834	-13.4
(025)	B	841	-13.9
	B*	843	-13.4
	B* 2*	840	-13.4
Whaikapo	A	834	-13.6
(029)	B	854	-13.3
	1* 2*	852	-13.5
	1*	861	-13.2
Waihimia	A	790	-14.5
(020)	C	819	-14.1
Motutere	A	808	-14.0
(008)	B	854	-12.8
	C	832	-13.7
	D	855	-12.8

Table E-2 con't

Unit	grain	Temperature	-log oxygen fugacity
Opepe	A	847	-13.0
(031)	B	860	-12.7
	C	828	-13.6
	D	850	-13.0
	1*	822	-13.9
	1* 2*	809	-14.3
	1* 3*	830	-13.8
Poronui	A	865	-12.5
(009)	B	840	-13.5
	C	818	-13.4
	D	871	-12.3
	1*	791	-14.7
	1* 2*	811	-14.1
Karapiti	A	826	-13.7
(010)	B	813	-14.2
	C	821	-13.8
Oruanui	A	787	-15.2
(050)	B	793	-14.1
	C	791	-14.1
	D	812	-13.9
	A*	809	-13.5
Okaia	A	781	-15.1
(047)	B	798	-14.1
	C	812	-13.0
	B* B	803	-13.5
Tihoi	A	798	-13.9
(054)	C	767	-15.4
	A*	786	-14.2
	B* A*	796	-14.0

Table E-2 con't
Okataina Volcanic Center tephras

Unit	grain	Temperature	-log oxygen fugacity
Kaharoa	A	825	-12.4
(080)	B	786	-13.2
Whakatane	A	778	-13.5
(068)	B	799	-13.0
	C	786	-13.7
	D	804	-12.9
	1*	772	-14.3
	2*	770	-14.4
Mamaku	A	776	-13.1
(066)	B	791	-13.6
	C	795	-12.8
	D	806	-12.5
	B*	792	-13.6
	B*	784	-13.9
Rotoma	A	775	-12.9
(064)	B	797	-13.1
	C	793	-12.7
	D	806	-12.4
Waiohau	A	789	-13.1
(081)	B	793	-12.8
	C		-12.8
	1* A	796	-13.3
	2* B	805	-13.0
	3* C	804	-13.0
Rotorua	A	843	-11.3
(085)	B	837	-11.5
	C	834	-11.5
	A 1*	842	-12.1
Okareka	1*	766	-14.8
	2* 1*	767	-14.8
Te Rere	A	805	-12.6
(059)	B	798	-12.8
	C	795	-13.3
Awakeri	A	807	-12.7
(072)	B	805	-12.8
	C	812	-12.5
	B*	804	-13.3
	B*	819	-12.8

Table E-2 con't

Unit	grain	Temperature	-log oxygen fugacity
Mangaone (071)	A	798	-12.0
	B	800	-12.2
	C	808	-11.8

APPENDIX F

Calculated solubility of H_2O and fragmentation depths for Taupo Volcanic Rhyolites

Solubility of water

Burnham (1975, 1979a and b) devised a model for solubility of H_2O in magmas which allows theoretical solubilities to be calculated for any given magma as long as the chemical composition is known. This model explains that H_2O dissolves in melts by breaking Si-O-Si bridges, and bonding with the available oxygen. If cations are present, balancing the charge on Al tetrahedra, they will move to occupy a position near the broken bridge site to maintain electrical neutrality. The reaction is the following, and will occur for up to 50 mole % H_2O in a pure albite melt. Terms used in all of the following equations are defined in Table F-1.

$$H_2O_{(v)} + O^{2-}{}_{(m)} + Na^+ = OH^-{}_{(m)} + ONa^-{}_{(m)} + H^+{}_{(m)} \qquad \text{(F-1)}$$

If no cations are available, H_2O will dissolve according to the following reaction, producing 2 moles of OH^- for every mole of dissolved H_2O. This reaction will take place if more than 50 mole % H_2O is present in the

Table F-1. Definition of equation variables, in order of occurrence

v	:	vapor phase
m	:	melt phase
M_e	:	equivalent mass of melt relative to H_2O
n_i^x	:	moles of exchangeable cations
n_{Si}	:	moles of silica
a_w	:	activity of water in the melt
k	:	constant (must be calculated for each case)
x_w^m	:	mole % of H_2O in melt
T	:	temperature in degrees Kelvin
W_w^m	:	weight % H_2O in melt
M_e'	:	equivalent mass of melt relative to H_2O for greater than 50 molecular percent
kW_w^m	:	weight fraction of H_2O in melt in excess of 50 molecular percent

melt.

$$H_2O_{(v)} + O^{2-}_{(m)} = 2OH^-_{(m)} \qquad (F-2)$$

Burnham's solubility model is for a pure albite melt, but he has found that it can be applied to any magma by calculating the mass of rock melt which will interact with one mole of H_2O. Calculation of this mass is different for amounts of water greater or less than 50 mole %, because of the different solubility mechanisms operating at the different water contents. When the water content is more than 50 mole %, the reaction is simple (eq. F-2), and is proportional to the molecular percentage of oxygen, as long as there was not more than 1 mole of exchangeable cations present in the original melt.

If less than 1 mole of water is present, the reaction is more complex because of the interaction of exchangeable cations. The exchangeable cations are proportional to the amount of Al in tetrahedral co-ordination, so in a melt with no normative corundum, the number of moles of melt which will react with water is proportional to the moles of Al. When there is normative corundum, the process is more complex, and the amount of melt which will react with water is shown by the equation:

$$1M_e = 1/[\Sigma n_i^x + 0.19(n_{Si} - 3\Sigma n_i^x)] \qquad (F\text{-}3)$$

The masses of one mole of rock melt, in terms of interaction with water, are calculated for an average Taupo Volcanic Zone rhyolite (Table F-2).

Burnham (1975) showed that there is a linear relationship between the activity and molecular percentages of water for less than 50 mole % H_2O in the melt:

$$a_w = k(x_w^m)^2 \qquad (F\text{-}4)$$

When there is more than 50 mole % H_2O, the relationship changes from linear to exponential because 2 moles of OH^- are produced for each mole of H_2O in solution:

$$a_w = 0.25ke^{(6.52 - 2667/T)(x_{wm} - 0.5)} \qquad (F\text{-}5)$$

Based on these equations, a solubility curve can be calculated for an albite melt at 750° C, using values for k

Table F-2. Calculation of equivalent weights of Taupo Volcanic Zone Rhyolite to albite. Average analysis of rhyolite from Reid (1983)

element	weight %	mole % cation	mole % oxygen
SiO_2	73.7	1.23	2.46
TiO_2	0.29	0.004	0.008
Al_2O_3	13.3	0.261	0.391
Fe_2O_3	1.82	0.023	0.034
MgO	0.36	0.009	0.009
CaO	1.67	0.030	0.030
Na_2O	4.28	0.138	0.069
K_2O	3.17	0.067	0.034
total	98.62	1.762	3.056

Equivalent mass: 98.62 [1 /(0.267 + 0.19{1.23 - (3 x 0.267)}] = 283
(less than 50 mole % H_2O)

Equivalent mass: 98.62 (8/3.056) = 258
(greater than 50 mole % H_2O)

from chart 16-3 (Burnham, 1979). The maximum solubility is shown by setting the activity of water equal to 1, and assuming that a very small amount of vapor is present. Values graphed in Fig. F-1 and listed in Table F-3.

Once this solubility curve for albite has been determined, the solubility of H_2O at a range of pressures can be calculated for Taupo rhyolite at 750°C by using the following two equations: For less than 50 mole% H_2O:

$$x_w^m/(1 - x_w^m) = (M_e W_w^m)/[18.02(1 - W_w^m)] \quad \text{(F-6)}$$

For greater than 50 mole % H20:

$$x_w^m/(1 - x_w^m) = 1 + [(M_e' kW_w^m)/[18.02(1 - kW_w^m)\}] \quad \text{(F-7)}$$

Values calculated for the TVZ rhyolite are shown in Fig. F-2, and are listed in Table F-3. Terms for equations F-6 and F-7 are defined in Table F-1.

Fragmentation depth calculations

Once the solubility of H_2O is known for a rhyolite, the depth at which bubbles make up a given volume

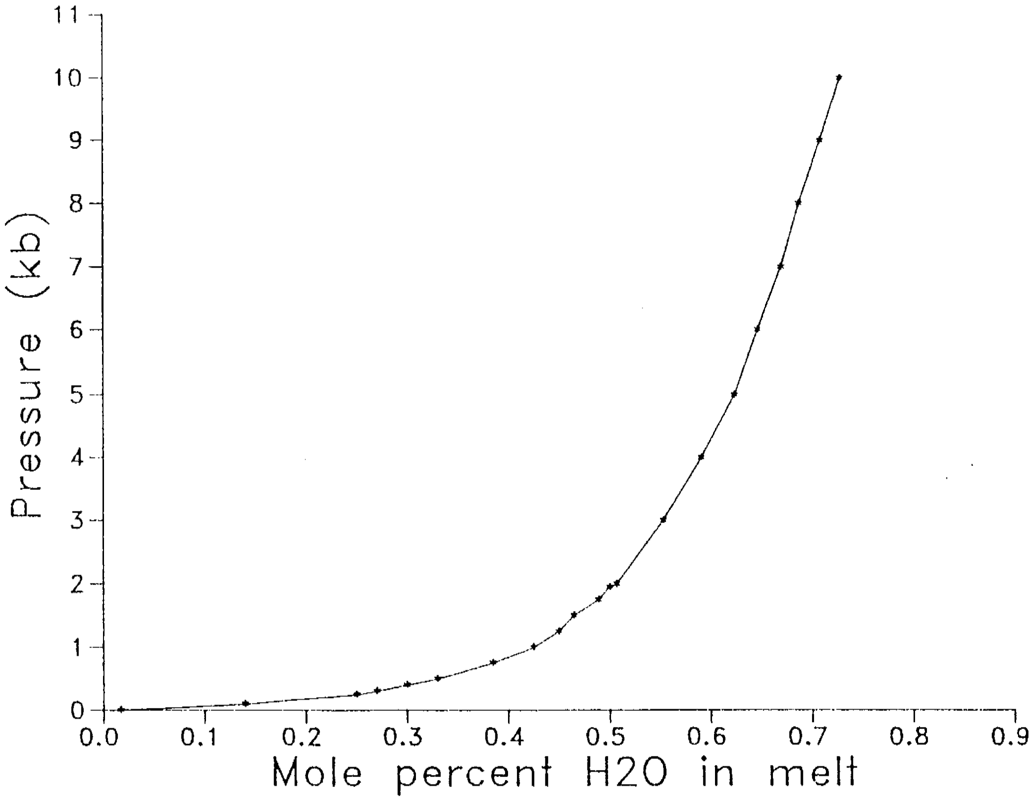

Figure F-1. Molar solubilty of H_2O in an albite melt at 750°C. Calculations are made following Burnham (1975, 1979a and b).

Table F-3. Maximum solubility of water in an albite melt at 750°C and maximum solubility of water in a Taupo rhyolite at 750°C. Solubility of albite is calculated from equations F-4 and -5. Values for k are taken from Fig. 16-3 (Burnham, 1979). Solubility for rhyolite is calculated from equations F-6 and F-7 in text and equivalent masses calculated earlier.

Pressure (kb)	ln k	mole % water in albite (x^m_w)	Weight % water in rhyolite (W^m_w)
0.001	8.2	0.017	0.11
0.1	4.0	0.14	1.02
0.25	2.8	0.25	2.06
0.3	2.6	0.27	2.30
0.4	2.4	0.30	2.66
0.5	2.2	0.33	3.00
0.75	1.90	0.38	3.83
1	1.71	0.42	4.49
1.25	1.60	0.45	4.95
1.5	1.55	0.46	5.30
1.75	1.43	0.49	5.74
1.95	1.39	0.50	5.98
2	1.36	0.51	6.09
3	1.18	0.55	7.52
4	1.03	0.59	8.90
5	0.90	0.62	10.29
6	0.82	0.65	11.39
7	0.72	0.67	12.60
8	0.65	0.69	13.65
9	0.57	0.71	15.01
10	0.49	0.73	16.45

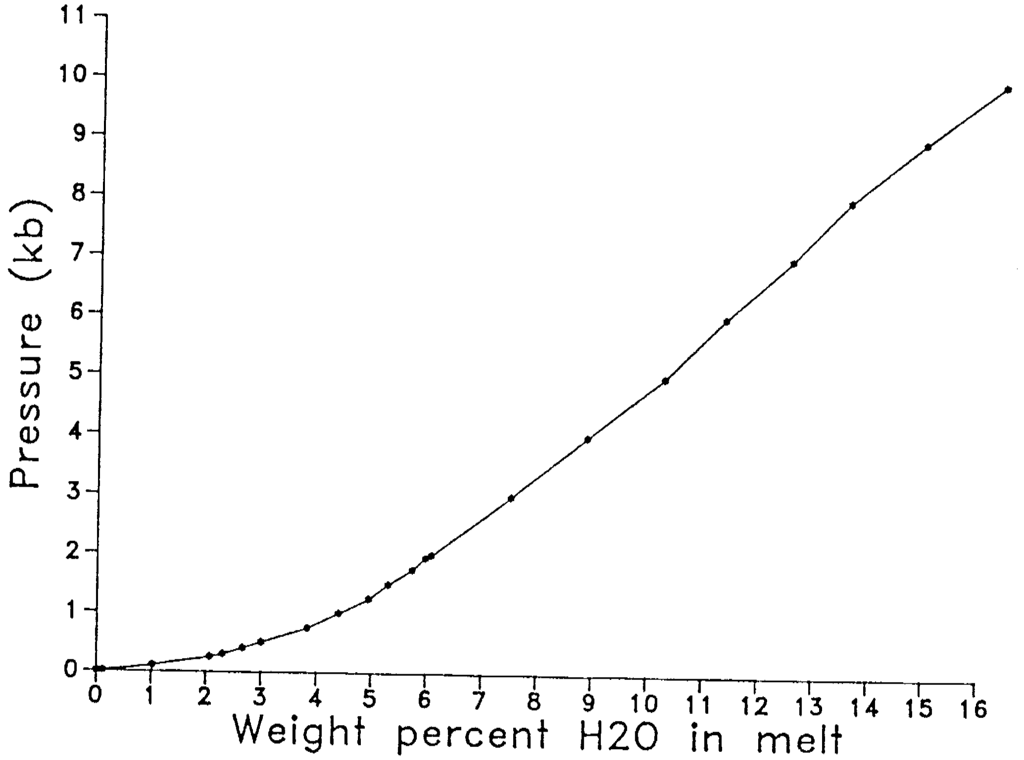

Figure F-2. Solubilty of H_2O in a TVZ rhyolite at 750°C. Calculations are made following Burnham (1975, 1979a and b).

percentage of the melt can be calculated from first principles, assuming ideal behavior of the water vapor. This has been done for the Taupo rhyolites for a 3:1 vapor/melt ratio, where fragmentation of the melt occurs.

The calculations used to determine these values are as follows. First, the molecular weight of the vapor-free melt is calculated for a variety of pressures, taking into account the amount of dissolved H_2O which would be present. The the density of the melt is then determined, using the relationship: density = 2.35 g/cm^3 - 5 (weight fraction of H_2O in melt). This assumes that the melt is a liquid, and that the density is pressure-independent. With the molecular weight and density of the melt known, the molecular volume can be calculated. For a ratio of 75% vapor to 25% melt, the number of moles of water vapor which will occupy 3 times the molecular volume of the melt at the given pressure is calculated using the ideal gas law. The weight percent of water vapor in the vapor-melt system can then be calculated. This can be added to the dissolved water remaining in the melt to determine the total water content of the melt necessary to cause fragmentation at a given pressure.

The values calculated for Taupo rhyolite are given in Table F-4, and in Fig. 7-1.

Table F-4. Calculations of initial melt water content necessary to cause fragmentation at given pressures. Ideal gas behavior of water is assumed.

Pressure (kb)	Wt% H_2O in melt	Mole. wt of melt (g)	Density of melt (g/cm^3)	Mole. vol of melt (cm^3)	Wt% deg. H_2O	Initial H_2O of melt
0.001	0.11	69.1	2.34	29.5	0.26	0.37
0.1	1.0	68.4	2.29	29.8	2.8	3.83
0.25	2.1	67.7	2.25	30.1	7.1	9.17
0.3	2.3	67.5	2.24	30.1	8.6	10.90
0.4	2.7	67.3	2.22	30.3	11.6	14.26
0.5	3.0	67.1	2.20	30.5	13.4	16.4
0.75	3.8	66.5	2.16	30.8	22.4	26.2
1.0	4.5	66.0	2.13	31.0	30.2	34.7
1.25	5.0	65.7	2.22	31.3	38.4	43.4

APPENDIX G

MAGMATIC INCLUSIONS: A KEY TO PRE-ERUPTIVE VOLATILE CONTENTS OF MAGMAS

INTRODUCTION

Melt inclusions are small samples of magma which are trapped in crystals during their growth. If unaltered, these inclusions will provide direct samples of pre-eruptive magma. They will also contain the magmatic volatile elements which would otherwise exsolve and escape to the atmosphere during the eruptive process. Melt inclusions are often subject to alteration which can change their pristine magmatic composition. This paper discusses the applicability of inclusions to analysis of pre-eruptive magmatic volatiles, and reviews current research on this topic.

Contents of melt inclusions

Melt inclusions, also known as magmatic or glass inclusions, can trap any material which is present at the time a magma is crystallizing (Roedder, 1984). This includes some combinations of melt, exsolved fluid, and smaller crystals. Afterward, when the magma is erupted and an inclusion cools, a number of different phases can appear.

Contraction bubbles sometimes form during cooling of a melt inclusion when differential contraction causes the melt to shrink more than the surrounding crystal while the glass is still plastic (Roedder, 1984). In this form, a melt inclusion may closely resemble a fluid inclusion, but can be distinguished by the lack of Brownian motion of the contraction bubble (Roedder, 1979). Also, fluid inclusions will contain only one bubble, which will be against the inclusion wall, whereas melt inclusions can contain any number of bubbles situated anywhere in the glass (Roedder, 1984).

Contraction bubbles which form in a melt inclusion can contain either a void space or a volatile phase, usually H_2O or CO_2. Formation of a shrinkage bubble, and the amount of vapor in the bubble, respectively, depend on the nucleation and diffusion rates of the specific melt (Roedder, 1984). Bubbles are more common in hydrous silicic melts than in drier basaltic magmas, and larger inclusions in a given melt will more commonly contain bubbles than small ones (Roedder, 1984). Also, inclusions which cool slowly will more commonly contain bubbles, because more time is available for contraction and diffusion before the glass is solid (Roedder, 1984). Simple optical observation cannot distinguish between a void or vapor filled bubble. Void contraction bubbles can be differentiated from bubbles which contain vapor by crushing the inclusion in oil, and observing whether the oil fills the bubble with or without the release of any vapor. (A. Rankin, pers. comm.). As an inclusion containing melt and fluid phases cools, the fluid phase will cease to be supercritical, and may exsolve into liquid and vapor phases if the density is great enough (Belkin et al., 1985), or it may remain a single vapor phase.

Daughter minerals, which were grown from trapped material are present in some melt inclusions. There are two main types of daughter minerals, those which crystallize from the magma, such as pyroxene, plagioclase and ilmenite, and those which crystallize from a trapped saline fluid, such as halite and sylvite (Roedder, 1984). Daughter minerals are generally crystalline, although immiscible phases are also seen, such as sulfide blebs in basaltic melts. The presence and size of daughter minerals is a function of cooling rate, inclusion size, and final quench temperature. The cooling rate has a significant effect on the final contents of melt inclusions, in general, the slower the cooling rate, the more phases a given inclusion will contain (Roedder, 1979). Inclusions may also contain microphenocrysts which were trapped at the time of crystallization. These can be distinguished primary daughter minerals by the inclusion volume:crystal size ratio. If this ratio is constant for a number of inclusions, the microphenocrysts are daughter minerals, but if it is variable, the crystals are trapped phases.

In summary, simple optical study of material contained in melt inclusions can give information about the phases present in the magma chamber, and the post-entrapment cooling rates undergone by the inclusions.

Types of melt inclusions

Melt inclusions are formed primarily by magmatic materials adhering to irregularities on the growing faces of a crystal. This occurs particularly when crystals are growing in a skeletal habit, which has experimentally been determined to be a result of high degrees of melt supercooling or rapid cooling rates (Lofgren, 1980).

Three types of inclusions are defined based on how they are trapped: primary, secondary and pseudosecondary. Primary inclusions are the most common and are trapped along the growth planes of the mineral during crystal growth. Secondary inclusions are trapped in fractures which develop in the crystal and subsequently reheal. A train of secondary inclusions will crosscut the growth planes of the crystal. Pseudosecondary inclusions appear to be secondary, but are actually primary, or co-genetic with the crystal where they are trapped. These inclusions can form if a crystal is resorbed or broken, and then begins to recrystallize, creating an unconformity. The distinction between primary, secondary, and pseudosecondary is not as critical in the study of melt inclusions as it is in the study of ore-deposit-related fluid inclusions, because the composition of the magma probably does not change very much while a small phenocryst is growing. An exception to this is a xenocryst introduced into a magma where it is no longer in equilibrium trapping inclusions of the second magma. The safest policy when studying magmatic inclusions is to only analyse inclusions which are obviously primary.

APPLICATIONS OF MELT INCLUSIONS AND METHODS OF ANALYSIS

A number of magmatic parameters can be analysed in primary, unaltered melt inclusions, including temperatures, pressures of magmatic systems, and major and volatile element chemistry. Analysis of melt inclusions requires specialized techniques because of their small size.

Temperature measurements

Temperature measurements involve heating the inclusion on a heating stage and can determine two properties, the minimum melting temperature of the magma (T_m), and the minimum temperature at which the inclusion was trapped (homogenization temperature, T_h) (Roedder, 1984). The melting temperature is the temperature at which the glass is molten enough for the vapor bubble to move. This is difficult to measure and is relatively unimportant. The homogenization temperature is the temperature at which all phases present homogenize to a single phase (Roedder, 1984). A pressure correction to this temperature, which is essential when measuring T_h in ore deposit fluid inclusions is unnecessary for melt inclusions because silicate melt is relatively incompressible (Roedder, 1984).

Homogenization temperature may be difficult to measure, particularly in viscous rhyolitic melts where dissolution kinetics of vapor bubbles are slow. Roedder and Coombs (1967) suggest run times of 16 hours for high silica melts. Inclusions of lower silica compositions, such as anorthoclase phonolite from Mt. Erebus, Antarctica, homogenize in 15 minutes (Dunbar, unpublished data). A second difficulty encountered in making T_h measurements is that inclusions often decrepitate before homogenization is achieved. This may be due to overpressuring in inclusions composed of volatile-rich glass (Chaigneau et al., 1980). However, decrepitation temperatures may, in some cases, approximate actual trapping temperatures (Roedder, 1979). Several studies of melt inclusion trapping temperatures have yielded accurate results (Clochiatti et al., 1976; Chaigneau et al., 1980; Belkin et al., 1985; Cortini et al., 1985 and others). Homogenization temperatures can, in some cases, accurately approximate magmatic temperatures, as seen in Fig. G-1 (Dunbar and Kyle, 1987). However, this is not always the case, particularly for rhyolitic melts where melt inclusion geothermometry does not yield reasonable data (Beddoe-Stephens et al., 1983). Additional problems with melt inclusion geothermometry include inclusions leaking due to incompetent host crystals, solid phases which won't homogenize, and vapor bubbles which won't dissolve for unknown reasons (Cortini et al., 1985). Magmatic inclusions should only be used as temperature indicators if no better geothermometric techniques are available.

Pressure measurements

Geobarometry, or estimation of trapping pressures of an inclusion, can be calculated from inclusions which contain both liquid and vapor phases of CO_2, as shown by Belkin et al., 1985). This is not a widely used technique, and the accuracy of the results is difficult to evaluate. Initially, the T_h of two-phase CO_2 inclusion containing liquid and vapor, is measured. The T_h can then be used to determine the density of the CO_2 phase at the time of trapping, using the phase diagram for CO_2 showing temperature vs. density. The density of trapped CO_2 can be used to estimate the trapping pressure of the inclusion.

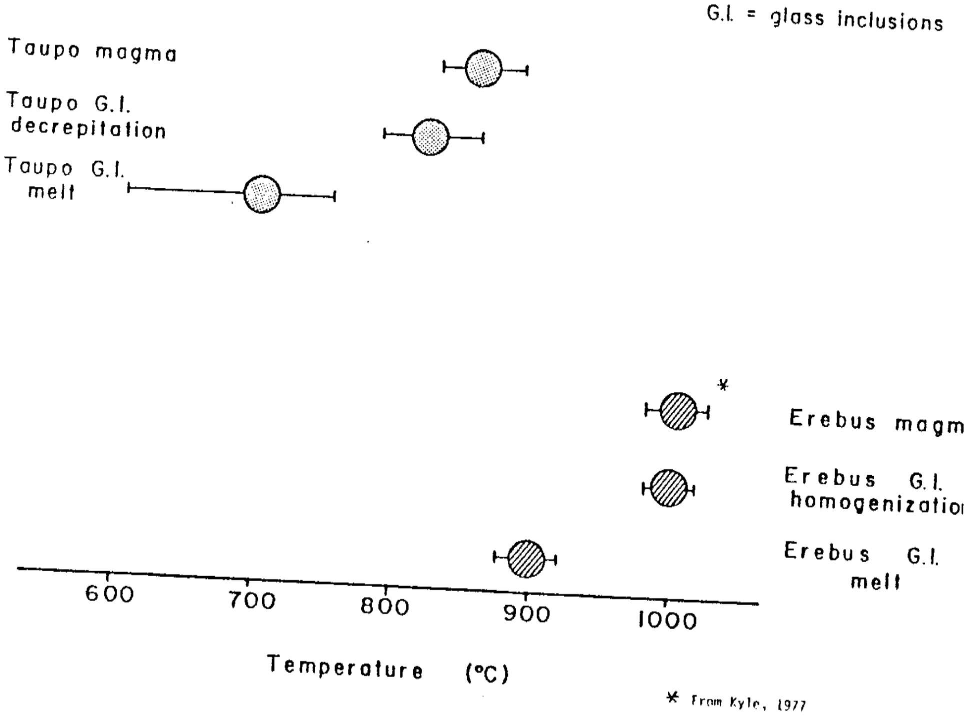

Figure G-1. Melt and homogenization/decrepitation temperatures of melt inclusions from the TVZ and Mt. Erebus, Antarctica as determined by high-temperture-stage analysis. These temperatures are compared with magmatic temperatures determined by other techniques (Fe-Ti oxide geothermometry for TVZ inclusions, and optical pyrometry for Mt. Erebus).

The temperature of trapping must be determined by an independent means.

Major element chemistry

Determination of major element chemistry in unaltered magmatic inclusions is important because it can show the melt composition at the time of crystallization. However, analysis is difficult because most melt inclusions are small. The most suitable way to analyse melt inclusions is in situ, with a microbeam technique, such as the electron microprobe (Roedder, 1984). Analysis by electron microprobe involves bombarding the sample with a small (1 to 50 microns) beam of electrons, exciting the atoms of the sample, and analysing the resultant secondary x-rays which have characteristic wavelengths and energies. This technique has been widely used for melt inclusion analysis (e.g. Dunbar et al., 1987; Sommer and Schramm, 1983; Anderson, 1973). However, there are a number of problems with this technique which must be considered when analysing melt inclusions. First, volatilization of elements such as sodium (Na) can occur under the energetic electron beam. This is corrected by broadening the beam to 20 to 50 microns (Kyle, 1977; Beddoe-Stephens, 1983), or by correcting the Na content based on known volatilization curves (Devine et al., 1984). A second problem is that a narrow beam may penetrate through the glass into the underlying host crystal, generating secondary x-rays from the crystal as well as the glass. This can be overcome by broadening the beam, or by analysing only the centers of larger inclusions. Despite these problems, the electron microprobe can give accurate data for melt inclusion major element chemistry.

Volatile Chemistry

Analysis of volatile elements in melt inclusions is difficult, particularly for H_2O and CO_2, but can provide the only available direct measurement of pre-eruptive magmatic volatile contents. This approach has been used by a number of different workers, using diverse analytical techniques. These analytical techniques and the results of some of this research are discussed below and results of a number of studies are summarized in Table G-1.

A. Electron microprobe

An early and widely used technique for analysing H_2O is the electron microprobe "analysis by difference" method (Anderson, 1979). This method assumes that the difference from 100% of the sum of major elements is representative of the volatile content of the melt, principally H_2O. There are a number of problems with this technique (Sommer and Schramm, 1983). First, the analysis is not specifically for H_2O, but determines the total weight percent of all the elements which are not specifically determined by the major element analysis. This includes all volatile elements, as well as any trace elements in the sample. Second, the volatilization of Na may significantly lower the final total of major elements. In addition, microprobe analyses are imprecise instruments, and totals of replicate analyses may vary by $\pm 1\%$. This technique is useful for very rough volatile determinations, but will not yield accurate data.

A number of early workers used the "analysis by difference" technique. Anderson (1979) worked on subduction-related basalts and andesites, and found a range of H_2O contents in different systems. The Pavlof region of Alaska showed H_2O concentrations of between 0.4 and 2.9 wt.%, averaging 1.4 wt.% for glass inclusions in pyroxene from andesites, and H_2O averaging 2.5 wt.% for inclusions in olivine from basalts. Inclusions in a basaltic to rhyolitic suite from Asama, Japan showed water contents between 0 and 4 wt.%. No systematic difference in H_2O contents was seen with compositional variation. At Arenal volcano, in Costa Rica, inclusions in andesitic material contained between 0 and 7 wt.% H_2O. Basaltic and andesitic inclusions from Mount Shasta ranged from 0 to 12 wt.% H_2O. Glass inclusions in phenocrysts from Paracutin volcano showed between 1.2 and 1.7 wt.% H_2O.

Based on these data, plus extrapolations based on a supposed $K_2O:H_2O$ correlation, Anderson (1979) suggested that subduction related basaltic magmas contain between 2 and 4 wt.% H_2O, and associated andesites between 2 and 6 wt.% H_2O, based on the K_2O contents of the melts. He concluded that the high levels of H_2O estimated for these magmas are directly related to the subduction process and that water is introduced into the magmas by the subducted oceanic crust.

Sommer (1977) estimated the total volatile concentrations of glass inclusions using the "analysis by difference" technique, and then determined the relative abundances of volatiles in the inclusions by mass spectrometry. He analysed rhyolitic glass inclusions in quartz phenocrysts from Bandelier pyroclastic-fall and ash-flow tuffs. In general, glass inclusions from explosive, high silica eruptions tend to give better results than those from more mafic or intrusive material, probably because they have slower chemical diffusion rates than mafic magmas, and cool faster than intrusive magmas. Sommer (1977) found that inclusions in quartz were clear, glassy, and had rhyolitic compositions. "Analysis by difference" gave total volatile content between 2.4 and 7 wt.%, averaging 5.4 wt.%, and mass spectrometry showed 91.9% H_2O, 2.7% CO_2, and 4.8% CO. This yielded an average bulk composition of 4.9 wt.% H_2O, 0.15 wt.% CO_2 and 0.24 wt.% CO in the melt. An unusual point here is that CO_2 is generally thought to be more abundant in magmatic volatiles than CO (Fisher and Schmincke, 1984). This problem was not addressed in the paper.

Beddoe-Stephens at al. (1983) studied rhyolitic glass inclusions in quartz, plagioclase, and potassium feldspar from the Toba tuff. They determined that 4 $\pm$ 1 wt.% H_2O was present in the magma, based on the "analysis by difference" technique, but they attached little significance to this result because of the analytical technique.

Melson (1983) analysed melt inclusions in phenocrysts from dacitic plinian phase-dome building phase pairs from Mount St. Helens. He studied all eruptions which occurred between May 18, 1980 and March 19, 1982. The H_2O content of melt inclusions varies from 0.8 to 7.5 wt.%, as determined by the "analysis by difference" technique, and shows trends of decreasing H_2O contents with time throughout the entire eruptive sequence, and within individual plinian-dome pairs. Melson interpreted these trends as representing H_2O gradients within the melt from which units were erupted. In comparison, Mertzbacher and Eggler (1984) estimated based of experimental data that the May 18, 1980 magma contained 4 wt.% H_2O decreasing to 1 wt.% H_2O over a period of several years, based on experimental data.

Although there are definite trends in the water contents seen by Melson (1983), the data are questionable, due to the large range in water contents seen within glass inclusions of individual samples, for example, 3 to 11 wt.% H_2O in his sample 3. Melson interpreted this as variability in H_2O content of the parental magma. Sample 3 is from the May 18, 1980 plinian phase, which is a small volume event, and it is difficult to envisage such strong H_2O variability in a small body of magma. Also, the inferred re-equilibration times of the water gradient in the magma chamber are extremely rapid. For example, the plinian-dome phase of June 12 decreased from 5 wt.% to about 2 wt.% H_2O, and then the July 22 plinian phase contained 4.5 wt.% H_2O. This would imply almost total re-equilibration within a time of 40 days. This could not be accomplished by simple diffusion of H_2O as the dominant process. Possibly convection or some other process might allow extremely rapid re-equilibration to take place. Melson's study should be repeated using a better analytical technique, because if these results are valid, they have major implications for magma chamber processes.

The volatile elements Cl and S are less abundant than H_2O and CO_2, but are important nevertheless, especially in the study of magmatic volatiles in relation to ore deposits. Both of these elements can be successfully analysed by electron microprobe (e.g. Anderson, 1974; Devine et al., 1984; Palais and Sigurdsson, 1988; Dunbar and Kyle, 1986). The essential points in the use of electron microprobe for volatile analyses are that the beam must be widened to at least 20 microns to reduce volatilization, and count times must be long (e.g. 150 seconds on the peak, and 75 seconds on the background) due to low abundances of these elements. Detection limits for both S and Cl are about 50 ppm (Devine et al., 1984).

Electron microprobe analysis of S and Cl have been applied by many workers, and some results are summarized in Table G-1. An important studies using only this technique for volatile analyses has been published by Devine et al. (1984) and Palais and Sigurdsson (1988). These authors have taken a slightly different approach to magmatic volatiles, being concerned with the atmospheric input of volatiles S and Cl during volcanic eruptions. The method they used was to analyse the content of S and Cl in both glass inclusions and in degassed matrix glass from volcanic eruptions. Then, based on the difference between the two, and the mass of erupted material, they calculated the minimum atmospheric input. They have analysed a number of major magma types, and found that S contents vary from to 40 to 1900 ppm, and Cl from 150 to 4000 ppm. In addition to absolute abundances, they determined a number of trends. First, the S content of a magma shows a good correlation to the Fe content. Correspondingly, the amount of sulfur lost on eruption varies inversely with increasing SiO_2 content of the melt. Cl, however, shows no particular correlations. They concluded that basaltic eruptions of equal magnitude to rhyolitic eruptions release an order of magnitude more S, and would therefore have a greater climatic impact.

B. Ion Microprobe

A second type of microbeam technique which has shown great promise is the ion microprobe. This technique involves bombarding the sample with an ion beam, sputtering positive or negative ions off the sample surface, and analysing these secondary ions (Morrison and Slodzian, 1975). Volatile elements H (presumed to occur only in H_2O) and F can be analysed by this technique with accuracies of $\pm$0.5 wt.% and $\pm$50 ppm or better, respectively. The main drawbacks to this technique are that it is expensive, ion microprobes are scarce, and the calibration for H is difficult.

Hervig et al. (1986) have used the ion microprobe in order to analyse the H_2O and F contents of melt inclusions from explosive rhyolitic plinian eruptions from the Taupo Volcanic Zone, New Zealand. In this, plus later work, they determined a mean of 4.5 wt.% H_2O and 420 ppm F and 4.5 wt.% H_2O and 440 ppm F for two explosive eruptions from the Taupo center closely spaced in time, and 6.0 wt.% H_2O and 440 ppm F for an older eruption. The mean H_2O and F contents for different phenocryst types are very similar.

Based on this data, the two younger eruptions appear to be derived from the same magma batch, whereas the older eruption could be from a slightly different melt. This conclusion is supported by trace element data (Dunbar, unp).

C. Capacitance manometry

Two techniques, used by Sommer and Schramm (1983), and Harris (1981a) both involve analysing the volatile contents of melt inclusions in a single crystal by capacitance manometry and estimating the volume of glass by an independent technique. Harris (1981a) analysed for H_2O, CO_2, and SO_2 by heating the sample to 1200^{o}C to drive the volatiles out of the glass, condensing them in a cold trap, and then measuring the pressure as individual volatile components vaporize during reheating. The volume of glass in a wafer of crystal containing melt inclusions was estimated optically (Harris, 1981a). This technique has the ability to analyse small volumes of sample (containing as little as 1.7×10^{-6} grams of H_2O), and to analyse several volatile components simultaneously on the same sample. There are, however, several problems. First, visual estimates of glass volume may introduce a significant error, and second, peaks of H_2S and CO_2 are indistinguishable, which requires the assumption that no H_2S is present (Harris, 1981a).

In studies of basalts from Hawaii, Harris analysed H_2O, CO_2, and S were determined in large (100-250 micron) glass inclusions in olivine phenocrysts (Harris, 1981b; Harris and Anderson, 1983, 1984). Analyses of melt inclusions showed 2-8 wt.% post-entrapment crystallization, and volatile values were corrected accordingly. Three samples were analysed and gave H_2O content of .46, .19, and .27 wt.%, CO_2 of .31, .024, and .08 wt.%, and S of .06 to .14 wt.% (Harris and Anderson, 1983).

The same analytical techniques were used to determine H_2O and CO_2 in the subduction-related basalt from Fuego volcano (Harris and Anderson, 1984). The inclusions show a range in major element chemistry from 51 to 54 wt.% SiO_2. This effect could be due to some of the phenocrysts growing in a more differentiated thermal boundary layer of the magma chamber. The inclusions contain 1.6 to 3.5 wt.% H_2O, .17 to .5 wt.% CO_2, and 1100 to 2800 ppm S. The H_2O content increases with increased differentiation, and the S content decreases, as would be expected.

The method of Sommer and Schramm (1983) is similar to that of Harris (1981a). The sample is heated to 1300^{o}C for 2 hours, resultant gas is transferred to a liquid nitrogen cold trap. As the sample is warmed to room temperature, pressures of each species are then determined by capacitance manometer and related to the number of moles present in the sample by the ideal gas law. In order to estimate the volume of glass, the authors determine an element which is present only in the melt inclusions, not in the host crystal, by electron microprobe. Then a whole phenocryst is chemically analysed, and the crystal:glass ratio can be estimated based on the dilution of the chosen element.

Sommer and Schramm (1983) applied this technique to a sequence of samples through the lower and upper Bandelier tuff plinian and pyroclastic flow deposits. The lower Bandelier airfall averages 3.99 wt.% H_2O, the lower ashflow 1.71, the upper airfall 2.11 and the upper ashflow 0.79. The authors found this data consistent with other geochemical observations in the Bandelier tuff, indicative of a zoned magma chamber. This interpretation, if correct, implies that these quartz crystals grew in a magma chamber which was already zoned with respect to water, and that no significant mixing of the zoned layers occurred during the eruptive process.

PROBLEMS WITH MELT INCLUSION ANALYSES

A number of factors may cause melt inclusion compositions to deviate from true magmatic compositions. First, if a crystal which trapped a droplet of pristine magma remains at high temperature, additional host crystal present in the sample by the ideal gas law. In order to estimate the volume of glass, the authors determine an element which is present only in the melt inclusions, not in the host crystal, by electron microprobe. Then a whole phenocryst is chemically analysed, and the crystal:glass ratio can be estimated based on the dilution of the chosen element.

Sommer and Schramm (1983) applied this technique to a sequence of samples through the lower and upper Bandelier tuff plinian and pyroclastic flow deposits. The lower Bandelier airfall averages 3.99 wt.% H_2O, the lower ashflow 1.71, the upper airfall 2.11 and the upper ashflow 0.79. The authors found this data consistent with other geochemical observations in the Bandelier tuff, indicative of a zoned magma chamber. This interpretation, if correct, implies that these quartz crystals grew in a magma chamber which was already zoned with respect to water, and that no significant mixing of the zoned layers occurred during the eruptive process.

PROBLEMS WITH MELT INCLUSION ANALYSES

A number of factors may cause melt inclusion compositions to deviate from true magmatic compositions. First, if a crystal which trapped a droplet of pristine magma remains at high temperature, additional host crystal may be deposited on the crystal walls (Fig. G-2). This will leave the remaining glass concentrated or depleted in elements which are respectively incompatible or compatible in the crystal. This "post-entrapment crystallization" has been recognized by a number of workers (Watson, 1976; Anderson and Wright, 1972). Watson (1976) used analyses of modified inclusions from several different phenocryst phases to project back to primary magma chemistry (Fig. G-3), and confirmed that post-entrapment crystallization had taken place. This phenomenon is a serious problem, especially if the inclusions are to be used for volatile analysis, because the volatile elements are concentrated in the remaining glass. Less than about 10% crystallization is tolerable, because most analytical techniques used today have at least this much error in an individual analysis.

The extent of post-entrapment crystallization in a melt inclusion can be assessed by detailed electron microprobe analyses of the inclusion. First, if the major element chemistry of the inclusion agrees closely with the major element chemistry of the whole rock, not much post-entrapment crystallization has taken place (Beddoe-Stephens et al., 1983). Figure 5-2 in text shows a close similarity between major element chemistry in inclusion glass, bulk rock, and quenched magma (obsidian) from the Taupo Volcanic Zone (Dunbar and Kyle, 1987). If the compositions are different, the amount of post-entrapment crystallization

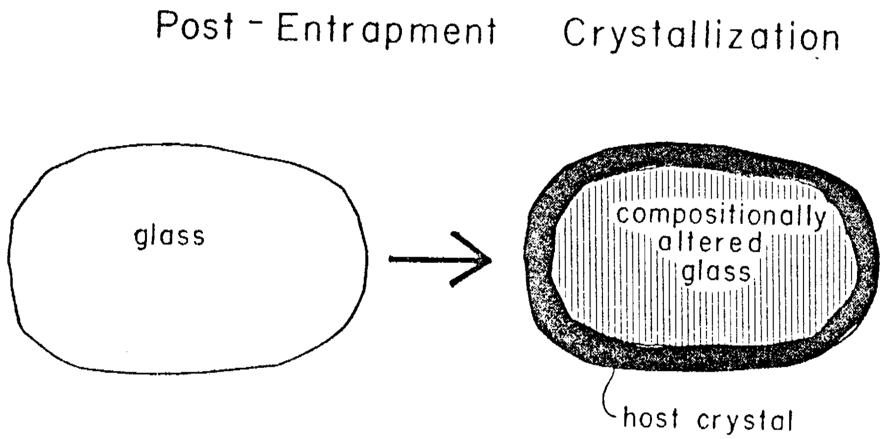

Figure G-2. Diagramatic effects of post-entrapment crystallization.

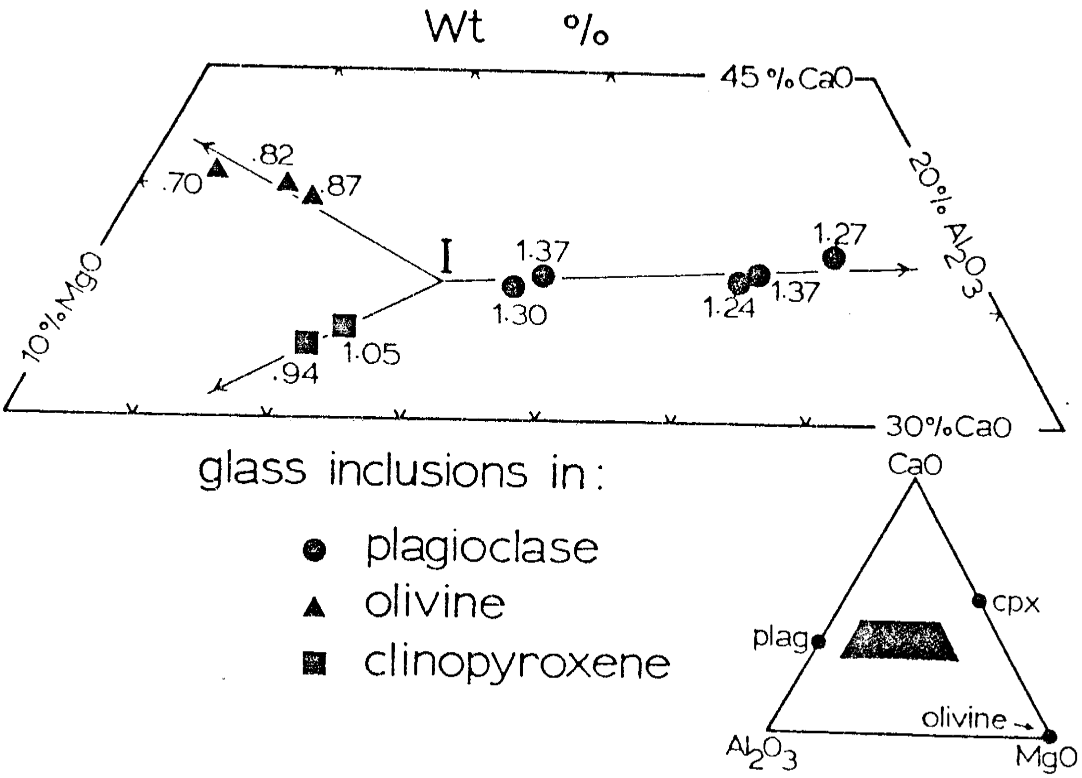

Figure G-3. CaO-MgO-Al_2O_3 plot of melt inclusions analyses in different phenocryst types. Numbers plotted next to points denote MgO/FeO weight ratios. Point 1 represents the intersection of olivine, clinopyroxene and plagioclase fractionation lines, and represents the composition of the magmatic liquid at the moment of melt inclusion formation. (From Watson, 1976).

which has taken place can be assessed using partition coefficients of various elements between the glass and the host phenocryst. Another test is to analyse individual spots in an inclusion, scanning from the core to the rim of the glass. If any crystallization has occurred in the inclusion, the glass shows progressive chemical zonation. Results of this type of test are shown in Table C-6, for Taupo Volcanic Zone inclusions, in which no zonation is seen.

The second major problem with melt inclusions, is that they may not trap pristine magma. This would occur if the crystal grew faster than elements could diffuse away from the crystal-magma interface thus forming an envelope of anomalous melt around the growing crystal. The same assessment method used for post-entrapment crystallization could be used here. In other words, if the bulk magma chemistry and inclusion chemistry match, the inclusion is probably pristine.

CONCLUSIONS

Glass inclusions, when carefully evaluated and analysed, have potential to give the best available direct estimates of pre-eruptive volatile contents of a magma, when not affected by problems such as volatile gradients and post-entrapment crystallization. At present, the main problem to be overcome is that of analytical technique, and progress is being made in this area. Microbeam techniques, some of which are available now and others which will be available in the near future, are the most promising analytical methods, due to their ability to analyse single inclusions, or even domains within one inclusion. The currently available techniques include electron microprobe, for elements Cl, F, and S, and ion microprobe for H_2O, and F. The ion microprobe may also be able to determine oxygen isotopic ratios, which could be applied to melt inclusions. Other microbeam techniques which may soon be applicable to melt inclusions include proton induced x-ray emission (PIXE); proton induced gamma-ray emission (PIGE); nuclear reaction analysis; Raman spectoscopy; and infrared spectroscopy. A final technique is a system which couples a laser beam with a mass spectrometer (Yonover et al., 1986). Other techniques, such as the capacitance manometry methods mentioned in this paper, are useful, but will never offer the ability to choose a very small and precise area of analysis on the sample available with microbeam techniques.

Table G-1. Volatile determinations in pre-eruptive magmas using melt inclusions.

Worker	Magma composition	Technique	Volatile component	abundance (wt.%)
Anderson	and-bas	ABD	H_2O	1.4 to 2.5
		EM	Cl	0.1 to 0.5
	rhy-bas	ABD	H_2O	0 to 4
		EM	Cl	0.1 to 0.3
	and	ABD	H_2O	0 to 7
		EM	Cl	0.22 to 0.78
	and-bas	ABD	H_2O	0 to 12
		EM	Cl	0.08 to 0.66
Sommer and Schramm	rhy	ABD+MS	H_2O	4.9
			CO_2	0.15
			CO	0.24
	rhy	CM	H_2O	0.79 to 3.99
Beddoe-Stephens	rhy	ABD	H_2O	4.0
Melson	dac	ABD+IM	H_2O	0.8 to 7.5
Harris	bas	CM	H_2O	0.19 to 0.46
		CM	CO_2	0.03 to 0.31
		EM	S	0.06 to 0.14
	bas	CM	H_2O	1.6 to 3.5
		CM	CO_2	0.17 to 0.5
		EM	S	0.11 to 0.28
		EM	Cl	0.08 to 0.13
Sigurdsson Devine Palais	rhy-bas	EM	S	0.005 to 0.14
		EM	Cl	0.015 to 0.4
Dunbar and Hervig	rhy	IM	H_2O	4.3 and 5.9
		IM	F	0.04
		EM	Cl	0.17 to 0.25
		EM	S	$<$ 0.005

rhy = rhyolite
and = andesite
dac = dacite
bas = basalt

ABD = analysis by difference (EM)
EM = electron microprobe
MS = mass spectrometry
CM = capacitance manometry
IM = ion microprobe

APPENDIX H.

REVIEW OF VOLATILES

Volatile components are always present in terrestrial magmas and play an important role in the formation of igneous rocks. Volatiles, especially H_2O and CO_2, influence the viscosity and crystallization patterns of magmas and are a major driving force behind explosive volcanic eruptions (Fisher and Schmincke, 1984). The full importance of volatile elements is not clearly understood because it is difficult to assess the chemical state and abundances of these constituents in natural magmatic systems. In order to address this problem, a number of different theoretical and analytical approaches have been taken to assess the solubility mechanisms, concentrations, and relative proportions of volatiles in magmas.

The dominant volatile elements in igneous melts are hydrogen, carbon, fluorine, chlorine, and sulfur. Water is usually the most abundant molecular volatile species (35-90 mole %), with carbon dioxide composing 5-50 mole % (Fisher and Schmincke, 1984). Sulfur species are important in mafic magmas, with sulfur dioxide dominant at high temperature and oxygen fugacity, and hydrogen sulfide otherwise. As the silica content increases and the iron content decreases in a melt, the S content decreases (Devine et al., 1984). Low concentrations of chlorine and fluorine are usually present in magmas, but these volatiles have a disproportionately high effect on reducing melt viscosity, and environmental impact during explosive eruptions (Devine et al., 1984).

Volatile solubilities in magmas

Magmatic volatiles are defined as "chemical species in gaseous or supercritical fluid state at temperatures over 300-400^{o}C" (Holloway, 1981), but this is not necessarily how they occur in magmas. Volatile components may be present in a fluid state, but also occur dissolved in melts (Fisher and Schmincke, 1984). Solution of volatiles can involve whole molecules or dissociated molecules that form complexes which bond with the framework of a silicic magma.

Knowledge of the solubility mechanisms of volatile species in silicate melts is important in understanding the role of volatiles in the petrogenesis of igneous rocks, because volatiles control the equilibrium phase relations (Burnham, 1979a). Solubility mechanisms cannot be easily examined in natural systems, but can be modelled experimentally. The most common approach has been to study a simple system, such as the solution of a volatile in a mono-mineralic melt, and from that extrapolate to more complex systems. This approach has been taken for the volatiles H_2O, CO_2, F, and Cl.

Water

The solubility mechanism of water has been studied by a number of workers, but is still debated (Fisher and Schmincke, 1984). The amount of water that is soluble in a melt is dependent on the composition and pressure of the melt, but is virtually independent of melt temperature (Holloway, 1981). Effects of H_2O dissolution on melt properties include lowering of viscosity and density and increasing electrical conductivity of the melt (Burnham, 1975).

Wasserburg (1957) suggested that water dissolves into a silicate melt by breaking bridging Si-O-Si bonds between tetrahedra and bonding with the open O and Si:

$$\text{Si-O-Si} + H_2O = \text{Si-OH} + \text{HO-Si}$$

this model explains the melting point depression of albite in a water-albite melt, because the melt becomes depolymerized, resulting in lower albite stability. If this is correct, then the molar solubility of H_2O should be proportional to the pressure of water in the system.

However, experimental systems have shown that the behavior is non-linear (Fig. H-1, Mysen, 1977). Wasserburg's model is not adequate to describe the behavior of the albite-water system at high water concentrations.

Burnham (1975), proposed a more refined model, which is also based on the water-albite system. The Burnham model is derived from experimentally determined effects of H_2O on the viscosity, electrical conductivity and thermodynamic properties of the system. It involves the same reaction of H_2O with the bridging Si-O bonds between silica/alumina tetrahedra, but also calls for exchange of an H^+ proton with the Na^+ that was providing the charge balance on the AlO_4 tetrahedra (Fig. H-2) (Burnham, 1979a). The reaction of H_2O with Na^+ (the right-hand side of Fig. H-2) will go to completion, or will continue up to the point that there is excess H_2O or albite. If the H_2O is greater than 50 mole % of the melt, the reaction on the right side of Fig. H-2 will begin. The equations for the two reactions are as follows:

1) $NaAlSi_3O_8 + H_2O = NaAlSi_3O_8(OH)^- + H^+$

2) $NaAlSi_3O_8(OH)^- + H^+ + nH_2O = NaAlSi_3O_{8-n}(OH)_{n+1} + H^+$

The second reaction will occur because all of the Na in the melt occupy charge-balancing positions, so a new mechanism for charge balance must be found. When the first

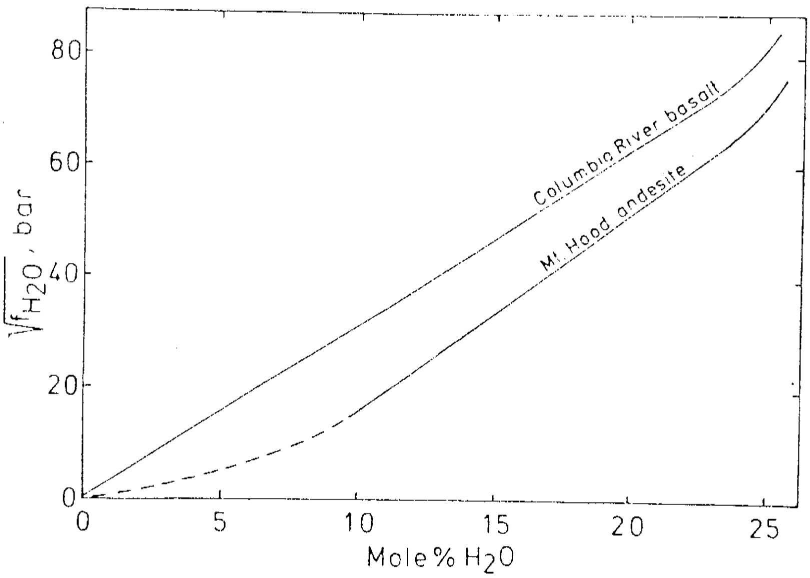

Figure H-1. Molar solubility of H_2O versus water fugacity for an andesitic and tholeiitic melt. (From Mysen, 1977.)

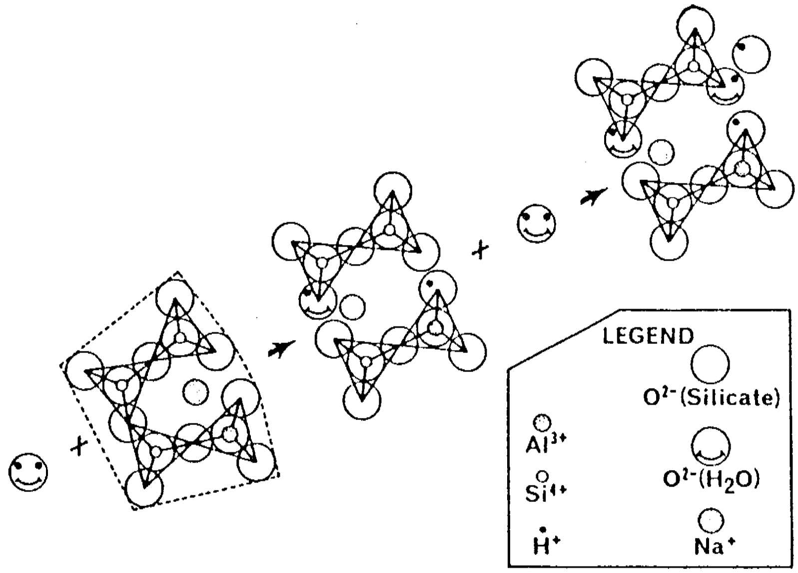

Figure H-2. Diagramatic reaction scheme for H_2O in an albite melt as proposed by Burnham (1979a). (From Burnham, 1979a).

reaction occurs, one mole of OH^- ion associated with the silica tetrahedra is produced. The relationship between the activity of H_2O and the square of its mole fraction in the melt is linear, but once the second reaction begins, this relationship becomes exponential because 2 moles of OH are being produced for every mole of H_2O (Burnham, 1979a). The reaction of H_2O with the silicate melt has the effect of depolymerizing the liquid by breaking the tetrahedral bridge bonds and therefore decreasing the stability of polymerized minerals (especially feldspars). This depolymerization also decreases the density of the melt; for example, a mole fraction of 0.5 H_2O, can lower the viscosity of an anhydrous melt by a factor of 10^5 - 10^6 (Burnham, 1975). The exchange of H^+ for Na^+ results in greater mobility of Na^+, which increases the electrical conductivity of the melt. To determine if this model was applicable to more varied igneous systems, Burnham compared experimental solubility data for different composition rocks. Although the actual weight percent of dissolved H_2O at a given pressure was different for each sample, the molecular percentage of H_2O was the same. This suggests that the dissolution mechanism of H_2O in the different composition melts was the same (Fig. H-3). Burnham concluded that, as long as each mole of melt contains 1 mole of exchangeable cations, solution of water will behave the same regardless of melt composition.

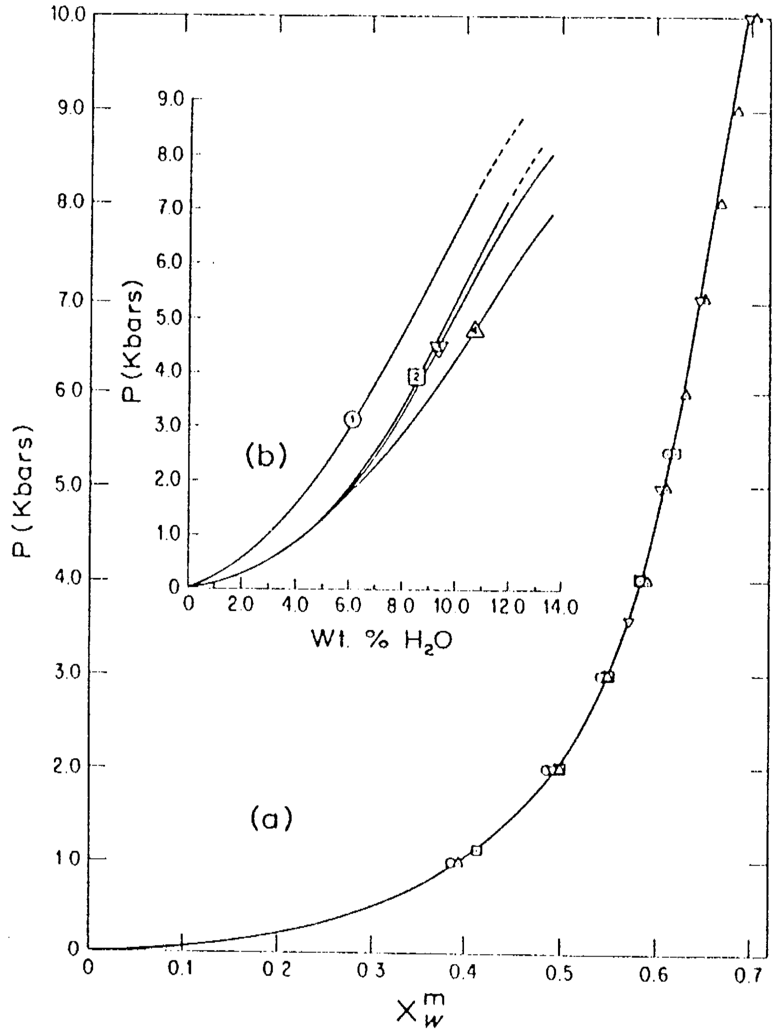

Figure H-3. Solubility of H_2O in different composition aluminosilicate melts. Circles (1), Columbia River basalt. Squares (2) Mt. Hood andesite. Inverted triangles (3) albite. Upright triangles (4) Harding pegmatite. Portion (a) of the diagram shows eqimolal solubilities at 1373°K calculated from experimental weight-percent solubilities in portion (b) (calculated from equations in Burnham, 1979a) (From Burnham, 1979a).

Infrared spectroscopy (IR) data on water quenched in natural glasses lead Stolper (1982a and b) to propose another refinement to the water solubility model. He found that molecular water, as well as OH^- ions, are present in quenched glass. Assuming that the speciation of water in glass is representative of that in the melt, he proposed that the reaction $H_2O + O_2 = 2OH^-$ is controlled by an equilibrium constant rather than proceeding to completion. The relationship observed between H_2O and OH^- groups is summarized in Fig. H-4. At water contents below 0.5 wt% in an albite, all water is present as hydroxyl groups, but as water contents become higher, molecular water becomes more prevalent, consistent with the equilibrium constant model. Also, the IR data demonstrate that water is structurally bound in the glass and does not occur as fluid inclusions, because no ice bands are present at liquid nitrogen temperatures. If the water speciation changed during quenching of the melt to a glass, this theory would be invalid, but the water content and species distribution were found to be independent of quenching history (Stolper, 1982a). Stolper's model explains the same phenomena as Burnham's (electrical conductivity, viscosity, depression of feldspar liquidus) but also explains why water solubilities in melts seem to be independent of melt composition at high water contents, and vary at lower water contents. The bonding of OH^-

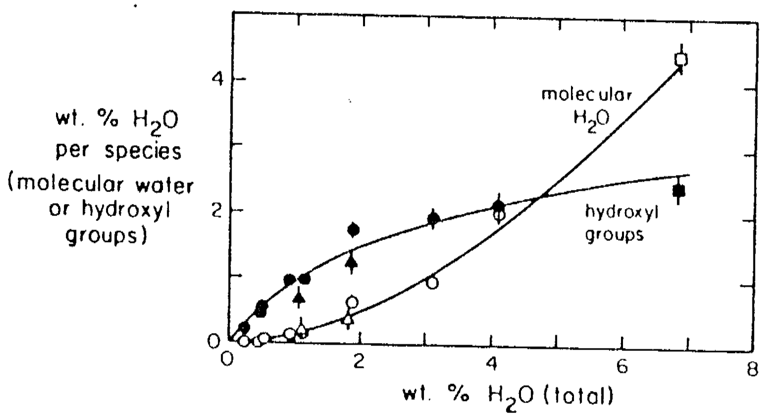

Figure H-4. Speciation of H_2O in silicate glass as determined by infrared spectroscopy. Molecular water is shown as open symbols, and water present as hydroxyl groups is shown by closed symbols. The curves show the trends of these species concentrations as total water content increases. Symbols: circles-rhyoltic glass; triangles-basaltic glass; squares-albite glass. (From Stolper, 1982b).

groups would be compositionally dependent because of the limited number of tetrahedral bridges available as bonding sites, but structurally bound H_2O groups could enter a melt in the same proportions, regardless of composition (Stolper, 1982b). Burnham's model for OH^- configuration is probably correct, but the undissociated H_2O that Stolper describes is probably present at higher H_2O concentrations.

Mysen et al (1980) and Mysen and Virgo (1986) have investigated the solubility mechanisms of H_2O with use of Raman spectroscopy. This technique allows identification of chemical bonds based on spectrum changes of monochromatic light that passes through the sample. They found that, in general, H_2O dissolves in melts either as molecular H_2O groups or as dissociated OH^- groups which bond with positive cations, in particular Si^{4+}, Al^{3+}, Ca^{2+}, and Na^+. Mysen and Virgo (1986) investigated the relationship between OH^- groups and Si^{4+}, Al^{3+}, Ca^{2+}, Na^+ and H^+ in melts. They found that in SiO_2 and SiO_2-Al melts, H_2O exists both as free molecules and as dissociated OH^- complexed with Si^{4+} and Al^{3+}. In SiO_2-Ca and SiO_2-Na melts, H_2O also partially dissociates but OH^- only complexes with the Ca^{2+} and Na^+ ions, not the Si^{4+}. Non-bridging oxygens, formed by modification of the SiO_2 tetrahedral network, are created in all cases except pure SiO_2 melts. Non-bridging oxygens result in decreased melt viscosity. They determined the relative stability of hydroxyl complexes to be Si***OH > Na***OH > Al***OH > Ca***OH. Mysen and Virgo (1986) concluded that the equilibrium constant for OH^-/H_2O solubility in melts is compositionally dependent, contrary to Stolper's (1982b) conclusion.

In summary, there is no single agreed-upon moded for solubility of H_2O in silicic melts, although general solubility mechanisms proposed by a number of authors are similar. However, Burnham's solubility model, while probably oversimplified, seems to allow accurate calculation of melt H_2O contents at a variety of pressures.

Carbon dioxide

CO_2, the second most abundant volatile in magmas, is much less soluble than H_2O, and dissolves by quite different processes. CO_2 is not able to break bridging Si-O-Si bond and depolymerize the melt, but instead reacts with oxygen to form the carbonate ion CO_3^{2-}, which is completely miscible in silicate melts (Eggler, 1978).

$$2SiO_4 + CO_2 = Si_2O_7 + CO_3^{2-}$$

Infrared spectroscopy of silicate glasses show that CO_3^{2-} is the dominant form of carbon, but that some CO_2

ions are also present (Mysen and Virgo, 1980). The amount of undissociated CO_2 dissolved in low pressure melts (<10 kb) is probably negligible, because there are no spaces in the three dimensional network that are large enough to house such a large species. But, above 10kb, Al changes coordination, allowing CO_2 to fit into the framework (Burnham, 1979b). Another reaction that can take place is bonding of CO_2 with a metal ion (M) to form a neutral metal carbonate (Holloway, 1981).

$$MO + CO_2 = MCO_3$$

Because the solubility of CO_2 is dependent on the availability of oxygen with which to bond, it is also dependent on the degree of polymerization of the melt, and so is more soluble in mafic than silicic melts (Fig. H-5) (Holloway, 1981).

<u>Fluorine and Chlorine</u>

The solubility mechanisms of subordinate volatile elements F and Cl are not as well studied as H_2O and CO_2. Burnham (1979a) proposed that when HF and HCl are introduced into a melt, the solubility mechanisms are as

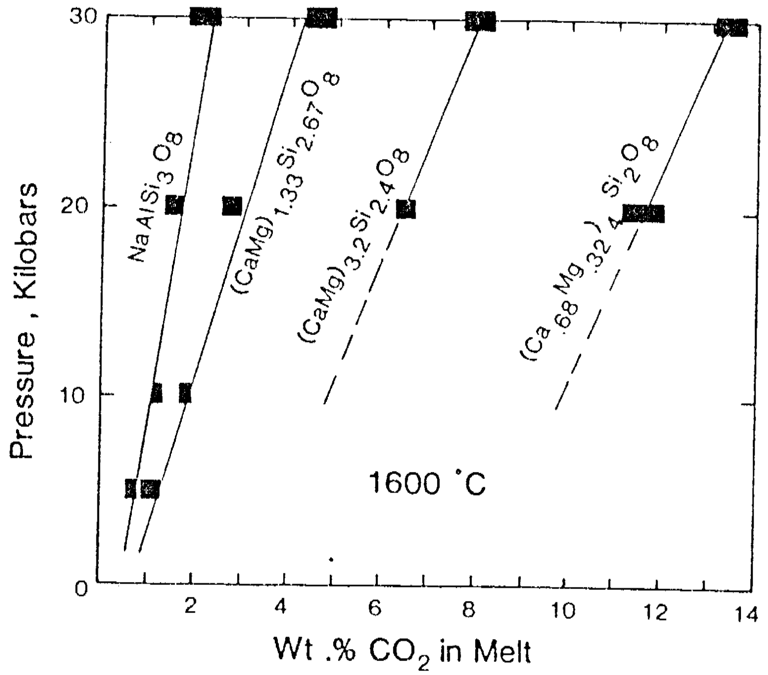

Figure H-5. CO_2 solubility as a function of pressure for several compositions at 1600°C (from Holloway, 1981).

follows:

$$HF\ (fluid) + O^{2-}\ (melt) \rightarrow F^{-}\ (melt) + OH^{-}\ (melt)$$

and

$$HCl\ (fluid) + O^{2-}\ (melt) \rightarrow Cl^{-}\ (melt) + OH^{-}\ (melt)$$

This mechanism is analagous to the dissolution of H_2O in a silicate melt, and produces the same type of melt depolymerization.

Many authors agree that HF is soluble in melts by the mechanism shown above, but more specific mechanisms for certain types of melts have been suggested. Manning (1981) found that in a quartz-albite-orthclase melt in presence of excess H_2O, F forms AlF^{3-}_6 complexes, as well as forming free F^- ions. He noted that in a dry melt, silicofluoride complexes would be more stable than aluminofluoride complexes.

Foley et al. (1986) studied high pressure (28 kb) melts of the system $KAlSiO_4$-Mg_2SiO_4-SiO_2 by IR spectroscopy. They found that in a dry melt, F^- complexes with K, Mg, and Al. At high concentrations of F^- (~1%) tetrahedral $KAlO_2$ groups are complexed by F^-. This causes polymerization of the residual melt by increasing the (Si)/(Si + Al) ratio. However, they noted that F^- is generally introduced to a melt as an HF molecule, and dissolution of this molecule causes melt depolymerization.

In this case, F^- behaves in a similar fashion to OH^-, bonding with the network-modifying cations, without formation of Si-F bonds.

Mysen and Virgo (1986) investigated the behavior of F in an anhydrous $NaAlO_2$-SiO_2 melt with Raman spectroscopy. They found that F complexes with Na and Al, but did not see evidence of Si-F bonds. They also found that F is a more efficient melt depolymerizer than H_2O, and suggested that this difference is due to the stabilities of fluoride and hydroxyl complexing with Na and Al.

Little detailed research has been done to determine the exact solubility mechanisms of Cl^- ions in silicic melts. Cl is assumed to dissolve by a similar mechanism as F, but is probably much less soluble due to the large size of Cl^- compared to F^- and OH^-. Expermental studies on the solubility of Cl in rhyolitic melts has been done by Webster and Holloway (1988). They found that Cl solubility is dependent on the major element composition of the melt, but is independent of F content. Experimental work on the solubility of Cl in rhyolitic melts has been done by Webster and Holloway (1988). They found that Cl solubility is dependent on the major element composition, but is independent of the F content of the melt.

Determination of magmatic volatiles

A number of approaches can be used to arrive at pre-eruptive magmatic volatile contents. These include measuring gases emitted from lava lakes or fumeroles, estimations of volatile fugacities from mineral stabilities or actual measurements of volatiles in melt inclusions or quenched magma. A number of specific techniques, and determinations of pre-eruptive volatile contents will be listed below. This discussion focusses primarily on volatile determinations in rhyolitic melts.

Sampling of volcanic gases directly from fumeroles or lava lakes is difficult and the gases will not be representative of magmatic volatiles because volatiles have different solubilities, so some may be preferentially retained. Contamination by reaction with meteoric water and/or the atmosphere is a problem. Methods used to overcome these problems involve restoration of true gas contents by complex computer calculations (Gerlach, 1981).

However, in well-understood magmatic systems, which undergo continuous degassing, detailed gas sampling in conjunction with other geologic data can yield high quality estimates of magmatic gas contents. Gerlach and Graeber (1985) and Greenland et al. (1985) made very similar estimates of magmatic gas content and gas emissions of Kilauea volcano using different techniques of evaluating fumerolic and eruptive gasses. The technique of sampling volcanic gas emissions from active volcanoes has not been applied to rhyolitic systems.

Volatile fugacities in magmas may be determined by the composition and content of phenocrysts in a melt. Merzbacher and Eggler (1984) have experimentally documented a magmatic geohydrometer based on compositional equilibrium between glass and phenocrysts, generally plagioclase and pyroxene. Presence of varying amounts of water will change the equilibrium of these components. From this information, they suggest magmatic water of 4 wt% for the May 18, 1980 eruption of Mount St. Helens dacites.

Naney (1983) made an extensive experimental study of mineral stabilities in a granitic melt at 2 and 8 kilobars (kb), and at a variety of temperatures. The experimental melt that most closely approximates the conditions and mineralogy of the young Taupo rhyolites contains a minimum of 3 to 4 wt% H_2O.

Another common method of estimating the volatile content of a magma, based on the phenocryst assemblage is by thermodynamic calculations. It is not possible to determine the fugacity of all volatiles in the magma from a given phenocryst assemblage, but only ones that are buffered by the phases present. For example, sulfur fugacity can be calculated with an assemblage of pyrrhotite, titanomagnetite and olivine (Rutherford and

Heming, 1978), hydrogen fugacity with biotite, sanidine and magnetite (Wolff and Storey, 1983), and carbon dioxide with olivine, diopside and magnesian ilmenite (Carmicheal et al., 1974).

The fugacity of water can be determined with an assemblage of cummingtonite, orthopyroxene, and quartz (Ewart et al., 1975). Ewart et al. (1975) have calculated pre-eruptive water fugacities from Taupo Volcanic Zone tephra samples containing the above phenocryst assemblage. They also showed that $P_{H2O} \sim P_{total}$, and calculate pre-eruptive water content between 5.2 and 7.9 wt%. Rutherford and Heming (1978) determined magmatic water contents within about the same range for older TVZ ignimbrites, using a buffer assemblage of biotite, sanidine, and magnetite. Using similar calculations, Hildreth (1979) estimated volatile contents of 2.8 to 4.9 wt% H_2O for the rhyolitic Bishop Tuff, increasing upwards in the magma chamber..

The third method, direct analysis of volatiles in volcanic material can be done by a number of different techniques. The material analysed must be quenched volcanic glass, whether extruded magma or melt inclusions in phenocrysts. Eichelberger and Westrich (1981), analysed water in rhyolitic obsidians from small, young tephra deposits in Long Valley, Ca. by thermogravinometric analysis. Their values ranged from between 0.5 and 3.0

weight percent, decreasing through the eruptive sequence until the final non-explosive flows that contain 0.2 wt% H_2O. These analyses, coupled with delta deuterium (delta D) values (Taylor et al., 1983), which become more negative with increased degassing, show that the original H_2O content of the magmas was close to 3.0 wt% (see Fig. 6-13). This suggests that obsidians can trap all or part of volcanic H_2O.

Volatile contents and their ratios have been determined on volcanic glasses by mass spectrometer (Muenow, 1973; Delaney et al., 1978; Garcia et al., 1979); and by infrared methods (Neuman et al., 1986). Electron microprobe analyses of glass inclusions, using the difference method, have been widely used (Anderson, 1973; Sommer, 1977). Water contents are inferred to be the difference between the analytical totals and 100%. This is not an accurate method because, first, the analytical error of microprobe analysis can be 2 wt.%, and also it is impossible to assure that H_2O is accounting for the difference from 100% total, but it can be used for general approximations. Water cannot be directly determined by microprobe analysis, but the technique is applied to higher atomic number volatile elements, such as S, Cl and F. An analytical method that involves long count times is described by Devine et al. (1984).

Sommer and Schramm (1983), have devised a method for glass inclusion volatile determinations that requires two major steps: 1) determination of glass concentrations in phenocrysts, and 2) determination of volatile concentrations in the melt inclusions. The amount of glass is determined by calculating the dilution factor of an element that is present in the glass, but not in the host mineral, and volatiles are measured by a partial pressure capacitance manometer. This method, although it seems difficult, yields satisfactory results. Values measured for silicic melt inclusions range from 2.11 wt% to 3.99 wt% for material from plinian fall deposits and from 0.79 wt% to 1.71 wt% for associated ignimbrites. Sommer and Schramm's analytical method for melt inclusions assumes that there are no volatiles included in crystals as dissolved species or as fluid inclusions, but this assumption may not be true.

Druitt et al. (1982) determined H_2O contents of melt inclusions from the Bishop Tuff, also by the capacitance manometry technique. They found which inclusions from the early erupted material contain 4.9 wt% H_2O, and in the late material >2 wt% H_2O. This agrees with Hildreth's (1979) thermodynamic estimates.

Devine et al. (1984) and Palais and Sigurdsson (1988) analysed the Cl and S contents of melt inclusions from a number of chemically diverse eruptions by electron microprobe. For all samples analysed in these studies, the Cl ranged from 0.02 to 0.4 wt.%, and S from 0.004 to 0.19 wt.%.

Fluorine is known to be extremely soluble in granitic melts (up to 4 wt%, Bailey 1977), but very few determinations of pre-eruptive F in melts have been reported. Nash (1987) reports 2 wt% F in glass from a Cenozoic rhyolitic eruption in the western US.

Appendix I
Abstracts and publications related to this project

Dunbar, N.W., Hervig, R., and Kyle, P.R., 1988. Determinations of pre-eruptive H_2O, F and Cl contents of silicic magmas using melt inclusions, examples from Taupo Volcanic center, New Zealand. Bull. Volcan., (in press).

Dunbar N.W., Hervig, R., and Taylor, B.E., 1987. Volatile contents and degassing behavior of rhyolitic magmas from the Taupo Volcanic Zone, New Zealand (abstr). I.U.G.G., V3-5, p. 404.

Dunbar, N.W., and Kyle, P.R., 1985. Investigation of volatiles in rhyolitic magma chambers (abstr). New Mexico Geological Society Abstract volume, spring, 1985, p. 23.

Dunbar, N.W., and Kyle, P.R., 1986. H_2O and Cl contents, and temperature of Taupo Volcanic Zone rhyolitic magmas (abstr.). Abstract Volume, International Volcanological Congress, New Zealand, p. 148.

Dunbar, N.W., and Kyle, P.R., 1987. Studies of magmatic volatiles using glass inclusions in crystals from the Taupo Volcanic Zone, New Zealand, and Mount Erebus, Antarctica (abstr). American Current Research on Fluid Inclusions, Abstracts with Programs.

Dunbar, N.W., Kyle, P.R., and Taylor, B.E., 1986. H_2O and Cl contents, and isotopic composition of Taupo Volcanic Zone rhyolitic magmas. Norman D. Watkins symposium on Environmental Impact of Volcanism Abstract Volume.

Dunbar, N.W., Kyle, P.R., and Wilson, C.J.N, (in review). Evidence for limited zonation in silicic magma systems, Taupo Volcanic Zone, New Zealand. Submitted to Geology

Hervig, R., Dunbar, N.W., Westrich, H., and Kyle, P., 1986. Direct determination of initial H_2O and F contents of rhyolitic magmas by ion microprobe (abstr). Geological Society of America Abstracts with Programs, 18, 636.

Hervig, R., Dunbar, N.W., Westrich, H., and Kyle, P., (1988). Pre-eruptive water content of rhyolitic magmas as determined by ion microprobe analysis of melt inclusions in phenocrysts. J. Volcan. Geoth. Res. (in press).

Taylor, B.E., Dunbar, N.W., and Kyle, P.R., 1986. Stable isotope studies of the volatile history and degassing of rhyolitic magmas in the Taupo Volcanic Zone, New Zealand (abstr.). Abstract Volume, International Volcanological Symposium, New Zealand, p. 217.

REFERENCES CITED

Andersen, D.J., and Lindsley, D.H., 1985. New (and final) models for the Ti-magnetite/ilmenite geothermometer and oxygen barometer (abstr). EOS, 66, 416.

Anderson, A.T., 1973. The before-eruption water content of some high alumina magmas. Bull. Volcan., 37, 530-552.

Anderson, A.T., 1974. Chlorine, sulfur and water in magmas and oceans. Geol. Soc. Am. Bull., 85, 1485-1492.

Anderson, A.T., 1979. Water in some hypersthenic magmas. J. Geol., 87, 509-531.

Anderson, A.T. and Wright, T.L., 1972. Phenocrysts and glass inclusions and their bearing on oxidation and mixing of basaltic magmas, Kilauea Volcano, Hawaii. Am. Mineral., 57, 188-216.

Ando, A., Mita, N., and Terashma, S., 1987. 1986 values for fifteen GSJ rock reference samples. "Igneous rock series". Geostandards Newsletter, 11, 159-166.

Bailey, J.C., 1977. Fluorine in granitic rocks and melts: A review. Chem. Geol., 19, 1-42.

Beddoe-Stephens, B., Aspden, J.A., and Shepherd, T.J., 1983. Glass inclusions and melt compositions of the Toba Tuffs, Northern Sumatra. Contrib. Mineral. Petrol., 83, 278-287.

Belkin, H.E., De Vivo, B., Roedder, E., and Cortini, M., 1985. Fluid inclusion geobarometry from ejected Mt. Somma-Vesuvius nodules. Am. Mineral., 70, 288-303.

Bence, A.E., and Albee, A.L., 1968. Empirical correction factors for the electron microanalysis of silicates and oxides. J. Geol., 76, 382-403.

Blake, S., 1984. Volatile oversaturation during the evolution of silicic magma chambers as an eruption trigger. J. Geophys. Res., 89, B10, 8237-8244.

Blake, S., and Ivey, G.N., 1986. Density and viscosity gradients in zoned magma chambers, and their influence on withdrawal dynamics. J. Volcan. Geother. Res., 30, 201-230.

Blattner P., and Reid, F.W., 1982. The origin of lavas and ignimbrites of the Taupo Volcanic Zone, New Zealand, in light of oxygen isotope data. Geochim. Cosmichim. Acta, 46, 1417-1429.

Brimhall, G.H., and Crerar, D.A., 1987. Ore Fluids: Magmatic to supergene. In: Reviews in Mineralogy, 17, 235-321.

Buddington, A.F., and Lindsley, D.H., 1964. Iron-titanium oxide minerals and synthetic equivalents. J. Petrol., 5, 310-357.

Burnham, C.W., 1975. Water and magma; a mixing model. Geochim. Cosmochim. Acta, 39, 1077-1084.

Burnham, C.W., 1979a. Importance of volatile constituents. In: Evolution of igneous rocks, 50 anniversary perspectives. Ed: H.D. Yoder. Princeton Univ. Press, Princeton, N.J., 439-482.

Burnham, C.W., 1979b. Magmas and hydrothermal fluids. In: Geochemistry of hydrothermal ore deposits. Ed: H.L. Barnes. John Wiley and Sons, New York.

Burnham, C.W., 1981. Physiochemical constraints on porphry mineralization. In: Relations of tectonics to ore deposits in the Southern Cordillera. Eds: W.R. Dickenson and W.D. Payne. Ariz. Geol. Soc. Digest, 14, 71-77.

Cadle, R.D., 1980. A comparasion of volcanic with other fluxes of atmospheric trace gas constituents. Revs. Phys. Sp. Phys., 18, 746-752.

Candela, P.A., and Holland, H.D., 1984. The partitioning of copper and molybdenum between silicate melts and aqueous fluids. Geochim. Cosmichim. Acta, 48, 373-380.

Candela, P.A., and Holland, H.D., 1986. A mass transfer model from copper and molybdenum in magmatic hydrothermal systems: the origin of porpyry-type ore deposits. Econ. Geol., 81, 1-19.

Carmichael, I.S.E., Turner, F.J., and Verhoogen, J., 1974. Igneous Petrology. McGraw-Hill Book company, New York.

Chaigneau, M., Massare, D., and Clochiatti, R., 1980. Contributions a l'etude des inclusions vitreuses et des elements volatiles contenus dans les phenocristaux des quartz des roches volcaniques acides. Bull. Volcan., 43, 233-240.

Chappell, B.W., and White, A.J.R., 1974. Two contrasting granite types. Pacific Geol., 8, 173-174.

Clemens, J.D., 1984. Water contents of silicic to intermediate magmas. Lithos, 17, 273-287.

Clochiatti, R., Desnoyers, C., Sabroux, J-C, Tazieff, H, and Wilhelm, S., 1976. Relations entre les anorthoses de l'Erebus et leurs inclusions vitreuses. Bull. Soc. Fr. Mineral. Cristallogr., 99, 98-110.

Cole, J.W., 1979. Structure, petrology, and genesis of cenozoic volcanism, Taupo Volcanic Zone, New Zealand--a review. New Zealand J. Geol. Geophys., 22, 631-657.

Cole, J.W., 1982. Tonga-Kermadec-New Zealand. In: Andesites. Ed: R.S. Thorpe. John Wiley and Sons, 245-258.

Cole, J.W., 1984. Taupo-Rotarua Depression: an ensialic marginal basin of North Island, New Zealand. In: Marginal Basin Geology Eds: B.P. Kokelaar and M.F. Howells. Blackwell Scientific Publications.

Cortini, M., Lima, A., and De Vito, B., 1985. Trapping temperatures of melt inclusions from ejected Vesuvian mafic xenoliths. J. Volcan. Geother. Res., 26, 167-172.

Delaney, J.R., Muenow, D.W., and Graham, D.G., 1976. Abundance of water, carbon, and sulfur in the glassy rims of submarine pillow basalts. Geochim. Cosmichim. Acta, 42, 587-594.

Devine, J.D., Sigurdsson, H. and Davis, A.N., 1984. Estimates of sulfur and chlorine yield to the atmosphere from volcanic eruptions and potential climatic effects. J. Geophys. Res., 89, 6309-6325.

Druitt, T.H., Anderson, A.T., and Nagle, F., 1982. Water in rhyolitic magma, Bishop, California (abstr). EOS, 63, 451.

Dunbar, N.W., Hervig, R., and Kyle, P.R., 1988. Determinations of pre-eruptive H_2O, F and Cl contents of silicic magmas using melt inclusions, examples from Taupo Volcanic center, New Zealand. Bull. Volcan., (in press).

Dunbar N.W., Hervig, R., and Taylor, B.E., 1987. Volatile contents and degassing behavior of rhyolitic magmas from the Taupo Volcanic Zone, New Zealand (abstr). I.U.G.G., V3-5, p. 404.

Dunbar, N.W., and Kyle, P.R., 1986. H_2O and Cl contents, and temperature of Taupo Volcanic Zone rhyolitic magmas (abstr.). Abstract Volume, International Volcanological Congress, New Zealand, p. 148.

Dunbar, N.W., and Kyle, P.R., 1987. Studies of magmatic volatiles using glass inclusions in crystals from the Taupo Volcanic Zone, New Zealand, and Mount Erebus, Antarctica (abstr). American Current Research on Fluid Inclusions, Abstracts with Programs.

Dunbar, N.W., Kyle, P.R., and Wilson, C.J.N, (in review). Evidence for limited zonation in silicic magma systems, Taupo Volcanic Zone, New Zealand. Geology

Eggler, D.H., 1972. Water-saturated and -undersaturated relations in a Parucutin andesite and an estimate of water content in the natural magma. Contrib. Mineral. Petrol., 34, 261-271.

Eggler, D.H., 1976. Does CO_2 cause partial melting in the low-velocity layer of the mantle? Geology, 4, 69-72.

Eggler, D.H., 1978. The effect of CO_2 upon partial melting of peridotite in the system Na_2O-CaO-Al_2O_3-MgO-SiO_2-CO_2 to 35 kb. with an analysis of melting in a peridotite-H_2O-CO_2 system. Am. J. Sci., 278. 305-343.

Eichelberger, J.C., Carrigan C.R., Westrich, H., and Price, R.H., 1986. Non-explosive silicic volcanism. Nature, 323, 589-602.

Eichelberger, J.C., and Westrich, H.R., 1981. Magmatic volatiles in explosive rhyolitic eruptions. Geophys. Res. Let., 8, 757-760.

Esperanca, S., and Holloway, J.R., 1986. The origin of high-K latites from Camp Creek, Arizona: constraints from experiments with variable fO_2 and a_{H2O}. Contrib. Mineral. Petrol., 93, 504-512.

Ewart, A., 1963. Petrology and petrogenesis of the quaternary pumice ash in the Taupo area, New Zealand. J. Petrol., 4, 392-431.

Ewart, A., 1966. Review of mineralogy and chemistry of the acidic volcanic rocks of the Taupo Volcanic Zone, New Zealand. Bull. Volcan., 29, 147-172.

Ewart, A., Green, D.C., Carmichael, I.S.E., and Brown, F.H., 1971. Voluminous low temperature rhyolitic magmas in New Zealand. Contrib. Mineral. Petrol., 33, 128-144.

Ewart, A., Hildreth, W., and Carmichael, I.S.E., 1975. Quaternary acid magma in New Zealand. Contrib. Mineral. Petrol., 51, 1-27.

Ewart, A., and Taylor, S.R., 1969. Trace element geochemistry of the rhyolitic volcanic rocks, Central North Island, New Zealand. Phenocryst data. Contrib. Mineral and Petrol., 22, 127-146.

Fisher, R.V., and Schmincke, H.U., 1984. Pyroclastic Rocks. Springer-Verlag, New York.

Foley, S.F., Taylor, W.R., and Green, D.H., 1986. The effect of fluorine on phase relationships in the system $KAlSiO_4-Mg_2SiO_4-SiO_2$ at 28 kilobars and the solution mechanism of fluorine in silicate melts. Contrib. Mineral. Petrol., 93, 46-55.

Friedman, I., and Long, W., 1976. Hydration rate of obsidian. Science, 191, 347-352.

Friedman, I., and Smith, R.L., 1958. The deuterium content of water in some volcanic glasses. Geochim. Cosmich. Acta, 15, 218-228.

Froggatt, P.C., 1981. Karapiti Tephra Formation: a 10,000 year B.P. rhyolitic tephra from Taupo. New Zealand J. Geol. Geophys., 24, 96-98.

Froggatt, P.C., 1982a. Review of methods of estimating rhyolitic tephra volumes; applications to the Taupo Volcanic Zone, New Zealand. J. Volcan. Geother. Res., 14, 301-318.

Froggatt, P.C., 1982b. A study of some aspects of the volcanic history of the Lake Taupo area, North Island, New Zealand. Unpublished Ph.D. thesis, lodged in the Library, Victoria University of Wellington.

Garcia, M.O., Liu, N.W.K., and Muenow, D.W., 1979. Volatiles in submarine volcanic rocks from the Mariana Island arc and trough. Geochim. Cosmichim. Acta, 43, 305-312.

Gerlach, T.M., 1981. Restoration of new volcanic gas analyses from basalts of the Afar region: Further evidence of CO_2 degassing trends. J. Volcan. Geother. Res., 10, 83-91.

Gerlach, T.M., and Graeber, E.J., 1985. Volatile budget of Kilauea volcano. Nature, 313, 237-277.

Greenland, L.P., Rose, W.I., and Stokes, J.B., 1985. An estimate of gas emissions and magmatic gas content from Kilauea volcano. Geochim. Cosmichim. Acta, 49, 125-129.

Gustavson, L.B., and Hunt, J.P., 1975. The porphyry copper deposit at El Salvador, Chile. Econ. Geol., 70, 857-912.

Harris, D.M., 1981a. The microdetermination of H_2O, CO_2, and SO_2 in glass using a 1280°C microscope heating stage, cryopumping, and vapor pressure measurements from 77 to 273 K. Geochim. Cosmichim. Acta, 45, 2023-2036.

Harris, D.M., 1981b. The concentration of CO_2 in submarine tholeiitic basalts. J. Geol., 89, 689-701.

Harris, D.M., and Anderson, A.T., 1983. Concentrations, sources and losses of H_2O, CO_2, and S in Kilauean basalt. Geochim. Cosmichim. Acta, 47, 1139-1150.

Harris, D.M., and Anderson, A.T., 1984. Volatiles H_2O, CO_2 and Cl in a subduction related basalt. Contrib. Mineral. Petrol., 87, 120-128.

Hervig, R., Dunbar, N.W., Westrich, H., and Kyle, P., 1986. Direct determination of initial H_2O and F contents of rhyolitic magmas by ion microprobe (abstr). Geological Society of America Abstracts with Programs, 18, 636.

Hervig, R., Dunbar, N.W., Westrich, H., and Kyle, P., (1988). Pre-eruptive water content of rhyolitic magmas as determined by ion microprobe analysis of melt inclusions in phenocrysts. J. Volcan. Geother. Res. (in press)

Hildreth, W., 1979. The Bishop Tuff: Evidence for the origin of compositional zonation in silicic magma chambers. Geol. Soc. Am. Special Paper 180, 43-85.

Hildreth, W., 1981. Gradients in silicic magma chambers: Implications for lithospheric magmatism. J. Geophys. Res., 86, B11, 10153-10152.

Hollister, V.F., 1978. Geology of the porphyry ore deposits of the Western Hemisphere. A.I.M.E. press, New York.

Holloway, J.R., 1981. Volatile interactions in magma. In: Thermodynamics of minerals and melts. Eds: R.C. Newton, A. Navrotsky and B.J. Wood.. Springer-Verlag, Germany, 273-293.

Howorth, R., 1976. Late Pleistocene tephras of the Taupo and Bay of Plenty regions. Ph.D. thesis, Victoria Univ., Wellington, New Zealand.

Hurlibut, C.S., and Klein, C., 1977. Manual of Mineralogy. John Wiley and Sons, New York. 532 pp.

Huppert and Sparks, 1988. The generation of granitic magmas by intrusion of basalt into continental crust. J. Petrol (in press)

Jezek, P.A., and Noble, D.C., 1978. Natural hydration and ion exchange of obsidian: an electron microprobe study. Am. Mineral., 63, 266-273.

Jacobs, J.W., Korotev, R.L., Blanchard, D.P., and Haskins, L.A., 1977. A well-tested procedure for instrumental neutron-activation analysis of silicate rocks and minerals. J. of Radioac. Chem., 40, 93-114.

Johnston, D.A., 1980. Volcanic contributions of chlorine to the stratosphere: More significant to ozone than previously estimated? Science, 209, 491-493.

Kilinc, I.A. and Burnham, C.W., 1972. Partitioning of chloride between a silicate melt and coexisting aqueous phase from 2 to 8 kilobars. Econ. Geol., 67, 231-235.

Korotev, R.L., 1987. National Bureau of Standards Fly-Ash (1633A) as a multielement standard for instrumental neutron activation analysis. J. Radionucliide Anal., 110, 159-177.

Korotev, R.L., and Lindstrom, D.J., 1985. Interferences from fission of U-235 in INAA of rocks. Trans. Am. Nucl. Soc., 49, 177-178.

Krauskopf, K.B., 1979. Introduction to geochemistry. McGraw-Hill Book Company. 617 pp.

Kyle, P.R., 1977. Mineralogy and glass chemistry of recent volcanic ejecta from Mt Erebus, Ross Island, Antarctica. New Zealand J. Geol. Geophys., 20, 1123-1146.

Lofgren, G., 1980. Experimental studies on the dynamic crystallization of silicate melts. In: Physics of Magmatic Processes. Ed: R.B. Hargrave. 487-543

London, D., Morgan, G.B., and Hervig, R.L., 1987. Element partitioning and fractionation trends in volatile and LILE-rich rhyolite (abstr). EOS, 68, 450.

Lowe, D.J., 1986. Revisions of the age and stratigraphic relationships of Hinemaiaia Tephra and Whakatane Ash, North Island, New Zealand, using distal occurences in organic deposits. New Zealand J. Geol. Geophys., 29, 61-73.

Lowell, J.D., and Guilbert, J.M., 1970. Lateral and vertical alteration-mineralization zoning in porphyry ore deposits. Econ. Geol., 65, 373-408.

Luth, W.C., 1969. The system $NaAlSi_3O_8-SiO_2$ and $KAlSi_3O_8-SiO_2$ to 20 kb and the relationship between H_2O content, P_{H2O} in granitic magmas. Am. J. Sci., 267-A, 325-341.

Manning, D.A.C., 1981. The effect of fluorine on liquidus phase relationships in the system Qz-Ab-Or with excess water at 1 kilobar. Contrib. Mineral. Petrol., 76, 206-215.

McBirney A.R. and Murase,T., 1984. Rheological properties of magmas. Ann. Rev. Earth Plan. Sci., 12, 337-358.

Melson, W.G., 1983. Monitoring the 1980-1982 eruptions of Mount St. Helens: compositions and abundances of glass. Science, 221, 1387-1391.

Merzbacher, C. and Eggler, D.H., 1984. A magmatic geohydrometer: Applications to Mount St. Helens and other dacitic magmas. Geology, 12, 587-590.

Micheal, P.J., 1983. Chemical differentiation of the Bishop Tuff and other high-silica magmas through crystallization processes. Geology, 11, 31-34.

Mitchell, A.H.G. and Garson, M.S., 1983. Mineral deposits and global tectonic settings. Academic Press Geology series, London, U.K.

Morrison, G.H., and Slodzian, G., 1975. Ion Microscopy. Anal. Chem., 47, 933A-943A.

Muenow, D.A., 1973. High temperature mass spectrometric gas-release studies of Hawaiian volcanic glass: Pele's Tears. Geochim. Cosmochim. Acta, 37, 1551-1561.

Mysen, B.O., 1977. The solubility of H_2O and CO_2 under predicted magma genesis conditions and some petrologic and geophysical implications. Revs. Geophys. Sp. Phys., 15, 351-361.

Mysen, B.O. and Virgo, D., 1980. The solubility behavior of CO_2 in melts on the join $NaAl_3O_8$-$CaAl_2Si_2O_8$ at high pressures and temperatures: a Raman spectroscopic study. Am. Mineral., 65, 1166-1175.

Mysen, B.O. and Virgo, D., 1986. Volatiles in silicate melts at high pressure and temperature, parts 1 and 2. Chem. Geol., 57, 303-331.

Mysen, B.O., Virgo, D., Harrison, W.J., and Scarfe, C.M., 1980. Solubility mechanisms of H_2O in silicate melts at high pressures and temperatures: a Raman spectroscopic study. Am. Mineral., 65, 900-914.

Nairn, I.A., 1972. Rotoehu ash and the Rotoiti breccia formation, Taupo Volcanic zone, New Zealand. New Zealand J. Geol. Geophys., 15, 251-261.

Nairn, I.A., 1980. Source, age, and eruptive mechanism of Rotarua ash. New Zealand J. Geol. Geophys., 23, 193-207.

Nairn, I.A., 1981. Some studies of the geology, volcanic history, and geothermal resources of the Okataina volcanic center, Taupo volcanic zone, New Zealand. Ph.D. thesis, Victoria Univ., Wellington, New Zealand.

Naney, M.T., 1983. Phase equilibria of rock-forming ferromagnesian silicates in granitic systems. Am. J. Sci., 283, 993-1033.

Nash, W.P., 1987. Pre-eruptive gradients in pegmatitic magmas (abstr). I.U.G.G., V3-4, p 404.

Neuman, S., Stolper, E.M., and Epstein, S., 1986. Measurement of water in rhyolitic glasses: Calibration of an infrared spectroscopic technique. Am. Mineral., 71, 1527-1541.

Norrish, K., and Chappell, B.W., 1977. X-ray fluorescence spectrometry. In: Physical Methods in Determinative Mineralogy Ed: J. Zussman. Academic Press.

Palais, J.M., and Sigurdsson, H., 1987. Petrologic evidence of volatile emissions from major historic and pre-historic volcanic eruptions. Contributions of Geophysics to Climate change studies (Eds. A. Berger and R. Dickenson) A.G.U. Monogr. Geophys. 15 (in press).

Rampino, M.R. and Self, S., 1984. Sulfur-rich volcanic eruptions and stratospheric aerosols. Nature, 310, 677-679.

Rampino, M.R., Strothers, R.B., and Self, S., 1985. Climatic effects of volcanic eruptions. Nature, 313, 272.

Reid, F., 1983. Origin of the rhyolitic rocks of the Taupo Volcanic Zone, New Zealand. New Zealand J. Geol. Geophys., 15, 315-338.

Roedder, E., 1979. Origin and significance of magmatic inclusions. Bull. Mineral., 102, 487-510.

Roedder, E., 1984. Fluid Inclusions. In: Reviews in Mineralogy. Ed: Paul H. Ribbe, volume 12.

Roedder, E., and Coombs, D.S., 1967. Immiscibility in granitic melts, indicated by fluid inclusions in ejected granitic blocks from Ascension Island. J. Petrol., 8, 417-451.

Rutherford, N.F. and Heming, R.F., 1978. The volatile component of quaternary ignimbrite magmas from the North Island, New Zealand. Contrib. Mineral. Petrol., 65, 401-411.

Rutherford, M.J., Sigurdsson, H., Carey, S., and Davis, A., 1985. The May 18, 1980 eruption of Mount St. Helens 1. Melt composition and experimental phase equilibria. J. Geophys. Res., 90, 2929-2947.

Self, S., 1983. Large-scale phreatomagatic silicic volcanism: a case study from New Zealand. J. Volcan. Geother. Res., 17, 433-469.

Shimizu, N., Semet, M.P., and Allegre, C.J., 1978. Geochemical applications of quantitative ion-probe analysis. Geochim. Cosmochim. Acta, 42, 1321-1334.

Silltoe, R.H., Halls, C., and Grant, J.N., 1975. Porphyry time deposits in Bolivia. Econ. Geol., 70, 913-927.

Smith, R.L, 1979. Ash-flow magmatism. Geol. Soc. Am. Sp. Paper 180, 5-27.

Smith, R.L., and Bailey, R.A., 1966. The Bandelier Tuff: A study of ash-flow eruption cycles from zoned magma chambers. Bull. Volcan., 29, 83-104.

Sommer, M.A., 1977. Volatiles H_2O, CO_2 and CO in silicate melt inclusions in quartz phenocrysts from the rhyolitic Bandelier air-fall and ash-flow tuff, New Mexico. J. Geol., 85, 423-432.

Sommer, M.A. and Schramm, L.S., 1983. An analysis of the water concentrations in silicate melt inclusions in quartz phenocrysts from the Bandelier Tuff, Jemez Mountains, New Mexico. Bull. Volcan., 46, 299-320.

Sparks, R.S.J., 1978. THe dynamics of bubble formation and growth in magmas: A review and analysis. J. Volcan. Geother. Res., 3, 1-37.

Stanton, T.R., Holloway, J.R, Hervig, R.L., and Stolper, E., 1985. Isotope effect on water diffusivity in silicic melts: an ion microprobe and infrared analysis (abstr). EOS, 66, 1131.

Stern, T.A., 1985. A back-arc basin formed within continenetal lithosphere; the Central Volcanic region of New Zealand. Tectonophys., 112, 385-409.

Stern, T.A., 1987. Asymmetric back-arc spreading, heat flux and structure associated with the Central Volcanic Region of New Zealand. Ear. Plan. Sci. Let., 85, 265-276.

Stolarski, R.S. and Cicerone, R.J., 1974. Stratospheric chlorine: a possible sink for ozone. Can. J. Chem., 52, 1610-1615.

Stolper, E., 1982a. Water in silicate glasses: an infrared spectroscopy study. Contrib. Mineral. Petrol., 81, 1-17.

Stolper, E., 1982b. The speciation of water in silicate melts. Geochim. Cosmichim. Acta, 46, 2609-2620.

Stormer, J.C., 1983. The effects of recalculation on estimates of temperature and oxygen fugacity from analyses of multicomponent iron-titanium oxides. Am. Mineral., 68, 586-594.

Symonds, R.B., Rose, W.I., and Reed, M.H., 1988. Contributions of Cl- and F-bearing gases to the atmosphere by volcanoes. Nature, 334, 415-418.

Taylor, B.E., Dunbar, N.W., and Kyle, P.R., 1986. Stable isotope studies of the volatile history and degassing of rhyolitic magmas in the Taupo Volcanic Zone, New Zealand (abstr.). Abstract Volume, International Volcanological Symposium, New Zealand, p. 217.

Taylor, B.E., Eichelberger, J.C., and Westrich, H.R., 1983. Hydrogen isotopic evidence of rhyolitic magma degassing during shallow intrusion and eruption. Nature, 306, 541-545.

Taylor, H.P., 1979. Oxygen and hydrogen isotope relationships in hydrothermal mineral deposits. In: Geochemistry of Hydrothermal Ore deposits, 2nd edition. Eds: H.L. Barnes. Wiley-Interscience.

Topping, W.W., and Kohn, B.P., 1973. Rhyolitic tephra marker beds in the Tongariro area, North Island, New Zealand. New Zealand J. Geol. Geophys., 16, 375-395.

Turco, R.P., 1985. The photochemistry of the stratosphere. In: The Photochemistry of Atmospheres. Ed: J.S. Levine. Academic Press.

Vié Le Sage, R., 1983. Chemistry of the volcanic aerosol. In: Forecasting Volcanic Eruptions. Eds: H.Tazieff and Sabroux. Elsevier Press.

Vucetich, C.G., and Howorth, R., 1976. Late pleistocene tephro-stratigraphy in the Taupo District, New Zealand. New Zealand J. Geol. Geophys., 19, 51-69.

Vucetich, C.G., and Pullar W.A., 1973. Holocene tephra formations erupted in the Taupo area, and interbedded tephras from other volcanic sources. New Zealand J. Geol. Geophys., 16, 745-780.

Vucetich, C.J., and Pullar, W.A., 1969. Stratigraphy and chronology of late Pleistocene ash beds of central North Island, New Zealand. New Zealand J. Geol. Geophys., 12, 784-837.

Walker, G.P.L., 1980. The Taupo Pumice: product of the most powerful known (ultraplinian) eruption? J. Volcan. Geother. Res., 8, 69-94.

Walker, G.P.L., 1981a. Characteristics of two phreatoplinian ashes, and their water-flushed origin. J. Volcan. Geother. Res., 9, 395-407.

Walker, G.P.L., 1981b. Generation and dispersal of fine ash and dust by volcanic eruptions. J. Volcan. Geother. Res., 11, 81-92.

Walker, G.P.L., 1981c. The Waihimia and Hatepe plinian deposits from the rhyolitic Taupo Volcanic Center. New Zealand J. Geol. Geophys., 24, 305-325.

Wang, W.C., Wuebbles, D.J., Washington, W.M. Isaacs, R.G., and Molnar, G., 1986. Trace gases and other potential perturbations to global climate. Rev. Geophys., 24 (1), 110-140.

Wasserburg, G.J., 1957. The effect of H_2O in silicate systems. J. Geol., 65, 15-23.

Watson, E.B., 1976. Glass inclusions as samples of early magmatic liquid: determinative method and application to a South Atlantic basalt. J. Volcan. Geother. Res., 1, 73-84.

Webster, J.D., and Holloway, J.R., 1988. Experimental constraints on the partitioning of Cl between topaz rhyolites and H_2O and H_2O+CO_2 fluids: New implications for granitic differentiation and ore deposition. Geochim. Cosmich. Acta (in press)

Westrich, H.R., 1987. Determination of water in volcanic glasses by Karl Fischer titration. Chem. Geol., 63, 335-340.

Wilson, C.J.N., 1985. The Taupo Eruption, New Zealand. II. The Taupo Ignimbrite. Phil. Trans. R. Soc. Lond., 314, 229-310.

Wilson, C.J.N., Ambraseys, N.N., Bradley, J., and Walker, G.P.L, 1980. A new date for the Taupo eruption, New Zealand. Nature, 288, 252-253.

Wilson, C.J.N., Houghton, B.F., and Lloyd, E.F., 1986. Volcanic history and evolution of the Maroa-Taupo area, Central North Island. R. Soc. New Zealand, Bull. 23, 194-223.

Wilson, C.J.N., Rogan, A.M., Smith, I.E.M, Northey, D.J., Nairn, I.A., and Houghton, B.F., 1984. Caldera volcanoes of the Taupo Volcanic Zone, New Zealand. J. Geophys. Res., 89, 8463-8484.

Wilson, C.J.N., Switsur, V.R., and Ward, A.P., 1988. A new date for the Oruanui eruption, New Zealand. Geol. Mag., 125, 297-300.

Wilson, C.N.J., and Walker, G.P.L., 1985. The Taupo Eruption, New Zealand, I. General Aspects. Phil. Trans. R. Soc. Lond., 314, 199-228.

Wilson, L., 1980. Relationship between pressure, volatile content and ejecta velocity in three types of volcanic explosions. J. Volcanol. Geother. Res., 297-313.

Wilson, L., Sparks, R.S.J., Huang, T.C., and Watkins, N.D., 1978. The control of volcanic column height by eruption energies and dynamics. J. Geophys. Res., 83, 1829-1836.

Wilson, L., Sparks, R.S.J., and Walker, G.P.L., 1980. Explosive volcanic eruptions - IV. The control of magma properties and conduit geometry on eruption column behavior. Geophys. J. R. Astron. Soc., 63, 117-148.

Wolff, J.A. and Storey, M., 1983. The volatile conponent of some pumice-forming alkaline magmas from the Azores and Canary Islands. Contrib. Mineral. Petrol., 82, 66-74.

Yonover, R.N., Sinton, J.M., and Sommer, M.A., 1986. Petrology and laser decrepitiation volatile composition of the Galapagos 95.5^{o}W propagating/dying rift system (abstr). Abstract Volume, International Volcanological Congress, New Zealand, p. 225.

This dissertation is accepted on behalf of the faculty of the Institute by the following committee:

____
Advisor

____

____

____

____

January 18, 1989
____
Date